Simulation of secondary arcs in ehv systems employing single-pole autoreclosure.

Al-Rawi, Akram M.

Award date:
1981

Awarding institution:
University of Bath

SIMULATION OF SECONDARY ARCS IN EHV SYSTEMS EMPLOYING SINGLE-POLE AUTORECLOSURE

by

AKRAM M. AL-RAWI
B.Sc., M.Sc.

Thesis submitted for the degree of
Doctor of Philosophy
of
the University of Bath
1981

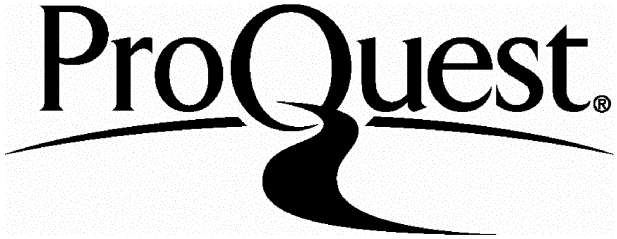

CONTENTS

CHAPTER 7 PARAMETERS OF SYSTEM STUDIED

CHAPTER 8 SYSTEM STUDIES: UNCOMPENSATED LINE

SUMMARY

The effectiveness of single-pole autoreclosure in maintaining power system stability is largely determined by the speed with which secondary arc extinction and hence autoreclosure can be achieved. Realistic simulation techniques are of obvious importance in relation to the design of systems employing single pole autoreclosure and, in this thesis, digital methods are developed to enable the faulted response of e.h.v. feeders subjected to secondary arcing phenomena to be more realistically simulated than hitherto had been possible. The new techniques are also of importance in relation to programmable based protection test equipment. The realistic simulation of the secondary arcing phenomena is of obvious importance in relation to pre-determining the shunt reactor compensation necessary to achieve acceptable autoreclosure dead-times in long line applications. Based upon experimental data, methods of modelling the non-linear behaviour of the earth fault arc path in both conducting and extinction states are described, together with the techniques developed for incorporating such models into practical e.h.v. system interconnections. The thesis concludes by illustrating and discussing the results of computational studies relating to typical 500 kV feeders employing single-pole autoreclosure.

ACKNOWLEDGEMENTS

The work presented in this thesis was carried out under the supervision of Dr. A.T. Johns, of the School of Electrical Engineering, University of Bath, whose constant encouragement and guidance are gratefully acknowledged.

Sincere thanks are due to Dr. R.K. Aggarwal for his cooperation.

Thanks are also due to the staff of the University of Bath Computer Centre for their assistance.

Finally the author is very grateful to his brother, Ismail, for his encouragement and financial support.

LIST OF SYMBOLS

p.p.s.,z.p.s.	=	positive and zero phase sequences
C_1, C_o	=	p.p.s. and z.p.s. shunt capacitance of assumed ideally transposed line
ℓ	=	length of faulted line section
x_f	=	distance to fault from end S
h_1,h_o	=	degree of p.p.s. and z.p.s. shunt compensation
B_{L1},B_{LO}	=	magnitude of p.p.s. and z.p.s. inductive susceptance of shunt reactor bank at nominal system frequency
B_{C1},B_{CO}	=	magnitude of p.p.s. and z.p.s. capacitive susceptance of any line section at nominal system frequency, assuming ideal transposition
Z_p,Z_n	=	phase and neutral impedances of shunt reactor bank
L_p, L_n	=	phase and neutral inductance of shunt reactor bank
ω_o	=	nominal system angular frequency
ω	=	angular frequency
ω_r	=	natural angular frequency of recovery voltage ($2\pi f_r$)
B_ℓ,B_u	=	susceptance of lower and upper arm
E	=	base voltage (E_a)
E_a,E_b,E_c	=	normal phase-to-neutral voltage
I_b	=	normal positive-sequence charging current ($j\omega_o C_1 E$)
I_{sec}	=	residual (secondary) current of phase-to-ground fault

$I_{sec(p.u.)}$ = normalized secondary arc current (I_{sec}/I_b)

j = imaginary unit $(-1)^{\frac{1}{2}}$

k = capacitance ratio of line (C_o/C_1)

V_r = steady-state recovery voltage

$V_{r(p.u.)}$ = normalized recovery voltage (V_r/E)

Γ_1, Γ_o = p.p.s. and z.p.s. reciprocal inductance of shunt reactor

$\bar{V}, \bar{I}$ = voltage and current transforms

U, O = unit and zero matrices

S = voltage eigenvector matrix

γ = modal propagation constant matrix

ψ = $S\gamma S^{-1}$

Z_o = $Y_o^{-1} = S\gamma^{-1}S^{-1}Z$ = polyphase surge impedance matrix

Z = series-impedance matrix per unit length of line

Y = shunt-admittance matrix per unit length of line

Z_S, Z_R = sending- and receiving-end main source impedance matrices

Z_{SS}, Z_{SR} = sending- and receiving-end composite-source impedance matrices

s.c.l. = short-circuit level

Z_{SO}/Z_{S1} = ratio of z.p.s. to p.p.s. impedance of lumped sources (at 50 Hz)

A_1, B_1, C_1, D_1 = matrices defining line section up to point of fault

A_2, B_2, C_2, D_2 = matrices defining line section beyond point of fault

$f(\omega)$ = Fourier transform of $f(t)$

α = frequency shift constant

Ω = truncation frequency

$f(\omega - j\alpha)$ = modified Fourier transform

$h(t)$ = unit step function

Z_F = fault resistance matrix

R_F = primary fault arc resistance

$\bar{E}_{fS}, \bar{E}_{fR}$ = transform of voltages at point of fault

$\bar{V}_{fS}$ = transform of prefault voltages at point of fault

$\bar{V}_{ff}, \bar{E}_{ff}$ = transform of superimposed voltages at point of fault

$\bar{V}_{SS}, \bar{I}_{SS}$ = transform of prefault voltages and currents at sending end of line

$\bar{V}_{RS}, \bar{I}_{RS}$ = transform of prefault voltages and currents at receiving end of line

$\bar{V}_S, \bar{V}_R$ = sending-and receiving-end voltage transforms

$\bar{I}_S, \bar{I}_R$ = sending- and receiving-end current transforms

$\bar{V}_{Sf}, \bar{I}_{Sf}$ = transform of superimposed voltage and current at sending end of line

$\bar{I}_{fSf}, \bar{I}_{fRf}$ = transform of superimposed currents at fault point

$\bar{V}_{Rf}, \bar{I}_{Rf}$ = transform of superimposed voltage and current at receiving end of line

V_p, I_p = voltage and current parameters of arc cyclogram

T_e = secondary arc extinction time (measured from time of initiation of secondary arc)

t = any time t

$h(t - T)$ = delayed unit step function $0, t < T$

$1, t > T$

$v_r(t)$ = arc re-ignition voltage

$\ell_a(t)/\ell_o$ = per-unit arc length variation

n = integer sample step n

ΔT = time sampling interval

$v(t), i(t)$ = voltage and current time variation

$\mathcal{F}^{-1}$ = inverse Fourier transform

τ = Convolution time variable

V_S/V_R = ratio of steady-state power frequency pre-fault bus-bar voltages

Z_{sr} = shunt reactor impedance sub-matrix

Y_{SR} = shunt admittance matrix

T_{ob} = observation time

T_1 = fault inception time

T_2 = sending end breaker opening time (measured from time of initiation of fault)

T_3 = receiving end breaker opening time (measured from time of initiation of fault)

T_4 = secondary arc extinction time measured from secondary arc initiation

T_5 = sending end breaker reclosing time (measured from time of initiation of fault)

T_6 = receiving end breaker reclosing time (measured from time of initiation of fault)

N = number of frequency sample

θ = line angle

Subscripts

S,R,F	=	sending end, receiving end, and fault points
a,b,c	=	phases a,b,c

Superscripts

T	=	transpose of matrix

CHAPTER 1

INTRODUCTION

1.1 Literature Review

It is well known that the majority of all line faults affecting e.h.v. networks are of the single-line-to-ground type and that most of these are transitory. From the standpoint of minimizing the disturbances, especially loss of synchronism, caused by such faults, it is desirable to clear them by opening the breaker poles of the faulted phase and to reclose them rapidly.

With regard to the cost of transmission lines, the increasing difficulty in obtaining rights-of-way and the growth of the system voltages, the question of attaining a good balance between cost and security leads to serious consideration of single-pole switching as a means of attaining this balance. Further, for a variety of reasons, there appears to be many cases where only a single transmission circuit is used. In such case, single-pole switching is almost a necessity. It is obvious that for a multi-phase fault, single-phase switching is not applicable. The modern approach is not to confine attention to the most severe cases, but rather to look at the whole spectrum of disturbances from a probabilistic point of view. The search for improved system performance in the case of a single phase-to-ground fault is in line with this outlook.

The required dead time (dead time is here defined as the period of time in which the whole line or just one phase of it remains de-energised) for single-pole switching is considerably longer than for three-phase switching, if no special measures are taken. In the past, single-pole

switching (s.p.s.) was little used, since the techniques which could permit sufficiently fast autoreclosure in such schemes were not developed[1]. It is for this reason that three-phase switching of lines was generally the solution adopted. The fact that the necessary dead time increased with the length and voltage of the transmission line further discouraged the use of s.p.s.[2].

The duration of the short circuit current is dependent only on the speed of the circuit breaker and associated relay equipment. For successful autoreclosure, the necessary dead time which must be allowed is dictated by the speed of the extinction of the secondary arc and the recovery of the dielectric strength of the fault path, and not by the mechanical reclosing time of the circuit breakers. When a line-to-ground fault is isolated by s.p.s., the current flowing in the fault path does not extinguish instantaneously. As a result of the capacitive and inductive coupling of the switched phase with the sound phases, a secondary arc current will continue to flow in the highly ionized fault path. As the arc path is elongated and cooled, a successful extinction may take place in one of the zero values of the residual current[3]. Here again, the sound phases will determine the recovery voltage (the recovery voltage is defined as the phase to earth voltage induced in the de-energized conductor at the fault point subsequent to the current extinction), which will determine whether a further re-strike may take place. At the time of re-energization of the switched phase the residual fault path has to withstand the normal phase voltage plus any transient over-voltage due to the reclosure, if a successful operation is to result.

The principal factors associated with s.p.s., that determine the probability of extinction of residual (or secondary) arcing fault in a given time are believed to be:

1. Effective value of steady state residual fault current.
2. The magnitude and rate of rise of the recovery voltage.
3. Length of air gap.
4. Effective value and duration of short circuit current.
5. Weather.

Items 1 and 2 are the most important factors. It depends mainly on system voltage, line length, and loading conditions. The magnitude of the secondary arc current and recovery voltage can be reduced by transposition[4,5,6], and by using high conductivity earth wires[7]. The magnitude and duration of the short circuit current as well as the wind strength have a certain influence on the extinction time[8]. Maikopar[9] provides data regarding the duration of the required pause in three-pole and single pole switching for transmission lines up to 400 kV. He concludes that the necessary dead time for s.p.s., with 20A (r.m.s.) residual current, may be taken as 0.4 second. With an 80A secondary arc, the dead time should be increased to 1.8 seconds.

The relation between system voltage, line length, and extinction time, has been described by Ozaki[8]. The author shows that, with a secondary arc current of about 20A, the average extinction time is 10-15 cycles. It also shows that, for 500 kV system, the extinction time is 15-20 cycles, for a line length of approximately 100 km, from 15-25 cycles for a line length of approximately 150 km, and more than 25 cycles for a line length of approximately 250 km. Other laboratory tests on 400 kV system[10] show that for recovery voltages higher than 20 kV extinction time increases with an increase of the secondary arc

current, while for lower recovery voltages the extinction time is practically independent on the value of the secondary arc current in the range examined (18-43A), and in all cases lower than 0.15s. While, if the recovery voltage is over 50 kV (r.m.s.), extinction time becomes extremely long.

Based on the above results, it is seen that the dead time can be too long and consequently can eliminate the use of s.p.s. for stability considerations. Therefore, the length of the line sections where s.p.s. is used has to be limited so that the limiting magnitudes of residual current and recovery voltage are not exceeded.

The continuous increase in transmission voltage over long distances has emphasised the importance in e.h.v. systems of the excessive line reactive power and the associated means to control them so that a reasonably constant voltage along the line can be maintained. In particularly long a.c. lines energized through relatively weak sources, the adoption of shunt reactors to compensate a portion of the line charging volt-amperes reactive (VAR's) is an indispensable method for excessive voltage and reactive power control[11]. High voltage shunt reactors connected to the line may increase the induced voltage in the disconnected phase[12,13]. Resonance may occur in conjunction with a high degree of compensation, where voltages on the disconnected phase may exceed the normal voltage to ground. However, the magnitude of the secondary arc current changes only insignificantly when shunt compensation is introduced. This means that the arc extinction is not necessarily more difficult, as long as the resonance region is avoided. A high degree of shunt compensation will probably nevertheless make single-pole reclosing impossible, unless special measures are taken to limit the induced voltage on the disconnected phase.

In 1962 Knudsen[14] proposed a method for reducing the capacitively induced voltage, and thus also the secondary arc current, for shunt compensated lines to such low values that single-pole reclosing could be used for longer lines and for higher degree of shunt compensation than would otherwise be possible. Independently of Knudsen, Kimbark[15] proposed the same system solution two years later. According to Knudsen the capacitive coupling can be reduced or completely eliminated, if the shunt reactors are designed so that their zero-sequence reactance becomes greater than their positive sequence reactance ($x_o/x_1 > 1.0$). This can be brought about by installing a separate reactor between earth and neutral of a star connected shunt reactor connected to the line. The neutral point reactor will be small in relation to the main reactor. This means that the cost of this reactor arrangement will be only slightly higher than a conventional shunt reactor. Maikopar[11] has also suggested the installation of a neutral reactor to avoid the resonance conditions, but the author does not mention the possibility of reducing the secondary arc current.

Relevant results of staged fault tests have been published in the description of the first practical application of specially connected reactors as an adjunct of the s.p.s. of the line[16,17].

Peterson[18] has suggested another method to eliminate the capacitive coupling. It requires the connection of capacitors of special value across the circuit breaker contacts. When the breakers open following a non-permanent line to ground fault the faulted phase conductor is connected to the source through these capacitors. Values of the capacitors can be selected to minimise the potential of the faulted phase conductor with respect to ground, thereby extinguishing the residual arc. Jahn et al[6] has suggested the use of ACSR ground wires to reduce the magnetic coupling. Forced extinction of the

residual arc, by shunting with jets of conducting salt solution was tried on the French 220 kV system and is discussed by Muller et al[19]. A modification of the above idea, where discharge resistors are connected through switches at the two ends of the faulted conductor, has also been suggested. Heinemann[20] describes how this could also be used to reduce switching surge overvoltages during reclosing.

Recently, two papers[21,22] concerning the use of shunt reactors for the purpose of secondary arc extinction have been presented and analysed for untransposed e.h.v. lines. The authors developed a modified 4-legged reactor scheme for installation at one end of the line, to be used in conjunction with a conventional 4-legged reactor at the other end. The modified reactor bank includes four switches whose operations are coordinated with the line breaker.

Several authors analysed the problem of single pole autoreclosure from different aspects. Shipley et al[23] used a digital computer, the effect of line transposition, the position of the 4-legged reactor, and the degree of compensation on the secondary arc extinction was analysed. Eaton et al[24] analysed the problem from the steady state point of view. The latter study is concerned with the effect on the magnitude of the steady state recovery voltage due to changes in the value of the shunt and neutral reactor. Haubrich et al[5] analysed the influence of various line parameters, and of the compensation reactors on the extinction of secondary arc in case of single phase autoreclosure. ASEA[17] has reported the installation of 100 MVAR, 400 kV shunt reactor in a 400 km long line. A study was performed to predict the influence of the reactor on the secondary arc current and the voltage occurring at the fault location after arc extinction and to calculate the transient voltage stresses on the neutral-point reactor

in conjunction with s.p.s.[13].

As mentioned previously, if the transmission line length or voltage is raised, the self extinction time of the secondary arc becomes longer and hence the reclosing time, or the no voltage time has to be elongated[2]. The increase in the reclosing time is not only unfavourable to system stability, but also increases the instantaneous torque on generators at the instant of reclosing, giving them unfavourable shocks.

To determine the reclosing time or to take suitable measures for reducing it, a knowledge of the self-extinction time of the secondary arc as well as its mechanism is essential. Several papers have discussed the characteristics of the secondary arc, however, its self-extinction mechanism has not been studied theoretically in detail[3,9,25,26,27] Maury[3] reviews the effect of the arc resistance on the magnitude of the secondary arc current and the recovery voltage waveform. The author concludes that the arc resistance does not, in practice, influence the value of the capacitive current flowing in the arc path. On the other hand, Dobson et al[28] has shown a different result which indicated that the arc resistance could decrease the magnitude of the secondary arc current to a significantly low value. However, both authors used the same equation to calculate the secondary arc current, but they used different values of secondary arc resistance which lead to their disagreement. Based on an extensive literature survey, the secondary arc resistance does not exceed 1000 Ω before the extinction[26,29,30], and this resistance is very small compared to the coupling impedance, so from the secondary arc current magnitude point of view, the secondary arc resistance can be neglected. However, from the extinction of the secondary arc current point, the arc path has to be represented as accurately as possible.

Milne[26] has investigated the stability of the secondary arc, in single-pole reclosing tests on long 275 kV transmission lines. The author shows that the secondary arc resistance varied between 200 and 800 Ω, the lower value holding soon after fault isolation and increasing till final arc extinction. Anjo et al[30], has analysed the self extinction mechanism of the secondary arc produced in the long air gap in the 500 kV line, by taking the voltage and current oscillograms and also by observing the arc on a high speed camera. The authors found that the arc voltage generally tends to increase with time, however, the measured self extinction time scatters extensively. Gary et al[31] analysed the probability of successful single pole autoreclosure in the 765 kV French system. The authors concluded that 40 ms is required for the re-establishment of the dielectric strength between the arc electrodes after the arc extinction.

Balser et al[32] analysed the electrical characteristics of a 500 kV transmission line during s.p.s., using a hybrid computer. A time dependent arc is used in their study. The authors assume that the arc resistance increases linearly with time until reaching a value at which the arc is extinguished. This representation requires four items of data:

1. The initial resistance (immediately after isolation of the faulted conductor).
2. The final resistance (immediately before arc extinction.
3. The lapsed time, or the rate of rise of resistance.
4. The time required for deionization sufficient to withstand line voltage upon reclosure.

The paper uses values of the first three items derived from test on the TVA line[16], the fourth item was not considered in the paper.

Single pole autoreclosure requires more complex protective relaying for the line[33]. In addition, the problem of zero-sequence current circulation in the adjacent lines is of great concern. These currents will flow when one phase of the line is open and can lead to false operation of the ground relays at a time when one can least afford such mal-operation. From a protection point of view, the significant voltage which appears on the faulted phase line-side of the breakers during the dead time could be a significant determining factor in respect of the optimum position and type of voltage transducer necessary for satisfactory phase-selection in single pole autoreclosure schemes[34].

1.2 Transient Calculation Methods

Power system analysis generally falls into three broad categories of study: steady-state operation, transient stability, and electrical transients. Much effort has been expended in recent years to improve the techniques of steady-state analysis, in view of the enormous increase in size and complexity of power netowrks. Electrical transients are associated with the circuitry in power systems, and therefore are very fast phenomena usually ranging from micro-seconds to milliseconds. The nature of electrical transients make it necessary to accurately model the distributed nature of transmission lines, as well as the dynamic behaviour of the associated apparatus.

In transient studies there are numerous calculation methods available. Some of them present some advantages over the others, but it is very difficult to define which one is the best. However each method presents its own merit and its choice depends very much on the

accuracy of the results, and the available means of tackling the problem, and on the time taken to get the results. They may be separated into three main groups, namely, methods using a scaled model of the actual system, mathematical methods and methods using a combination of analogue and digital computers. The first method uses a transient network analyser (TNA) where actual system parameters are scaled down. It presents some advantages such as the system response to any study can be obtained in a very short time and that once the model is established various studies can be done on it with ease. On the other hand it has some disadvantages due to the fact that it cannot accurately represent frequency dependent parameters of the system or simultaneously scale down all system parameters. In addition to these it requires a lot of time to remodel the system for different system parameters.

In recent years, however, much progress has been made in the use of computer simulation for the study of electrical transients. Based on the travelling wave phenomena, a number of methods are available to solve the system eqns. (1.1) and (1.2):

$$\frac{d}{dx}\left[\bar{V}\right] = -\left[\bar{Z}\right]\left[\bar{I}\right] \qquad (1.1)$$

$$\frac{d}{dx}\left[\bar{I}\right] = -\left[\bar{Y}\right]\left[\bar{V}\right] \qquad (1.2)$$

where $\bar{Z}$ and $\bar{Y}$ are the series-impedance and shunt-admittance matrices per unit length, respectively. $\bar{V}$ and $\bar{I}$ are column vectors, the elements of which represent the voltage to ground and the current flowing through the various conductors of the line. One of the most widely known methods is the Bewley lattice technique. This method is based on the assumption of lossless or distortionless propagation

and requires the use of reflection coefficients at discontinuities in transmission system. This method was used in much of the earlier works on computer simulation of travelling waves in power systems[35]. Another more recent method of simulating travelling waves was employed by Domel[36] in the development of the Boneville Power Administration (BPA) system transient program. This method also requires the assumption of lossless or distortionless propagation, but does not require the use of reflection coefficients. Boonyubol et al [37] has made use of the Laplace transform method and evaluated the fault transient, employing the residue theorem for the inverse Laplace transformation. In this method the line is assumed to be transposed and the line parameters used in the calculations are computed at a single fixed frequency.

Most power lines have small losses, and for transmission circuits without earth wires the line distributed parameters can be considered nearly constant over a wide range of frequency. In such a case, the digital simulation technique, previously mentioned, among others, may give reasonable results. For transmission lines involving the earth, line resistance and inductance vary significantly with frequency, and therefore a lossless or distortionless model is not satisfactorily represented if extreme accuracy is required. In such a case, the modified Fourier transform method is used for calculation[38,39]. By the use of a theory recently developed by Wedepohl[39], it is possible to represent the line in an accurate way, taking into account both the frequency dependence of the line parameters and the asymmetry of the multiconductor line. To account for a non-linearity, caused by the arc for example, the modified Fourier transform is used in conjunction with Duhamel's integral[40]. Recently, Bickford et al[41] demonstrated

the application of the modified Fourier transform and the Bowley lattice methods to the calculation of transient fault currents and voltages in power system networks. The results obtained using these techniques are compared and discussed on the basis of both waveform and frequency spectral. It is concluded that both methods are capable of yielding acceptable and near identical results.

1.3 Scope of the Present Work

In the present work, the modified Fourier transform method is used for calculation. It can easily represent frequency-dependence parameters of the system, and the asymmetry of the multiconductor line. To account for the non-linearity caused by the secondary arc, the modified Fourier transform is used in conjunction with time domain Convolution.

The main objective behind the present work is to develop mathematical and digital modelling techniques for simulating the secondary arc behaviour and the mechanism of its extinction, in both compensated and uncompensated systems. To use this in the study of:

1. The extinction time of the 500 kV uncompensated system.
2. The determination of the degree of shunt reactor compensation necessary to achieve acceptable auto-reclosure dead time in long line applications.
3. The determination of the secondary arc transient and recovery voltages for the purposes of evaluating the performance of protective gear utilising, in particular, voltage transducers connected on the line side of the circuit breakers.

4. Over voltages arising on the system and the neutral reactor, during the whole process of fault inception and single pole opening and reclosure.
5. Effect of line length, prefault power flow, source parameter, busbar termination and fault position on the secondary arc extinction time.
6. The possibility of using 4-legged shunt reactors in untransposed long lines.

The formulation should be as accurate as possible and should be sufficiently general to allow inclusion of different line types, transposed or non-transposed line, different line terminations, different fault position, sequential or simultaneous breaker opening and reclosure, compensated or uncompensated lines. The secondary arc path can be represented by a constant linear resistance, or a time dependent linear resistance or a full non-linear arc representation. The re-ignition voltage characteristic is also simulated.

Chapter 2 describes the simulation of the system under fault conditions. The methods used to incorporate 4-reactor schemes into single/multi-section feeder systems are also presented. The analysis of the multi-section feeder and line transposition scheme are described. In the same chapter, a brief review of the effect of shunt compensation on the secondary arc is presented.

The simulation of the breakers opening and isolation of the fault are described in chapter 3. It is considered, in this chapter, that the primary and secondary arc path are represented by a constant linear resistance (0.5 Ω).

Chapter 4 studies arc phenomena. The secondary arc path of transmission systems and the mechanism of extinction is modelled.

Chapter 5 formulates the secondary arc current and voltage, after fault isolation, by considering the non-linearity effect of the secondary arc path. The sending and receiving end voltage and current waveforms are also formulated.

The techniques used to simulate the breakers reclosure is described in chapter 6.

In chapter 7 the configuration of system studied is detailed. This covers line construction, line parameters, source parameters and the 4-reactor scheme parameters.

Digital computer results are presented in chapters 8 and 9. In chapter 8 digital examination of the secondary arc extinction time for the uncompensated (single feeder) system is presented. The problem of neutral reactor overvoltages and secondary arc extinction time in long line shunt compensated (single and 4-section feeder) systems is described in chapter 9.

General conclusions are presented in chapter 10.

CHAPTER 2

SIMULATION OF SHUNT COMPENSATED SINGLE/MULTI SECTION FEEDER SYSTEMS

2.1 Introduction

Shunt compensation of long lines serves two purposes:

1. Limitation of power-frequency overvoltages, especially at an open end of the line and at buses having transformers or loads[42].
2. Neutralization of shunt-capacitive coupling between phases, making s.p.s. feasible on a long line[14,15, 23,24,43,44,45].

For serving the first purpose alone, one or two banks of Y-connected shunt reactors with solidly grounded neutral are commonly employed. The size of the reactors can be expressed (a) as the three phase reactive power (MVAr's) consumed at rated voltage, (b) as the reactance per phase X_p, or (c) as the degree of positive sequence shunt compensation h_1. For serving both purposes simultaneously, the neutral point of the reactors selected for the first purpose is grounded through a fourth reactor, the neutral reactor. The bank of reactors then becomes a four-pointed star (fig. 2.1).

In this chapter, the method of determining the reactance of the neutral reactor is described[43]. Mathematical techniques to incorporate the 4-reactor scheme under steady-state and transient-fault conditions are described[45,46]. Methods used to represent the line transposition and composite source network are also described.

2.2 Secondary Arc Current and Recovery Voltage for Uncompensated Line

When one phase of a 3-phase line is opened at both ends to clear a ground fault, the faulted phase is capacitively and inductively coupled to the two sound phases[3]. This coupling has two effects:

1. Before extinction of the fault arc, it feeds current to the fault and maintains the arc.
2. After the arc current becomes zero, the coupling causes a voltage across the arc path. If the rate of rise of this voltage is too high, it will re-ignite the arc.

The current which will flow in the arc path after the breakers open is called the secondary arc and it has two components. Its shunt component is proportional to the length of the line. The series component is theoretically proportional to the loading and to the square of the line length. Its maximum value occurs at one end or the other, where the vector sum of the two components is also maximum. The voltage across the fault path after the extinction of the secondary arc current and before reclosure of the breakers is called the recovery voltage. The shunt component of the recovery voltage is proportional to the voltages of the energized conductors. The series component is proportional to the length of the line and its loading. The two components of recovery voltage differ in phase, and the actual recovery voltage at any point of the line is their vector sum. The ratio of the recovery voltage to the secondary arc current is the Thevenin's impedance.

Consider a 3-phase symmetrical transmission line connected to an ideal source at one end, the other end being open. Representing the line in terms of lumped capacitance (neglecting the line inductance and resistance), as shown in fig. 2.2, where C_1 and C_o are the positive and zero sequence capacitances for the line length under consideration. A line to ground (LG) fault (represented by switch F in closed position) occurs on phase 'a' and the circuit breaker S is opened to clear the fault. The system can be further simplified in the form of an equivalent circuit shown in fig. 2.3 by means of Thevenin's theorem. With switch F closed, the induced secondary arc current assuming zero arc resistance is given by:

$$I_{sec} = - j \frac{1}{3} E_a \omega_o (C_1 - C_o) \qquad (2.1)$$

where ω_o is the system frequency in rad/sec, and E_a is the phase voltage. If switch F is open (cleared fault) the induced voltage on phase 'a' is given by:

$$V_r = - E_a \frac{C_1 - C_o}{2C_1 + C_o} \qquad (2.2)$$

The Thevenin admittance seen from the fault terminals is given by:

$$Y_T = \frac{j\omega_o}{3} (2C_1 + C_o) \qquad (2.3)$$

Equations 2.1, 2.2, and 2.3 represent the components which are due to the electrostatic coupling only. For lines longer than 300 km, the component which is induced electromagnetically by the current in the sound phases must be taken into consideration[14].

2.3 Simulation of Shunt-Reactor Bank

The shunt capacitances of a transmission line are usually described by either a capacitance matrix or by a mesh circuit (fig. 2.4a). Assuming ideal transposition, the phase to phase and phase to ground

capacitive susceptances are B_{Ch} and B_{Cg} respectively. The symmetrical components of these susceptances are[44]:

$$\begin{aligned} B_{Co} &= B_{Cg} \\ B_{Cl} &= B_{Cg} + 3B_{Ch} \end{aligned} \qquad (2.4)$$

In terms of the positive-phase sequence (p.p.s.) and zero-phase sequence (z.p.s.) values of the line capacitive susceptances (B_{Cl},B_{Co}), the parameters of the shunt reactor bank when arranged to compensate one half of any line section of length ℓ are[44]:

$$\begin{aligned} B_{Ll} &= h_l B_{Cl}\, \ell_l \\ B_{Lo} &= h_o B_{Co}\, \ell_l \end{aligned} \qquad (2.5)$$

where h_l and h_o are the degrees of p.p.s. and z.p.s. shunt compensation, and $\ell_l = \ell/2$.

Because of the independence of the sequence circuit corresponding to a symmetrical actual circuit, these circuits are decoupled so that:

$$\begin{aligned} X_{Lo} &= 1/B_{Lo} \\ X_{Ll} &= 1/B_{Ll} \end{aligned} \qquad (2.6)$$

Examination of the circuit of fig. 2.1 with positive-sequence current and zero sequence current into the terminals gives:

$$\begin{aligned} X_{Ll} &= X_p \\ X_{Lo} &= X_p + 3X_n \end{aligned} \qquad (2.7)$$

or

$$\begin{aligned} X_p &= 1/(h_l B_{Cl} \ell_l) \\ X_n &= (h_l B_{Cl} - h_o B_{Co})/(3\ell_l h_l B_{Cl} h_o B_{Co}) \end{aligned} \qquad (2.8)$$

It follows from eqn. 2.8 that the phase and neutral inductances are as given in eqn. 2.9.

$$\begin{aligned} L_p &= X_p/\omega_o \\ L_n &= X_n/\omega_o \end{aligned} \qquad (2.9)$$

The resistances of the shunt reactor are relatively very small, a typical Q factor of each limb at power frequency (50 Hz) being 250. The impedance of the shunt reactor (fig. 2.5) are given by eqn. 2.10.

$$\begin{aligned} Z_p &= R_p + j\omega L_p \\ Z_n &= R_n + j\omega L_n \end{aligned} \qquad (2.10)$$

There are a number of factors which determine the degrees of shunt compensation (h_1, h_o), and for a typical line they generally lie between zero and 1.2[15,43,44,45]. The line shunt susceptances (B_{C1}, B_{Co}) are evaluated in the usual manner from the average sum of all the self and mutual susceptances per unit length of the line section under consideration.

It is convenient to combine the shunt-reactor arrangements with the line sections involved and for this purpose the canonical form of the two port or transfer matrix function defining the arrangement of fig. 2.5 is particularly useful[45,46,47].

$$\begin{bmatrix} \bar{V}_1 \\ \bar{I}_1 \end{bmatrix} = \begin{bmatrix} U & 0 \\ Y_s & U \end{bmatrix} \begin{bmatrix} \bar{V}_2 \\ \bar{I}_2 \end{bmatrix} \qquad (2.11)$$

where U is a unity matrix. The difference of the current vectors $[\bar{I}_1 - \bar{I}_2]$ define the current which flows in the reactor $[\bar{I}_s]$ and the latter is seen to be simply related to the impedance matrix $[Z_{sr}] = [Y_s]^{-1}$ of the shunt reactor by eqn. 2.12.

$$\begin{bmatrix} V_{2a} \\ V_{2b} \\ V_{2c} \end{bmatrix} = \begin{bmatrix} Z_{sr} \end{bmatrix} \begin{bmatrix} \bar{I}_s \end{bmatrix} = \begin{bmatrix} Z_p + Z_n & Z_n & Z_n \\ Z_n & Z_p + Z_n & Z_n \\ Z_n & Z_n & Z_p + Z_n \end{bmatrix} \begin{bmatrix} \bar{I}_{sa} \\ \bar{I}_{sb} \\ \bar{I}_{sc} \end{bmatrix} \qquad (2.12)$$

The submatrix $\begin{bmatrix} Y_s \end{bmatrix} = \begin{bmatrix} Z_{sr} \end{bmatrix}^{-1}$ which is used in the transfer matrix representation of the reactor is thus as given below:

$$\begin{bmatrix} Y_s \end{bmatrix} = \begin{bmatrix} Z_{sr} \end{bmatrix}^{-1} = \frac{1}{Z_p(Z_p + 3Z_n)} \begin{bmatrix} Z_p + 2Z_n & -Z_n & -Z_n \\ -Z_n & Z_p + 2Z_n & -Z_n \\ -Z_n & -Z_n & Z_p + 2Z_n \end{bmatrix}$$

2.4 The Effect of the Shunt Reactor on Reducing Capacitive Coupling Effect

Several authors have analysed how the shunt reactor supresses the secondary arc current and recovery voltage[14,15,43,44,24,23]. Kimbark[43] has produced useful sets of families of curves that can be suited to certain line construction. Secondary arc current, steady-state recovery voltage and natural frequency of transient recovery voltage have been considered and the loci of each of them has been plotted in a rectangular coordinates h_o versus h_1. However, the charts are true for a line with $C_o/C_1 = 0.7$ only.

In order to determine these three important curves, consider the equivalent circuit for a three-phase line, fig. 2.6a. The fault is assumed to occur on phase 'a' by closure of switch F and is isolated by opening of circuit breaker CB, whereupon it becomes a secondary arc current I_{sec}. Extinction of the arc is represented by opening switch F. The voltage V_r across the open switch is then the recovery voltage.

I_{sec} and V_r can be calculated more simply from the reduced circuit of fig. 2.6b, where the sound phases 'b' and 'c' are replaced by conductor 'bc' having an applied voltage equal to the average of E_b and E_c. In fig. 2.6b if the reactor scheme designed for quenching the secondary arc, the inductance of the upper arm resonates with the corresponding capacitance at the supply frequency, giving a high impedance. The lower arm generally does not resonate, hence the recovery voltage $V_r = 0$. While the residual fault is present, it bypasses the lower arm, and the current I_{sec} is proportional to the susceptance of the upper arm. With this arm adjusted for resonance, I_{sec} as well as V_r, is zero (neglecting the magnetic coupling effect). On any line with shunt reactors, the recovery voltage has in addition to the steady state component, a transient component of a natural frequency f_r, generally different from the supply frequency f_o. The circuit for determining the natural frequency is that of fig. 2.6c, formed from that of fig. 2.6b by setting the applied voltage equal to zero, thus making nodes 'bc' and 'g' become one[43].

Appendix (2.1) states the formula for the secondary arc current, the steady state recovery voltage, and the natural frequency component of recovery voltage:

$$I_{sec} = -j(E\,\omega_o/3)\left[C_1(1 - h_1) - C_o(1 - h_o)\right] \qquad (2.13)$$

$$V_r = -E\,\frac{C_1(1 - h_1) - C_o(1 - h_o)}{2C_1(1 - h_1) + C_o(1 - h_o)} \qquad (2.14)$$

$$\omega_r = \left(\frac{2h_1\omega_o^2C_1 + h_o\omega_o^2C_o}{2C_1 + C_o}\right)^{\frac{1}{2}} \qquad (2.15)$$

Or in p.u. quantity, the base current is the normal charging current I_b where $I_b = j\omega_o C_1 E$

$$I_{sec(p.u.)} = I_{sec} / I_b = -(H_1 - K\,H_o)/3 \qquad (2.16)$$

where $H_1 = (1 - h_1)$, $H_o = (1 - h_o)$, and $k = C_o/C_1$.

The base voltage is the normal line to ground voltage E.

$$V_{r(p.u.)} = V_r/E = -\frac{H_1 - kH_o}{2H_1 + kH_o} \tag{2.17}$$

and $$f_{r(p.u.)} = \omega_r/\omega_o = \left(\frac{2h_1 + kh_o}{2 + k}\right)^{\frac{1}{2}} \tag{2.18}$$

From these equations it is obvious that the condition to be met for eliminating the secondary arc current and recovery voltage is $(1 - h_1) = k(1 - h_o)$. It can be noticed from eqn. 2.8 that the inductance of the neutral reactor is zero when $h_o = h_1/k$. A close examination of eqn. 2.16 shows that the magnitude of the secondary arc current, under such condition ($h_o = h_1/k$), is equal to the secondary arc current when the line is uncompensated (as shown in eqn. 2.1). However, the recovery voltage in this case ($h_o = h_1/k$) could be higher than the uncompensated case and it depends on the value of h_1.

2.5 Simulation of Discretely Transposed Line Section

The effect of transposition is to provide an equivalent equilateral spacing. This means that the voltage drops should be equal in all conductors when balanced load conditions prevail (in the transposed line the voltage drops in each phase are directly proportional to the own phase current but independent of the current in the other phases).

In long distance transmission systems, discrete transposition of the line conductors is often performed at the terminal of each section or at intermediate points thereon. Transposition of the line can reduce its RI^2 loss. Furthermore it equalizes the three phase-to-phase shunt capacitances and thus makes it feasible to use simple four-legged bank of shunt reactors[22]. Transposition can assist on the secondary

arc extinction even if the line is not equipped with shunt reactor[6,17]. It is particularly important to simulate the effect of such transpositions, because they represent an abrupt point of discontinuity from which incident wave components are reflected[45].

Consider a transmission line of length, ℓ, having a complete cycle of transposition as shown in fig. 2.7. In section I, a two-port matrix equation can be written as[45,46,47]:

$$\begin{bmatrix} \bar{V}_{sa} \\ \bar{V}_{sb} \\ \bar{V}_{sc} \\ \bar{I}_{sa} \\ \bar{I}_{sb} \\ \bar{I}_{sc} \end{bmatrix} = \begin{bmatrix} A_1 & B_1 \\ & \\ & \\ & \\ & \\ C_1 & D_1 \end{bmatrix} \begin{bmatrix} \bar{V}_{R1a} \\ \bar{V}_{R1b} \\ \bar{V}_{R1c} \\ \bar{I}_{R1a} \\ \bar{I}_{R1b} \\ \bar{I}_{R1c} \end{bmatrix} \qquad (2.19)$$

where

$$A_1 = S \cosh(\gamma\ell/3)S^{-1}, \quad B_1 = S \sinh(\gamma\ell/3)S^{-1}Z_o$$
$$C_1 = Y_o B_1 Y_o \quad , \quad D_1 = Y_o A_1 Z_o$$

and

$$\begin{bmatrix} \gamma \end{bmatrix} = \begin{bmatrix} \gamma_1 & 0 & 0 \\ 0 & \gamma_2 & 0 \\ 0 & 0 & \gamma_3 \end{bmatrix} \qquad (2.20)$$

$$Z_o = S\,\gamma^{-1}S^{-1}Z, \quad Y_o = Z_o^{-1}$$

The variables in the above equations are explained in more detail in the modal analysis of the system studied considered in Appendix (2.2). In section II,

$$\begin{bmatrix} \bar{V}_{S2a} \\ \bar{V}_{S2b} \\ \bar{V}_{S2c} \\ \bar{I}_{S2a} \\ \bar{I}_{S2b} \\ \bar{I}_{S2c} \end{bmatrix} = \begin{bmatrix} A_2 & B_2 \\ & \\ & \\ & \\ & \\ C_2 & D_2 \end{bmatrix} \begin{bmatrix} \bar{V}_{R2a} \\ \bar{V}_{R2b} \\ \bar{V}_{R2c} \\ \bar{I}_{R2a} \\ \bar{I}_{R2b} \\ \bar{I}_{R2c} \end{bmatrix} \tag{2.21}$$

It is now required to define A_2 , B_2 , C_2 , and D_2 . In section II, a two-port matrix equation can also be written by using the two-port constants A_1 , B_1 , C_1 , and D_1 of section I, if the following order is used:

$$\begin{bmatrix} \bar{V}_{S2b} \\ \bar{V}_{S2c} \\ \bar{V}_{S2a} \\ \bar{I}_{S2b} \\ \bar{I}_{S2c} \\ \bar{I}_{S2a} \end{bmatrix} = \begin{bmatrix} A_1 & B_1 \\ & \\ & \\ & \\ & \\ C_1 & D_1 \end{bmatrix} \begin{bmatrix} \bar{V}_{R2b} \\ \bar{V}_{R2c} \\ \bar{V}_{R2a} \\ \bar{I}_{R2b} \\ \bar{I}_{R2c} \\ \bar{I}_{R2a} \end{bmatrix} \tag{2.22}$$

On the other hand:

$$\begin{bmatrix} \bar{I}_{S2} \end{bmatrix} = \begin{bmatrix} \bar{I}_{S2a} \\ \bar{I}_{S2b} \\ \bar{I}_{S2c} \end{bmatrix} = \begin{bmatrix} 0 & 0 & 1 \\ 1 & 0 & 0 \\ 0 & 1 & 0 \end{bmatrix} \begin{bmatrix} \bar{I}_{S2b} \\ \bar{I}_{S2c} \\ \bar{I}_{S2a} \end{bmatrix} \tag{2.23}$$

$$\left[\bar{I}_{S2}\right] = \left[M\right]\begin{bmatrix}\bar{I}_{S2b}\\ \bar{I}_{S2c}\\ \bar{I}_{S2a}\end{bmatrix}, \left[\bar{V}_{S2}\right] = \left[M\right]\begin{bmatrix}\bar{V}_{S2b}\\ \bar{V}_{S2c}\\ \bar{V}_{S2a}\end{bmatrix} \tag{2.24}$$

The same for

$$\left[\bar{I}_{R2}\right] = \begin{bmatrix}\bar{I}_{R2a}\\ \bar{I}_{R2b}\\ \bar{I}_{R2c}\end{bmatrix} = \left[M\right]\begin{bmatrix}\bar{I}_{R2b}\\ \bar{I}_{R2c}\\ \bar{I}_{R2a}\end{bmatrix} \tag{2.25}$$

$$\left[\bar{V}_{R2}\right] = \begin{bmatrix}\bar{V}_{R2a}\\ \bar{V}_{R2b}\\ \bar{V}_{R2c}\end{bmatrix} = \left[M\right]\begin{bmatrix}\bar{V}_{R2b}\\ \bar{V}_{R2c}\\ \bar{V}_{R2a}\end{bmatrix} \tag{2.26}$$

From eqns. 2.22 to 2.26, it gives:

$$\begin{bmatrix}\bar{V}_{S2}\\ \bar{I}_{S2}\end{bmatrix} = \begin{bmatrix}M\,A_1\,M^{-1} & M\,B_1\,M^{-1}\\ M\,C_1\,M^{-1} & M\,D_1\,M^{-1}\end{bmatrix}\begin{bmatrix}\bar{V}_{R2}\\ \bar{I}_{R2}\end{bmatrix} \tag{2.27}$$

From eqns. 2.21 and 2.27, it gives:

$$\begin{aligned} A_2 &= M\,A_1\,M^{T}\\ B_2 &= M\,B_1\,M^{T}\\ C_2 &= M\,C_1\,M^{T}\\ D_2 &= M\,D_1\,M^{T} \end{aligned} \tag{2.28}$$

where $\left[M\right]^{T} = \left[M\right]^{-1}$

A post-multiplication of the matrix $\left[A_1\right]$ by the transposed of the connection matrix, $\left[M\right]^{T}$, leads to a shift on the column vectors. A

pre-multiplication of the matrix A_1 by the connection matrix, M , leads to a shift in row vectors. Hence A_2 , B_2 , C_2 , and D_2 can be obtained respectively from A_1 , B_1 , C_1 , and D_1 , with no need of doing the matrix multiplications as shown in eqn. 2.28, by just reshuffling the elements in matrices A_1 , B_1 , C_1 , and D_1 as outlined below.

If a line having its phase conductors changing from positions 1 to 3, 2 to 1 and 3 to 2, as shown in fig. 2.7, a matrix K can be formed such that:

$$\left[K\right] = \left[3 \quad 1 \quad 2\right]$$

It can be shown that:

$$\left[M\right] A_1\,(I,J) \left[M\right]^T = A_1\,(K(I), K(J))$$

or $$A_2\,(I,J) = A_1(K(I), K(J)) \qquad (2.29)$$

The same can be applied to B_2 , C_2 , and D_2 .

Two-port constants for section III can also be calculated as those in section II. A matrix K_1 can be formed such that:

$$\left[K_1\right] = \left[2 \quad 3 \quad 1\right]$$

and $$A_3\,(I,J) = A_1\,(K_1(I), K_1(J)) \qquad (2.30)$$

The overall transfer matrices between the sending and receiving end for unfaulted transposed line can be described by:

$$\begin{bmatrix} \bar{V}_S \\ \bar{I}_S \end{bmatrix} = \begin{bmatrix} A_1 & B_1 \\ C_1 & D_1 \end{bmatrix} \begin{bmatrix} A_2 & B_2 \\ C_2 & D_2 \end{bmatrix} \begin{bmatrix} A_3 & B_3 \\ C_3 & D_3 \end{bmatrix} \begin{bmatrix} \bar{V}_R \\ \bar{I}_R \end{bmatrix} \qquad (2.31)$$

Similar methods are likewise used to describe the overall transfer matrices between the fault point and the sending and receiving ends

for fault at any point along the line[45].

2.6 Combination of Line and Shunt Reactor Bank

For computational purposes, it is convenient to combine the line sections with the shunt reactors in the manner illustrated in fig. 2.8 to form a line/reactor equivalent circuit. From the previously developed equation 2.11

$$\begin{bmatrix} \bar{V}_R \\ \bar{I}_{RL} \end{bmatrix} = \begin{bmatrix} U & O \\ Y_s & U \end{bmatrix} \begin{bmatrix} \bar{V}_{R1} \\ \bar{I}_R \end{bmatrix} \tag{2.32}$$

or

$$\begin{bmatrix} \bar{V}_R \\ \bar{I}_{RL} \end{bmatrix} = \begin{bmatrix} Y_{SR} \end{bmatrix} \begin{bmatrix} \bar{V}_{R1} \\ \bar{I}_R \end{bmatrix}, \quad \begin{bmatrix} Y_{SR} \end{bmatrix} = \begin{bmatrix} U & O \\ Y_s & U \end{bmatrix}$$

At the fault point

$$\begin{bmatrix} \bar{V}_F \\ \bar{I}_{FR} \end{bmatrix} = \begin{bmatrix} A_{RT} & B_{RT} \\ C_{RT} & D_{RT} \end{bmatrix} \begin{bmatrix} \bar{V}_R \\ \bar{I}_{RL} \end{bmatrix} \tag{2.33}$$

$$\begin{bmatrix} \bar{V}_F \\ \bar{I}_{FR} \end{bmatrix} = \begin{bmatrix} A_{RT} & B_{RT} \\ C_{RT} & D_{RT} \end{bmatrix} \begin{bmatrix} Y_{SR} \end{bmatrix} \begin{bmatrix} \bar{V}_{R1} \\ \bar{I}_R \end{bmatrix}$$

$$= \begin{bmatrix} A_{2T} & B_{2T} \\ C_{2T} & D_{2T} \end{bmatrix} \begin{bmatrix} \bar{V}_{R1} \\ \bar{I}_R \end{bmatrix} \tag{2.34}$$

The same way could be used to describe the equivalent line section linking points F and S.

$$\begin{bmatrix} \bar{V}_F \\ \bar{I}_{FS} \end{bmatrix} = \begin{bmatrix} A_{1T} & B_{1T} \\ C_{1T} & D_{1T} \end{bmatrix} \begin{bmatrix} \bar{V}_{S1} \\ \bar{I}_S \end{bmatrix} \qquad (2.35)$$

The equivalent line/reactor representation of the unfaulted sections can be obtained in a similar way. In this case the transfer matrix describing the line section has to be pre- and post-multiplied by the transfer matrix describing the shunt reactors to give the overall equivalent.

$$\begin{bmatrix} \bar{V}_{S1}=\bar{V}_S \\ \bar{I}_S \end{bmatrix} = \begin{bmatrix} Y_{SR} \end{bmatrix} \begin{bmatrix} A_1 & B_1 \\ C_1 & D_1 \end{bmatrix} \begin{bmatrix} A_2 & B_2 \\ C_2 & D_2 \end{bmatrix} \begin{bmatrix} A_3 & B_3 \\ C_3 & D_3 \end{bmatrix} \begin{bmatrix} Y_{SR} \end{bmatrix} \begin{bmatrix} \bar{V}_{R1}=\bar{V}_R \\ \bar{I}_R \end{bmatrix} \qquad (2.36)$$

2.7 Simple/Composite Source Simulation

In power system transient analysis, it is usual to assume that the line under consideration is energized from infinite-busbar source. A more realistic form of representation is necessary taking into consideration the source-side network representation. The complexity of the source-side network terminating in a busbar from which a transmission line is energized has been recognized. This mainly is due to the fact that, in general, this source is not a localised generation source whose reactance can be derived from the system short-circuit apparent power and the system voltage. Terminating at the busbar may be other transmission lines originating at remote points in the network and these may in turn be fed from other generating points. There is thus, in fact, no limit to the extent of such detailed source arrangement. In dealing with transient switching voltages the source side plays a very important role in the shape and magnitude of the transient voltage waveform[39]. It is not always necessary to represent the entire network source configuration, since from computation

points of view, this may not be economical. Sometimes it is not even necessary to consider the entire source-side network, since transient times to the distant points of such networks and back may exceed the observation time chosen and hence would be of no direct relevance to the study.

A general source model based upon arbitrarily defined short-circuit levels at the terminating busbars, is shown in fig. 2.9, and possesses an impedance matrix of the form given in eqn. 2.37. The parameters of eqn. 2.37 are explained in Appendix (2.3).

$$\left[Z_S \right] = \begin{bmatrix} Z_{S1} + Z_{n1} & Z_{n1} & Z_{n1} \\ Z_{n1} & Z_{S1} + Z_{n1} & Z_{n1} \\ Z_{n1} & Z_{n1} & Z_{S1} + Z_{n1} \end{bmatrix} \tag{2.37}$$

$$\text{or} \quad \left[Z_{S6} \right] = \begin{bmatrix} U & Z_S \\ 0 & U \end{bmatrix} \tag{2.38}$$

Fig. 2.10 represents a composite source network to be considered in this work. Analysis of a general composite source network has been reported[45]. The impedance matrix of each local infeed/outfeed (Z_S, Z_R, Z_{S3}, Z_{S4}, Z_{S5}) is calculated from a knowledge of the power frequency short-circuit levels and the ratio of zero-phase sequence to positive-phase sequence impedance of the source in question.

With reference to figs. 2.9-2.13, the transfer-matrix eqn. 2.39 defines the response of the line/reactor combination of the first source section (sending end side).

$$\begin{bmatrix} \bar{V}_S \\ \bar{I}_{S1} \end{bmatrix} = \begin{bmatrix} A_{L1} & B_{L1} \\ C_{L1} & D_{L1} \end{bmatrix} \begin{bmatrix} \bar{V}_{00} \\ \bar{I}_{00} \end{bmatrix} \tag{2.39}$$

Now the total current entering busbar S is

$$\bar{I}_S = \bar{I}_{S1} + \left[Z_{S3}\right]^{-1}\bar{V}_S \qquad (2.40)$$

where Z_{S3} is a 3 x 3 matrix and represents the impedance of the infeed/outfeed s.c.3 and is calculated in the same way of calculating the main source impedance Z_S.

At the main source $\left[\bar{V}_{00}\right] = \left[Z_S\right]\left[\bar{I}_{00}\right]$ (2.41)

Substituting eqns. 2.41 and 2.40 in 2.39, the total composite source impedance matrix at sending end Z_{SS} is then finally computed from eqn. 2.42.

$$\left[\bar{V}_S\right] = (A_{L1}Z_S + B_{L1})(C_{L1}Z_S + Z_{S3}^{-1}A_{L1}Z_S + D_{L1} + Z_{S3}^{-1}B_{L1})^{-1}\left[\bar{I}_S\right] \qquad (2.42)$$

or

$$\left[Z_{SS}\right] = (A_{L1}Z_S + B_{L1})(C_{L1}Z_S + Z_{S3}^{-1}A_{L1}Z_S + D_{L1} + Z_{S3}^{-1}B_{L1})^{-1}$$

Similar procedures are likewise performed to define the total complex source impedance Z_{SR} at the receiving end.

2.8 Fault Simulation

The fundamental relationships developed in sections 2.5-2.7 have been deliberately formulated in such a way as to effectively enable any compensated/uncompensated feeder arrangement to be reduced to the faulted circuit model shown in fig. 2.14. Details of the methods of digitally simulating a fault on such a model by using matrix functions and numerically evaluated Fourier transforms are reported by Johns and Aggarwal[47]. It is worthwhile noting that the latter methods were developed for studying uncompensated single section homogeneous feeders.

The basis of the method hinges upon representing the voltage at the fault point by the sum of two voltages $\bar{V}_{fS}$, $\bar{V}_{ff}$ as shown in fig. 2.15. $\bar{V}_{fS}$ is sinusoidal and is equal to the steady-state voltage at the fault point before the disturbance. $\bar{V}_{ff}$ is a suddenly applied voltage, which when added to $\bar{V}_{fS}$, represents the post fault voltage. A solution may be obtained by performing two separate calculations in which the desired voltages and currents are evaluated when $\bar{V}_{fS}$ is applied to the energized system, and the superimposed voltage $\bar{V}_{ff}$ is applied to the line with all source voltages set at zero. The method is essentially one of superposition. Under steady state conditions, three quantities are required, namely, sending end current, receiving end current, and the voltage at fault point (F) before the fault occurs.

From fig. 2.15, under steady state conditions, eqn. 2.43 represents the relationship between voltage and current.

$$\begin{bmatrix} \bar{V}_{SS} \\ \bar{I}_{SS} \end{bmatrix} = \begin{bmatrix} A_L & B_L \\ C_L & D_L \end{bmatrix} \begin{bmatrix} A_R & B_R \\ C_R & D_R \end{bmatrix} \begin{bmatrix} \bar{V}_{RS} \\ \bar{I}_{RS} \end{bmatrix} \qquad (2.43)$$

$$= \begin{bmatrix} A & B \\ C & D \end{bmatrix} \begin{bmatrix} \bar{V}_{RS} \\ \bar{I}_{RS} \end{bmatrix}$$

where A_L, B_L, C_L and D_L represent the matrix constant of the line/reactor between the fault point and the sending end. A_R, B_R, C_R and D_R represent the matrix constants of the line/reactor between the fault and the receiving end.

The sending and receiving end current before the fault is thus given by:

$$\begin{aligned} \bar{I}_{SS} &= \left[C - DB^{-1}A \right] \bar{V}_{RS} + DB^{-1}\bar{V}_{SS} \\ \bar{I}_{RS} &= B^{-1}\left[\bar{V}_{SS} - A\bar{V}_{RS} \right] \end{aligned} \tag{2.44}$$

At the fault point

$$\begin{bmatrix} \bar{V}_{fS} \\ \bar{I}_{fRS} \end{bmatrix} = \begin{bmatrix} A_R & B_R \\ C_R & D_R \end{bmatrix} \begin{bmatrix} \bar{V}_{RS} \\ \bar{I}_{RS} \end{bmatrix} \tag{2.45}$$

Solving eqns. 2.45 and 2.44

$$\bar{V}_{fS} = \left[A_R - B_R B^{-1} A \right] \bar{V}_{RS} + B_R B^{-1} \bar{V}_{SS} \tag{2.46}$$

Each of the above equations are evaluated at power frequency, because the prefault condition is essentially a steady-state one. Indeed, the voltage and current vectors may be considered in phasor form and converted directly to the time domain without invoking the inverse transform[45]. The analysis for phase-a-to ground fault requires the calculation of the components due to the superimposed voltage $\bar{V}_{ff}$. These components should be added to the corresponding prefault steady state components to obtain the complete fault-transient waveform. The formulation of the equations required for a complete solution is discussed in detail in Appendix (2.4).

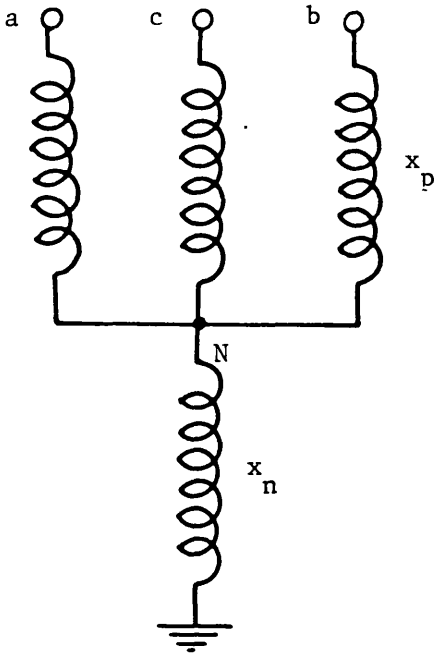

Fig. 2.1 Four-branched symmetrical star circuit for shunt compensation of balanced single circuit line

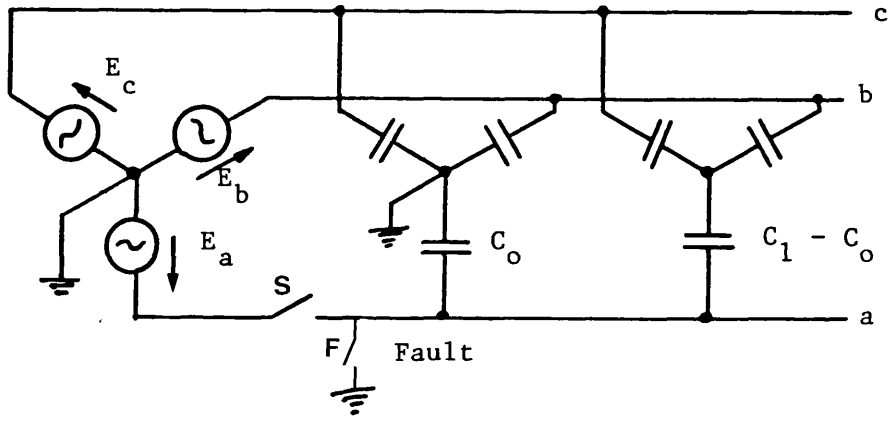

Fig. 2.2 Lumped capacitance three-phase system

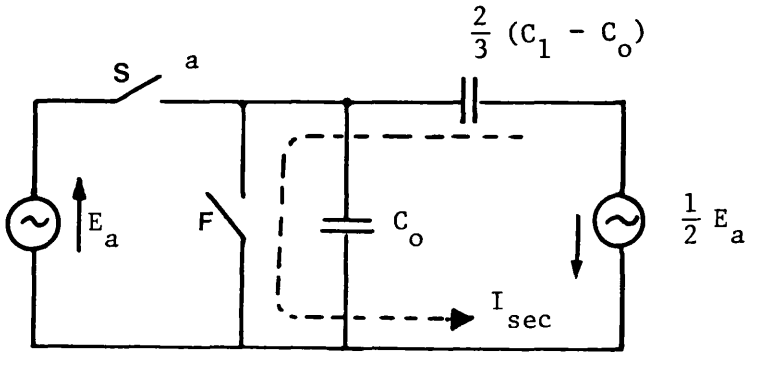

Fig. 2.3 Equivalent circuit for system of fig. 2.2

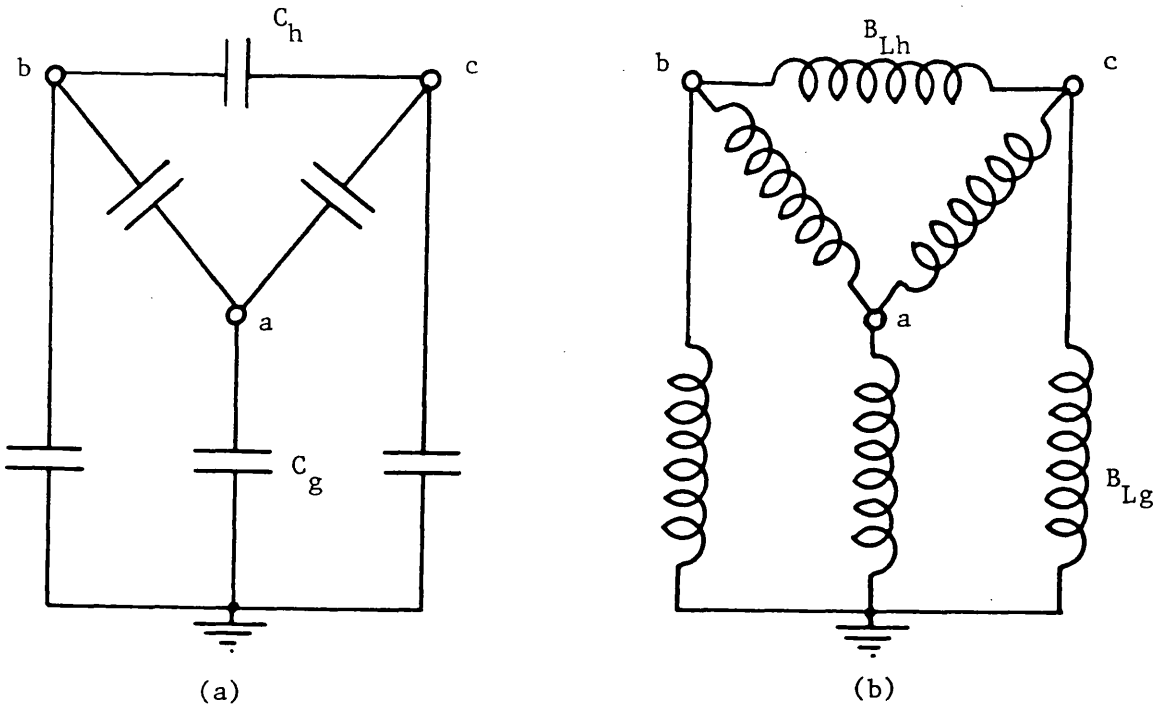

Fig. 2.4 (a) Mesh circuit representing shunt capacitances of balanced single-circuit line

(b) Symmetrical circuit equivalent to the symmetrical star of fig. 2.1

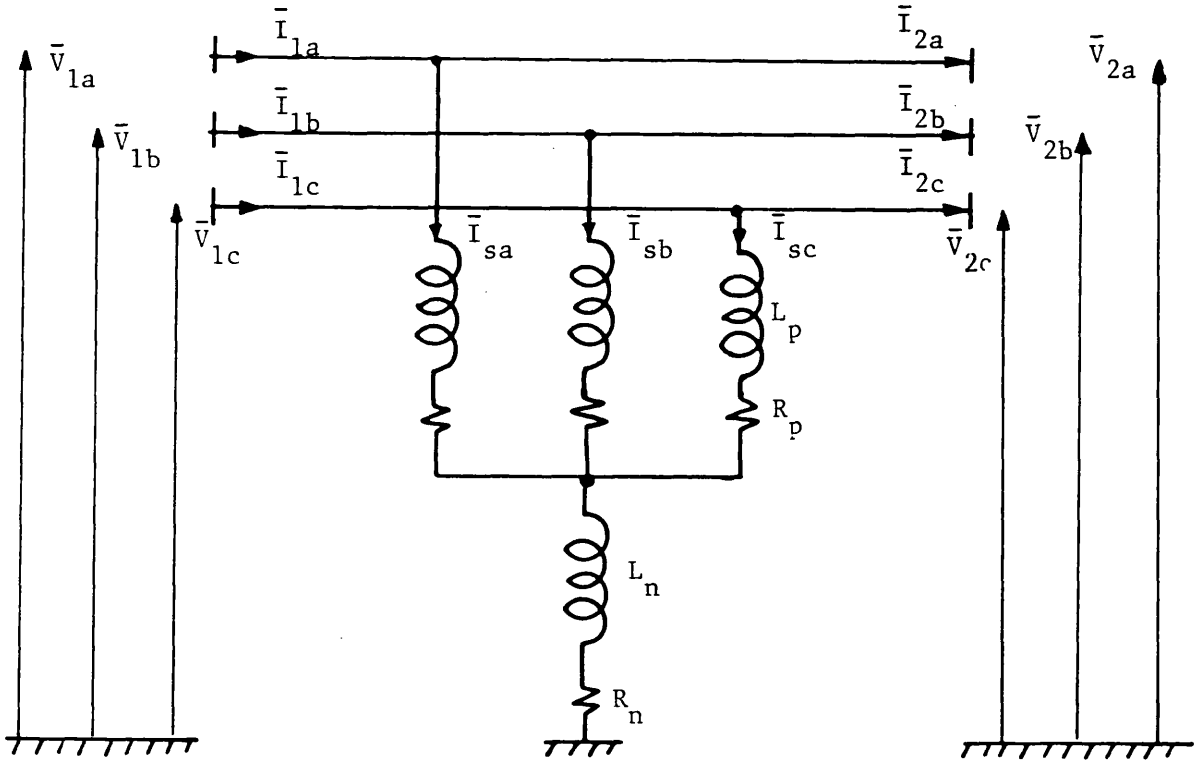

Fig. 2.5 Shunt reactor arrangement

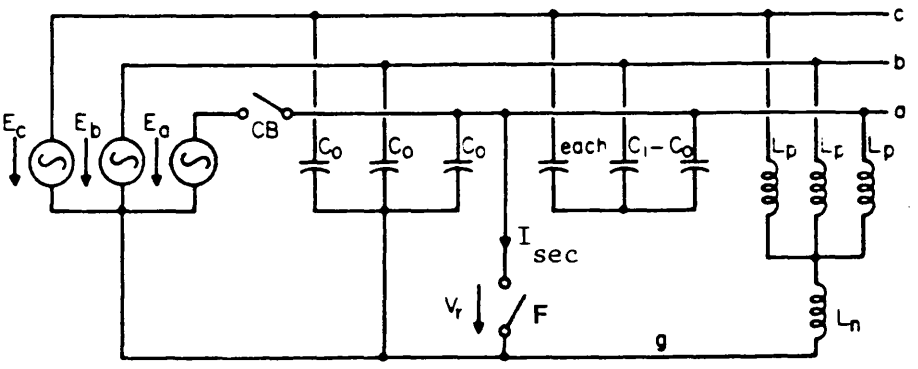

Fig. 2.6a Three-phase circuit with faulted phase disconnected

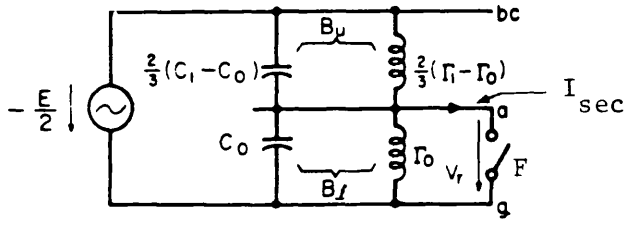

Fig. 2.6b Circuit result from reduction of circuit of fig. 2.6a

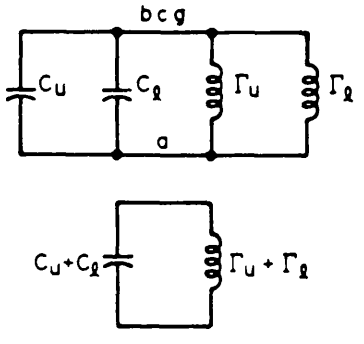

Fig. 2.6c Circuit for determination of natural frequency of recovery voltage

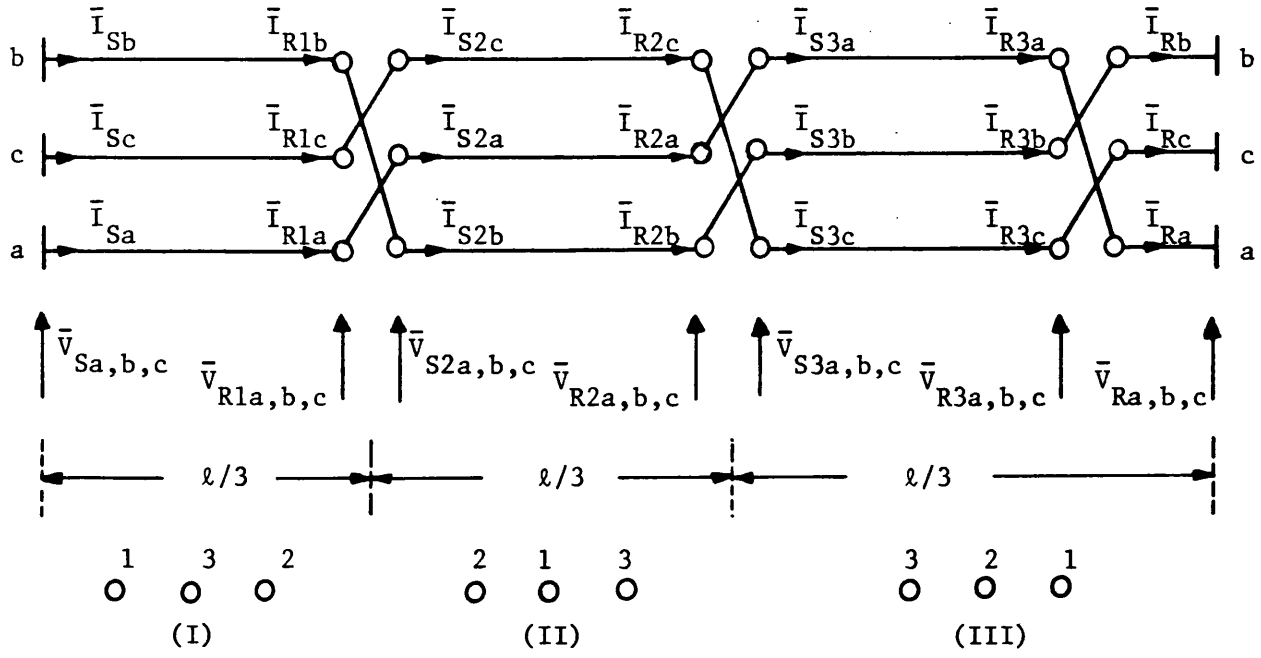

Fig. 2.7 Schematic diagram of a transmission line with a complete cycle of transposition

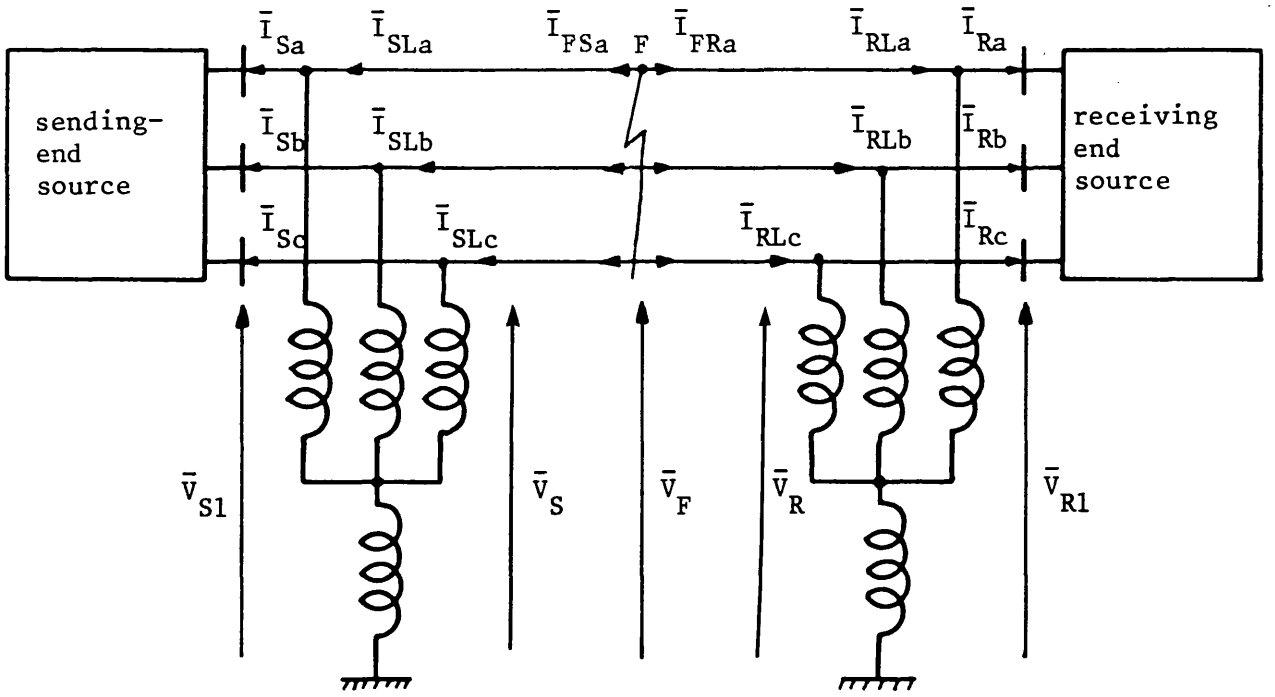

(a)

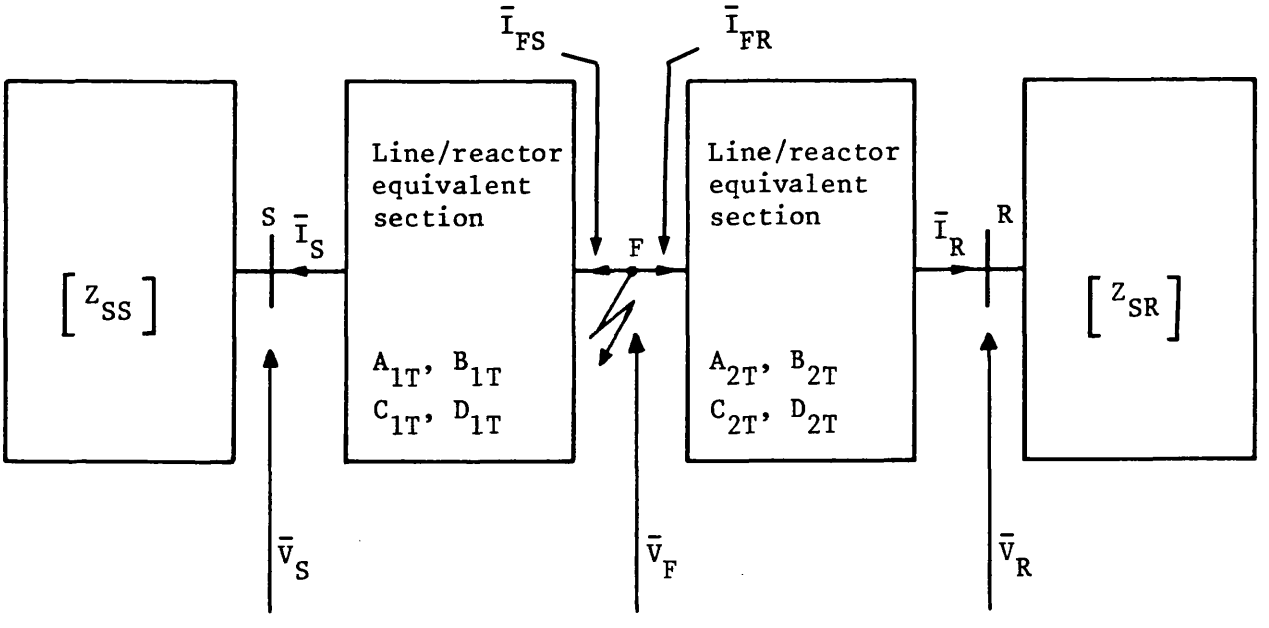

(b)

Fig. 2.8 Combination of line and shunt-reactor banks

(a) actual circuits

(b) equivalent arrangement

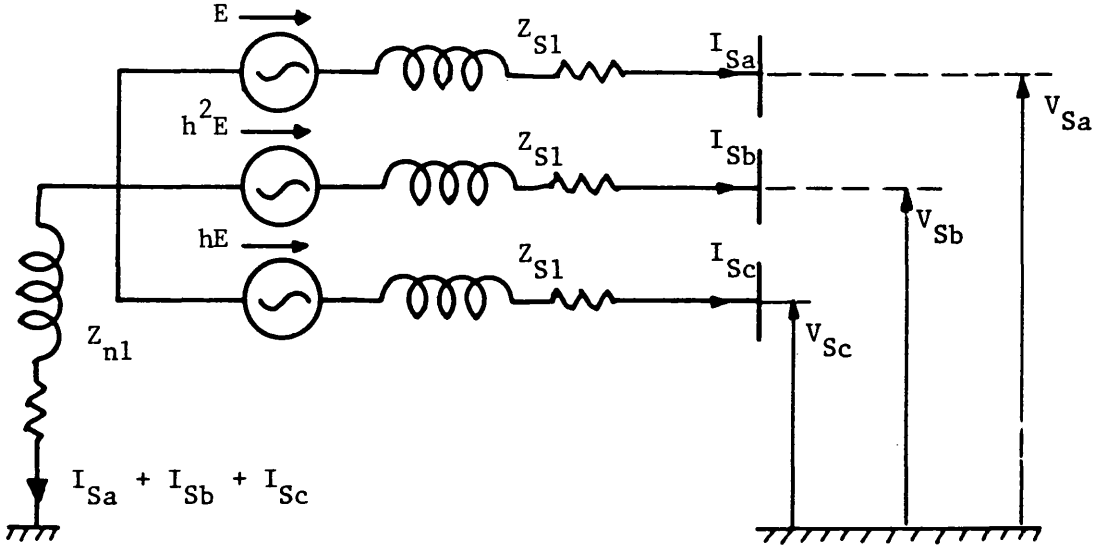

Fig. 2.9 Main source network model

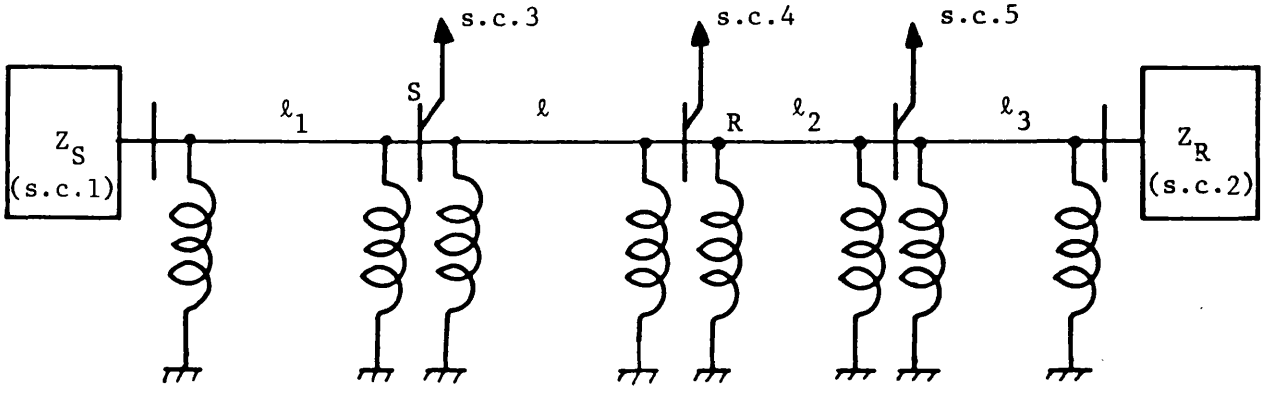

Fig. 2.10 Basic system model

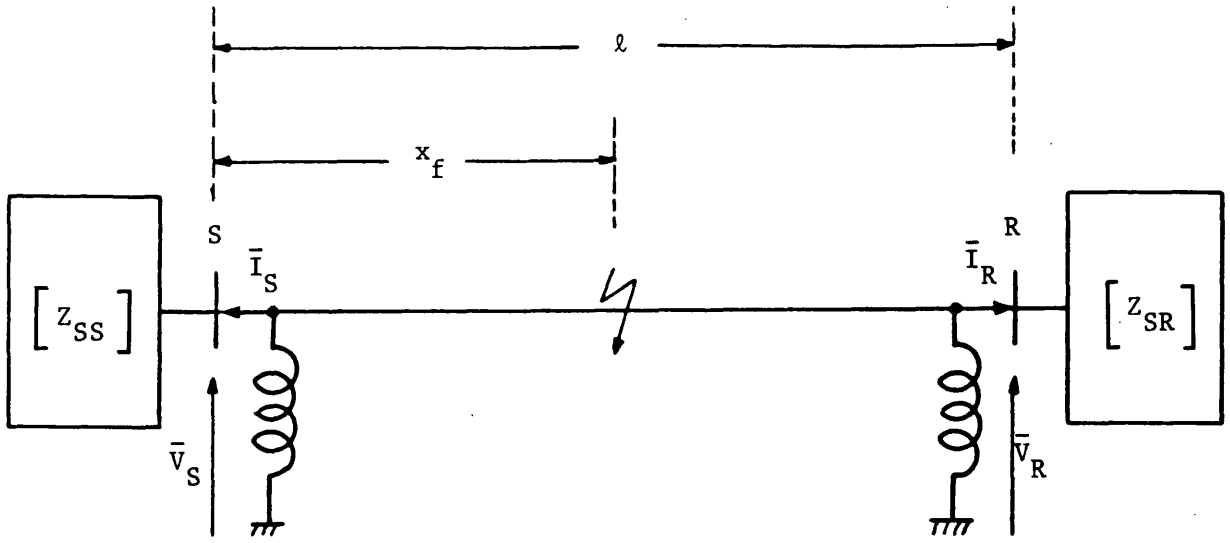

Fig. 2.11 Equivalent system models

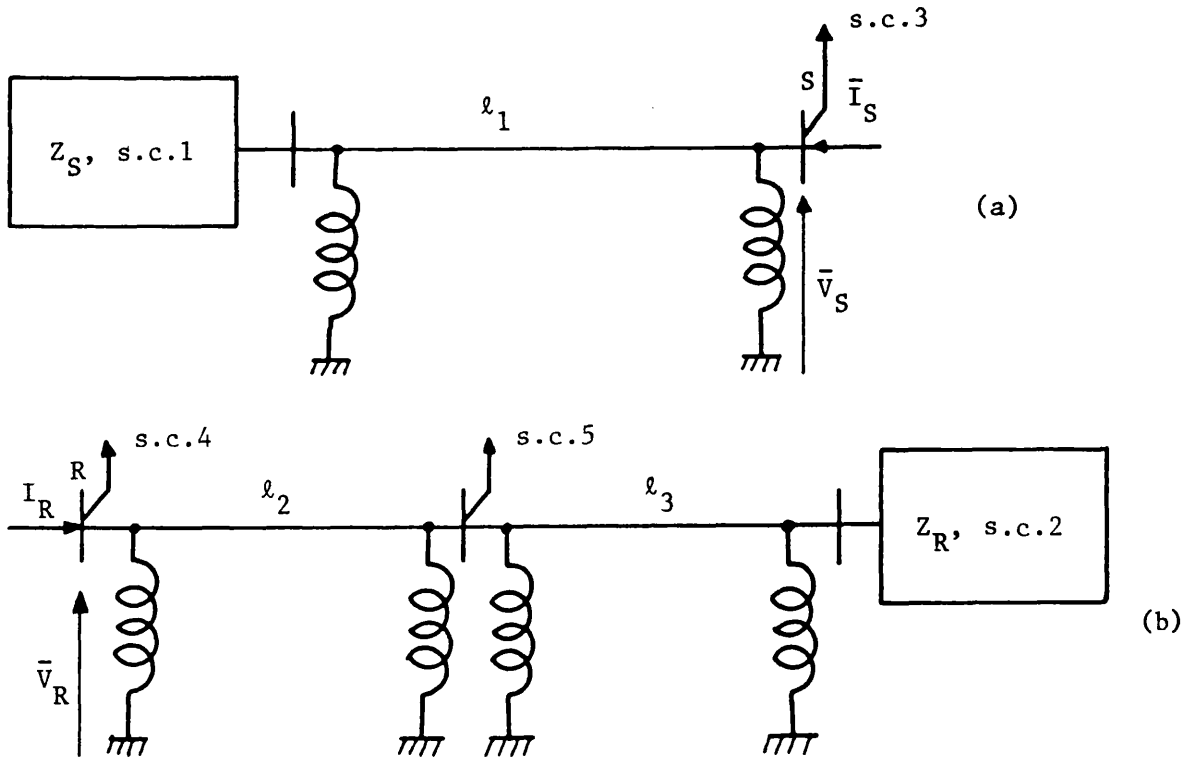

Fig. 2.12 Composite source network

(a) sending end

(b) receiving end

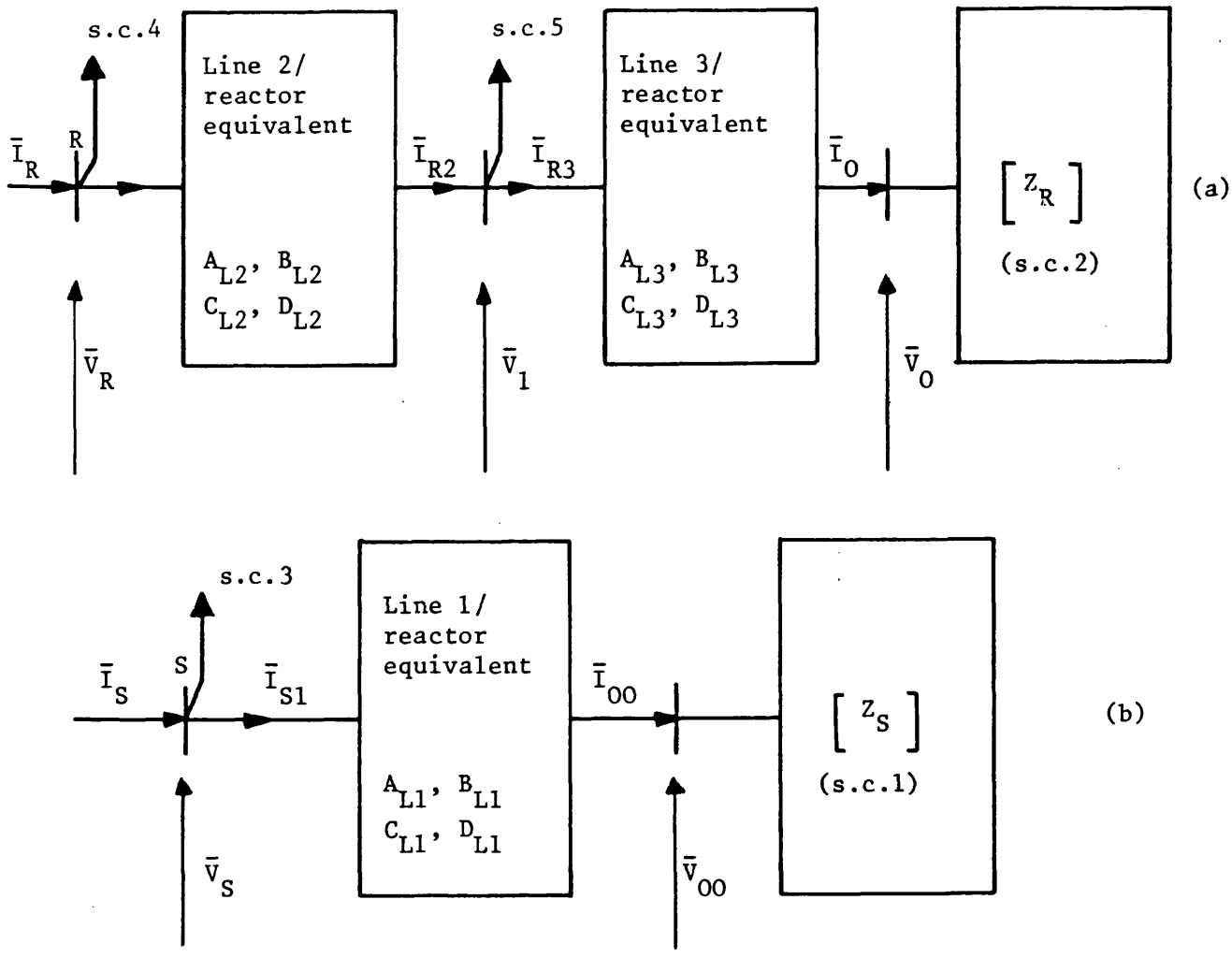

Fig. 2.13 Composite source equivalent

(a) composite receiving end source Z_{SR}
(b) composite sending end source Z_{SS}

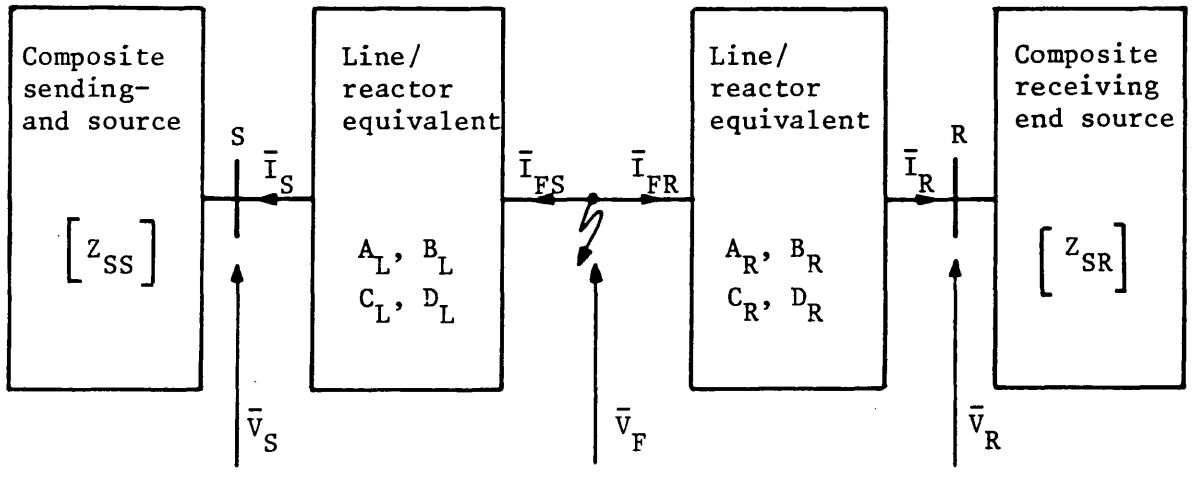

Fig. 2.14 Equivalent arrangement to fig. 2.13

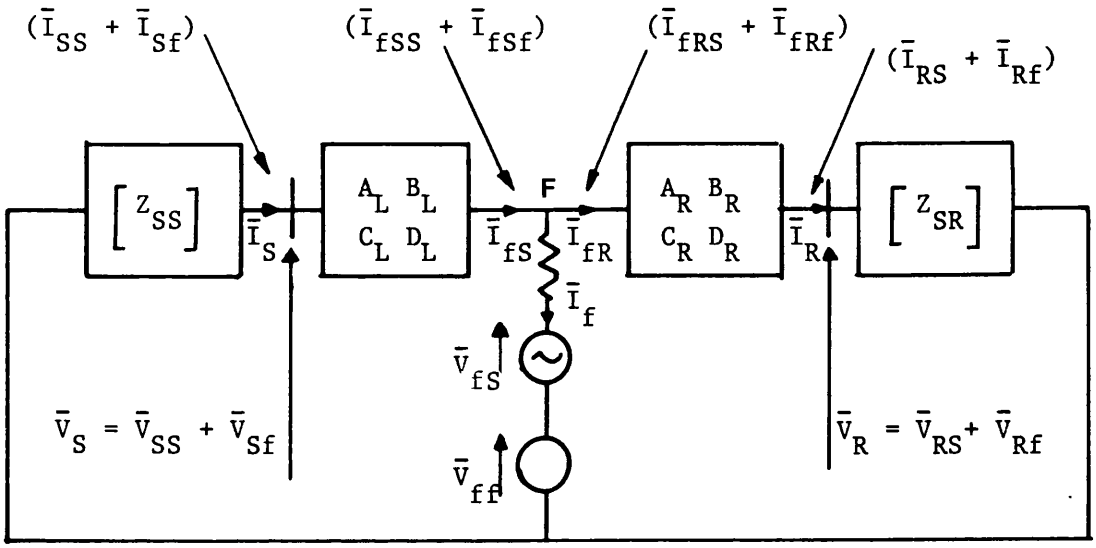

Fig. 2.15 Faulted compensated/uncompensated system

Steady state components:

$\bar{V}_{SS}$, $\bar{I}_{SS}$, $\bar{I}_{fSS}$, $\bar{I}_{fRS}$, $\bar{I}_{RS}$, $\bar{V}_{RS}$

Transient components:

$\bar{V}_{Sf}$, $\bar{I}_{Sf}$, $\bar{I}_{fSf}$, $\bar{V}_{ff}$, $\bar{I}_{fRf}$, $\bar{I}_{Rf}$, $\bar{V}_{Rf}$

CHAPTER 3

DIGITAL SIMULATION OF SINGLE-POLE OPENING

3.1 Introduction

When a fault occurs on an electric power transmission system, it is necessary to isolate the fault as quickly as possible, so as to prevent damage to the system plant, which could be caused by overheating or mechanical stress. The time taken to trip the faulted section out depends on the time to detect the fault and to decide to trip, and the time taken by the breaker to clear the fault[48]. Recent experimental installation of 1/4 cycle relay schemes by Bonneville Power Administration [48,49] has demonstrated the feasibility of ultra-high-speed relaying and 3/4 cycle breakers are expected to be installed in 1980 by BPA.

Internally developed overvoltages are caused by a switching operation; either the opening or closing of a circuit breaker. Because of their importance in the design of switchgear, the transient voltages generated by the opening of a circuit breaker have, until comparitively recently, been regarded with more interest than those due to the closing of a circuit breaker. However, at e.h.v. systems the significant overvoltages are those caused by the energisation of transmission lines, since given the necessary conditions, overvoltages of as much as four times the phase-to-ground voltage of the system are theoretically possible.

The problem of opening surges has been solved with modern circuit breakers, by opening the breaker at a zero current. The problem of closing surges has been overcome by two different methods. The first

method based upon energising the line in stages, by closing resistors. The second method provides for the closing of the circuit breaker at the precise instant when the voltage is zero at the terminals (synchronous closing)[50,51].

Sequential pole tripping and closure take place in practice, the effect that such action may have on the system transient response should be taken into account. Theoretically, the action of the breaker poles when a circuit is being energised involves a change of system conditions at the switching point. Using the matrix method of analysis for polyphase transmission system, this condition can be represented mathematically by an input matrix at the switching point. As this input matrix changes at the instant of breaker-pole operation, the problem ceases to be linear[52]. This type of problem, where the system matrix changes with time, will be referred to as a nonlinear problem. The problem of such nonlinearities has been solved using the lattice technique[53] and more recently using the modified Fourier transform method[52,34].

In this chapter, the development of frequency domain simulation techniques for the opening of the breaker is discussed. A constant linear fault path resistance (R_f) is assumed, during the fault and after the breakers opening. Breakers are simulated to open at any time after the fault inception. They could open either when the current waveform goes through zero or randomly.

3.2 Method of Simulation

As the transient phenomena associated with s.p.s. schemes is very complex, the analysis and therefore the rather difficult problem of simulation is split up into several distinct stages. By using a

frequency domain based method of simulation, the time variant non-linear fashion in which the various breakers poles and fault arc behave are overcome. Fig. 3.1 shows the fault transient model, a knowledge of the transient response due to fault inception is obtained (section 2.8) by using the theory developed by John and Aggarwal[47] in conjunction with the theory of natural modes developed by Wedepohl[54].

3.3 First Pole Opening Technique

On fault inception, the faulted phase relaying point currents (sending and receiving end) are checked for zero crossings. The opening of the pole in which the current first passes through zero, is simulated by injecting a current, equal and opposite to the relaying point current at the breaker point. This part of the simulation is essentially one of superposition and can be explained with reference to fig. 3.1 which shows the system model for an a-phase to earth fault[34,47].

If the time after fault (allowing for the breaker opening time) at which the first zero crossing of say the sending-end a-phase current occurs is T_{b1}, then the superimposed current is therefore given in the time domain by:

$$i_{S3a} = (i_{SSa} + i_{SFa})\, h(t - T_{b1})$$

where $(i_{SSa} + i_{SFa})$ = total instantaneous faulted phase current at the sending end.

The next stage of the computation involves finding the Fourier transform of the current i_{S3a}

$$\bar{I}_{S3a} = \int_{-\infty}^{\infty} i_{S3a} \exp\left[-j(\omega - j\alpha)\right] t.dt \qquad (3.1)$$

It is important to note that $i_{S3a} = 0$, $t < T_{b1}$, and the lower limit of integration in eqn. 3.1 is limited to time T_{b1}. Furthermore, it is only necessary to simulate the system response up to a finite observation time and it is therefore possible to reduce the upper limit of integration in order to increase the efficiency with which this and other similar integrals are digitally computed. So the frequency spectrum $\bar{I}_{S3a}$ of current which is injected into the opposite direction (fig. 3.2) to simulate a-phase sending pole opening is given by:

$$\bar{I}_{S3a} = \int_{T_{b1}}^{T_{ob}} i_{S3a} \exp\left[-j(\omega - j\alpha)\right] t.dt$$

where T_{ob} = observation time

α = frequency shift constant

In fig. 3.2 $\bar{E}_{S3a}$ is the frequency spectrum of a voltage source which arises due to the injection of a current $\bar{I}_{S3a}$. The transforms of the voltage components $\left[\bar{V}_{S3}\right]$ and $\left[\bar{V}_{R3}\right]$ on the line side of the breakers are obtained by noting that[34,47]:

$$\begin{aligned} \left[\bar{V}_{S3}\right] &= \left[Z_{SS}\right]\left[\bar{I}_{S3}\right] - \left[\bar{E}_{S3}\right] \\ \left[\bar{V}_{R3}\right] &= -\left[Z_{SR}\right]\left[\bar{I}_{R3}\right] + \left[\bar{E}_{R3}\right] \end{aligned} \qquad (3.2)$$

Also, the variation of the relaying point voltage and current components are related to the fault quantities by:

$$\begin{aligned} \begin{bmatrix} \bar{V}_{FF3} \\ \bar{I}_{FS3} \end{bmatrix} &= \begin{bmatrix} A_1 & B_1 \\ C_1 & D_1 \end{bmatrix} \begin{bmatrix} \bar{V}_{S3} \\ \bar{I}_{S3} \end{bmatrix} \\ \begin{bmatrix} \bar{V}_{FF3} \\ -\bar{I}_{FR3} \end{bmatrix} &= \begin{bmatrix} A_2 & B_2 \\ C_2 & D_2 \end{bmatrix} \begin{bmatrix} \bar{V}_{R3} \\ -\bar{I}_{R3} \end{bmatrix} \end{aligned} \qquad (3.3)$$

At the fault point

$$\left[\bar{V}_{FF3}\right] = \left[\bar{E}_{FF3}\right] + Z_F\left[\bar{I}_{FR3} - \bar{I}_{FS3}\right] = \left[\bar{E}_{FF3}\right] + Z_F\bar{I}_{F3} \qquad (3.4)$$

The transforms of the voltage across the neutral of the shunt reactors, at the sending and receiving ends, are:

$$\begin{aligned} \bar{V}_{Sn3} &= (\bar{V}_{S3a} + \bar{V}_{S3b} + \bar{V}_{S3c})\frac{Z_n}{Z_p + 3Z_n} \\ \bar{V}_{Rn3} &= (\bar{V}_{R3a} + \bar{V}_{R3b} + \bar{V}_{R3c})\frac{Z_n}{Z_p + 3Z_n} \end{aligned} \qquad (3.5)$$

where

A_1, B_1, C_1 and D_1 represent the line/reactor matrix constants between the fault and the sending end.

A_2, B_2, C_2 and D_2 represent the line/reactor matrix constants between the fault and the receiving end.

Z_{SS} , Z_{SR} represent simple/composite source matrix at the sending and receiving ends respectively.

The three foregoing relationships (3.2, 3.3, 3.4) effectively define a set of simultaneous equations, relating superimposed circuit transform currents to the associated transform voltages across each hypothetical current generator and they can be arranged in the alternative form of eqn. 3.6 (see Appendix 3.1).

$$\begin{bmatrix} \bar{I}_{F3} \\ \bar{I}_{S3} \\ \bar{I}_{R3} \end{bmatrix} = \begin{bmatrix} Y_1 & Y_2 & Y_3 \\ Y_4 & Y_5 & Y_6 \\ Y_7 & Y_8 & Y_9 \end{bmatrix} \begin{bmatrix} \bar{E}_{FF3} \\ \bar{E}_{S3} \\ \bar{E}_{R3} \end{bmatrix} \qquad (3.6)$$

Each of the sub-matrices in the admittance relationship of eqn. 3.6 is defined in terms of the basic parameters (R_F, A_1, Z_{SS} etc) of the system at any special frequency of interest. It is important to note

that each sub-matrix within the whole is a 3 x 3 matrix and that each sub-vector ($\bar{E}_{FF3}$, $\bar{I}_{F3}$ etc.) is a 3 x 1 column vector representing the voltage or current transforms of the individual phase conductors, e.g. $\left[\bar{I}_{S3}\right] = \left[\bar{I}_{S3a}\ \bar{I}_{S3b}\ \bar{I}_{S3c}\right]^T$. The 9 x 9 admittance matrix of eqn. 3.6 (derived in Appendix 3.1) is essentially a universal relationship which can be computed and stored at all spectral frequencies of interest. This equation can be used for fault simulation as well as breaker opening and closing.

When phase-a of the sending end is open, there are eight known zero-valued transforms associated with the sending end superimposed current. Furthermore, the ninth known value is the frequency transform of the superimposed current $\bar{I}_{S3a}$. Equation 3.6 could be written in the following form:

$$\begin{bmatrix} \bar{I}_{F3a} \\ \bar{I}_{F3b} = 0 \\ \bar{I}_{F3c} = 0 \\ \bar{I}_{S3a} \\ \bar{I}_{S3b} \\ \bar{I}_{S3c} \\ \bar{I}_{R3a} \\ \bar{I}_{R3b} \\ \bar{I}_{R3c} \end{bmatrix} = \begin{bmatrix} & & \\ Y_1 & Y_2 & Y_3 \\ & & \\ & & \\ Y_4 & Y_5 & Y_6 \\ & & \\ & & \\ Y_7 & Y_8 & Y_9 \\ & & \end{bmatrix} \begin{bmatrix} \bar{E}_{FF3a} = 0 \\ \bar{E}_{FF3b} \\ \bar{E}_{FF3c} \\ \bar{E}_{S3a} \\ \bar{E}_{S3b} = 0 \\ \bar{E}_{S3c} = 0 \\ \bar{E}_{R3a} = 0 \\ \bar{E}_{R3b} = 0 \\ \bar{E}_{R3c} = 0 \end{bmatrix} \qquad (3.7)$$

With reference to eqn. 3.7, all rows and columns that correspond to zero valued transforms in the voltage vector can be removed, to produce the reduced matrix relationship of eqn. 3.8.

$$\begin{bmatrix} 0 \\ 0 \\ \bar{I}_{S3a} \end{bmatrix} = \begin{bmatrix} Y_1(2,2) & Y_1(2,3) & Y_2(2,1) \\ Y_1(3,2) & Y_1(3,3) & Y_2(3,1) \\ Y_4(1,2) & Y_4(1,3) & Y_5(1,1) \end{bmatrix} \begin{bmatrix} \bar{E}_{FF3b} \\ \bar{E}_{FF3c} \\ \bar{E}_{S3a} \end{bmatrix} \qquad (3.8)$$

Now $\bar{I}_{S3a}$ is the ninth known transform which in turn enables the voltage vector in eqn. 3.8 to be determined. Substituting these quantities in eqn. 3.7, $\bar{I}_{F3}$, $\bar{I}_{S3}$ and $\bar{I}_{R3}$ are obtained. $\bar{V}_{S3}$, $\bar{V}_{R3}$ and $\bar{V}_{FF3}$ are obtained from equations 3.2 and 3.4 respectively.

These quantities are then transformed back into the time domain using the fast Fourier transform technique[47]. The total time domain response can be calculated by adding the three quantities: (1) steady state, (2) fault inception, and (3) sending end breaker opening.

At the sending end

$$\left.\begin{aligned} i_{St}(t) &= i_{SS}(t) + i_{SF}(t - T_f) - i_{S3}(t - T_{b1}) \\ v_{St}(t) &= v_{SS}(t) + v_{SF}(t - T_f) + v_{S3}(t - T_{b1}) \\ e_{St}(t) &= e_{S3}(t - T_{b1}) \\ v_{Snt}(t) &= v_{Snf}(t - T_f) + v_{Sn3}(t - T_{b1}) \end{aligned}\right\} \qquad (3.9)$$

Similar equations can be written at the receiving end, however $e_{Rt}(t)$ is still zero.

At the fault point

$$\left.\begin{aligned} v_{Ft}(t) &= v_{FS}(t) + v_{FF}(t - T_f) + v_{FF3}(t - T_{b1}) \\ i_{Ft}(t) &= i_F\ (t - T_f) + i_{F3}(t - T_{b1}) \end{aligned}\right\} \qquad (3.10)$$

where

$t = 0 \rightarrow T_{ob}$

T_f = time at which fault occurs

T_{b1} = time at which sending-end a-phase pole opens

3.4 Second Pole Opening Technique

The receiving-end a-phase current are next checked for zero crossing, say T_{b2} after fault, then the frequency spectrum $\bar{I}_{R4a}$ of current injected into opposite direction is given by:

$$\bar{I}_{R4a} = \int_{T_{b2}}^{T_{ob}} (i_{RSa} + i_{RFa} - i_{R3a}) \exp\left[-j(\omega - j\alpha)\right] t \, dt \qquad (3.11)$$

To determine the total response of the various quantities in the time domain, consider fig. 3.3, by following the same procedure as outlined previously the following eqn. can be written:

$$\begin{bmatrix} \bar{I}_{F4} \\ \bar{I}_{S4} \\ \bar{I}_{R4} \end{bmatrix} = \begin{bmatrix} Y_1 & Y_2 & Y_3 \\ Y_4 & Y_5 & Y_6 \\ Y_7 & Y_8 & Y_9 \end{bmatrix} \begin{bmatrix} \bar{E}_{FF4} \\ \bar{E}_{S4} \\ \bar{E}_{R4} \end{bmatrix} \qquad (3.12)$$

Assuming that the a-phase breaker pole at the sending end has previously opened, the zero-valued transforms are therefore $\bar{E}_{F4a}$, $\bar{E}_{S4b,c}$, $\bar{E}_{R4b,c}$, $\bar{I}_{S4a}$ and $\bar{I}_{F4b,c}$. Eqn. 3.12 can be written in the following form:

$$\begin{bmatrix} \bar{I}_{F4a} \\ 0 \\ 0 \\ 0 \\ \bar{I}_{S4b} \\ \bar{I}_{S4c} \\ \bar{I}_{R4a} \\ \bar{I}_{R4b} \\ \bar{I}_{R4c} \end{bmatrix} = \begin{bmatrix} & & \\ Y_1 & Y_2 & Y_3 \\ & & \\ Y_4 & Y_5 & Y_6 \\ & & \\ Y_7 & Y_8 & Y_9 \\ & & \end{bmatrix} \begin{bmatrix} 0 \\ \bar{E}_{FF4b} \\ \bar{E}_{FF4c} \\ \bar{E}_{S4a} \\ 0 \\ 0 \\ \bar{E}_{R4a} \\ 0 \\ 0 \end{bmatrix} \qquad (3.13)$$

The known quantities in eqn. 3.13 are Y_1-Y_9 and $\bar{I}_{R4a}$, so eqn. 3.13 can be reduced to:

$$\begin{bmatrix} 0 \\ 0 \\ 0 \\ \bar{I}_{R4a} \end{bmatrix} = \begin{bmatrix} Y_1(2,2) & Y_1(2,3) & Y_2(2,1) & Y_3(2,1) \\ Y_1(3,2) & Y_1(3,3) & Y_2(3,1) & Y_3(3,1) \\ Y_4(1,2) & Y_4(1,3) & Y_5(1,1) & Y_6(1,1) \\ Y_7(1,2) & Y_7(1,3) & Y_8(1,1) & Y_9(1,1) \end{bmatrix} \begin{bmatrix} \bar{E}_{FF4b} \\ \bar{E}_{FF4c} \\ \bar{E}_{S4a} \\ \bar{E}_{R4a} \end{bmatrix} \qquad (3.14)$$

From eqn. 3.14 $\bar{E}_{FF4b}$, $\bar{E}_{FF4c}$, $\bar{E}_{S4a}$ and $\bar{E}_{R4a}$ are obtained, substituting these quantities in eqn. 3.13 $\bar{I}_{F4}$, $\bar{I}_{S4}$ and $\bar{I}_{R4}$ are obtained. Then finally $\bar{V}_{S4}$, $\bar{V}_{R4}$, $\bar{V}_{FF4}$ and the voltage across the neutral reactor can be calculated.

These quantities are then transferred back into the time domain using the fast Fourier transform technique. The total time domain response can be calculated by adding the four quantities: (1) steady state, (2) fault inception, (3) sending end breaker opening, and (4) receiving end breaker opening. The total time domain response of say the receiving end (line side) current at this stage would then be:

$$\begin{aligned} i_{RT}(t) &= i_{RS}(t) + i_{RF}(t - T_f) - i_{R3}(t - T_{b1}) - i_{R4}(t - T_{b2}) \\ &= i_{Rt}(t) - i_{R4}(t - T_{b2}) \end{aligned}$$

The total fault current is given by:

$$\begin{aligned} i_{FT}(t) &= i_F\,(t - T_f) + i_{F3}(t - T_{b1}) + i_{F4}(t - T_{b2}) \\ &= i_{Ft}(t) + i_{F4}(t - T_{b2}) \end{aligned}$$

For $t > T_{b2}$, $i_{FT}(t)$ represent the secondary arc current assuming a constant fault path resistance R_F.

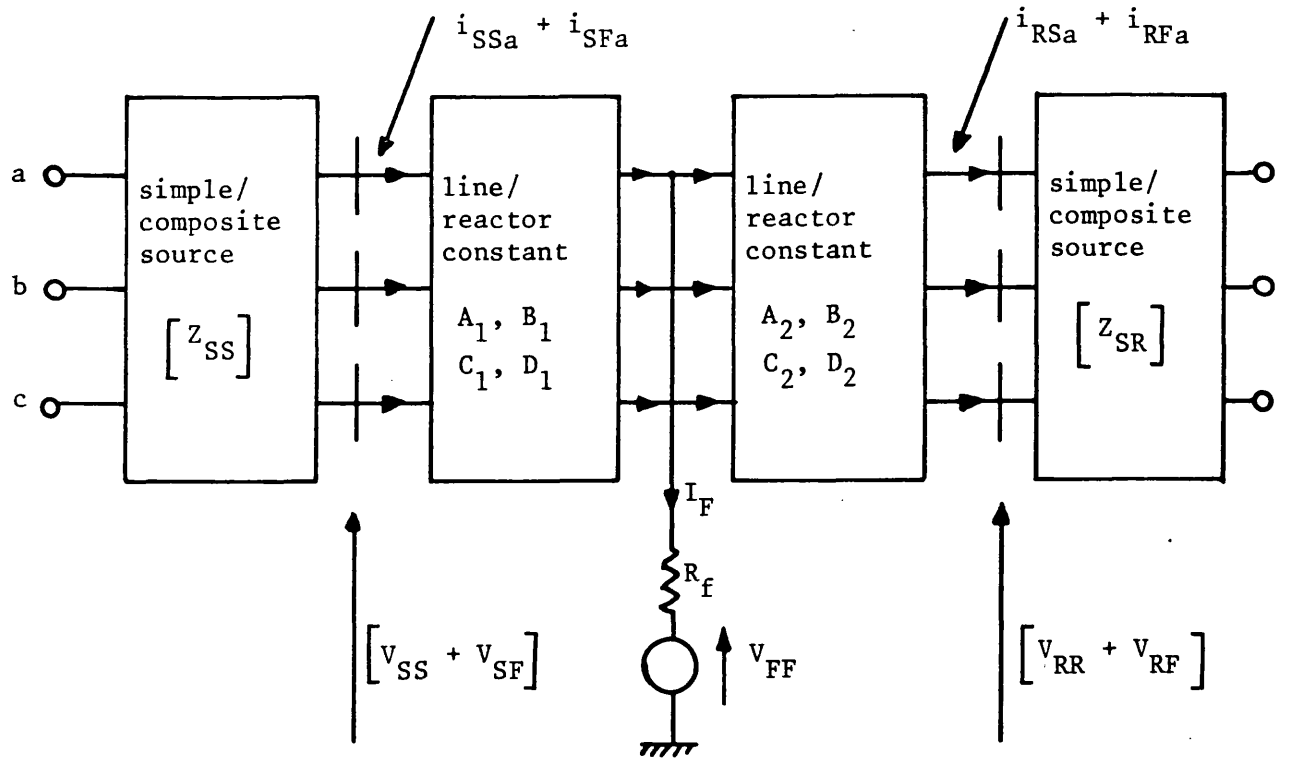

Fig. 3.1 Fault simulation models

i_{SSa}, i_{RSa}: steady-state current component

i_{SFa}, i_{RFa}: transient voltage vector component due to fault

V_{SS}, V_{RR}: steady-state voltage vector

V_{SF}, V_{RF}: transient voltage vector component due to fault

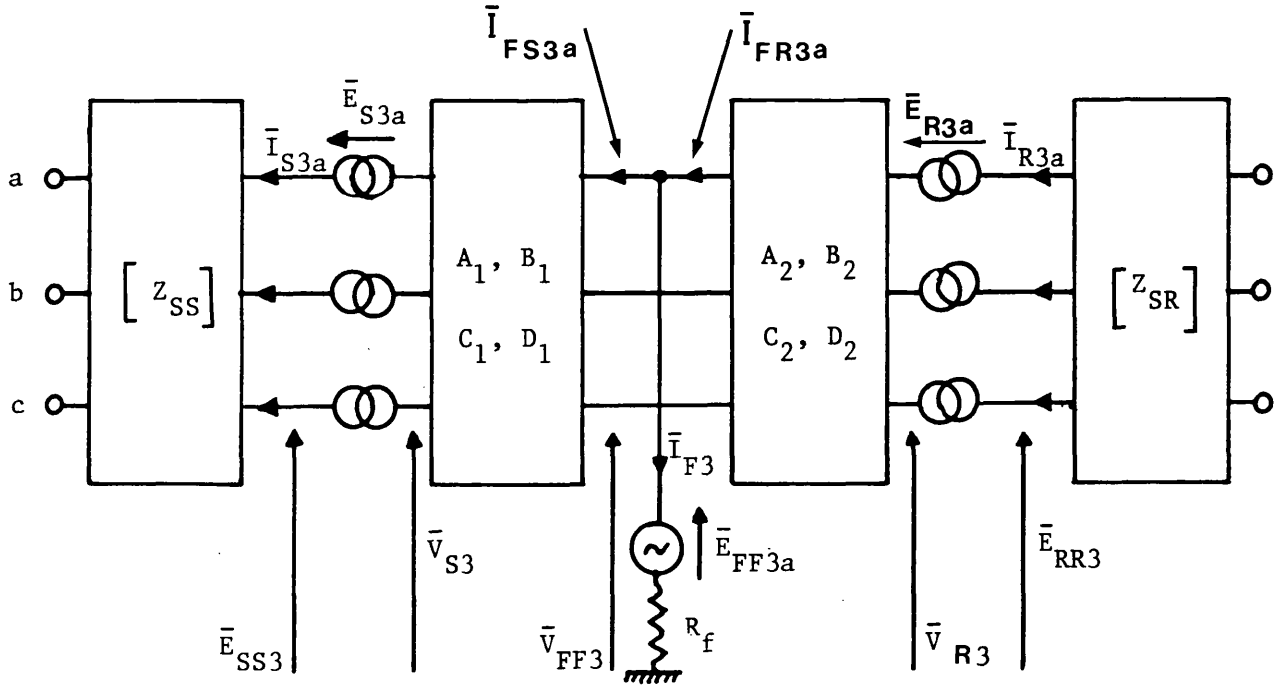

Fig. 3.2 Sending end 'a'-phase pole opening simulation

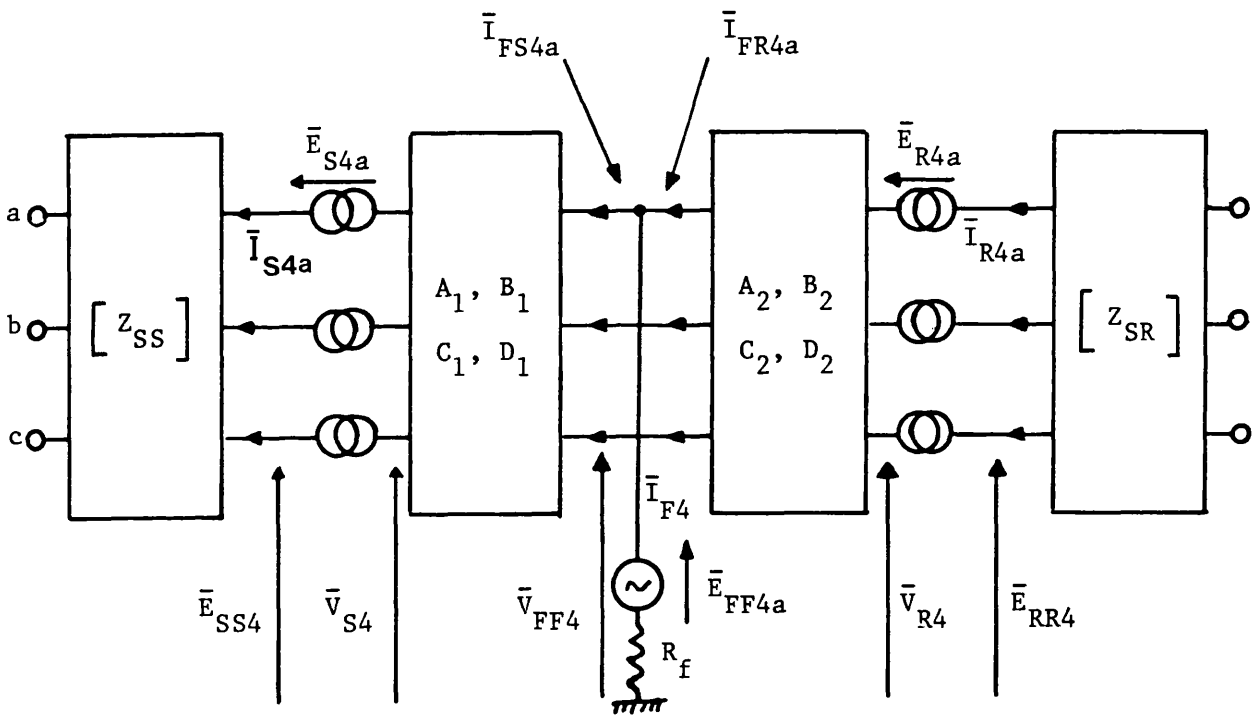

Fig. 3.3 Receiving end 'a'-phase pole opening simulation

CHAPTER 4

THE ELECTRIC ARC

4.1 Introduction

For the transient calculations undertaken in the previous chapter, the primary and secondary arc path was represented by a low constant resistance (R_F = 0.5 Ω). Faults in e.h.v. transmission lines are, however, mainly due to flashovers between conductor(s) and tower, or between phase conductors.

Recently, a paper[40] shows that the primary arc path can be simulated to a good degree of accuracy by a constant linear resistance. However, simulating the secondary arc path by a constant resistance is completely unacceptable, due to the bahaviour of the arc during the dead time. Its behaviour will be investigated in this chapter and a model of a long secondary arc in free air will be proposed.

4.2 Definition of the Electric Arc

The arc has a very complex structure and various definitions have been given to it. Edels[55] defined a fully developed arc as a steady state discharge having a positive column in thermal equilibrium and a cathode fall of small voltage and high current density. Compton[56] has defined the arc as a discharge of electricity, between electrodes in a gas or vapour, which has a voltage drop at the cathode of the order of the minimum ionizing or minimum exciting potential of the gas or vapour. However, the arc is a discharge characterised by a larger current and a lower voltage than any other type of gas discharge. The

total voltage across the arc is the sum of (1) the cathode drop, which has a value characteristic of the gas; (2) the anode drop, which depends on the size and shape of the anode as well as the nature of the gas and its degree of ionization; (3) the drop along the positive column, which is generally proportional to the length of the positive column and depends on the current, nature and density of the gas; (4) a voltage drop, generally negative but usually small, between the region of the cathode fall and the beginning of the positive column. The volt-ampere (VA) characteristic of an arc is generally negative, i.e. the voltage across the arc falls as the current is increased.

4.3 Static Arc Characteristic

Perhaps the most familiar electrical property of an arc under steady conditions is given by its so called volt-ampere characteristic, illustrated by the curve in fig. 4.1. A number of equations for this characteristic have been derived from experimental studies. The first and best known such equation is that due to Ayrton,

$$V_a = a + b.\ell_a + \frac{c + d\ell_a}{i} \qquad (4.1)$$

expressing the arc voltage, V_a, in terms of the arc length, ℓ_a, the current, i, and the constants a, b, c and d. The term a is the sum of the cathode and anode drops. The term $b.\ell_a$ is the voltage drop in the positive column, whose length is taken to equal the total arc length ℓ_a. The terms involving current i in the denominator take care of the negative characteristic feature of the arc. If in eqn. 4.1 the current is sufficiently large, the term containing the current becomes relatively small, and the arc voltage becomes a function only of the arc length according to the equation,

$$V_a = a + b.\ell_a \qquad (4.2)$$

For a long arc the term a may also be neglected, giving an arc voltage proportional to the length of the arc,

$$V_a = b.\ell_a \qquad (4.3)$$

Several authors have investigated the voltage gradient of a free-burning arc over different ranges of current. King[57] investigated the voltage gradient of the free burning arc in air, in the current range between 10^{-4} - 10^{4} amp. The author shows that at currents from 0.1 to 100 A the voltage gradient has the normal negative arc characteristic, while at currents above 100 A the voltage gradient of an arc remote from electrodes remains almost constant at 10 V/cm at least up to currents of 10,000 A (fig. 4.2).

Storm[58] has investigated the VA-characteristics for arcs of length 30-122 cm set up between brass electrodes, in the range of 100-20,000 A. Maikopar[59] has extended Storm's work, by the investigation of the voltage gradient of an open a.c. arc, 10-30 cm long for currents of 1-100 A. On the basis of these experiments, and also considering the results obtained by Storm, Maikopar plotted the static VA-characteristics of the open arc (fig. 4.3) for currents from 1-20,000 A. In the range of small values of the current (1-55 A) at which extinction of the secondary arc may be expected, the author has recommended to use the following empirical formula.

$$V_p = C.I_p^{-n} \qquad (4.4)$$

where $C = 75$, $n = 0.4$

V_p is the voltage gradient in V/cm

I_p is the arc current in A (peak)

The voltage gradient calculated from this equation is in agreement with the results shown by King[57].

Eaton et al[60] have done experimental studies on an arc set up between electrodes, for currents up to 800 A (peak). The authors' results indicated that the voltage gradient, for currents greater than 100 A (peak), is approximately 10 V/cm. However, for currents below this value the dispersion of the experimental points obtained is considerable.

4.4 Dynamic Arc Characteristics

At relatively low frequencies, say 50 Hz, the dynamic characteristic may follow the static characteristic closely except in the immediate vicinity of current zero, where the voltage reversal occurs.

Storm[58] has investigated the dynamic arc characteristic of a long arc in air at atmospheric pressure. At 100 A (r.m.s.), fig. 4.4, taken from the author's paper, shows a cyclogram for a 122 cm long vertical 60 cycle arc in air. The time records of current and voltage gradient are shown in the inset. It is clear that the arc characteristics are no longer unique but consist of two different branches, one for increasing and another one for decreasing current. This difference, termed arc hysteresis, is due to the heat capacity of the electrodes and arc gas, which are not able to follow the instantaneous conditions with rapid variation of the state. Fig. 4.5 shows the dynamic characteristics followed in two particular half-cycles by a similar arc 30.5 cm long carrying 15,000 A[58]. At this high current level the upward trend of the arc voltage with current in the 5,000-20,000 A range is clearly evident. It is clear that the arc characteristic does not always repeat itself for every successive cycle as may be seen in fig. 4.5.

Brown[61] has investigated the dynamic arc characteristic at low current. Fig. 4.6, taken from the author's paper, shows a rather different cyclogram for a 3.81 cm long 60-cycle in air between copper electrodes. The reversal of the loops near 1 A in this figure is thought to be due to phase errors in the measuring devices. Brown also shows a cathode-ray VA cyclogram (fig. 4.7) of the extinction after slightly more than one second of a 60 cycle magnetizing current (1.5 A r.m.s.) drawn vertically to 122 cm length in a 40 kv circuit.

Therefore it could be concluded that, for a long secondary arc in free air, the voltage gradient remains nearly constant (during part of the cycle) at an average value of $75\ I_p^{-0.4}$ V/cm. If the secondary arc current is greater than 55 A (peak) then the voltage gradient could be taken as 15 V/cm. It is also concluded that the re-ignition voltage increases as the arc goes towards extinction[61].

4.5 Arc Extinction Mechanisms

Arc extinction may result from two causes: (1) following a current zero, the recovery voltage across the arc terminals fails to reach a value equal to the dielectric strength of the arc path; (2) the arc length is increased by the wind (or otherwise) at such a rate that the voltage required to maintain the positive column of the arc is greater than that which can be supplied by the circuit[62]. The factors determining whether an a.c. arc will be extinguished at a current zero have been described by Slepian[63] as, first, the rate of recovery of the voltage across the arc and, second, the ability of the arcing medium to recover dielectric strength. If the rate of recovery of the voltage across the arc exceeds the rate at which the arcing medium recovers dielectric strength, the arc will persist.

Eaton et al[60] shows that the arc extinction in capacitive circuits is more severe than in an inductive or resistive circuit. This may be explained by the fact that after arc extinction (at zero) the voltage across the electrodes (recovery voltage) tends to rise to a value equal to the sum of the generated voltage and the voltage trapped on the equivalent capacitor in the circuit. The greater persistence of the arc in the capacitive circuit seems to indicate that not only is the rate of the recovery of arc voltage important but also the maximum value to which this voltage rises.

Eaton[62] analysed the dielectric strength of the arc following a current zero. The author shows that, following a current zero, and before the air becomes deionized, a minimum voltage of 250 V is required to establish the arc again. Slepian[63] has shown similar results. If the arc current stays at zero for some time, the arc space will cool down, and the voltage required to re-establish the arc will increase. A cathode-ray VA cyclogram of 122 cm arc in air[61], indicated that the re-ignition voltage increases with time until final extinction is reached.

4.6 Dielectric Recovery Characteristics of Long Air Gaps

In order for secondary arc extinction, dielectric recovery of the ionized fault-arc path must have proceeded to the point where application of the system recovery voltage will not produce sufficient current through the arc path to maintain ionization. The rate at which the insulator recovers its dielectric strength is believed to depend on:

1. The type of insulator string and the arcing horn[64,65].
2. The magnitude and duration of the short circuit current[66,67].

3. The wind speed, magnitude and duration of the secondary arc[68].

The dielectric strength recovery characteristics for different types of insulators in 500 kV transmission lines, after three phase interruption has been studied by Terase et al[64,69]. The authors concluded that the recovery speed is the highest in suspension strings. Another test indicated that suspension insulator strings with an intermediate horn exhibits the fastest dielectric recovery speed[65]. A laboratory study on 230 kV suspension insulator shows that the necessary deionization time increases linearly with the magnitude of the short circuit current[66].

The arc hysteresis cyclogram of fig.4.4 is only repeatedly obtained if the voltage across the arc is such that the time for which the arc current remains at zero following voltage reversal is sufficiently small to ensure that the arc is re-established without an appreciable re-striking voltage, i.e. negligible arc deionization occurs during zero current time. Where this is not the case, a significant re-ignition voltage has to be developed before the arc characteristic of fig. 4.4 is attained. In effect, fig. 4.4 is applicable only where the re-ignition voltage per centimetre length of the arc is very small. Relatively few experiments have been performed that enable the re-ignition voltage of long unconstrained arcs to be even loosely defined. However, of the available information, the work by Fukunishi et al[70] is probably the most useful in that it specifically relates to the extinction of long secondary arcs preceded by a high current primary arc. Fig. 4.8a shows some useful results relating to the re-ignition characteristics of a 500 kV suspension insulator string protected by 4.05 m arcing horn gaps. It is evident that the rate at which the re-ignition voltage increases is a function of the

time for which the arc exists. This feature is somewhat as expected because the levels of ionization within the main arc column gradually diminish after the transition from the high primary current to relatively low current secondary arc. Extinction at a time near the arc transition thus requires a lower re-ignition voltage for restriking to occur than does extinction at a later instant. Furthermore, the actual rate of increase of re-ignition voltage is seen to be lowest immediately at current interruption and a pessimistic model, in terms of arc re-ignition voltage, is obtained by assuming the linear approximations to the recovery characteristics as indicated in fig. 4.8b.

In the absence of more extensive experimental data, this latter approach will be followed here, and it follows that if the time from arc transition to any secondary arc extinction (either intermediate or final) is defined as T_e, the re-ignition voltage assumed varies with time as defined in eqn. 4.5.

$$|v_r(t)| = k(T_e)(t - T_e)h(t - T_e) \qquad (4.5)$$

The function $k(T_e)$ is the rate of increase of the re-ignition voltage, and when the effect of the arc length increase recorded during the tests performed to acquire the characteristics of fig. 4.8a is included[30], its value corresponds to approximately 5 V/ms and 15 V/ms per centimetre of arc length for T_e = 0 and 200 ms respectively. No further experimental results to enable the rate of increase of re-ignition voltage $k(T_e)$ to be estimated for other values of T_e have been located in the literature. In the absence of such information the author proposes a rather pessimistic linear change between and beyond the two known values as indicated in fig. 4.8c. The actual re-ignition voltage characteristic here used is therefore defined generally by eqn. 4.6.

$$|v_r(t)| = (5 + 50\ T_e)(t - T_e)h(t - T_e) \quad kV/cm \qquad (4.6)$$

It is important to note that both the initial value of $k(T_e)$ (5 V/cm) and the rate at which $k(T_e)$ is assumed to change are rather lower than is likely to be the case in many applications because the secondary arc is often preceded by a primary arc of lower duration and/or magnitude than that associated with deriving the assumed variation shown in fig. 4.8c. For example investigation into a 10 cycle, 40 A secondary arc that was not preceded by a primary arc[70] indicated a value of $k(T_e)$ of approximately 50 V/ms per cm of arc length for T_e = 200 ms. Fig. 4.8d shows graphically how the re-ignition voltage defined generally in eqn. 4.6 would vary subsequent to arc voltage polarity reversals at several values of T_e. It is worth noting that in terms of predicting minimum dead times for single-pole autoreclosure, the re-ignition characteristics here used are pessimistic from several points of view.

A paper, very recently published[71] demonstrated the rate of rise of the withstand voltage across the arc path after secondary arc interruption for a simulated 765 kV air gap with 4.2 m clearance. The author indicated that the withstand voltage reached 425 kV in 45 ms and its dependency on time can be used in conjunction with the rate of rise of recovery voltage for analyzing the application of various s.p.s. compensation schems.

4.7 Arc Length Variation

The techniques developed in this work enable any desired arc length variations to be simulated. However, the range of possible arc variations is extremely large[30, 60, 59, 72,3]. For example, under heavy current primary arc and high wind speed conditions the rate of

length increase is very high whereas, at the other extreme of a low current primary arc in still air, only an insignificant increase in secondary arc length may occur[5]. For the purpose of most studies it is useful to define a reasonably realistic variation between these extremes and this is the approach adopted here. In this respect, the work by Anjo et al[30] on observing the behaviour of arcs by using high speed photographic techniques is useful, and fig. 4.9 shows two typical apparent arc length variations obtained by using a single camera. Unfortunately, the secondary arc also bends in the direction of the camera axis, a factor which undoubtedly partially accounts for the different apparent arc lengths obtained in the two sets of results illustrated. Indeed, it has been concluded by the authors of reference 30 that the actual arc lengths are much longer than the apparent values reproduced in fig. 4.9 (2.24 times the arcing gap just before extinction) and it may reach up to 4 times the initial arc length[72,59]. The camera recordings do not reveal any significant arc length increase during the primary arc period and the length of the arc at the time of arc transition is therefore approximately equal to the length between the arcing horn (ℓ_o). With the foregoing consideration in mind, the linearised arc length/time variation indicated also in fig. 4.9 is used throughout the present work. This characteristic is described mathematically by eqn. 4.7 and provides for no secondary arc length increase for the first 100 ms after arc transition and approximately 1% increase in initial arc length (ℓ_o) per ms thereafter

$$\ell_a(t)/\ell_o = \begin{cases} 1, & t < 0.1 \text{ s} \\ 10t, & t > 0.1 \text{ s} \end{cases} \qquad (4.7)$$

4.8 Self-Extinction Time of Secondary Arc

It is a well known fact that the self-extinction time tends to increase as the secondary arc current increases[8,9,27,30,31,72,73]. However, the exact nature of this phenomena is not easily predictable.

The secondary arc stretches along the path having high ion density, hence, the secondary arc path winds considerably. Once the arc path is bent, electromagnetic forces act on the arc, and the arc path is stretched longer and longer until the final extinction[30]. The higher the secondary arc current, the higher the electromagnetic force generated, thus the arc length can be stretched more easily with high secondary arc currents than when the secondary arc current is small. When the arc path is long enough, the ignition point on the electrode moves, resulting in shortening of the arc path or short-circuiting of the secondary arc. In such a case, the arc power is reduced and the secondary arc begins to lengthen again. This causes the self extinction time to become long. Depending upon whether the secondary arc is short circuited or not and the number of short-circuits, the self extinction time varies greatly[30,73].

On the other hand, the dielectric recovery voltage ($v_r(t)$) of the arc gap decreases with increasing current[70,68]. No further experimental results to enable the rate of increase of the dielectric recovery voltage ($k(T_e)$) to be estimated for different values of secondary arc current have been located in the literature. It is shown in section 4.6 that the rate of increase of the re-ignition voltage depends also on the instantaneous arc length. Thus the effect of the increase in the secondary arc current can be simulated by a lower rate of increase of the arc length which leads to a lower rate of increase of re-ignition voltage.

In the absence of any information, required to simulate the effect of the increase in the magnitude of the secondary arc current on the rate of increase of the arc length and reignition voltage, the author proposes a rather pessimistic linear relationship between the rate of increase of re-ignition voltage and the magnitude of the secondary arc current, keeping the rate of increase of the arc length independent of the secondary arc. The actual re-ignition voltage characteristic is therefore defined generally by the following equation:

$$|v_r(t)| = (DV_o + DV_1 T_e)(t - T_e)10^3 \quad V/cm \qquad (4.8)$$

where

DV_o, DV_1 correspond to 5 and 50 in eqn. 4.6 and are inversely proportional to the magnitude of the secondary arc current (i_{sec}).

$$DV_o = 5 \frac{20}{i_{sec}}$$

$$DV_1 = 35 \frac{20}{i_{sec}}$$

where i_{sec} is in A (r.m.s.). It must be pointed out that the factor DV_1 is taken as 35, at 20 A, rather than 50 because the characteristics used in eqn. 4.6 are concerned with a 30 A secondary arc[70].

Under these assumptions, for the same recovery voltage, the secondary arc extinction time is almost linearly proportional to the magnitude of the secondary arc current. This conforms well with experimentally obtained results relating to the extinction times for different secondary arc currents[10,31].

4.9 Secondary Arc Path Representation and the Mechanism of its Extinction

Based on the information in sections 4.2-4.6, the work by Storm[58] is particularly relevant to the secondary arc situation because long arcs up to 122 cm have been studied and the laboratory tests were arranged to eliminate, as far as was practicable, any changes in the arc length. The results would therefore seem to safely represent the arc VA characteristic per unit length. Fig. 4.10 shows the result of Storm's investigation into an arc with a peak current of approximately 144 A. From a computational point of view it is difficult to simulate exactly such a characteristic as in any event the work by Storm and others[61] suggests that there is likely to be some, albeit for many practical purpose small, variation in the VA cyclogram from one half cycle to another. With the foregoing consideration in mind, the piecewise linear approximation indicated in fig. 4.10 is proposed.

The rather lower levels of current commonplace in secondary arcs make it necessary to scale the cyclograms along the current and voltage axes in accordance with the peak value of the arc current expected. Based upon values defining the points of discontinuity in the piecewise linear cyclogram of fig. 4.10 (I_ℓ, I_h, I_p), the scaled version shown in fig. 4.11 is used. The value of I_p is taken as the peak value of the steady state secondary arc current, in amps, assuming a constant fault path resistance (0.5 Ω) during the secondary arc period. The assumption of small resistance made for this purpose is justified on the grounds that the impedance coupling the sound and faulty phases is in practice very high. For example, a typical 100 km 500 kV uncompensated line possesses a coupling impedance which appears in series with the secondary arc of some 12 kΩ. Even higher values are obtained when the line is compensated and, in consequence, simple steady-

state estimates of I_p vary little whatever value of secondary arc resistance is assumed[3].

In fig. 4.11, V_p represents the arc voltage gradient when the arc is burning in air, and is represented by[59]:

$$V_p = 75\ I_p^{-0.4} \quad V/cm$$

If I_p exceeds 55 A then V_p is taken as constant and is equal to 15 V/cm. The constant voltage (V_p) region of figure 4.11 is extended indefinitely to cater for transient current effects which may momentarily give rise to currents in excess of the value I_p associated with a particular study.

Fig. 4.12 shows how the effect of a finite re-ignition voltage ($v_r(t)$) is incorporated into the piecewise linear arc VA characteristic. Following arc voltage reversal, the arc current is held at zero for as long as the arc voltage magnitude remains below the value given by eqn. 4.8. In practice there is a current required to establish the pre-breakdown glow discharge, but this is so low in relation to the post break-down current that for practical purposes it can, as here, be safely disregarded. When the re-ignition voltage is exceeded, the arc voltage is assumed to attain the remainder of the VA cyclogram in the manner indicated in fig. 4.12. In this respect, the work of Brown[61] provides the only information that has been located in the literature which helps in defining the manner in which the arc voltage and current attain the voltage V_p after the re-ignition voltage has been exceeded. Although the work detailed in reference 61 does not enable this factor to be precisely defined, it does nevertheless broadly confirm the approach here used. It is important to note that the negative slope resistance path that is traversed for re-ignition voltage in excess of V_p (fig. 4.12) causes the post break-down current to increase very rapidly. In consequence the constant arc voltage condition (V_p) is

equally quickly attained under such conditions. This feature of the VA cyclogram here used conforms to experimentally obtained results relating to the high speed with which arc voltage gradients attain the constant voltage following first break-down[74,75].

4.10 Digital Simulation of the Arc

The method will be explained by reference to any positive half-cycle of the arc, exactly similar equivalent techniques being applied when the arc voltage and current traverse each negative halfcycle. With reference to fig. 4.12, the simulation process begins by checking the arc voltage against the total re-ignition voltage $v_r(t)\ell_a(t)$. The arc current is thus held at zero until the arc voltage exceeds the latter value, as defined mathematically in eqn. 4.9.

$$i_{arc}(t) = 0, \quad v_{arc}(t) < v_r(t)\ell_a(t) \tag{4.9}$$

If and when the arc voltage reaches the value $v_r(t)\ell_a(t)$, the required relationship of eqn. 4.10 is applied until the arc voltage $V_p\ell_a(t)$ is reached.

$$v_{arc}(t) = \left[(V_p - v_r(t))i_{arc}(t)/0.15\ I_p + v_r(t)\right]\ell_a(t), \quad v_{arc}(t) < V_p\ell_a(t) \tag{4.10}$$

For any current in excess of the value $0.15\ I_p$, the arc voltage per unit length takes the constant value V_p and the arc voltage is thus given by eqn. 4.11.

$$v_{arc}(t) = V_p\ell_a(t), \quad i_{arc}(t) > 0.15\ I_p \tag{4.11}$$

During most of the secondary arc period, the arc current increases to a value in excess of $0.38\ I_p$. The subsequent reduction in arc current causes current to again reach the latter value after which the arc voltage and current are constrained to reach the condition for extinction

according to eqn. 4.12.

$$v_{arc}(t) = \left[V_p i_{arc}(t)/0.38\ I_p\right] \ell_a(t), \quad i_{arc}(t) < 0.38\ I_p \qquad (4.12)$$

It is important to note that near the end of the secondary arc period, i.e. near final extinction, the current can start to reduce before reaching the value $0.38\ I_p$. In this case, the arc voltage and current are alternatively constrained to reach extinction along the line used also for increasing current where $v_r(t) = 0$. This path (A - O) is indicated in fig. 4.12 and is defined in eqn. 4.13.

$$v_{arc}(t) = \left[V_p\ i_{arc}(t)/0.15\ I_p\right] \ell_a(t), \quad 0 < i_{arc}(t) < 0.15\ I_p \qquad (4.13)$$

The above detailed processes are repeated again after each extinction. In effect, the piecewise linear arc characteristic of fig. 4.12 is thereby cyclically traversed for both positive and negative halfcycles until final extinction occurs when $|v_{arc}(t)|$ remains permanently below the arc re-ignition voltage $|v_r(t)|\ \ell_a(t)$. In eqns. 4.9 to 4.13, both $\ell_a(t)$ and $v_r(t)$ are known functions of time given by eqns. 4.9 to 4.11 and their negative half cycle equivalents can be written in the general form $v_{arc}(t) = f(i_{arc}(t), t)$. However, since it is necessary to compute both system and arc path responses digitally, the discrete form of eqn. 4.14 is used to relate the arc voltage and current at any instant of time $n\Delta T$ after arc transition

$$v_{arc}(n) = f(i_{arc}(n), n) \qquad (4.14)$$

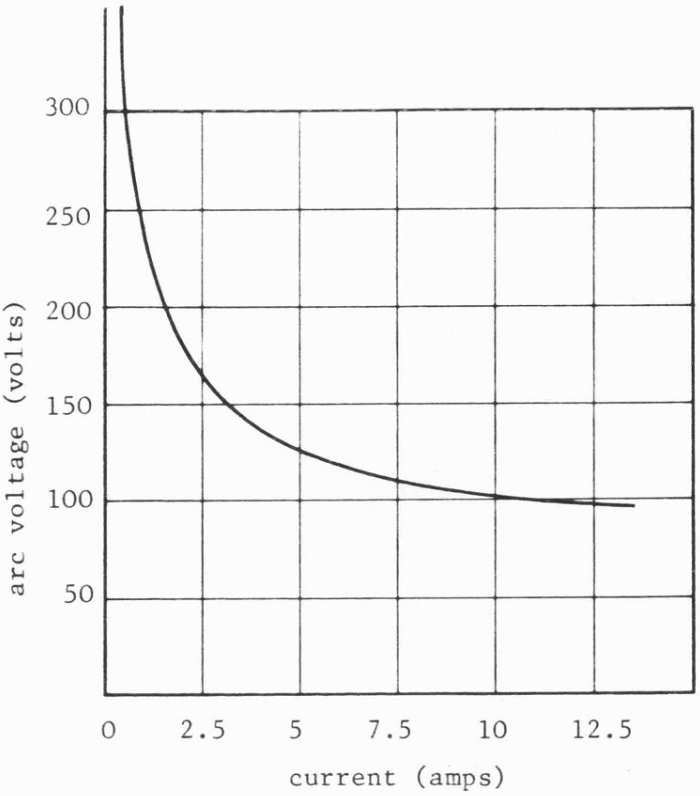

Fig. 4.1 Static characteristic of a 3.81 cm arc in air

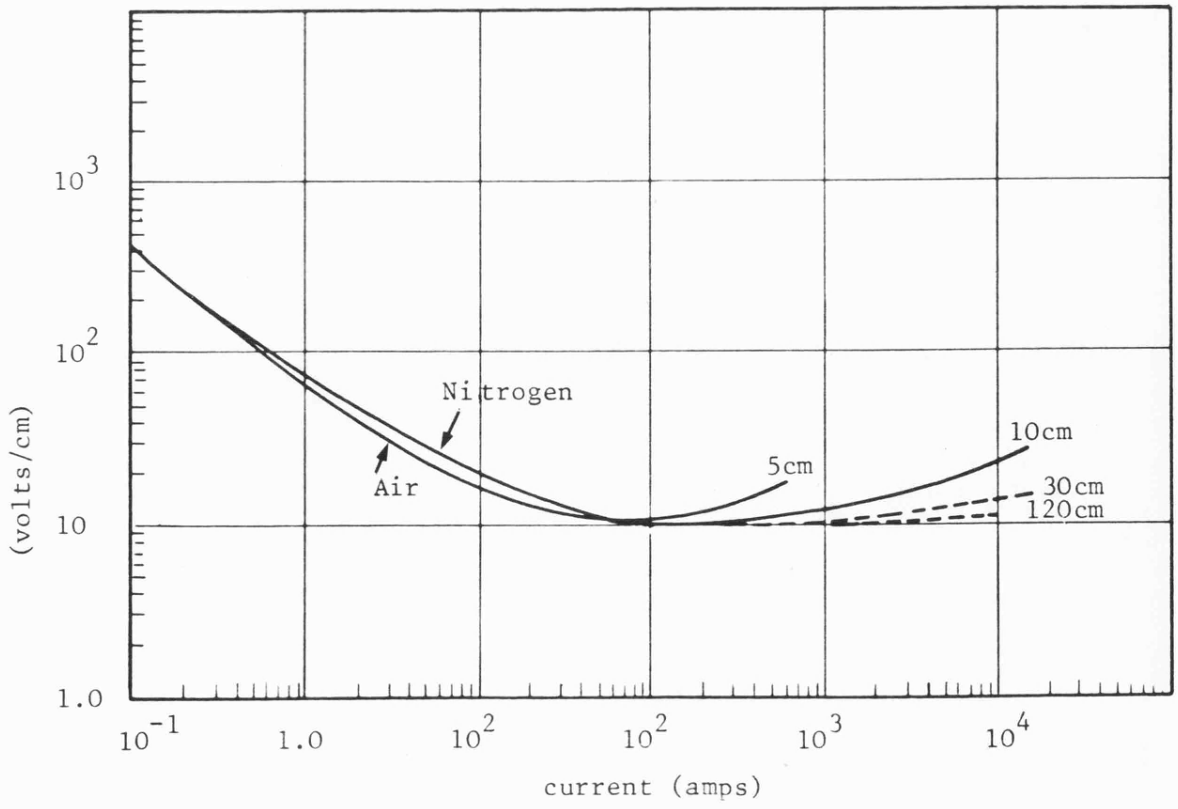

Fig. 4.2 Voltage gradient-current for an arc in air or nitrogen

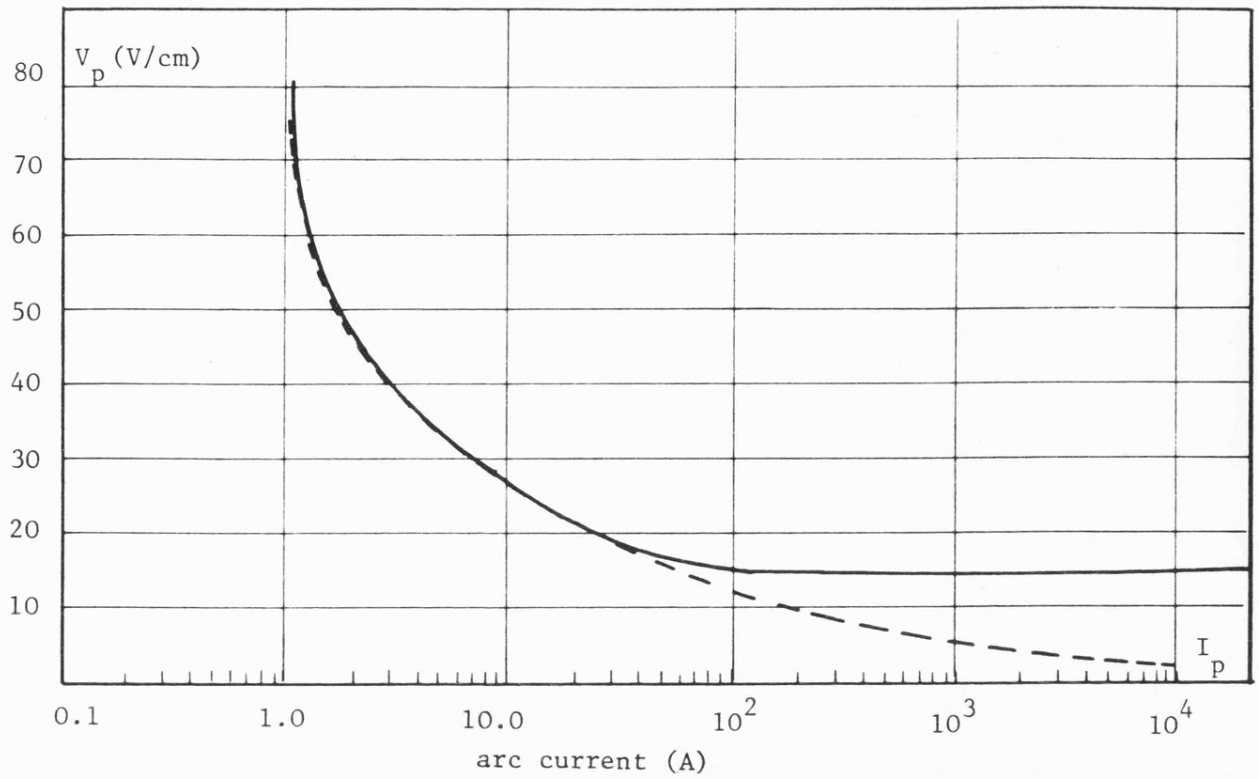

Fig. 4.3 Volt-ampere characteristics of an open electric arc

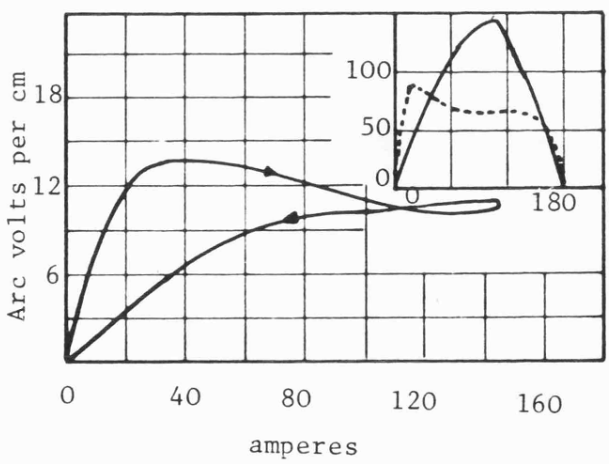

Fig. 4.4 Volt-ampere characteristics for a 100 r.m.s. ampere arc

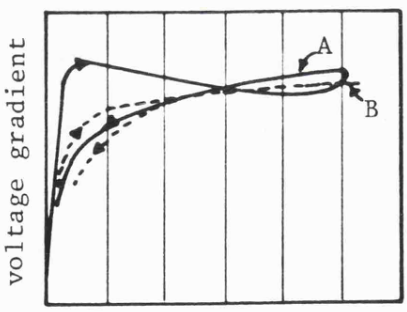

Fig. 4.5 Volt-ampere characteristics of a 15,000 r.m.s. ampere arc

arc length = 30.5 cm

A: second half cycle
B: fourth half cycle

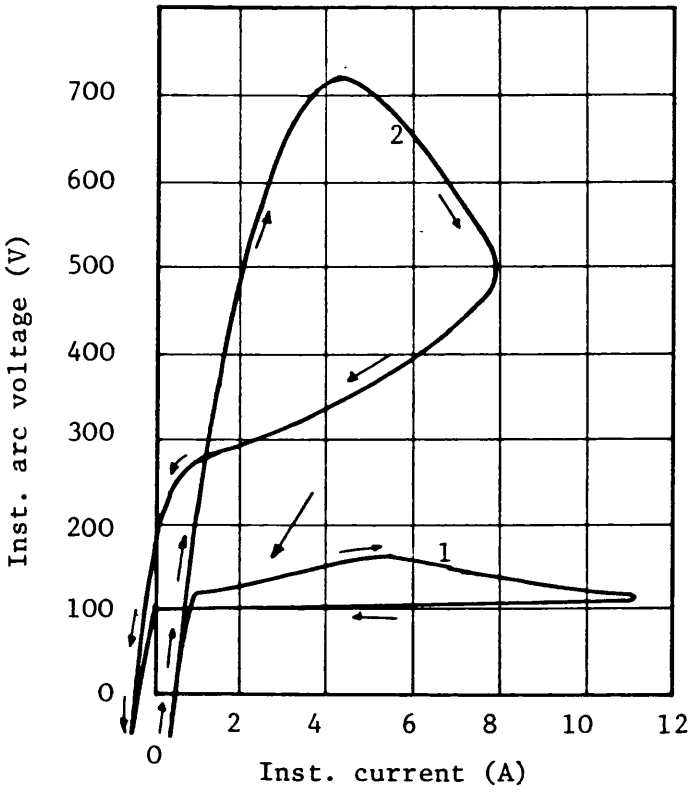

Fig. 4.6 Volt-ampere cyclograms of 60-cycle arcs in air between copper electrodes 3.81 cm apart

(1) arc still about 3.81 cm long
(2) arc lengthened to breaking point

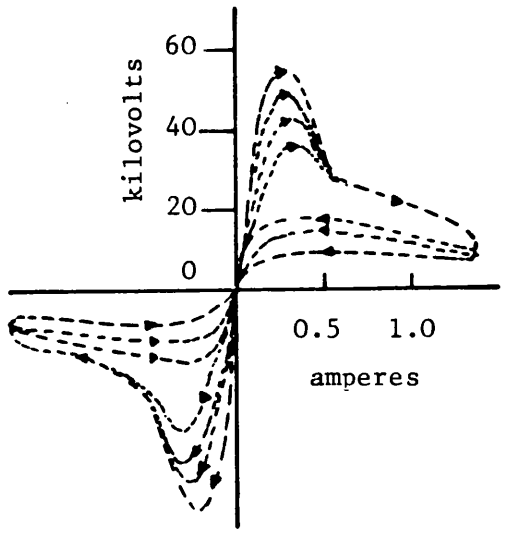

Fig. 4.7 Cathode-ray volt-ampere cyclograms of vertical 60-cycle arc drawn to a length of 122 cm in a 40-kV circuit in air

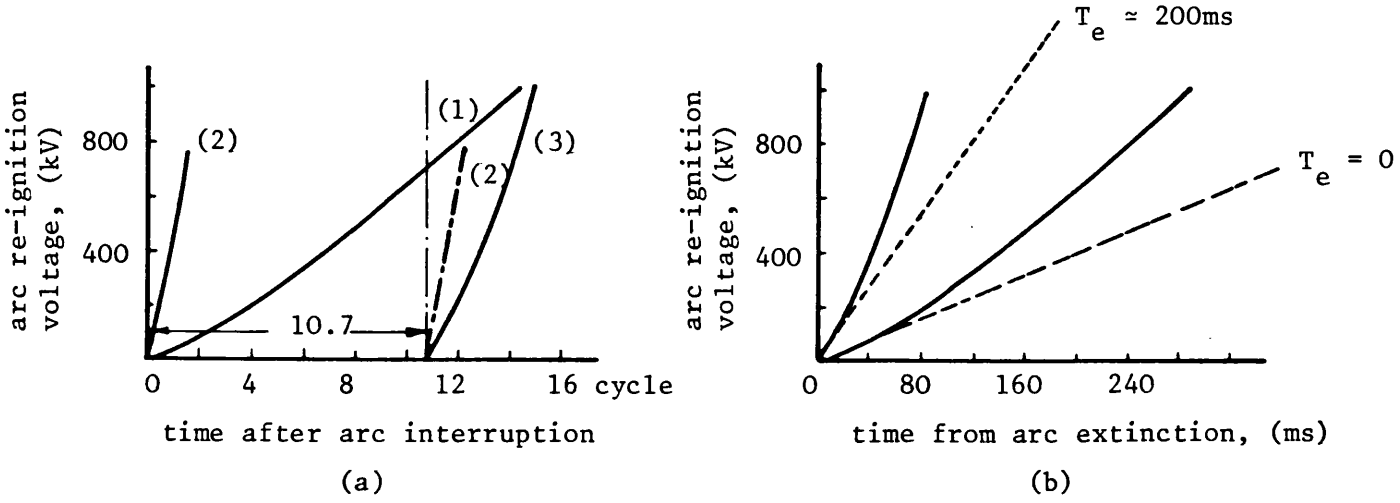

Fig. 4.8 Dielectric recovery characteristics of heavy current arc, small current arc, and secondary arc

(1) 8 kA, 5 cycles arc
(2) 40 A, 10 cycle arc
(3) 8 kA, 5 cycles and 30 A, 10 cycles secondary arc

(a) Typical arc recovery characteristics
(b) Pessimistic linearised approximation

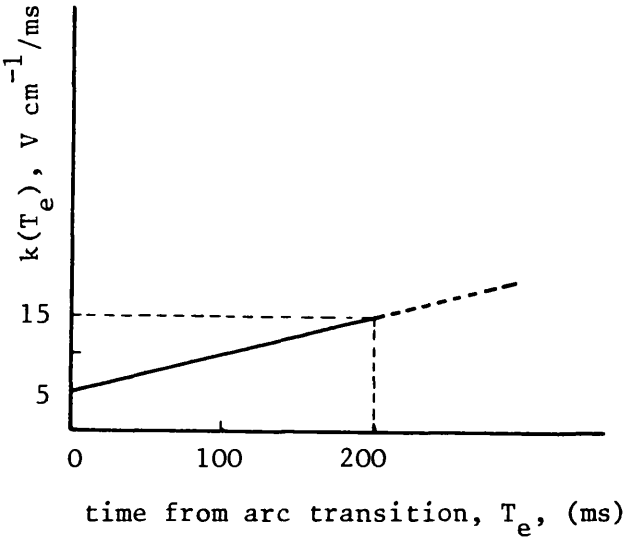

(c)

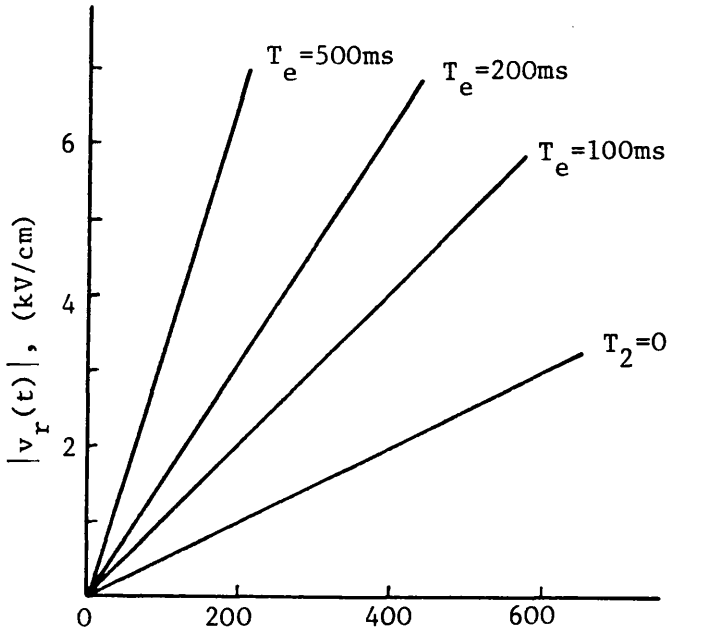

(d)

Fig. 4.8(continued)

(c) time variation of rate of change of re-ignition voltage gradient

(d) resulting time variation of re-ignition voltage gradient for discrete values of extinction time T_e

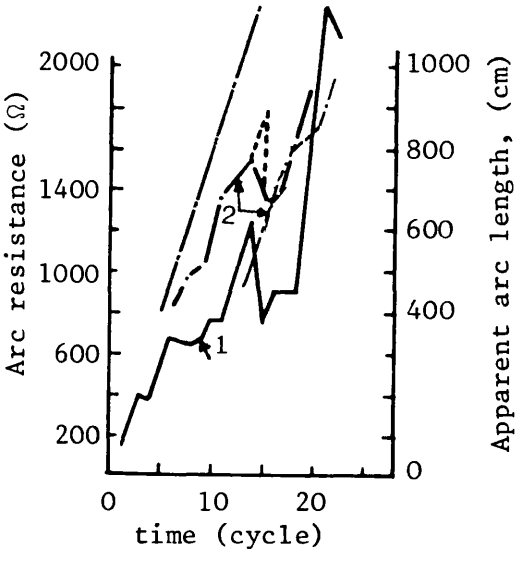

Fig. 4.9

Variation of secondary arc resistance and arc length

Primary arc: 8 kA, 5.74 cycles
Sec. arc: 315. A, self extinction time of 22.6 cycles

(1) arc resistance
(2) apparent arc length

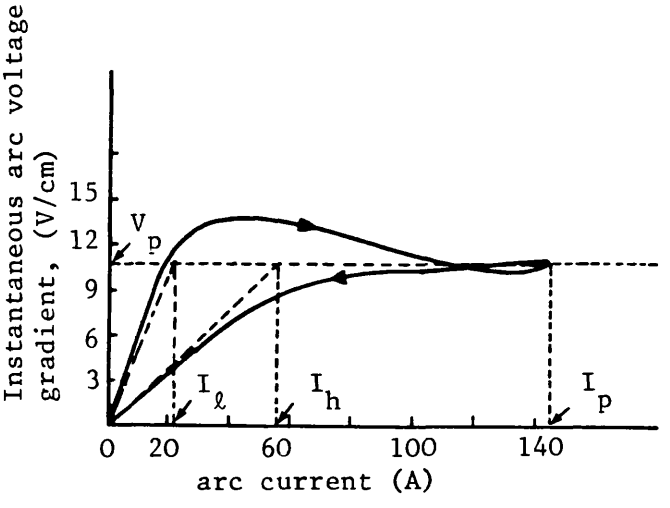

Fig 4.10 Typical long arc cyclogram

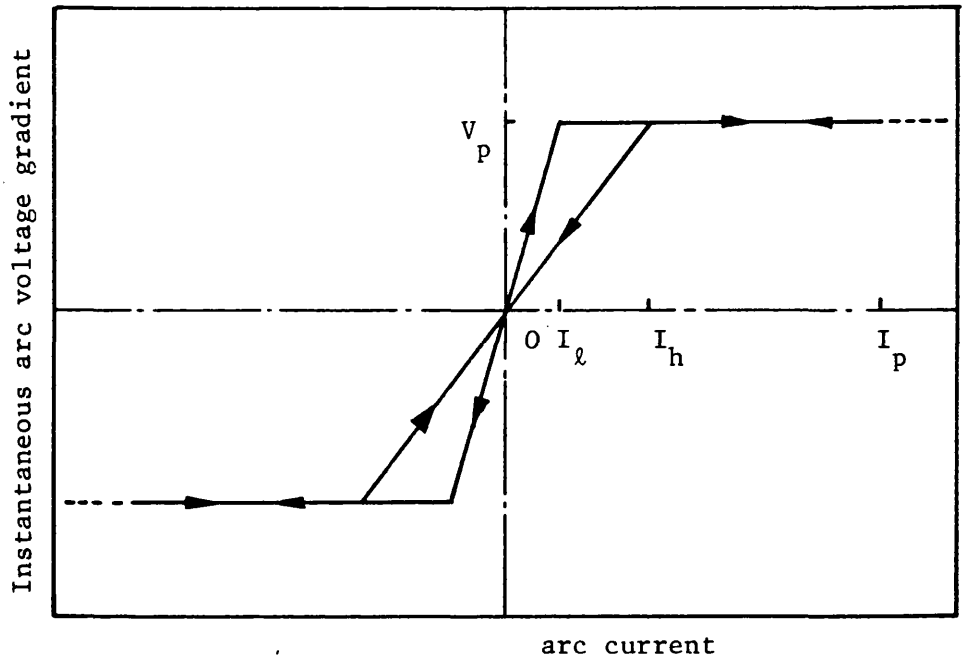

Fig. 4.11 Normalised linearised arc cyclogram

I_p = peak of steady-state secondary arc current

$I_\ell = 0.15\ I_p$

$I_h = 0.38\ I_p$, $V_p = 75\ I_p^{-0.4}$ V/cm

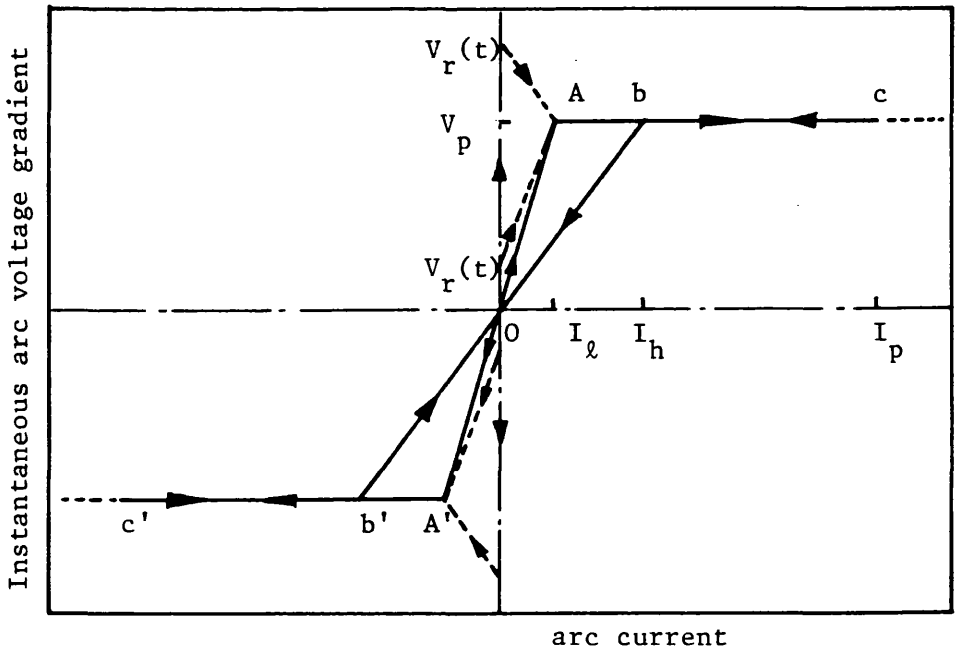

Fig. 4.12 Inclusion of re-ignition voltage in arc cyclogram

CHAPTER 5

SECONDARY ARC CURRENT AND VOLTAGE FORMULATION

5.1 Introduction

Having defined the secondary arc model, the secondary arc current and voltage waveforms are investigated. The system response at any point can be investigated, after calculating the secondary arc current and voltage waveforms, using the superposition and Thevenin theorems.

In the present chapter, a method is derived based on a combination of the Fourier technique and Time Domain Convolution. The accuracy of the Fourier method is thus retained in that all frequency dependent parameters are taken into account, while the non-linear analysis is carried out in the Time Domain using the superposition integral. In the method, the Thevenin voltage waveform is obtained in the absence of the secondary arc (assuming that the arc is removed immediately after the opening of the second breaker), together with system responses due to a unit step current injected into the system from the secondary arc terminals. Both sets of waveforms are obtained using the Fourier transform. The waveforms are then coupled with the secondary arc characteristics to yield the required secondary arc current and voltage using the Time Domain Convolution.

5.2 Basic Solution Method

Fig. 5.1 shows the circuit state following an 'a'-earth fault arc transition, i.e. conditions during the secondary arc (dead-time) period. At the instant of arc transition, the primary arc resistance (R_F) is replaced by the non-linear secondary arc model developed. However, in

order to determine the secondary arc response it is necessary to first consider the Thevenin equivalent of the system as viewed from the arc location. This is shown in fig. 5.2, from which it is seen that the secondary arc forms a simple termination of the equivalent driving circuit. By the definition of Thevenin equivalent circuits, the voltage $\bar{E}_T$ is the frequency spectrum of the voltage which would appear across the points F-E (see fig. 5.2) if the secondary arc extinguished immediately. In the course of this work, it is the time variation of the Thevenin voltage $e_T(t)$ that is used and this is in turn computed in discrete form $e_T(n)$ by using the Frequency Domain methods of reference 47. Essentially, the fault point voltage to earth is first computed for a hypothetical transient fault that fails to conduct current immediately following arc transition. By definition this voltage is, for all time after arc transition, equal to $e_T(t)$. Also by definition, the Thevenin impedance Z_T is the impedance which would be measured looking into point F-E with all system source voltage short circuited, i.e. the de-energised system impedance as viewed from F-E with the arc path open-circuited. The value of Z_T has to be computed over the complete range of frequencies of interest and the methods by which this is achieved are detailed in section 5.3. With reference to fig. 5.2, the Frequency Domain relationship of eqn. 5.1 relates the arc voltage and current.

$$\bar{V}_{arc} = \bar{E}_T - \bar{I}_{arc} Z_T \qquad (5.1)$$

However, the non-linear behaviour of the secondary arc demands that a solution during the secondary arc period be effected in the Time Domain and, in order to achieve this, the inverse Fourier transform is applied to eqn. 5.1.

$$v_{arc}(t) = e_T(t) - \mathcal{F}^{-1}(\bar{I}_{arc} Z_T)$$

$$= e_T(t) - \frac{1}{2\pi}\int_{-\infty}^{\infty}(\bar{I}_{arc} Z_T)\exp(j\omega t)d\omega \qquad (5.2)$$

The inverse Fourier integral of eqn. 5.2 can be evaluated in the Time Domain by means of the Convolution theorem and, when this is done, the full Time Domain solution of eqn. 5.3 emerges.

$$v_{arc}(t) = e_T(t) - \int_{-\infty}^{\infty} Z_T(t-\tau)i_{arc}(\tau)d\tau \qquad (5.3)$$

where

$$Z_T(t-\tau) = \frac{1}{2\pi}\int_{-\infty}^{\infty} Z_T \exp(j\omega(t-\tau))d\omega \qquad (5.4)$$

The impedance function $Z_T(t-\tau)$ is thus the voltage which would arise if a unit impulse of current were injected into the Thevenin impedance Z_T. In accordance with the usual requirements for the causality of real systems, the function $Z_T(t-\tau)$ must be equal to zero for $t-\tau < 0$, i.e. for $\tau > t$. For the purpose of solving eqn. 5.3, it is convenient to define the time $t = 0$ as the time of arc transition (start of secondary arc). Thevenin equivalent of fig. 5.1b is then only applicable for the time $t > 0$, the value of the secondary arc current ($i_{arc}(t)$) being zero for $t \leq 0$. It follows that $i_{arc}(\tau) = 0$ for $\tau < 0$ and with these conditions in mind, the limits of integration in eqn. 5.3 are modified as per eqn. 5.5.

$$v_{arc}(t) = e_T(t) - \int_{0}^{t} Z_T(t-\tau)i_{arc}(\tau)d\tau \qquad (5.5)$$

In common with previous work, the integral eqn. 5.4 is evaluated numerically in discrete sample data form by using the half range modified Fourier transform integral[47]. Thus, both $e_T(t)$ and $Z_T(t-\tau)$ are known in discrete sample data form, and it is shown in Appendix 5.1

that eqn. 5.5 can be written in the recursive form of eqn. 5.6 to relate the arc current at any time $n\Delta T$ to the known discrete value of Thevenin voltage $e_T(n)$.

$$e_T(1) = f(i_{arc}(1),1) + Z_T(0)\, i_{arc}(1)\, \Delta T/2$$

$$e_T(n) = f(i_{arc}(n),n) + Z_T(0) i_{arc}(n)\, \Delta T/2 + \sum_{k=1}^{n-1} Z_T(n-1) i_{arc}(k)\, \Delta T \quad (5.6)$$

The first of the above equations is solved using the value $e_T(1)$ to provide the arc current at the first sample step time ΔT after transition. From thereon, the second eqn. of 5.6 is solved recursively by noting that the terms within the summation over the range $k = 1 \rightarrow n - 1$ contain only past history of the arc current.

5.3 Digital Evaluation of Thevenin Impedance Z_T

The method of calculating Z_T is based on reducing the system network under study to a single-port equivalent network as viewed from the fault point. With reference to Figs. 5.1 and 5.2 it is required to determine the impedance measured between points F-E with all sources de-energised. Using two-port matrix function theory to describe the equivalent line/reactor section, the frequency domain relationship of eqn. 5.7 applies to the receiving end (see Fig. 5.1a).

$$\begin{bmatrix} \bar{V}_f \\ \bar{I}_{fR} \end{bmatrix} = \begin{bmatrix} A_2 & B_2 \\ C_2 & D_2 \end{bmatrix} \begin{bmatrix} \bar{V}_{R2} \\ \bar{I}_{R2} \end{bmatrix} \quad (5.7)$$

Because a de-energised condition is considered, eqn. 5.8 applies at the receiving end source.

$$\bar{V}_{R1} = Z_{SR}\, \bar{I}_{R1} \quad (5.8)$$

Now the conditions at the receiving end breakers are such that the constraints of eqn. 5.9 apply.

$$\begin{aligned} \bar{I}_{R1} = \bar{I}_{R2} &= \left[\bar{I}_{R2a} = 0 \quad \bar{I}_{R2b} \quad \bar{I}_{R2c}\right]^T \\ \left[\bar{V}_{R1b} \quad \bar{V}_{R1c}\right]^T &= \left[\bar{V}_{R2b} \quad \bar{V}_{R2c}\right]^T \end{aligned} \qquad (5.9)$$

The constraints of eqn. 5.9 can be applied to eqn. 5.8, in which the 'b' and 'c' phase voltages and currents are related by a sub-matrix of Z_{SR}, Z'_{SR}, say:

$$\left.\begin{aligned} \left[\bar{V}_{R2b} \quad \bar{V}_{R2c}\right]^T &= Z'_{SR}\left[\bar{I}_{R2b} \quad \bar{I}_{R2c}\right]^T \\ \text{or } \left[\bar{I}_{R2b} \quad \bar{I}_{R2c}\right]^T &= Y_{SR1}\left[\bar{V}_{R2b} \quad \bar{V}_{R2c}\right]^T \\ \text{where } Y_{SR1} &= \left[Z'_{SR}\right]^{-1} \end{aligned}\right\} \qquad (5.10)$$

It will be noted that $\bar{I}_{R2a} = 0$ and that consequently eqn. 5.7 can be written:

$$\left.\begin{aligned} \bar{V}_f &= A_2 \bar{V}_{R2} + B'_2 \left[\bar{I}_{R2b} \quad \bar{I}_{R2c}\right]^T \\ \bar{I}_{fR} &= C_2 \bar{V}_{R2} + D'_2 \left[\bar{I}_{R2b} \quad \bar{I}_{R2c}\right]^T \end{aligned}\right\} \qquad (5.11)$$

where B'_2, D'_2 are sub-matrices of B_2 and D_2 respectively. Substituting eqn. 5.10 into 5.11 yields:

$$\begin{aligned} \bar{V}_{fR} &= A_2 \bar{V}_{R2} + B'_2 Y_{SR1}\left[\bar{V}_{R2b} \quad \bar{V}_{R2c}\right]^T = A'_2 \bar{V}_{R2} \\ \bar{I}_f &= C_2 \bar{V}_{R2} + D'_2 Y_{SR1}\left[\bar{V}_{R2b} \quad \bar{V}_{R2c}\right]^T = C'_2 \bar{V}_{R2} \end{aligned}$$

$$\text{Therefore } \bar{V}_f = A'_2\left[C'_2\right]^{-1} \bar{I}_{fR} = Z_{Ra}\bar{I}_{fR} \qquad (5.12)$$

The part of the circuit linking the fault point to the sending end source is likewise treated to obtain, according to the current directions defined in Fig. 5.1:

$$\bar{V}_f = - A'_1 \left[C'_1\right]^{-1} \bar{I}_{fS} = - Z_{Sa} \bar{I}_{fS} \qquad (5.13)$$

The vector of fault point currents $\bar{I}_f = \bar{I}_{fS} - \bar{I}_{fR}$ is, from eqn. 5.12, 5.13 given by:

$$\bar{I}_f = -\left[Z_{Sa}^{-1} + Z_{Ra}^{-1} \right] \bar{V}_f$$

Therefore $$\bar{V}_f = - \left[Z_{Sa}^{-1} + Z_{Ra}^{-1} \right]^{-1} \bar{I}_f \qquad (5.14)$$

Now the fault point is constrained such that $\bar{I}_{fb} = \bar{I}_{fc} = 0$, and it follows from eqn. 5.14 that:

$$\bar{V}_{fa} = - Z_{11} \bar{I}_{fa} \qquad (5.15)$$

where Z_{11} is the leading element of $\left[Z_{Sa}^{-1} + Z_{Ra}^{-1} \right]^{-1}$. It should be noted that for the reference directions of current assumed (see Fig. 5.1), the Thevenin impedance Z_T is given by $- \bar{V}_{fa}/\bar{I}_{fa}$ which is in turn equal to the impedance function Z_{11} defined in eqn. 5.15. Z_T is thus computed at all spectral frequencies necessary.

5.4 Digital Evaluation of Thevenin Voltage

To calculate the Thevenin voltage $e_T(t)$, consider Fig. 5.3 at the fault point. v_{fo} is a voltage which is zero for all time up to the arc transition time T_o. It is also a voltage which forces the total current $i_a(t)$ to zero for all time after T_o. It follows that the Thevenin voltage $e_T(t)$ could be calculated as equal to the voltage $v_{f1}(t)$ after time T_o, i.e. $e_T(t) = v_{f1}(t)\ h(t - T_o)$.

Consider the current $i_a(t)$ (see Fig. 5.3), this will be equal to the sum of the response due to the application of v_{ff} and the injected current to simulate the opening of the faulted-phase breakers plus the current $i_{ao}(t)$ which flows in response to the application of v_{fo} to

the circuit with the breakers opened (Fig. 5.4). Consider Fig. 5.4 in the frequency domain.

$$\bar{E}_{fo} = \bar{V}_{fo} + \bar{I}_{ao} R_F \tag{5.16}$$

But $\bar{E}_{fo} = - \bar{I}_{ao} Z_T$

Therefore $\bar{V}_{fo} = - \bar{I}_{ao} (Z_T + R_F)$ (5.17)

Let the sum of the currents in the fault path due to the application of $\bar{V}_{ff}$ and the currents injected to simulate the opening of the breakers be given by $i_{a1}(t)$ ($i_{fT}(t)$ in chapter 3), then

$$i_{ao}(t) + i_{a1}(t)\, h(t - T_o) = 0$$

or $$\bar{I}_{ao} = - \int_{T_o}^{T_{ob}} i_{a1}(t) \exp(-j(\omega - j\alpha)t)dt \tag{5.18}$$

Therefore $\bar{V}_{fo}$ can be calculated in the frequency domain, and $v_{fo}(t)$ then obtained. The Thevenin voltage is then calculated in the time domain by eqn. 5.19.

$$e_T(t) = v_{f1}(t)\, h(t - T_o) \tag{5.19}$$

The time T_o is used as equal to the second breaker opening time T_{b2}.

5.5 Evaluation of Voltages and Currents at the Relaying Points

Having obtained the secondary arc current and voltage, the total fault point voltage throughout the pre-fault, primary and secondary arc periods are defined. If required, the total fault point voltage can then be used as a forcing voltage function in the simulation of the system voltages and currents at any other point.

Consider the system at the fault point, as shown in Fig. 5.5, where v'_{ff} is the new superimposed voltage which is no longer equal and opposite to the steady-state voltage v_{ss}. The current $i_A(t)$ is equal to the fault current $i_{al}(t)$ for $0 < t < T_o$, and is equal to the secondary arc current $i_{arc}(t)$, for $t \geq T_o$.

The voltage across the arc path for all time after the inception of the fault is given by:

$$e_f(t) = i_{al}(t)\, R_F\, h(t) - i_{al}(t)\, R_F\, h(t - T_o) + v_{arc}(t)\, h(t - T_o) \quad (15.20)$$

Consider Fig. 5.5,

$$i_A(t) = i_{al}(t)\, h(t) - i_{al}(t)\, h(t - T_o) + i_{arc}(t)\, h(t - T_o) \quad (15.21)$$

$$v_{ss}(t) + v'_{ff}(t) + i_A(t)R_F = e_f(t)$$

or $$v'_{ff}(t) = e_f(t) - i_A(t)R_F - v_{ss}(t) \quad (5.22)$$

The new superimposed voltage in the frequency domain is then obtained from eqn. 5.23.

$$\bar{V}'_{ff} = -\int_o^{T_{ob}} v'_{ff}(t)\exp(-j(\omega - j\alpha)t)dt \quad (5.23)$$

The new superimposed voltage is then injected to the system through a constant fault resistance R_F. The fault calculations and the breaker opening have to be repeated. The response at any point in the system is then found as a summation of all the separate components, i.e. steady-state, fault inception and breakers opening.

5.6 Evaluation of the Secondary Arc Current and Voltage: Computational Considerations

The solution for the secondary arc current and voltage is more complicated than has been indicated from eqns. 5.6. This is mainly due to the fact that the arc does not necessarily follow the whole halfcycle path o-a-b-c-b-o (or, o-a'-b'-c'-b'-o) as defined in Fig.5.6. During the first cycle, after arc transition, the arc may follow the path o-a-b then start decreasing before reaching b. Similar situation could happen along the path o-a or b-o. With the foregoing considerations in mind, the set of equations 5.6 could be solved as shown below (see Fig. 5.6). The arc characteristic is assumed to follow the path o-a (or, o-a'), i.e.

$$v_{arc}(1) = V_p \ell_a(1)\, i_{arc}(1)/0.15\, I_p \qquad (5.24)$$

By substituting for $v_{arc}(1)$ in eqn. 5.6, $i_{arc}(1)$ can be calculated. Now, $i_{arc}(1)$ has to be compared with $0.15\, I_p$ in sign and magnitude as shown:

1. If $|i_{arc}(1)| < 0.15\, I_p$ then the value of $v_{arc}(1)$ is calculated from eqn. 5.24 using the calculated value of $i_{arc}(1)$.

2. If $i_{arc}(1) \gtrsim 0.15\, I_p$ then the arc is assumed to follow the path o-a-b, i.e.

   $$v_{arc}(1) = V_p \ell_a(1) \qquad (5.25)$$

   Then by substituting for $v_{arc}(1)$ in eqn. 5.6, $i_{arc}(1)$ could be calculated.

3. If $i_{arc}(1) \lesssim -0.15\, I_p$ then the arc is assumed to follow the path o-a'-b', i.e.

   $$v_{arc}(1) = - V_p \ell_a(1) \qquad (5.26)$$

   Then, by substituting for $v_{arc}(1)$ in eqn. 5.6, $i_{arc}(1)$ could be calculated.

At this stage $i_{arc}(1)$ and $v_{arc}(1)$ could be obtained. Then $i_{arc}(2)$, $i_{arc}(3)$ ..., $i_{arc}(k)$ could be calculated until i_{arc} started to decrease, i.e. $|i_{arc}(k)| < |i_{arc}(k-1)|$. In this case, the following possibilities would exist (assuming $i_{arc}(1)$ is positive):

i) The current was increasing along the path o-a, but before reaching a it started to decrease. In such a case the current was assumed to follow the path a_o-o, where a_o corresponded to the latest calculated values of current and voltage before the current started to decrease. If the current started to increase again, it would have to continue doing so along the path o-a_o, but, when it exceeded the value which corresponds to a_o, it would then have to follow a new path a_o-a. The arc voltage, in this case, could be defined by eqn. 5.27 or 5.24 (depending upon the arc path).

$$v_{arc}(k) = \frac{v_{arc}(k-1)}{i_{arc}(k-1)\ell_a(k-1)}\, i_{arc}(k)\ell_a(k) \qquad (5.27)$$

ii) The current was increasing along the path a-b, but before reaching b it started to decrease. In this case the current was assumed to follow the path b-a as defined in eqn. 5.25.

iii) The current was increasing along the path b-c, then started to decrease. If the current decreased to a lower value than that which corresponded to b, it would then have to do so along the path b-o. But if it started to increase before reaching o, then it would have to do so along the path o-b-c. The arc voltage, in this case, could be represented by eqn. 5.28.

$$v_{arc}(k) = V_p \, i_{arc}(k) \ell_a(k) / 0.38 \, I_p \qquad (5.28)$$

In each of the above three cases the voltage/current relationship has to be defined before solving for $i_{arc}(k)$. The process of the calculation is repeated until voltage reversal (i.e. when the current passes through zero which means $i_{arc}(k)$ is negative). However, the arc current $i_{arc}(k)$ should be re-set to have the zero-value. In this case, the arc voltage ($v_{arc}(k)$) and the re-ignition voltage ($v_r(k)$) is thus as given below (see eqn. 5.6):

$$v_{arc}(k) = e_T(k) - \sum_{j=1}^{k-1} Z_T(k - j) i_{arc}(j) \Delta T \qquad (5.29)$$

The re-ignition voltage was calculated using eqn. 5.30.

$$v_r(k) = (DV_o + DV_1 T_e)(t - T_e) 10^3 \quad V/cm \qquad (5.30)$$

where $t = k.\Delta T$ and $(t - T_e)$, which is shown in fig. (5.7) can be defined by the following equation:

$$t - T_e = \frac{|i_{arc}(k)|}{|i_{arc}(k)| + |i_{arc}(k - 1)|} \Delta T \qquad (5.31)$$

By comparing the value for $v_{arc}(k)$ with the corresponding value for $v_r(k)$, the following possibilities result:

a) $v_{arc}(k) < -v_r(k) \ell_a(k)$

b) $v_{arc}(k) > v_r(k) \ell_a(k)$

c) $|v_{arc}(k)| \lesssim v_r(k) \ell_a(k)$

In the first case (a) the secondary arc current will continue along the path a_1'-a'. In this case the arc voltage could be defined by the following eqn.:

$$v_{arc}(k) = \left[(V_p - v_r(k))i_{arc}(k)/0.15\ I_p - v_r(k)\right]\ell_a(k) \qquad (5.32)$$

Now, $i_{arc}(k)$ can be recalculated from eqn. 5.6 and $v_{arc}(k)$ is thus calculated from eqn. 5.32. In the second case (b) the secondary arc current will continue along the path a_1-a. The arc voltage in this case is defined by:

$$v_{arc}(k) = \left[(V_p - v_r(k))i_{arc}(k)/0.15\ I_p + v_r(k)\right]\ell_a(k) \qquad (5.33)$$

While in the third case (c) the current $i_{arc}(k)$ will be kept at zero value and $i_{arc}(k + 1)$ is thus also set to have a zero value. Now $v_{arc}(k + 1)$ and $v_r(k + 1)$ can be calculated after re-adjusting the time intervals $(t - T_e)$ by the increment ΔT.

The process is repeated until the arc extinguishes at a current zero. The calculations for the recovery voltage should continue by using eqns. 5.29-5.32. Finally, the above procedure leads to the establishment of the secondary arc current and voltage waveforms.

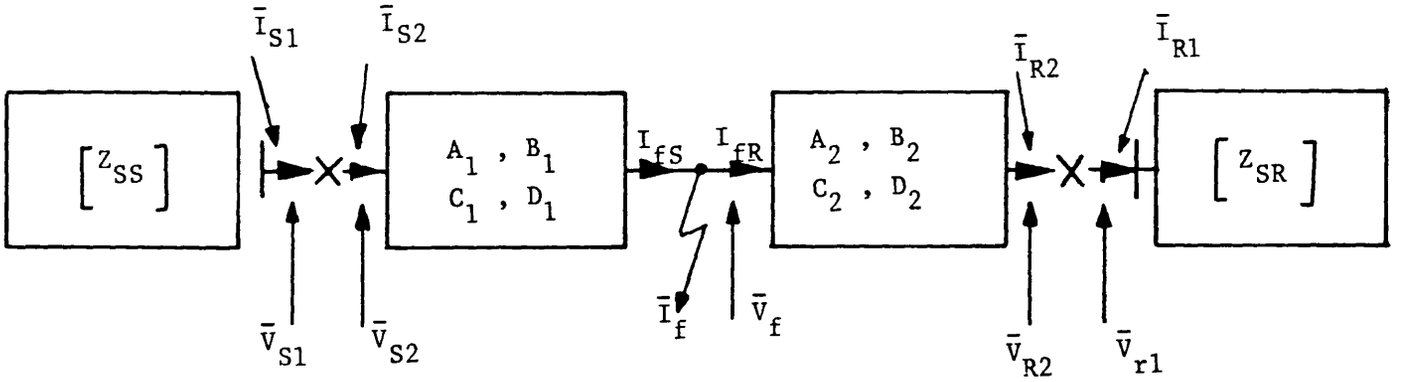

(a)

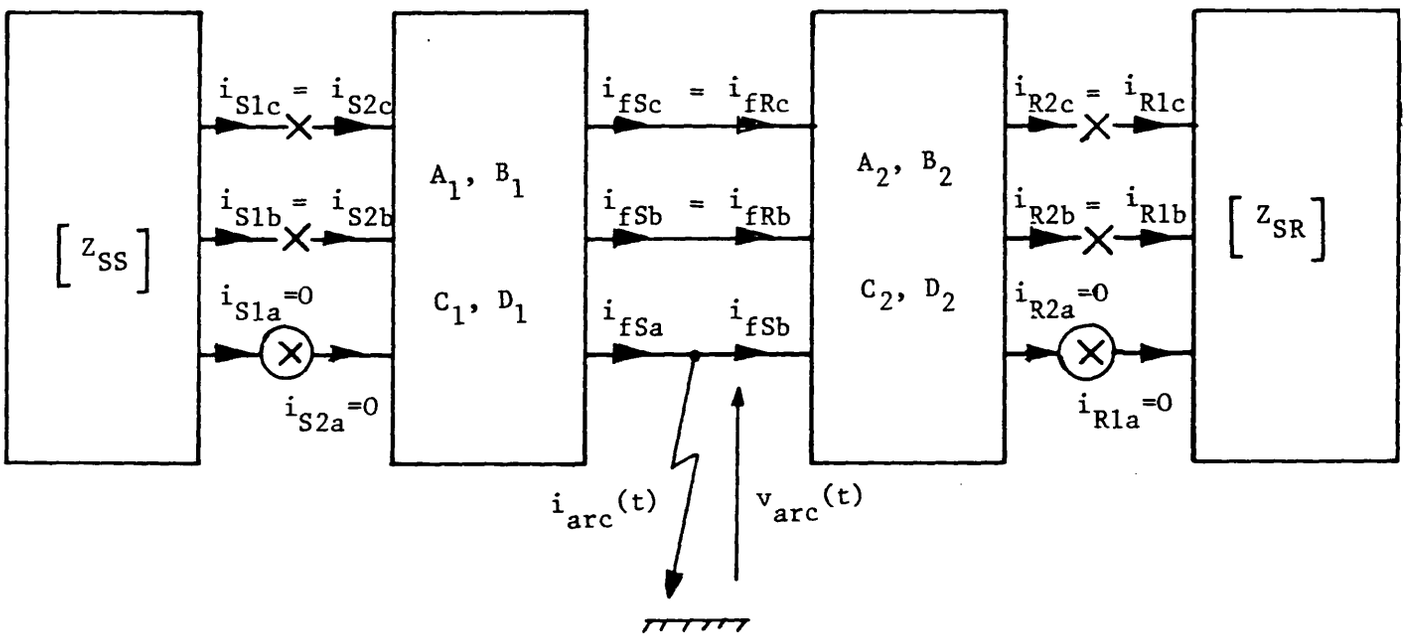

(b)

Fig. 5.1 (a) Basic system model
(b) Circuit state during secondary arcing period

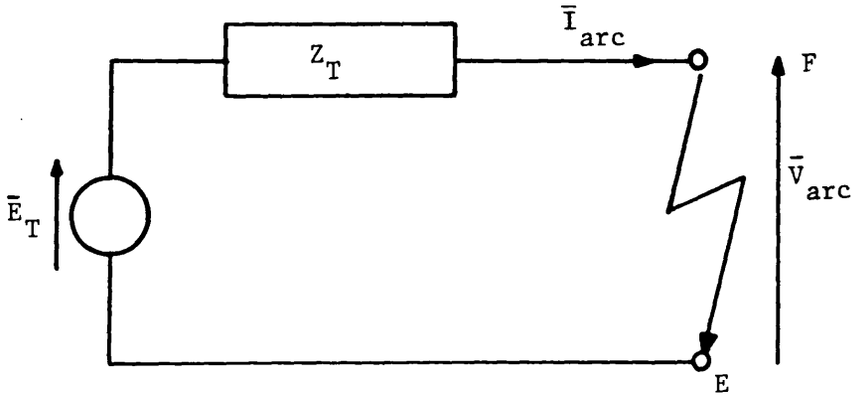

Fig. 5.2 Thevenin equivalent fault point circuit

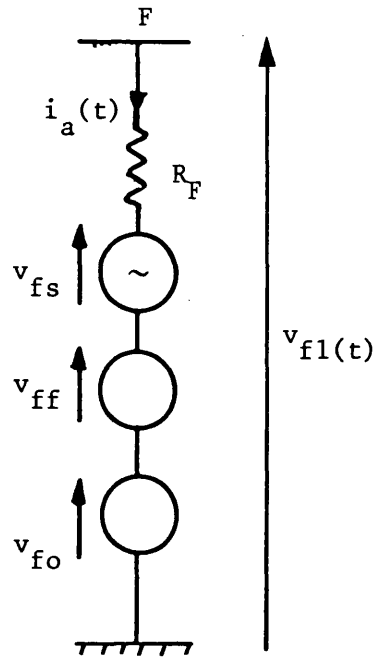

Fig. 5.3

Fault point equivalent circuit used to calculate Thevenin voltage

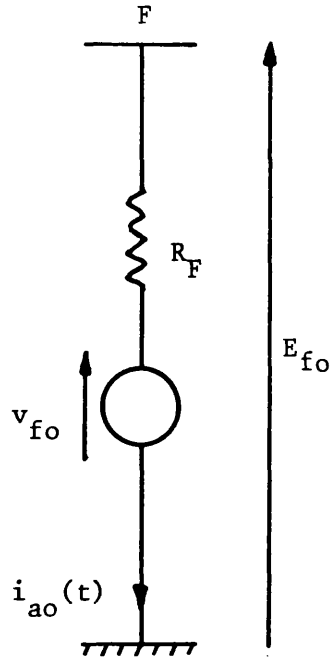

Fig. 5.4

Thevenin equivalent circuit

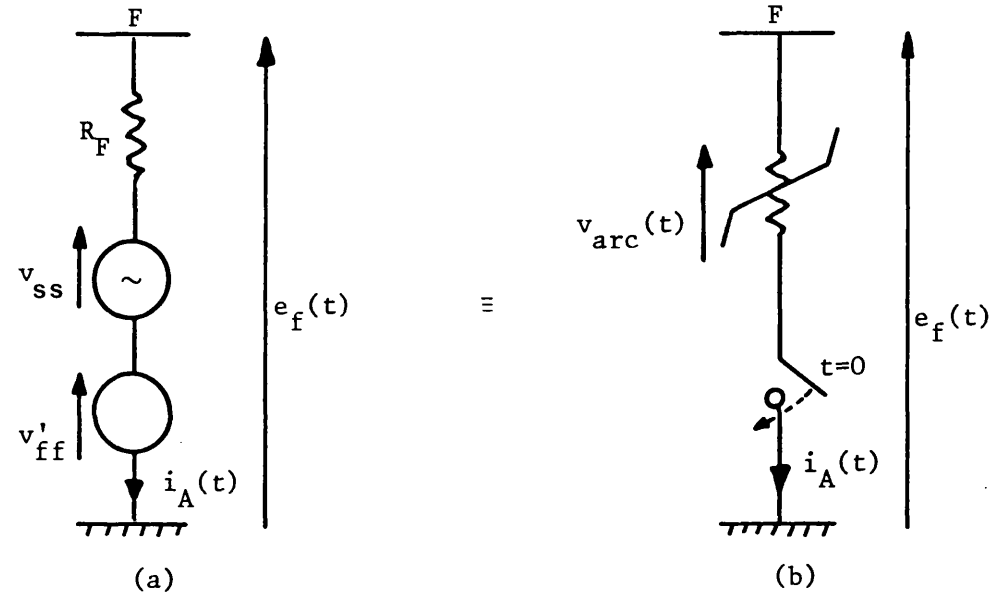

Fig. 5.5 Fault path equivalent circuit

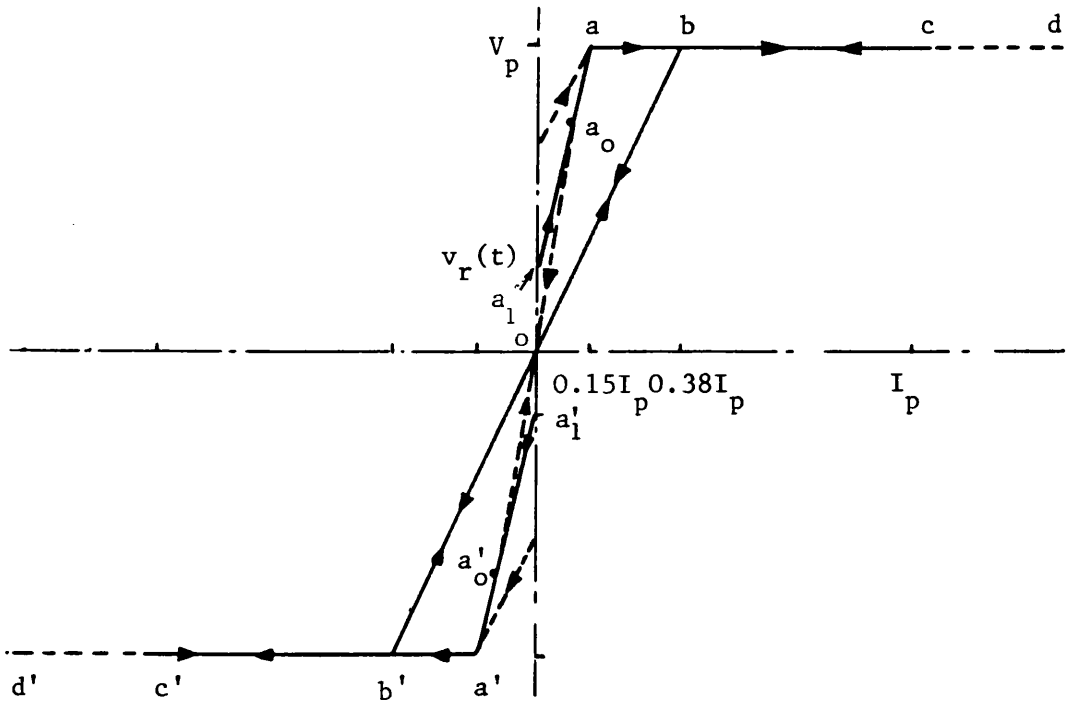

Fig. 5.6 Normalised linearised arc cyclogram

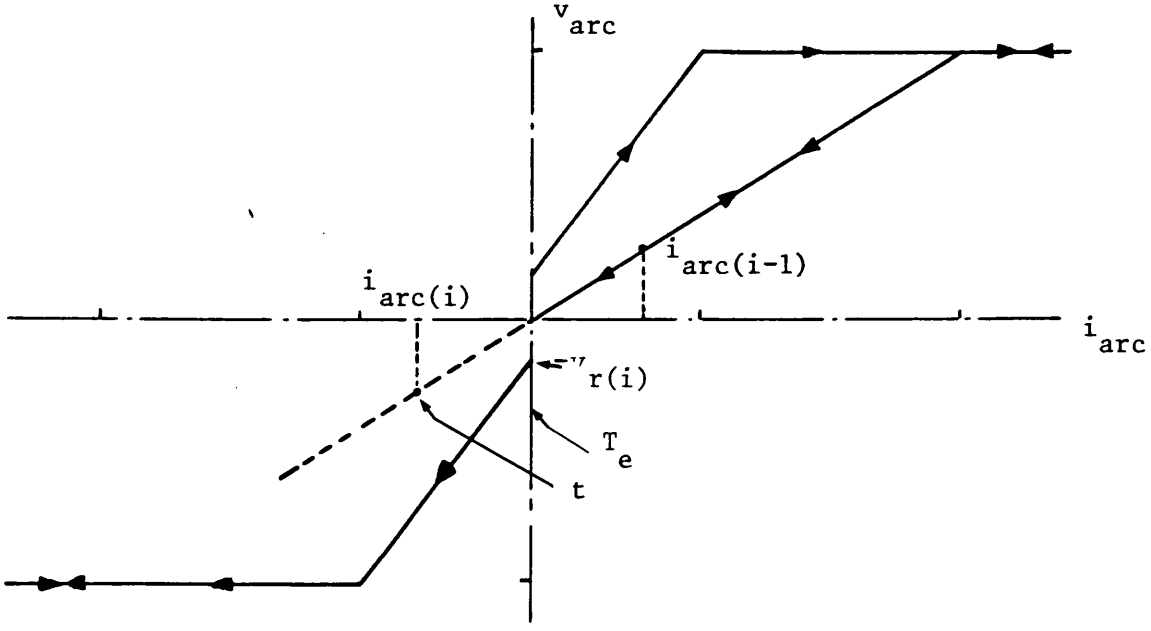

Fig. 5.7 Linearised re-ignition voltage characteristic at voltage reversal

CHAPTER 6

DIGITAL SIMULATION OF SINGLE-POLE RECLOSURE

6.1 Introduction

Single-pole reclosing is especially attractive from a switching surge point of view as surges associated with single-pole reclosing are significantly less than those associated with three-pole reclosing (51,76).

However, single-pole reclosure transients may still exceed the voltage level necessary in order to effect the desired reduction in the insulation level of the system. This voltage level is often specified in the range 2.0-2.5 p.u. of the peak phase-to-neutral voltage of the system, and, where energisation transient voltages do not fall inherently below this level, they must be restricted by other means.

The switching surges are dependent on the voltage across the circuit-breaker contacts at the instant of closing and are reduced considerably if this voltage is zero. The results of tests using the method of synchronous closing at voltage zero are described by Maury(50). The other well known method used for reducing switching overvoltages is to use breaker with closing resistor(s)(51,77).

Despite the fact that some reduction in the transient switching overvoltage is realised with the synchronous closing scheme, the critical tolerance on the breaker closing time and the need for additional voltage measurements make this technique unattractive. An optimum solution to the line energization problem in e.h.v. systems

includes a combination of adding switching resistance and adopting synchronous closing. This would make it possible to allow the breaker closing time to vary within certain limits and yet have the transient overvoltage limited to an acceptable level.

For successful single-pole reclosing there must be an adequate time between the extinction of the secondary arc and reclosure, for deionization and re-establishment of the dielectric strength between the arc electrodes. However, there is little information available about this time. The results of a staged-fault test on 230 kV systems indicated that 2 cycles provide sufficient time for deionization[78]. There is also information from laboratory tests on residual arcs over 400 kV and 765 kV V-strings insulators, with line capacitance simulated by capacitors. The paper[31] on those tests states that 40 ms is adequate for deionization. Some information is also available from the TVA tests[16], in one test the line was re-energized only one cycle (1/60 s) after arc extinction and the arc was re-established.

However, the result of a test on 500 kV suspension string shows that this time is dependent on the secondary arc extinction time[70]. This is due to the effect of the secondary post arc gas, i.e. when the arc extinction time of the secondary arc is considerably long, the primary luminous gas cloud has disappeared by that time, and the dielectric recovery resembled that of the independent secondary arc. This information, though perhaps inconsistent, gives a general idea of the necessary deionization time.

In this chapter, the methods used for simulating circuit breaker reclosures in the Frequency Domain, at the end of the dead time, are described[34]. The reclosure time is controlled so that closing the breaker will happen when the voltage across the breaker terminals is zero (or minimum).

6.2 Breaker Re-closure Technique

Having determined the total time varying response across the sending and receiving end breakers, it is possible to inject an equal and opposite voltage to the latter such that at breaker closure at time say T_{bc} the total voltage across the breaker is zero.

At a certain time, say 0.5s after fault inception, the sending and receiving end circuit breaker terminals is checked for zero voltage crossing. The closing of the pole in which the voltage first passes through zero is simulated by an injected voltage, equal and opposite to the relaying point voltage at the breaker terminals. As outlined in reference 34, this part of simulation is again essentially one of superposition and can best be explained with reference to Fig. 6.1 which shows a line to ground (LG) fault occurs and the breakers in phase 'a' are opened to clear the fault. The total voltage across the sending and receiving end breakers are $e_{Sa}(t)$ and $e_{Ra}(t)$ respectively.

$$e_{Sa}(t) = 0, \quad t < T_{b1}$$

$$e_{Ra}(t) = 0, \quad t < T_{b2}$$

T_{b1}, T_{b2} represent the time at which the sending and receiving end breakers open respectively.

If time after fault (allowing for the breaker opening time, arc extinction time, and insulator recovery time) at which the first zero crossing of say the sending-end a-phase voltage across the breaker terminals occur is T_{b5}, then the frequency spectrum $\bar{E}_{S5a}$ of voltage which is injected into the opposite direction to simulate a-phase sending-end pole reclosing is given by:

$$\bar{E}_{S5a} = -\int_{T_{b5}}^{T_{ob}} e_{Sa} \exp\left[-j(\omega - j\alpha)\right] t \, dt \qquad (6.1)$$

$\bar{I}_{S5a}$ in Fig. 6.2 is the frequency spectrum of a current source which arises due to the injection of voltage $\bar{E}_{S5a}$.

The 9 x 9 admittance matrix of eqn. 3.6 (chapter 3) is used again to define the current and voltage relationship shown in eqn. 6.2 (see Fig. 6.2).

$$\begin{bmatrix} \bar{I}_{F5a} \\ \bar{I}_{F5b} \\ \bar{I}_{F5c} \\ \bar{I}_{S5a} \\ \bar{I}_{S5b} \\ \bar{I}_{S5c} \\ \bar{I}_{R5a} \\ \bar{I}_{R5b} \\ \bar{I}_{R5c} \end{bmatrix} = \begin{bmatrix} & & \\ Y_1 & Y_2 & Y_3 \\ & & \\ & & \\ Y_4 & Y_5 & Y_6 \\ & & \\ & & \\ Y_7 & Y_8 & Y_9 \\ & & \end{bmatrix} \begin{bmatrix} \bar{E}_{FF5a} \\ \bar{E}_{FF5b} \\ \bar{E}_{FF5c} \\ \bar{E}_{S5a} \\ \bar{E}_{S5b} \\ \bar{E}_{S5c} \\ \bar{E}_{R5a} \\ \bar{E}_{R5b} \\ \bar{E}_{R5c} \end{bmatrix} \qquad (6.2)$$

Eqn. 6.2 can be solved in the same way used to solve eqn. 3.6 in the opening breaker technique. The eight known zero-valued transforms are $\bar{I}_{F5a,b,c}$, $\bar{I}_{R5a}$, $\bar{E}_{S5b,c}$ and $\bar{E}_{R5b,c}$. The ninth known value is $\bar{E}_{S5a}$.

With reference to eqn. 6.2, all rows and columns that correspond to zero-valued transforms in the voltage vector can be removed, to produce the reduced matrix relationship of eqn. 6.3 and its inverse 6.4.

$$\begin{bmatrix} 0 \\ 0 \\ 0 \\ \bar{I}_{S5a} \\ 0 \end{bmatrix} = \begin{bmatrix} Y_1(1,1) & Y_1(1,2) & Y_1(1,3) & Y_2(1,1) & Y_3(1,1) \\ Y_1(2,1) & Y_1(2,2) & Y_1(2,3) & Y_2(2,1) & Y_3(2,1) \\ Y_1(3,1) & Y_1(3,2) & Y_1(3,3) & Y_2(3,1) & Y_3(3,1) \\ Y_4(1,1) & Y_4(1,2) & Y_4(1,3) & Y_5(1,1) & Y_6(1,1) \\ Y_7(1,1) & Y_7(1,2) & Y_7(1,3) & Y_8(1,1) & Y_9(1,1) \end{bmatrix} \begin{bmatrix} \bar{E}_{FF5a} \\ \bar{E}_{FF5b} \\ \bar{E}_{FF5c} \\ \bar{E}_{S5a} \\ \bar{E}_{R5a} \end{bmatrix} \quad (6.3)$$

$$\begin{bmatrix} \bar{E}_{FF5a} \\ \bar{E}_{FF5b} \\ \bar{E}_{FF5c} \\ \bar{E}_{S5a} \\ \bar{E}_{R5a} \end{bmatrix} = \begin{bmatrix} Z_1(1,1) & Z_1(1,2) & Z_1(1,3) & Z_2(1,1) & Z_3(1,1) \\ Z_1(2,1) & Z_1(2,2) & Z_1(2,3) & Z_2(2,1) & Z_3(2,1) \\ Z_1(3,1) & Z_1(3,2) & Z_1(3,3) & Z_2(3,1) & Z_3(3,1) \\ Z_4(1,1) & Z_4(1,2) & Z_4(1,3) & Z_5(1,1) & Z_6(1,1) \\ Z_7(1,1) & Z_7(1,2) & Z_7(1,3) & Z_8(1,1) & Z_9(1,1) \end{bmatrix} \begin{bmatrix} 0 \\ 0 \\ 0 \\ \bar{I}_{S5a} \\ 0 \end{bmatrix} \quad (6.4)$$

From eqn. 6.4, $\bar{I}_{S5a} = \bar{E}_{S5a}/Z_5(1,1)$ (6.5)

Substituting for $\bar{I}_{S5a}$ in eqn. 6.4, the transforms $\bar{E}_{FF5a,b,c}$ and $\bar{E}_{R5a}$ are obtained. Further substitution of the resulting known voltage vector $\left[\bar{E}_{FF5a} \;\; \bar{E}_{FF5b} \;\; \bar{E}_{FF5c} \;\; \bar{E}_{S5a} \;\; \bar{E}_{R5a}\right]^T$ into the full admittance matrix eqn. 6.2 enables the remaining current transforms values to be obtained.

These are then transformed back into the time domain using the Fourier Transform techniques. The total time domain response of say the voltage across the sending and receiving end breakers at this stage would then be:

$$\left.\begin{aligned} e_{S1a}(t) &= e_{Sa}(t - T_{b2}) + e_{S5a}(t - T_{b5}) \\ e_{R1a}(t) &= e_{Ra}(t - T_{b3}) + e_{R5a}(t - T_{b5}) \end{aligned}\right\} \quad (6.6)$$

where $t = 0 \rightarrow T_{ob}$

The above process is then repeated for the second breaker reclosure, to give the total overall response.

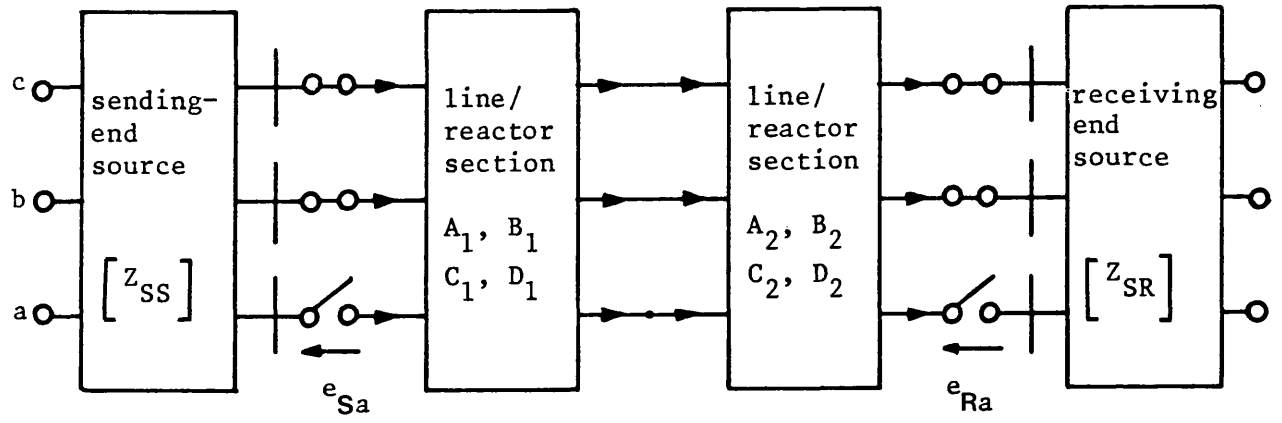

Fig. 6.1 Basic system model

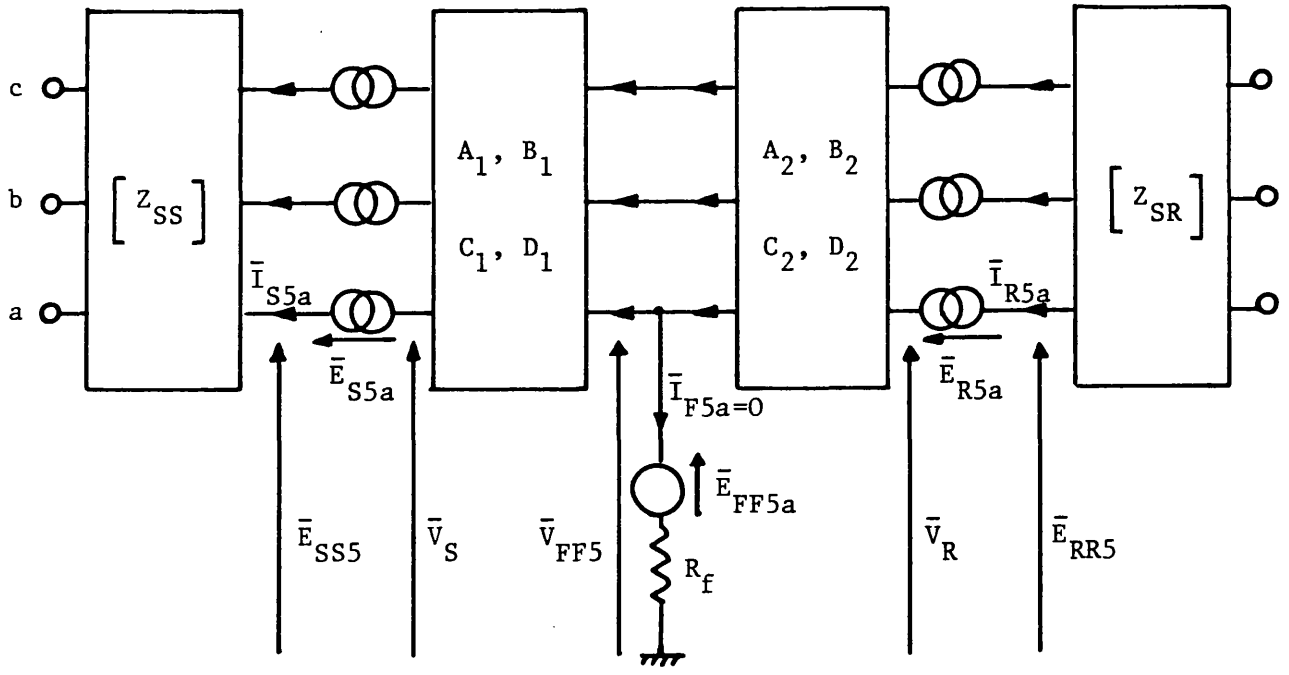

Fig. 6.2 Frequency-domain superimposed-system model

CHAPTER 7

PARAMETERS OF SYSTEM STUDIED

7.1 Introduction

The computational results presented in this work are for two different systems:

1) Uncompensated short line (120 km)
2) Compensated long line (300 km)

Both systems can be single-section or 4-section feeder systems. Both lines are regularly transposed through three equal intervals and the long line is compensated by the 4-reactor scheme located at each line end. The single-section feeder is fed at its remote-ends by the main sources s.c.1 and s.c.2. The 4-section feeder systems is fed by s.c.1 and s.c.2 at its remote-end; other infeed/outfeed s.c.3, s.c.4 and s.c.5 are also considered. Both systems compromise 500 kV, single-circuit transmission line(s).

In this chapter the parameters of transmission line(s), shunt reactors, line infeed/outfeed and that used in the Fourier transform routine are presented.

7.2 Transmission Line Parameters

7.2.1 Line construction

Fig. 7.1 shows the typical quad. conductor 500 kV line configuration considered. The positions of the conductors illustrated correspond to the positions over the first one third of the line

section from the sending end of any discretely transposed section.

The data for the line are:

1) Phase conductors = 4 x 477 MCM Al alloy,
   21.5 mm overall equivalent, 242 mm^2 Al equivalent,
   19/4.3 mm stranding
2) Shield wires = 7/3.5 mm Alumoweld
3) Earth resistivity = 100 Ωm
4) Distance between arcing horns (ℓ_o) = 4.05 m
5) Conductor resistance = 0.0217512 Ω/km (at 50 Hz)
6) Earth wire resistance = 1.0916841 Ω/km (at 50 Hz)
7) Conductor reactance = 0.00380647 Ω/km (at 50 Hz)
8) Earth wire reactance = 0.3877944 Ω/km (at 50 Hz)
9) For the two systems considered, line lengths are:
   a) For the single-section feeder system, uncompensated, ℓ = 120 km
   b) For the single-section feeder system, compensated, ℓ = 300 km. For the 4-section feeder system line lengths are 300, 300, 150 and 150 km from the sending-end to the receiving end respectively.

The frequency variation of all earth and conductor parameters is simulated.

7.2.2 Computed basic parameters

The line series impedance $[Z]$ and shunt admittance $[Y]$ matrices at power frequency are shown below. The methods used to calculate $[Z]$ and $[Y]$ are described in Appendix (2.2).

$$[Z] = \begin{bmatrix} .1019 + j.5011 & .0791 + j.1856 & .0813 + j.2273 \\ .0791 + j.1856 & .1019 + j.5011 & .0813 + j.2273 \\ .0813 + j.2273 & .0813 + j.2272 & .1049 + j.4979 \end{bmatrix} \times 10^{-3} \ \Omega/m \quad (7.1)$$

$$[Y] = \begin{bmatrix} .3443485 & -.01972752 & -.0643521 \\ -.01972752 & .3443486 & -.0643521 \\ -.0643521 & -.0643521 & .3586486 \end{bmatrix} \times j10^{-8} \ \Omega^{-1}/m \quad (7.2)$$

From eqns. 7.1 and 7.2, the propagation constant matrix γ, the surge impedance matrix Z_o, and the corresponding surge admittance matrix Y_o are calculated.

7.2.3 Secondary arc current and recovery voltage (capacitive components only)

The shunt admittance matrix Y is used to calculate the zero and positive sequence capacitances of the line as follows:

$$[Y] = \begin{bmatrix} Y_{11} & -Y_{12} & -Y_{13} \\ -Y_{21} & Y_{22} & -Y_{23} \\ -Y_{31} & -Y_{32} & Y_{33} \end{bmatrix} \ \Omega^{-1}/m \quad (7.3)$$

As the line is assumed to be transposed, averages of the self and mutual terms may be made

$$[Y_T] = \begin{bmatrix} Y_s & -Y_m & -Y_m \\ -Y_m & Y_s & -Y_m \\ -Y_m & -Y_m & Y_s \end{bmatrix} \ \Omega^{-1}/m \quad (7.4)$$

where

$[Y_T]$ is the shunt admittance matrix for a transposed line

$$Y_s = (Y_{11} + Y_{22} + Y_{33})/3.0$$

$$Y_m = (Y_{12} + Y_{13} + Y_{23})/3.0$$

With reference to the matrix eqn. 7.2

$$Y_s = j\ 3.4911523 \times 10^{-9} \quad \Omega^{-1}/m$$

$$Y_m = j\ 0.4947724 \times 10^{-9} \quad \Omega^{-1}/m$$

The transposed line capacitance matrix is[24]:

$$[C] = Y_T / j\omega_o = \begin{bmatrix} C_s & -C_m & -C_m \\ -C_m & C_s & -C_m \\ -C_m & -C_m & C_s \end{bmatrix} \quad F/m$$

where

$$C_s = 1.11126 \times 10^{-11} \ F/m$$

$$C_m = 0.15749 \times 10^{-11} \ F/m$$

From these self and mutual terms, the positive sequence and zero sequence values may be determined[24]:

$$C_1 = C_s + C_m = 1.26875 \times 10^{-11} \ F/m$$

$$C_o = C_s - 2C_m = 0.79628 \times 10^{-11} \ F/m$$

The line capacitance ratio[43] (K) is:

$$K = C_o/C_1 = 0.62761 \qquad (7.5)$$

The steady-state secondary arc current assuming a zero secondary arc resistance is[3,14,15]:

$$I_{sec} = -j\omega_o C_m E_a \qquad (7.6)$$

where

$$E_a = \frac{500{,}000}{\sqrt{3}}\sqrt{2} = 408248 \text{ peak volts}$$

$$I_{sec} = 2.01988 \times 10^{-4} \text{ A/m (peak)}$$

The steady-state recovery voltage is[3.14,15]:

$$V_r = -\frac{E_a}{2 + \frac{C_o}{C_m}} = -0.141722\, E_a \qquad (7.7)$$

$$= -57858 \text{ V (peak)}$$

7.3 Shunt Reactor Parameters

In this section, the calculated reactor parameters are presented. The shunt reactor has three quantities to be defined[43]:

1) The degree of the positive sequence shunt compensation h_1
2) The degree of the zero sequence shunt compensation h_o
3) The phase and neutral 'Q' factor, where Q = X/R

Eqn. 7.8 (which is described in chapter 2) is used to calculate the value of h_o required to limit the capacitive component of the steady-state secondary arc current to a certain value for an assumed value of h_1.

$$I_{sec.p.u.} = I_{sec}/I_b = -(H_1 - kH_o)/3 \qquad (7.8)$$

where

$$I_b = j\omega_o C_1 E_a$$

$$H_1 = (1 - h_1),\ H_o = (1 - h_o)$$

For a typical value of $h_1 = 0.75$

$I_{sec.p.u.} = 0$ when $h_o = 0.6016635$

This represents the optimum neutral reactor (neglecting the effect of the electromagnetic coupling). In this case

X_n = j 733.1 Ω (at power frequency)

X_p = j 2230.1 Ω (at power frequency)

Or under optimum conditions the ratio $X_o/X_1 = 1.986$.

For 300 km line, I_b = j 488 A (peak) and I_{sec} = j 60.6 A (peak). To limit the capacitive component of the steady-state secondary arc current to -j 20 A (r.m.s.), the value of h_o is:

$I_{sec.p.u.} = -0.0579595$

$h_1 = 0.75$

$h_o = 0.8787121$

The neutral inductance (X_n) in this case is equal to 267.5 Ω ($X_o/X_1 = 1.359$). The recovery voltage under this condition is equal to -123.2 kV (peak).

A 'Q' factor of 250 was assumed for neutral and phase reactor.

7.4 Source Parameters

7.4.1 Single-section uncompensated system (120 km)

Sending end source capacity s.c.1 = 1500 MVA.

Receiving end source capacity s.c.2 = 5000 MVA

Sources X/R ratio = 100

Sources $Z_{SO/ZS1}$ ratio = 0.5 - 1.0

7.4.2 Single-section compensated system (300 km)

Sending end source capacity s.c.1 = 5000 MVA

Receiving end source capacity s.c.2 = 5000 MVA

Sources X/R ratio = 100

Sources Z_{S0}/Z_{S1} ratio = 1.0

7.4.3 Four-section compensated system (300 km, 300 km, 150 km, 150 km)

Sources X/R ratio = 100

The sources Z_{S0}/Z_{S1} ratio and their capacities starting from sending end are:

s.c.1 = 0.25 GVA , Z_{S0}/Z_{S1} = 0.4

s.c.2 = 5.0 GVA , Z_{S0}/Z_{S1} = 1.0

s.c.3 = 5.0 GVA , Z_{S0}/Z_{S1} = 1.0

s.c.4 = 1.0 GVA , Z_{S0}/Z_{S1} = 0.5

s.c.5 = 5.0 GVA , Z_{S0}/Z_{S1} = 0.5

The line under study in this system is the second section from the left (300 km).

7.5 Modified Fourier Transform Parameters

In the single pole autoreclosure analysis, the Modified Fourier Transform method is used. In this case, the basic frequency ($\Delta\omega$), the maximum number of samples (N) and the frequency shift constant (α) may affect the system responses. Therefore appropriate values for these quantities should be used[79,80,81].

In the present studies, these parameters are taken as follows:

Observation time 'T_{ob}' = 0.8192 sec

Frequency shift constant 'α' = 7.67

Number of samples 'N' = 4096

Truncation frequency 'Ω' = 2.5 kHz

These quantities are calculated on the following basis:

$$\Delta\omega = \pi/T_{ob}$$

$$\alpha = 2\Delta\omega = 2\pi/T_{ob}$$

$$\Omega = N/2T_{ob} \quad \text{Hz}$$

The calculated responses are accurate only for a time up to about 85% of T_{ob}. Then the Gibbs oscillation appears in the waveshapes.

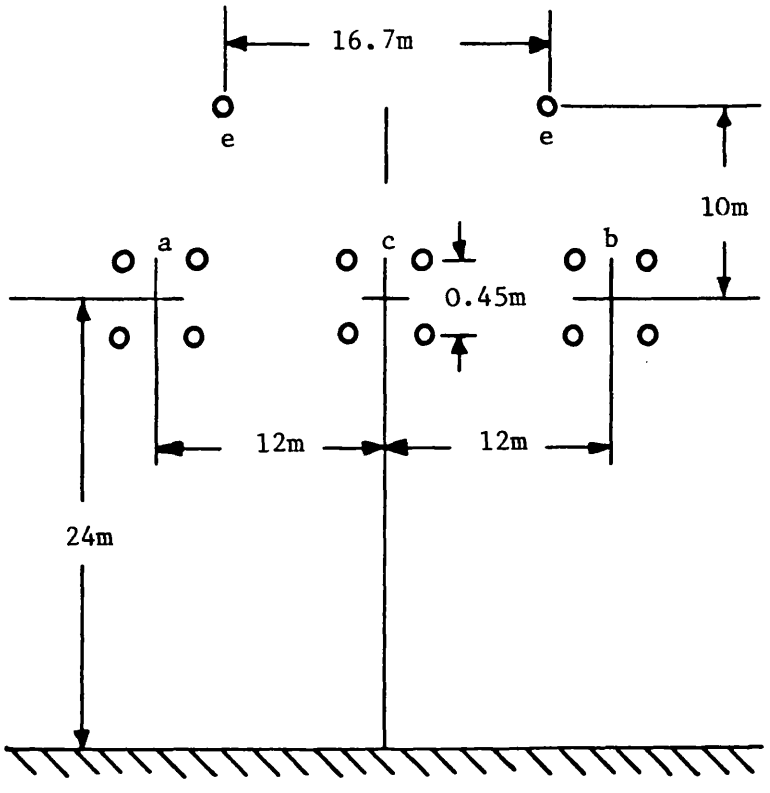

Fig. 7.1 500 kV horizontal line construction

CHAPTER 8

SYSTEM STUDIES: UNCOMPENSATED LINE

8.1 Introduction

The mathematical model of the secondary arc path, as developed in chapter 4 and 5, is used in this chapter to obtain the system response. The fault simulation, breakers opening and reclosure techniques are described in chapters 2, 3 and 6.

The results of many research works, both in the field and laboratories, show that the magnitude of the secondary arc current, amplitude and the steepness of wavefront of the recovery voltage, are among the most essential factors affecting the extinction time of the secondary arc[8,10,31,5,30]. Several factors can affect the ıdes of the secondary arc current and recovery voltage. These fault location, line length, transmission-line loading, ɔsition and parameters of terminal stations. However, there ıer factors which play important roles in the extinction time, ıs the wind velocity and the type and length of the insulator ngs.

To justify the digital simulation of the secondary arc path it felt necessary to consider the effect of the above mentioned factors ıe extinction time of the secondary arc. The transmission line ısidered to be discretely transposed at 40 km intervals along ɔngth of 120 km and to have the following features:

1) The capacitive component of the steady-state secondary arc current is approximately 17.14 A (r.m.s.) and, as such, is below the level generally deemed necessary for the use of shunt reactor compensation.
2) Faults are simulated on the 'a' phase at various point (x_f) along the feeder.
3) Various breaker opening times are studied with current interruption at the breakers occurring at or very close to a current zero, i.e. small current chopping.
4) Breakers reclosure occurs when the voltage across the breaker terminals is minimum.
5) The capacity of the sending and receiving end sources are 1500 and 5000 MVA respectively.
6) The fault is applied at the maximum point on the wave, except in one case where the fault is applied at zero voltage.
7) The arc length variation, unless otherwise stated, takes the following form:

$$\ell_a(t)/\ell_o = \begin{cases} 1.0 \ , & t < 0.1s \\ 10\ t \ , & t > 0.1s \end{cases} \qquad (8.1)$$

8.2 Effect of Fault Position: Zero Power Transfer ($V_S/V_R = 1\angle 0^o$)

8.2.1 Fault at the sending end

The system under study, as shown in fig. 8.1, is assumed to be at steady-state conditions until the occurrence of the fault at time T_1. The sending end phase 'a' breaker opens first at time T_2, followed by the receiving end breaker opening at time T_3. The steady state secondary arc current waveform is shown in fig. 8.2a. This

waveform is based upon a constant secondary arc resistance of 0.5 Ω as mentioned in chapter 3. The system Thevenin impedance (Z_T) and Thevenin voltage ($e_T(t)$) waveforms are shown in fig. 8.2b,c. The magnitude of the secondary arc current (fig. 8.2a) is approximately equal to the calculated value which has been shown in the previous chapter. The peak to peak value of the Thevenin voltage is approximately twice the peak value of the recovery voltage which has also been calculated in chapter 7. The Thevenin voltage waveform has a d.c. offset which characterises the breaking of a capacitive circuit.

Figs. 8.3-8.5 show several features of the system throughout the whole process of single phase fault clearing and autoreclosure, when the non-linear arc characteristic is used. With reference to fig. 8.3a it can be seen that the voltage at end S (voltage across arc path for this fault) drops on fault inception time (T_1) from the normal peak phase to earth voltage of approximately 408.2 kV to the relatively low primary arcing voltage. After fault isolation at time T_3 the arc voltage builds up gradually until final extinction at time T_4. It is of interest to note that the recovery voltage across the fault arc path in the period ($T_4 - T_5$) is almost fully offset. This phenomena, which has been experimentally observed by several authors[3,8,10,5,27], occurs because the faulted phase is effectively floating during the time interval T_4 to T_5. At arc extinction, all the energy within the faulted phase is thus manifested in the form of a steady uni-directional trapped charge voltage, the power frequency voltage coupled from the energised sound phases being superimposed thereon. The peak to peak value of the power frequency component of the recovery voltage is approximately 115.2 kV, and this compares with a theoretical value, as outlined by simple steady-state

analyses[3,14,15], of approximately 115.7 kV.

Successful autoreclosure is achieved at times T_5 and T_6, the arc reignition voltage being sufficiently high to withstand the momentary switching surge-type overvoltage that occurs principally during the 6 ms time interval between reclosure at ends S and R. It can be seen from fig. 8.4a that the voltage observed at the end R remote from the fault exhibits the usual high frequency travelling wave induced distortion during the primary arc period[47]. Considerable high frequency distortion also occurs subsequent to clearance at end R at time T_3, the most likely cause of which is low level clearing induced travelling waves within the faulted phase being in transit between the secondary arc point and the now open-circuited R end. Smilar effects are observed near final arc extinction at time T_4, but in this case the travelling waves giving rise to high frequency oscillations are induced by the collapse of voltage across the secondary arc following sudden re-strike. Figs. 8.3d and 8.4d show the variation of the faulted phase currents at either end. It is evident that the action of autoreclosure at end R produces uni-directional current waves for about 4 cycles of power frequency. This feature is of importance in relation to the performance of protection equipment. Figs. 8.3e,f and 8.4e,f illustrate also the sound phase currents at the sending and receiving ends. It is of interest to note that the sound phase currents do not reduce immediately subsequent to clearance at end S because, in the time interval T_2 to T_3 current is fed to the fault from the remote end R. The high current in the faulted phase causes a longitudinal induced voltage to occur along the whole length of the sound phases, and this in turn forces the relatively high sound phase currents to continue to flow throughout

the whole of the primary arc period T_1 to T_3.

The behaviour of the fault arc path is illustrated in fig. 8.5. With reference to fig. 8.5a, the reduction of the primary arc current following clearance at end S is evident. The transition to secondary arcing is also evident, although the secondary arc current is relatively so small that the detail in the period T_3 to T_4 has to be appreciated from fig. 8.5b. The effect of the arc length increase is most marked in the voltage waveform (fig. 8.5c) which exhibits the expected constant voltage type characteristic. Both the secondary arc voltage and current are characterised by an initial relatively high noise period of duration approximately 10 ms, during which time significant high frequency oscillations occur. The second stage of the arc consists of relatively smooth non-linear waveforms which contain only low levels of high frequency distortion. The partial extinctions of the arc as final extinction is approached are particularly evident from the current waveform of fig. 8.5b. A comparison of fig. 8.5b and c near final extinction shows clearly the rise in voltage across the arc path during zero current time, followed by rapid voltage collapse and an associated high current spike caused by arc re-ignition. It is of interest to note that the three distinct stages of the secondary arc and their characteristic features were first observed experimentally by Maury[3], but to the best of the author's knowledge, they have not previously been simulated. The fact that such phenomena are reproduced is of importance in that it provides some evidence of the validity of the new techniques presented in this study. It may further be noticed from fig. 8.5b that the peak of the secondary arc current during the essentially periodic second stage of the arc is nearly constant at approximately 25 A. This figure compares favourably with a value of approximately 24.3 A obtained for the line in question

when using the simple steady-state analytical method of Maury[3].

8.2.2 Fault at the mid-point

Fig. 8.6 illustrates the secondary arc behaviour following a mid-point fault. A comparison with fig. 8.5b shows that the extinction time is the same in the two cases. The faulted phase voltage and current waveforms at the sending and receiving end during the whole process of single pole autoreclosure is shown in fig. 8.7. It can be seen from fig. 8.7b that the high frequency distortion which occurs subsequent to clearance at end R is lower than the previous case, the same effect is observed near final arc extinction. A comparison of the faulted phase current (fig. 8.7c,d) at either end, following re-energisation, with the previous case, shows that the offset in the current waveform is much lower for the mid-point fault. This is mainly due to the effect of the sequence of the breaker reclosure rather than the fault position. In this case the two breakers closed simultaneously, 495.6 ms after the fault inception, when the voltage across the breakers terminal is minimum. Whilst in the previous case the receiving end breaker closed 6 ms after the reclosure of the sending end breaker.

A similar study of the extinction time for a remote end fault at R shows that the extinction time in this case is 11 ms shorter than the case of a sending end fault. Such results show that the extinction time does not vary significantly with fault position under lightly loaded conditions.

8.3 Effect of Prefault Loading

The variation of the extinction time with fault position is in fact more marked when the prefault power transfer is significant. Under such conditions, the larger sound-phase currents induce a much

more significant longitudinal voltage in the faulted phase during the secondary arc period[7,14,6]. These longitudinal electromagnetically induced voltages contribute to the total current that circulates through the secondary arc path and to the recovery voltage across the latter, following partial or final extinction with concomitant effect upon the final extinction time.

The magnitude and phase of the electromagnetically induced component of the secondary arc current and voltage, relative to the more significant and well known component due to electrostatic coupling between the faulted and sound phases, has been found to depend heavily on fault position[6,14].

8.3.1 Fault at the sending end: power transfer from sending to receiving end ($V_S/V_R = 1/10^o$)

Fig. 8.8 illustrates the secondary arc behaviour following a fault at end S when the prefault power transfer from end S is approximately 1262 MW. It is of interest to note that the secondary arc extinction time is significantly longer than the unloaded case. Also evident is the significantly greater post-extinction recovery voltage. In such cases, the arc recovery voltage thus rises more rapidly after extinction and this in turn largely accounts for the longer time required for final extinction to occur. It can be seen from fig. 8.9 that the voltage observed at the end R, remote from the fault, does not increase with time, during the period T_3 to T_4, as was the case for the unloaded line (fig.8.4d). This is due to the effect of the electromagnetic coupling. In this case it should be noted that the electromagnetic coupling component is essentially constant in magnitude during the period T_3 to T_4 and the component due to the voltage developed

A comparison of this case with 8.2.2 shows that the extinction time is 38 ms shorter, the secondary arc current and recovery voltage are also much smaller. These two cases should have the same results if the line is untransposed and has identical short circuit capacity at either end. It is of interest to note that the effect of the power transferdirection on the secondary arc current has been observed experimentally by Lambert et However, the authors have explained this phenomenon as being due to the difference between the sending and receiving end short circuit capacity. In this respect several Digital Computer results indicate that using two identical sources produces insignificant differences when compared with the results obtained with two different sources, especially if the fault occurs at the lower source capacity. It is concluded that the discrete transposition of the line is the main reason for this phenomenon.

8.3.4 Fault at the receiving end; power transfer from receiving to sending end = 1/-10°)

The behaviour of the secondary arc following a fault at the receiving end R is shown in fig. 8.15. A comparison of fig. 8.15 and 8.13 shows that the extinction time is increased by approximately 18.8 ms. The sending end voltage during the period T^ - T^ has the decreasing characteristics as shown in fig. 8.15c. It must be pointed out that the extinction time is still lower than the unloaded case by approximately 10 ms for the same fault position.

Two identical sources are used in another study, and the results show no significant difference in the extinction time or recovery voltage. Such results show that the extinction time varies significantly with fault position and direction of power transfer under normal loaded conditions. It is concluded that the secondary arc extinction time is

largest for faults near the power exporting end.

8.4 Effect of Source Sequence Impedance Ratio

The results presented so far assume the ratio of the zero sequence impedance to the positive sequence impedance (Z_{S0}/Z_{S1}) is unity. However, this is not always the case in practice. Based on steady-state calculations, it has been shown that the secondary arc current and the recovery voltage decreases slightly as the ratio Z_{S0}/Z_{S1} increases[18]. Fig. 8.16 shows the secondary arc current and voltage waveforms following a sending end fault, when V_S/V_R = $1 \angle 10^o$ and Z_{S0}/Z_{S1} = 0.5. A comparison with fig. 8.8 shows that the secondary arc extinction time increases slightly (about 10 ms) when Z_{S0}/Z_{S1} decreases from 1 to 0.5. The reduction of Z_{S0} actively results in an increase in the zero-phase sequence current flowing through the sound phase conductors during the secondary arc period and this in turn increases the electromagnetically coupled induced voltage in the faulted phase. This increased level of longitudinally induced voltage results in a slightly increased level of secondary arc current and recovery voltage as evidence from fig. 8.16. A considerable increase in the faulted phase voltage during the period $T_3 - T_4$ can also be observed from fig. 8.16c.

8.5 Effect of Breaker Operation Time

The results presented so far assume the normal fault duration ($2\frac{1}{2}$ - $3\frac{1}{2}$ cycle) which is in practice at the present time. However, a recently developed fast breaker has been tested which is able to isolate the fault 1 - $1\frac{1}{2}$ cycle after the fault inception[49]. The effect of the fault duration is examined for a mid-point fault, unloaded line, both breakers opened simultaneously 30 ms after the fault inception. The results of the secondary arc current and voltage

waveforms do not show any difference in the extinction time. Thus, although the duration of the fault can influence the rate and manner in which both the secondary arc length and re-ignition voltage vary[3], they do not otherwise significantly affect the extinction process in the uncompensated line.

8.6 Effect of Fault Inception Time

Fig. 8.17 illustrates the secondary arc behaviour following a mid point fault, unloaded line, when the prefault a-e voltage is zero. Although the primary fault current has a different waveform, the secondary arc extinction time does not change. This is due to the fact that the fault inception time does not affect the secondary arc current or recovery voltage waveforms in the uncompensated line.

8.7 Effect of Transposition

For a line with one complete round of conductor transpositions, the secondary arc current and recovery voltage for faults at the different phase conductors presents some symmetry about the mid point of the line. However, for an untransposed line, the secondary arc current and recovery voltage for the unlike conductors differ by an appreciable amount, with only a degree of symmetry in the middle phase. Fig. 8.18a,b illustrates the secondary arc behaviour following a fault at the sending end, untransposed line, when the power transfer from the receiving end is approximately 1262 MW. A comparison of figs. 8.18a,b and 8.13 shows the contribution of the conductor transposition in lowering the secondary arc extinction time.

Ignoring the electromagnetic coupling effect, the centre phase of an untransposed line possesses the greatest mutual coupling and hence

experiences the severest arcing conditions. Fig. 8.18c,d illustrates the secondary arc behaviour following a fault on the centre phase 'c', for an unloaded and untransposed line. A comparison of fig. 8.18c,d with fig. 8.5 shows that the secondary arc current and recovery voltage is much higher in this case, and in consequence the extinction time is 80 ms longer when the line is untransposed.

8.8 Effect of the Rate of Increase of Arc Length

The results presented so far assume the arc length to vary according to eqn. 8.1. However, wind velocity and the magnitude of the secondary arc current may alter these variations. Fig. 8.19 illustrates the secondary arc behaviour following a mid-point fault, unloaded line, with a relatively lower rate of increase of the arc length. The arc length variation in this study takes the following form:

$$\ell_a(t)/\ell_o = \begin{cases} 1 \ , \ t < 0.125 \text{ s} \\ 8t \ , \ t > 0.125 \text{ s} \end{cases} \qquad (8.2)$$

A comparison of figs. 8.19 and 8.6 shows that the extinction time is 30 ms longer in this case, even though the secondary arc current and recovery voltage are still the same. This phenomenon has been observed experimentally by Maury[3]. The author concluded that if the wind speed is 4 to 5 m/s the extinction time is very short. The author found also that the rate of increase of the arc length depends on the magnitude of the secondary arc current and it could reach 10 m/s in the 220 kV system.

8.9 Effect of the Line Length on Extinction Time

Several authors have shown that the extinction time increases almost linearly with the increase of the secondary arc current, for the same recovery voltage[10,5,31,8,30]. It is therefore felt necessary to examine the extinction times for different line length with the same recovery voltage (approximately 115 kV peak to peak). The lines are assumed to be unloaded and each line has a complete round of conductor transposition.

Fig. 8.20 illustrates the secondary arc currents following a fault at the sending end S for different line length (ℓ = 120, 135, 240, 300 km). It can be noticed from this figure that the extinction times increase significantly with the increase of the line length. It is of interest to note that the measured extinction times compare very favourably with experimental results obtained by several authors[10,8,31,8]. As an example, it can be seen from fig. 8.20d that the extinction time in the 300 km unloaded line (43.3 A r.m.s.) is approximately 453 ms, while reference 10 shows that the extinction time of a 42.5 A (r.m.s.) is 500 ms. However, the author used a shorter air gap (3.3 m) which leads to a higher recovery voltage gradient, and this accounts very much for the longer extinction time[8].

It must be pointed out that the extinction time will be almost independent of the line length, for the same recovery voltage, if the arc length variation ($\ell_a(t)$) and the re-ignition voltage ($v_r(t)$) are simulated to be independent on the magnitude of the secondary arc current. This can be explained with reference to figs. 8.21 and 8.2. It can be seen from these two figures that the steady-state value of the Thevenin impedance is inversely proportional to the line length,

while the steady-state value of the secondary arc current is linearly proportional to the line length. However, the peak to peak value of the Thevenin voltage is independent of the line length.

A close examination of the Convolution equation 5.5 which is described in chapter 5 indicates that the term $\sum_{k=1}^{n-1} Z_T (n - k) i_{arc}(k)$ is independent of the line length. This makes the factors which will determine the extinction time to be : (1) $v_{arc}(t)$, (2) $v_r(t)$, and (3) $e_T(t)$.

8.10 Representation of the Secondary Arc Path by a Time Dependent Linear Resistance

The effect of the secondary arc resistance on the magnitude of the secondary arc current and the extinction time has been discussed by several authors[3,28,30,26,32]. Balser et al[32] has simulated the secondary arc path by a linear resistance that is assumed to vary linearly with time up to final extinction and which then suddenly attains an infinite value. The latter approach is of generally rather limited value because it is specific to one system for which the results of fault throwing tests were previously obtained[16]. The point at which the arc resistance increases suddenly to infinity is rather difficult if not impossible to determine. Reference (73) states that, after arc transition the secondary arc voltage increases with time, while the secondary arc current hardly decreases, until it reaches 75% to 95% of the steady state recovery voltage after which the arc is self extinguished. However, the latter has simulated the line capacitance by an inductance. The extinction mechanism is different for a capacitive circuit than for an inductive circuit[60]. In the inductive circuit the recovery voltage is symmetrical, while

the recovery voltage in the capacitive circuit is almost fully offset. Furthermore, in the capacitive circuit the partial extinction in the secondary arc leads to higher peaks in the secondary arc voltage. This phenomenon does not exist in the inductive circuit[27,10,25]. In the compensated system the problem is more difficult, as the transient recovery voltage is more important than the steady state value. This makes the point at which the arc resistance increase to infinity is almost impossible to accurately define.

The variation of the secondary arc resistance with time has been described by Anjo et al[30]. Fig. 8.22a, taken from the authors' paper, shows the secondary arc resistance/time variation for a secondary arc current of 31.5 A preceded by 5.74 cycles of 8 kA primary arc. The experiment was carried out in a 500 kV suspension strings with 4.05 m arcing horn gap. The authors also show that even during a halfcycle period, there is a considerable change in arc resistance (fig. 8.22b).

It is felt necessary to simulate the secondary arc path by a linear resistance for the purpose of comparison. Fig. 8.22c illustrates the arc path representation, where R_f represents the primary arc resistance (0.5 Ω) and R_{ao} represents the arc resistance immediately after the breakers tripping at T_3 and its value varies between 150-200 Ω [26,30]. The rate of increase of the secondary arc resistance is highly dependent on wind velocity[3]. Several authors indicated that the value of the secondary arc resistance could reach 1000 Ω just before the final extinction[26,29,3,30].

Eqn. 5.5 is used to define the relationship between Thevenin voltage ($e_T(t)$), Thevenin impedance (Z_T), arc voltage ($v_{arc}(t)$), and

arc current ($i_{arc}(t)$). The relation between the arc voltage and current is simply defined by eqn. 8.3.

$$v_{arc}(t) = R_a(t)\, i_{arc}(t) \qquad (8.3)$$

Then eqn. 5.5 is solved as discussed in chapter 5. Fig. 8.23 illustrates the secondary arc current and voltage waveforms following a fault at the sending end S, of a transposed and unloaded line, with initial secondary arc resistance (R_{ao}) of 200 Ω and a rate of increase of 2000 Ω per second. A closer examination of fig. 8.23a shows that the secondary arc current decreases by only 11.6% when the arc resistance increases from 0.5 Ω to 1200 Ω (at 0.5s after the arc transition). The results presented here are in line with the simple steady-state calculations carried out by Maury[3] (see Appendix 8.1). However, such a simulation does not account for the prediction of the secondary arc extinction time. Therefore, it is felt necessary to increase the secondary arc resistance to infinity at a time corresponding to the extinction time predicted by the non-linear arc representation. In this case the initial arc resistance and its rate of increase is chosen to produce an arc voltage approximately equal to the one previously observed (fig. 8.5). Under these conditions:

$$R_{ao} = V_p \ell_o / I_p \qquad (8.4)$$

and

$$R_a(t)/R_{ao} = \begin{cases} 1 & , \quad t < 0.1 \text{ s} \\ 10t & , \quad 0.1 < t < 0.264 \text{ s} \\ \infty & , \quad t > 0.264 \text{ s} \end{cases} \qquad (8.5)$$

where I_p represents the steady-state peak value of the secondary arc current and V_p represents the arc voltage gradient as defined in chapter 4.

Fig. 8.24a,b illustrates the secondary arc current and voltage waveforms under such conditions. A comparison of this result with that of fig. 8.24c,d (which is obtained by the non-linear arc representation) shows the following points:

1. The secondary arc current has some similarity in the first 20 ms after arc transition. The second stage, which exhibits a smooth linear waveform, is rather different from that observed when using the non-linear arc representation.

2. The high frequency distortion observed in the arc voltage during the first 10 ms is higher in the case of a linear arc resistance representation. This is due to the fact that the arc voltage, in this representation, is linearly proportional to the arc current.

3. The voltage waveform is smooth and linear in this case, and does not exhibit the constant voltage characteristic which is observed in the non-linear arc representation. The peak value of the arc voltage just before arc extinction is only 35% of the steady-state peak value of the recovery voltage. While the peak value of the transient recovery voltage in the case of non-linear arc representation reaches 80% just before the final extinction.

4. The high current and voltage spike which is observed in the non-linear arc representation does not appear when the arc is represented by a linear resistance.

The secondary arc current and voltage waveforms which are observed experimentally are closer to the results obtained here, using a non-linear arc path, than the linear arc representation[3,8,5,10,31].

However, even though the second method cannot be used to predict the extinction time accurately, it is nevertheless less demanding from the point of view of computer programming.

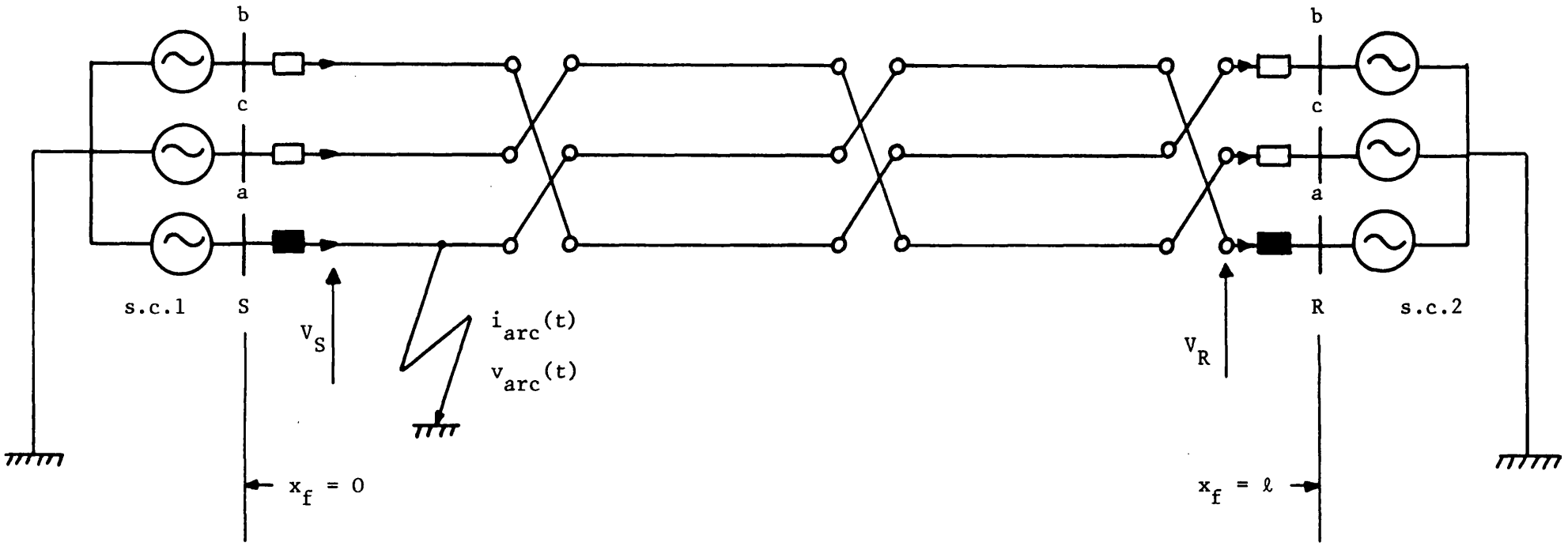

Fig. 8.1 System configuration

sen. end s.c.1 (s.c.1) = 1500 MVA
rec. end s.c.1 (s.c.2) = 5000 MVA

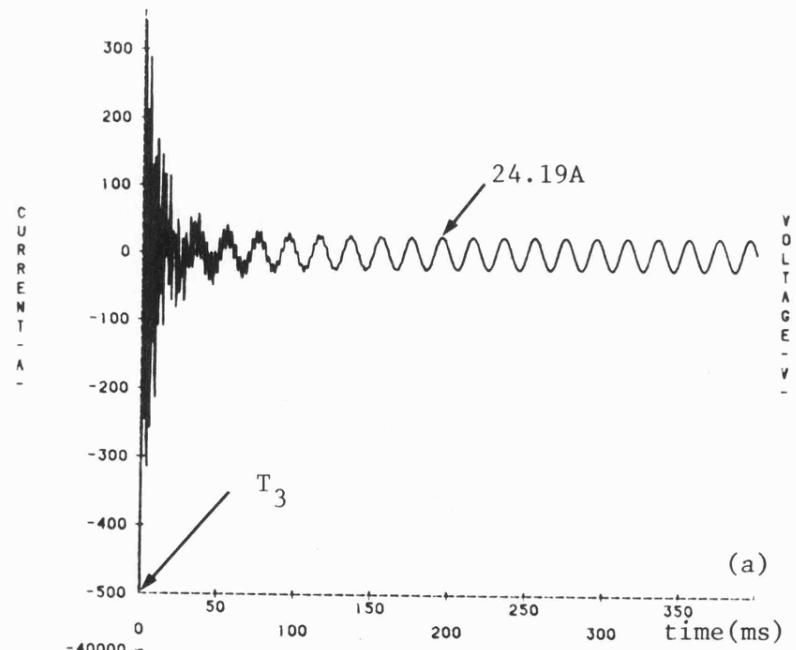

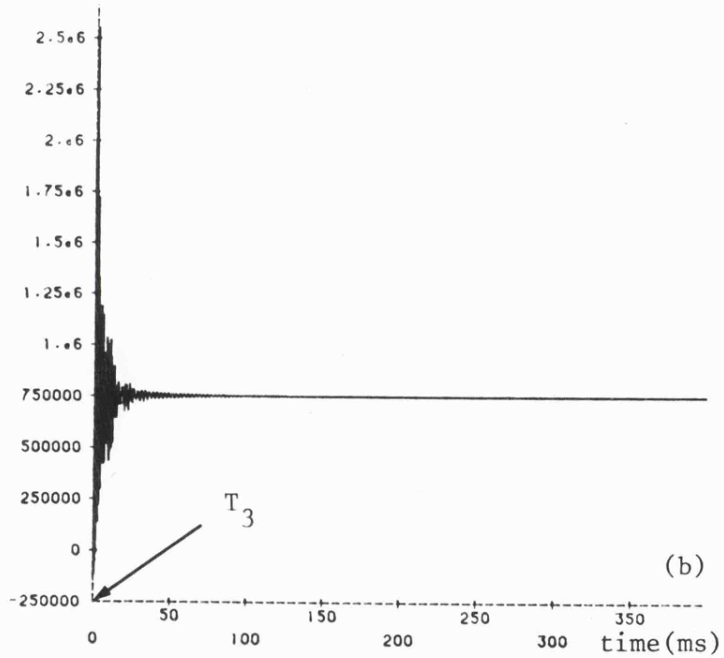

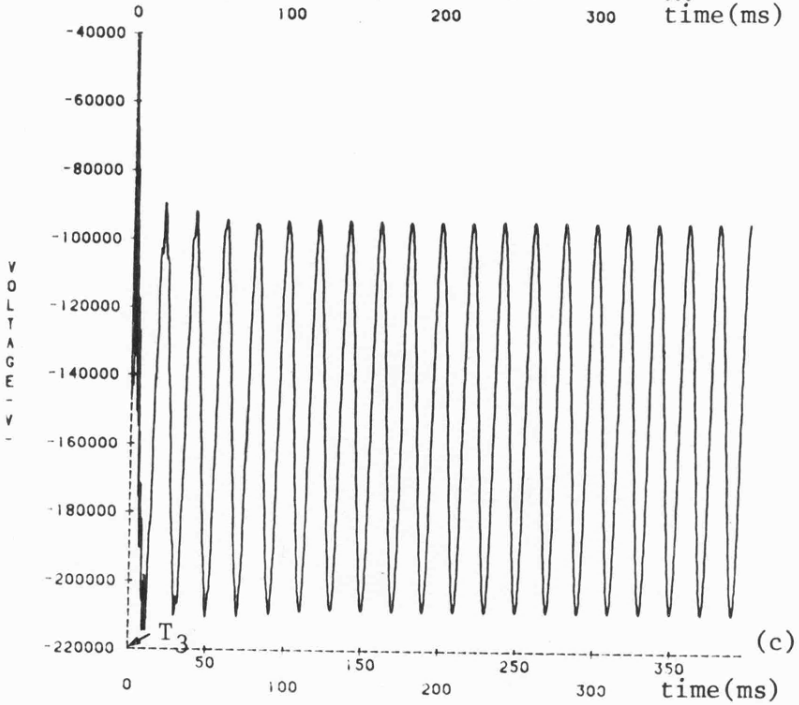

Fig. 8.2

System response for fault at end S

'a'-earth fault at peak of prefault 'a'-phase voltage

$x_f = 0$

ℓ = 120 km, transposed

sen. end s.c.l = 1500 MVA
rec. end s.c.l = 5000 MVA

$R_f = 0.5\Omega$

$V_S/V_R = 1\underline{/0^o}$

$Z_{S0}/Z_{S1} = 1.0$

T_3 = clearance by breaker at end R (70 ms after fault) = time of arc transition

(a) secondary arc current (constant arc resistance of 0.5Ω)
(b) Thevenin impedance
(c) Thevenin voltage

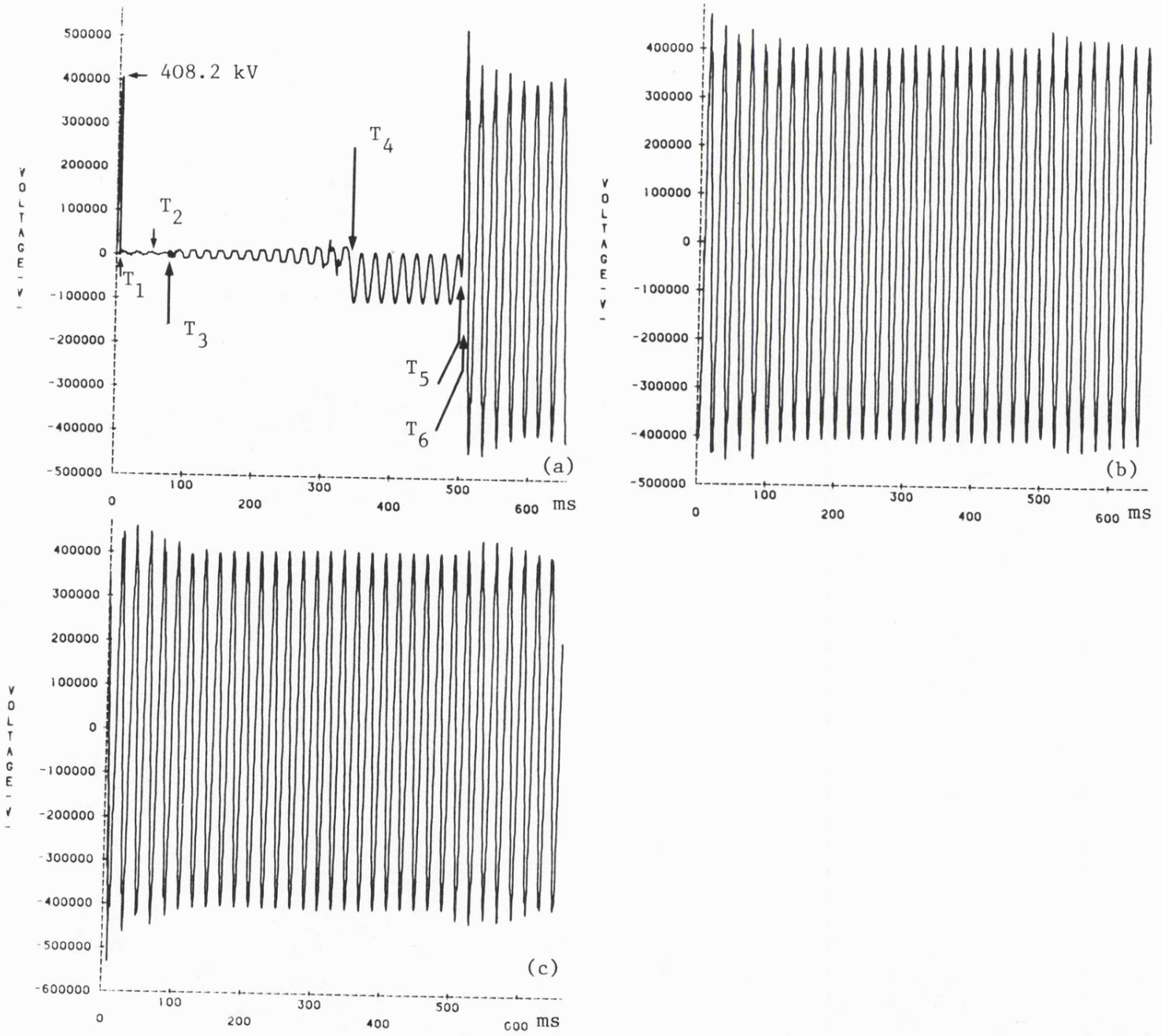

Fig. 8.3

Faulted and healthy phase-voltages and currents at end S

(a) 'a'-earth voltage
(b) 'b'-earth voltage
(c) 'c'-earth voltage
(d) 'a'-phase current
(e) 'b'-phase current
(f) 'c'-phase current

Fault conditions are stated in Fig. 8.2.

T_1 = fault inception (5 ms)

T_2 = clearance by breaker at S (50.2 ms after fault)

T_4 = final extinction of secondary arc (≃ 262.4 ms after arc transition)

T_5 = time of reclosure at S (≃ 495 ms after fault inception)

T_6 = time of reclosure at end R (≃ 500.8 ms after fault inception)

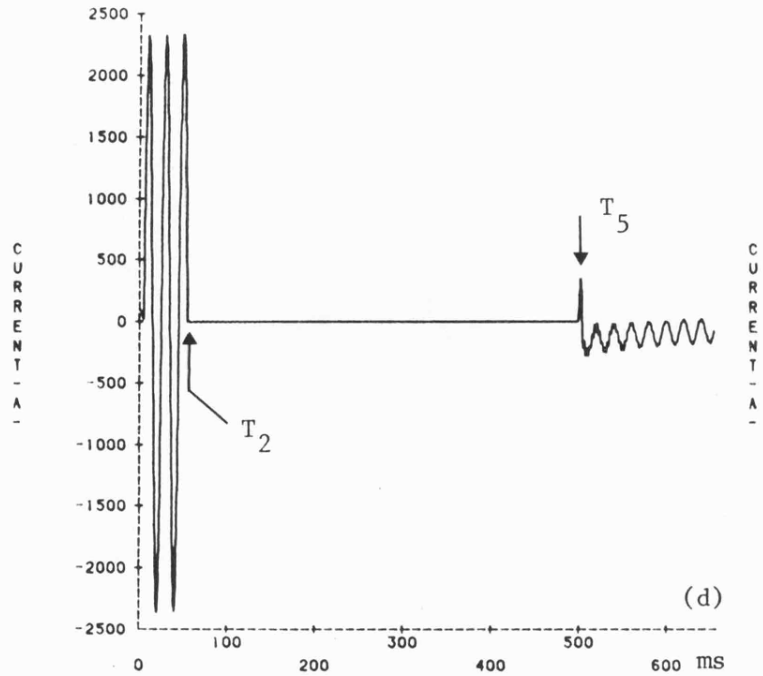

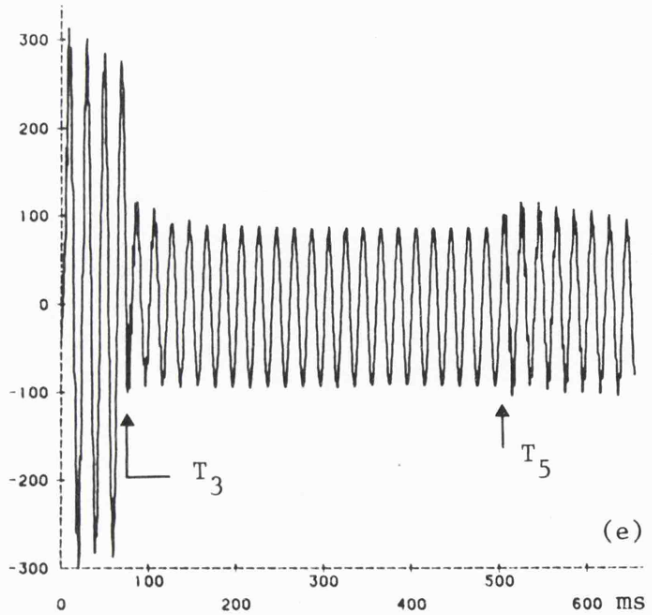

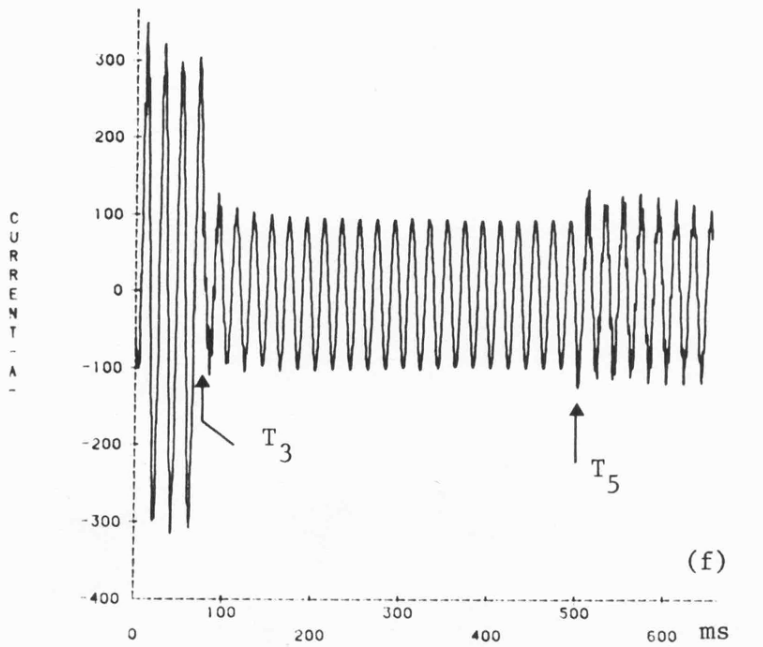

Fig. 8.3 (continued)

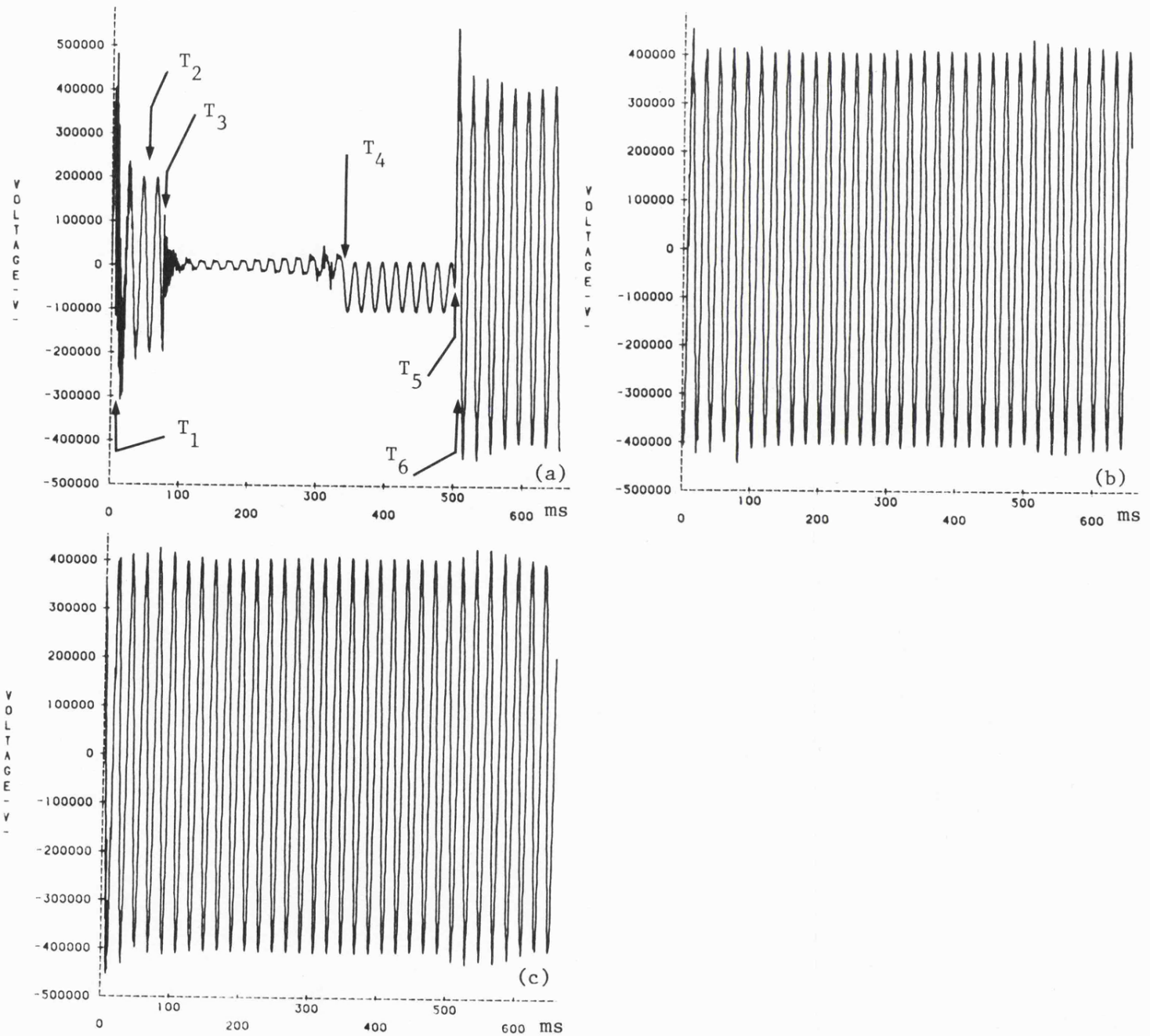

Fig. 8.4

Faulted and healthy phase-voltages and currents at end R

(a) 'a'-earth voltage
(b) 'b'-earth voltage
(c) 'c'-earth voltage
(d) 'a'-phase current
(e) 'b'-phase current
(f) 'c'-phase current

Fault conditions are stated in Fig. 8.2.

Fig. 8.4 (continued)

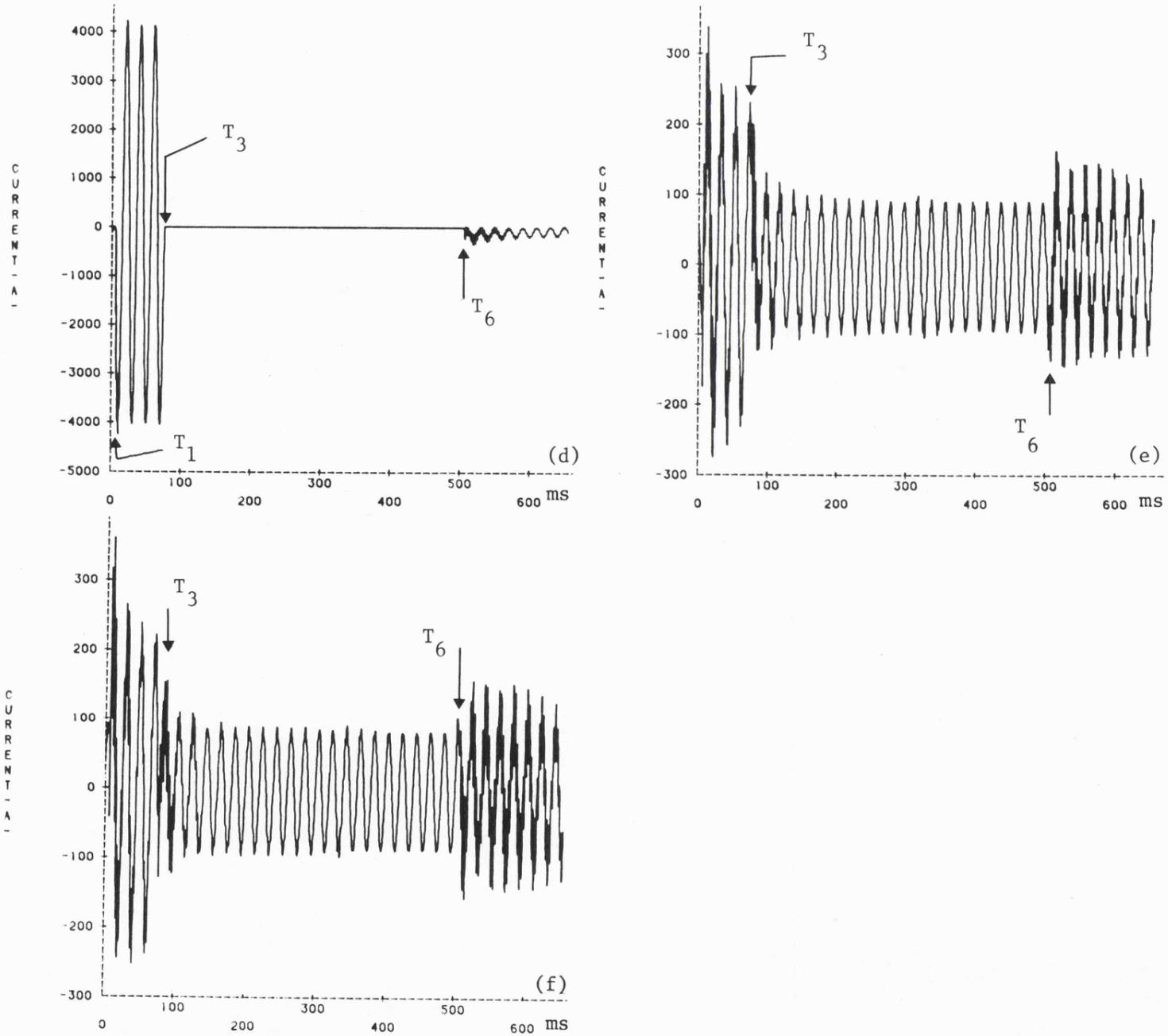

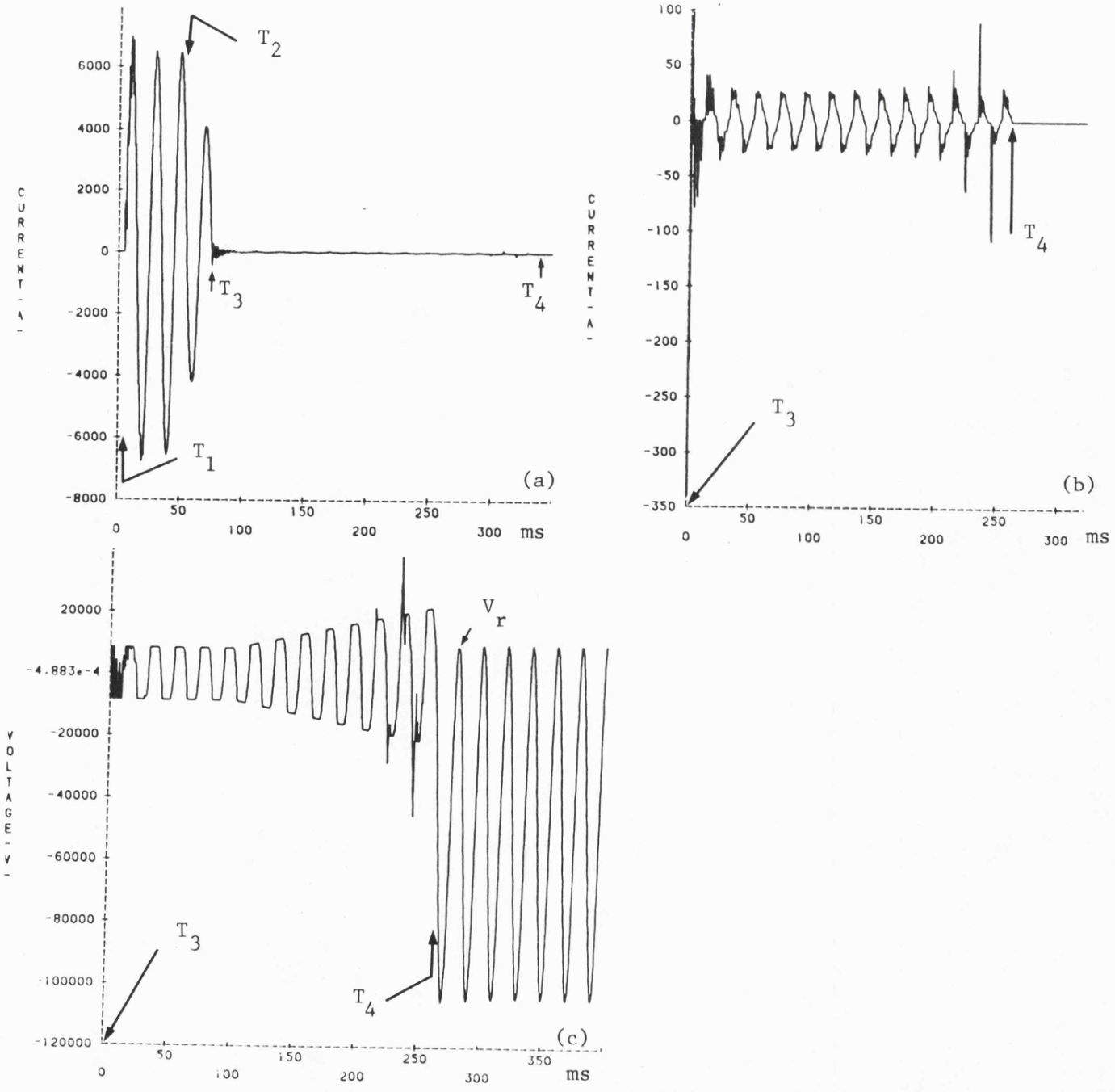

Fig. 8.5

Behaviour of secondary arc for fault at end S

(a) current in fault arc path
(b) secondary arc current
(c) secondary arc voltage

Fault conditions are stated in Fig. 8.2.

T_4 = 262.4 ms (after arc transition

V_r = 115.2 kV peak to peak

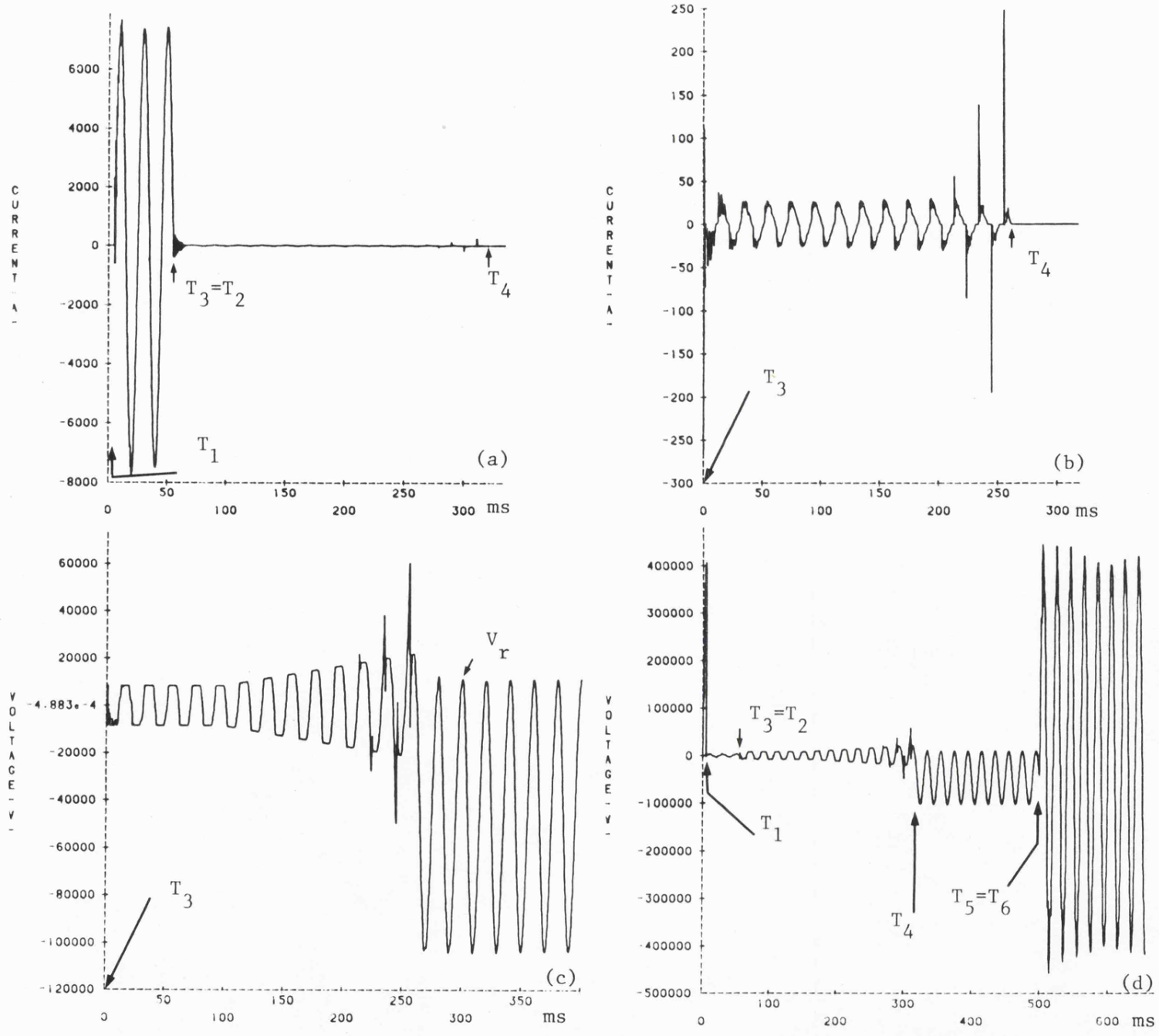

Fig. 8.6

Behaviour of secondary arc for midpoint fault

'a'-earth fault at peak of prefault 'a'-phase voltage

x_f = 60 km

T_1 = 5 ms

T_2 = 50 ms (after fault)

T_3 = 50 ms (after fault)

T_4 = 262.4 ms (after arc transition)

T_5 = 495 ms (after fault)

T_6 = 495 ms (after fault)

V_r = 115.2 kV (peak to peak)

Other fault conditions are similar to that of Fig. 8.2.

(a) current in fault arc path
(b) secondary arc current
(c) secondary arc voltage
(d) phase 'a' voltage at the fault point

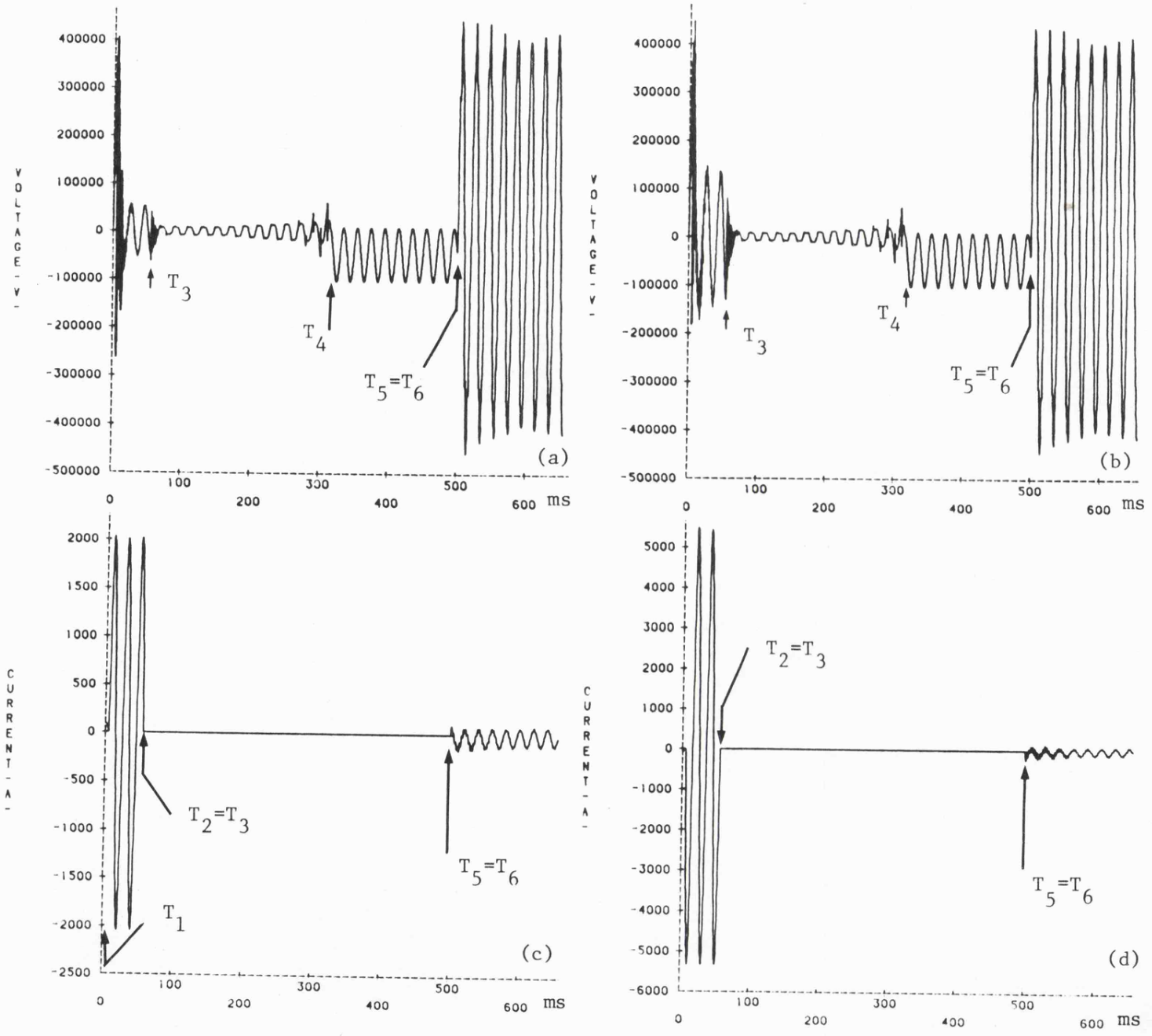

Fig. 8.7

Faulted phase-voltages and currents at ends S and R for midpoint fault

(a) 'a'-earth voltage at end S
(b) 'a'-earth voltage at end R
(c) 'a'-phase current at end S
(d) 'a'-phase current at end R

Fault conditions are stated in Fig. 8.6.

T_1-T_6 are stated in Fig. 8.6.

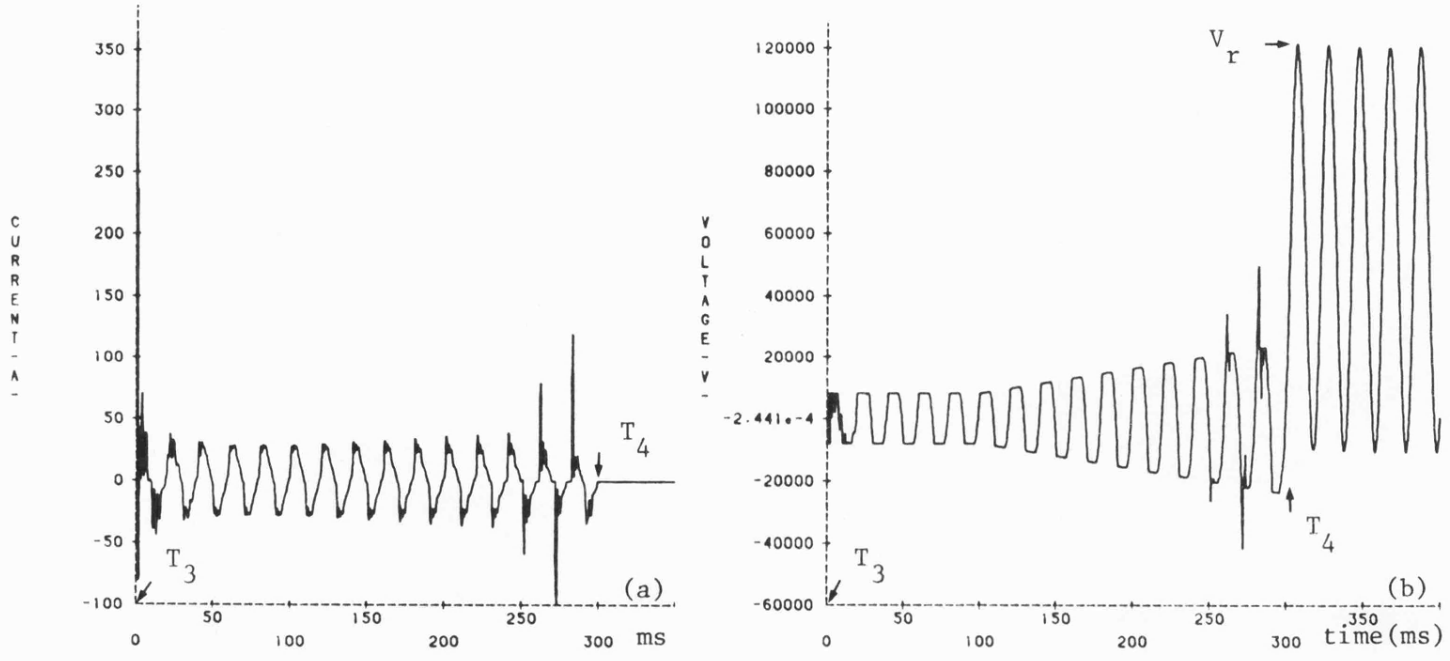

Fig. 8.8

Effect of pre-fault loading on arc extinction

'a'-earth fault at peak of prefault 'a'-phase voltage.

Fault at end S, $x_f = 0$

$V_S/V_R = 1/\underline{10}^o$ (pre-fault power exported from S to R)

$Z_{S0}/Z_{S1} = 1.0$

ℓ = 120 km, transposed

sending end s.c.l = 1500 MVA
receiving end s.c.l = 5000 MVA

$R_f = 0.5\Omega$

T_3 = 61.6 ms (after fault)

$T_4 \simeq$ 300 ms (after arc transition

$V_r \simeq$ 130.4 kV (peak to peak)

(a) secondary arc current
(b) secondary arc voltage

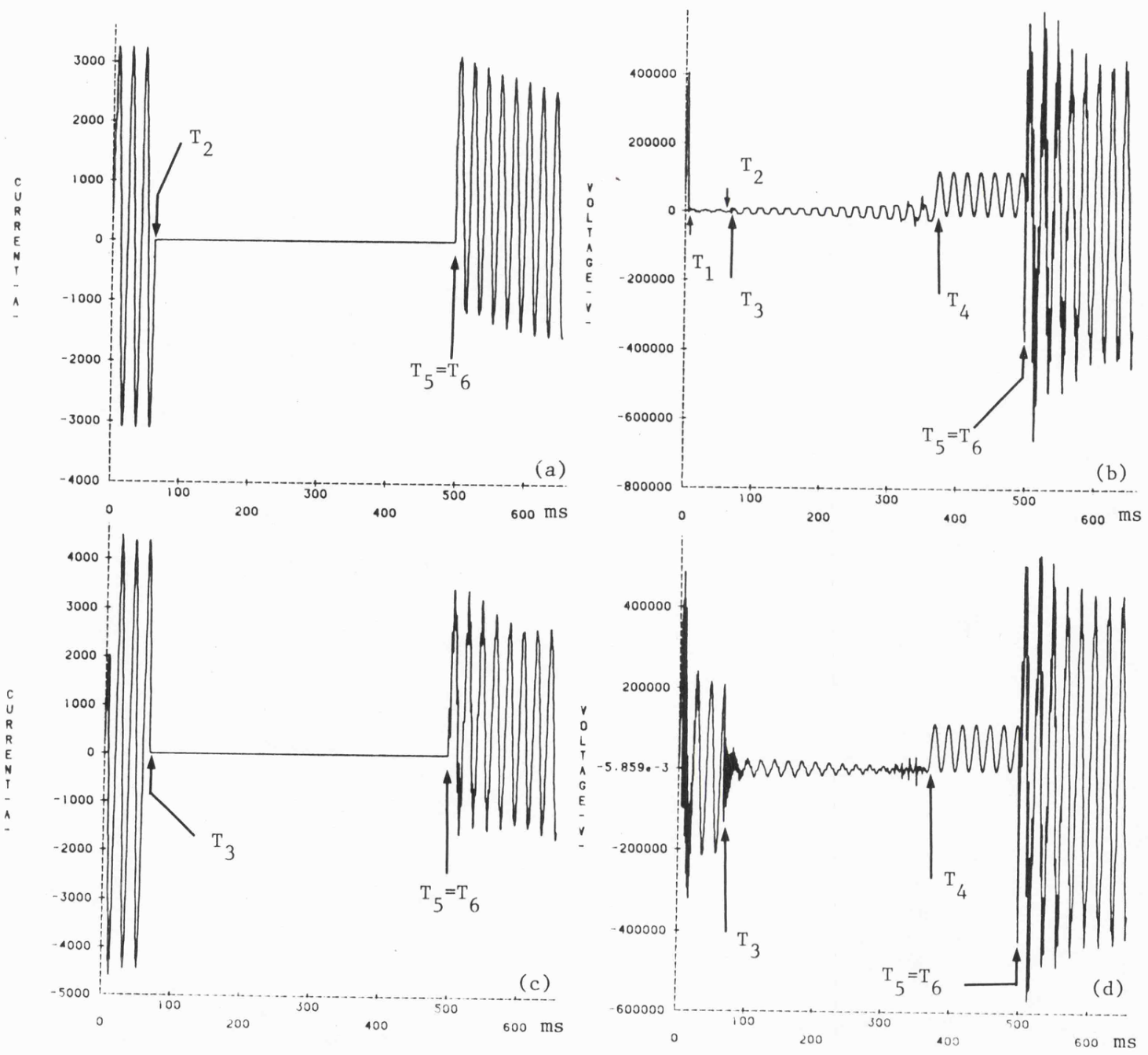

Fig. 8.9

Faulted phase-voltages and currents at ends S and R for fault at end S

T_1 = 4.5 ms
T_2 = 57.8 (after fault)
T_3 = 61.6 (after fault)
T_5 = 493.6 (after fault)
T_6 = 493.6 (after fault)

(a) 'a'-phase current at end S
(b) 'a'-earth voltage at end S
(c) 'a'-phase current at end R
(d) 'a'-earth voltage at end R

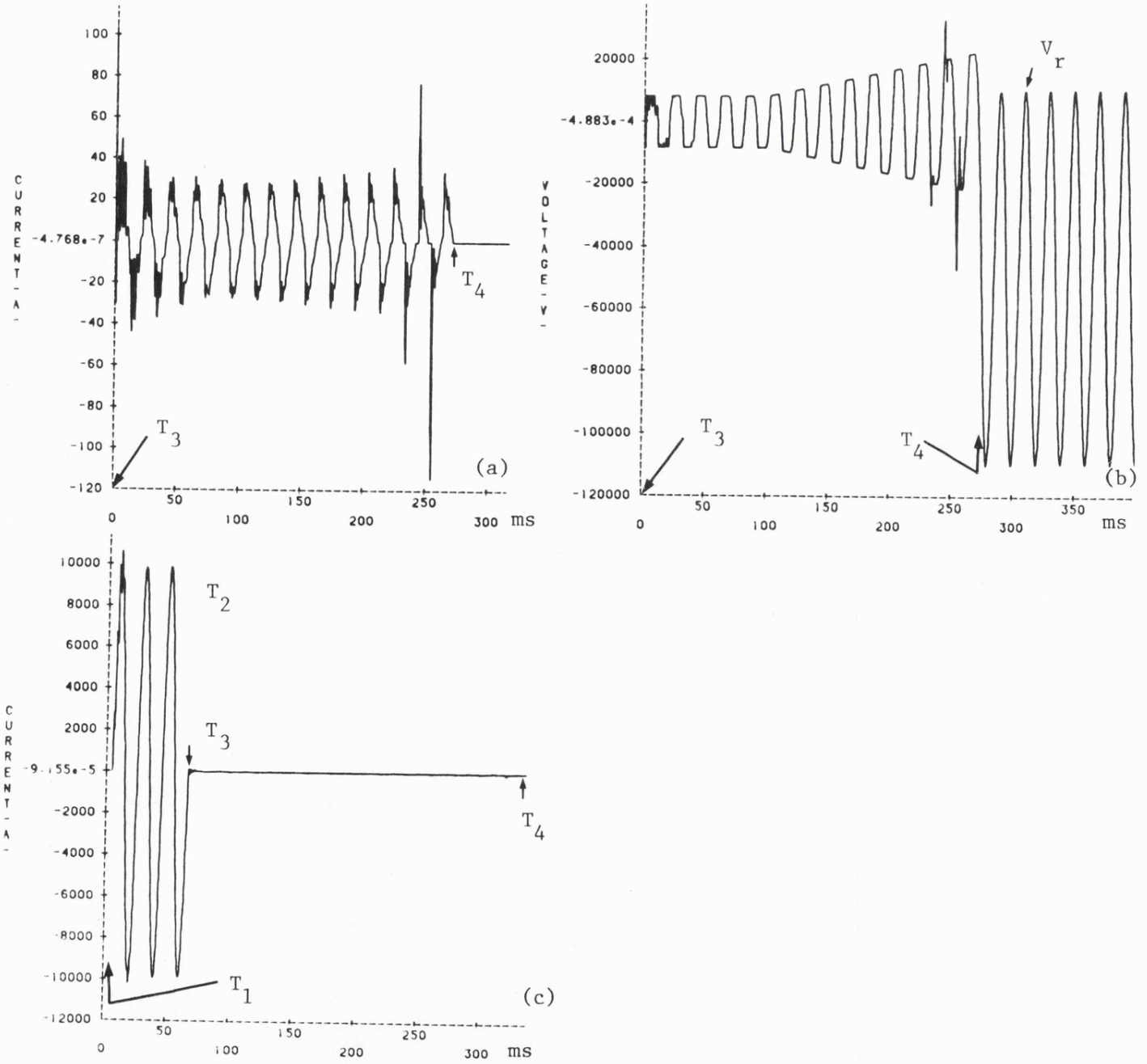

Fig. 8.10

Effect of pre-fault loading and fault position on arc extinction

'a'-earth fault at peak of pre-fault 'a'-phase voltage.

fault at end R, x_f = 120 km

$V_S/V_R = 1/\underline{10}^{\circ}$ (pre-fault power exported from S to R)

Z_{S0}/Z_{S1} = 1.0

ℓ = 120 km, transposed

sen. end s.c.l = 1500 MVA
rec. end s.c.l = 5000 MVA

$R_f = 0.5\Omega$

T_1 = 5 ms

T_2 = 57.2 ms (after fault)

T_3 = 60.8 ms (after fault)

T_4 = 272 ms (after arc transition)

$V_r \simeq$ 120.5 kV (peak to peak)

(a) secondary arc current
(b) secondary arc voltage
(c) current in fault arc path

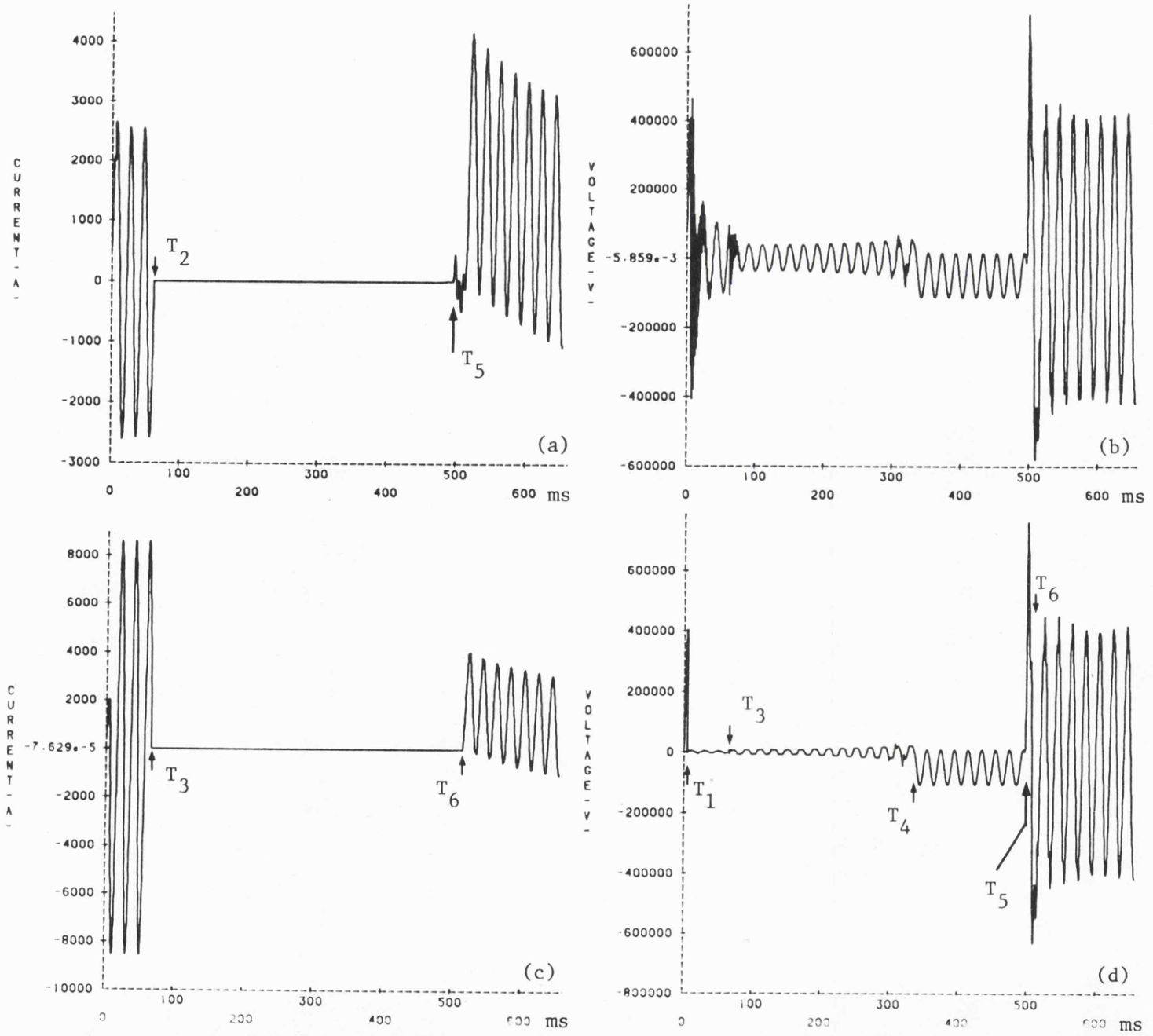

Fig. 8.11

Faulted phase-currents and voltages at ends S and R for fault at end R

T_5 = 492.4 (after fault)

T_6 = 510.8 ms (after fault)

Fault conditions are stated in Fig. 8.10

(a) 'a'-phase current at end S
(b) 'a'-earth voltage at end S
(c) 'a'-phase current at end R
(d) 'a'-earth voltage at end R

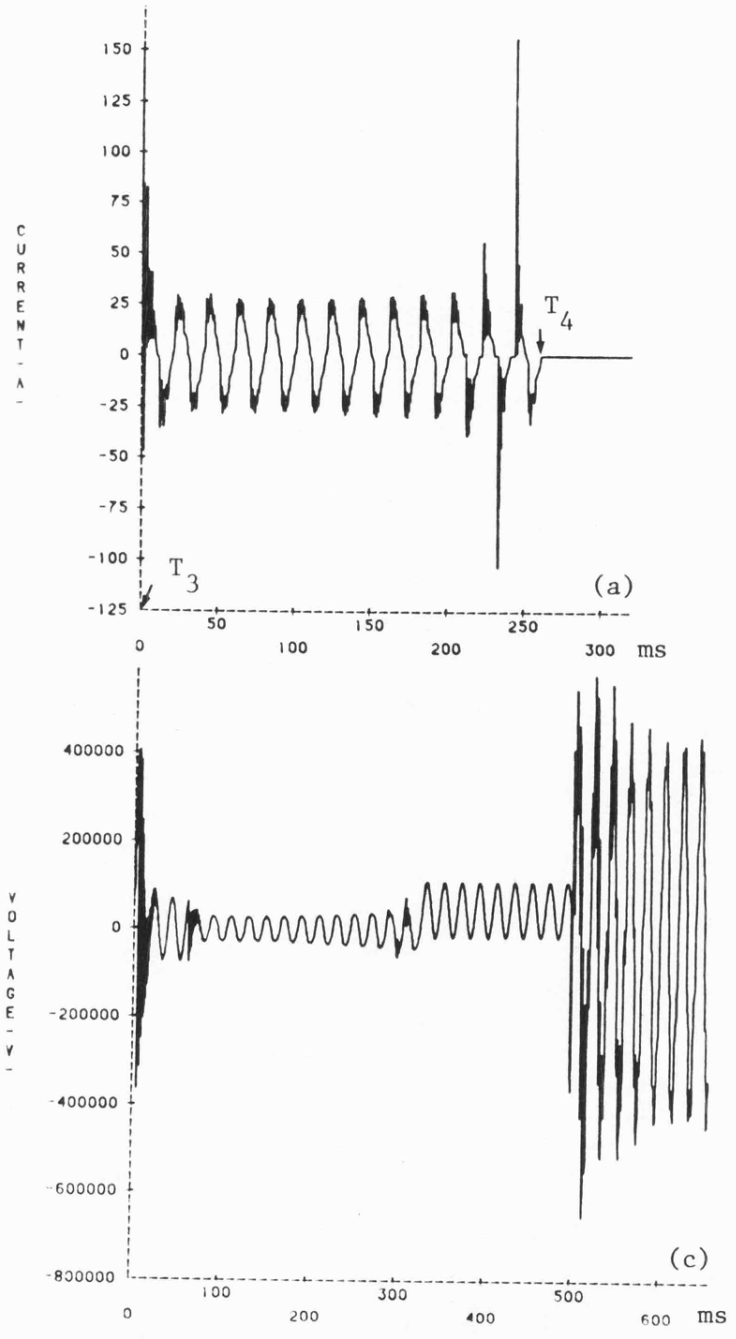

Fig. 8.12

Effect of fault position on arc extinction

'a'-earth fault at peak of prefault 'a'-phase voltage

fault at x_f = 80 km

ℓ = 120, transposed

$V_S/V_R = 1/\underline{10^o}$ (prefault power exported from S to R)

Z_{SO}/Z_{S1} = 1

sen. end s.c.1 = 1500 MVA

rec. end s.c.1 = 5000 MVA

T_1 = 5 ms

T_2 = 57.4 ms (after fault)

T_3 = 61 ms (after fault)

T_4 = 262.4 ms (after arc transition)

T_5 = 493.2 ms (after fault)

T_6 = 493.2 ms (after fault)

$V_r \simeq$ 116 kV (peak to peak)

(a) secondary arc current
(b) secondary arc voltage
(c) 'a'-earth voltage at end S
(d) 'a'-earth voltage at end R

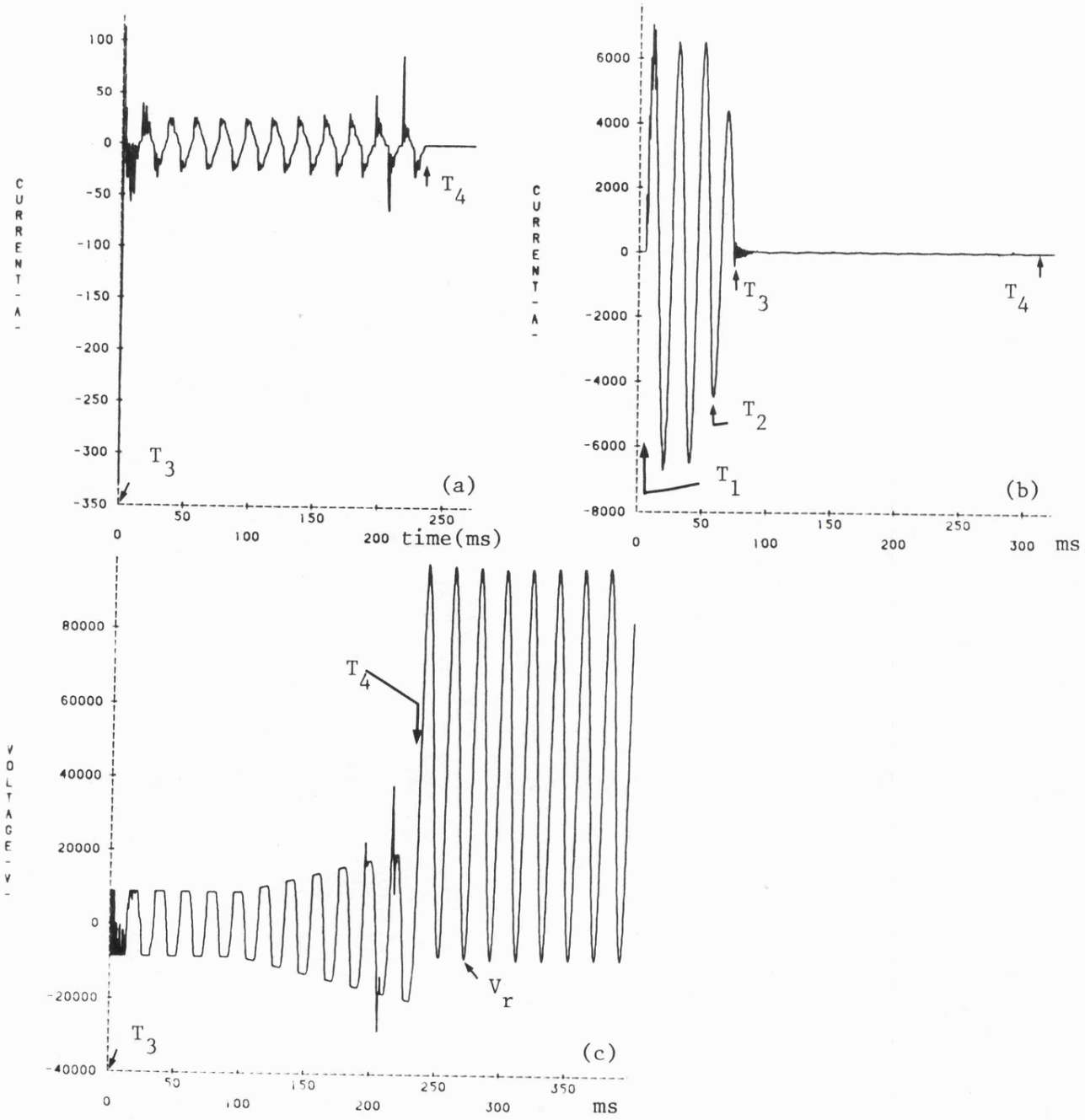

Fig. 8.13

Effect of power transfer direction on arc extinction

'a'-earth fault at peak of pre-fault 'a'-phase voltage

fault at end S, $x_f = 0$

ℓ = 120 km, transposed

$V_S/V_R = 1/\underline{-10^o}$ (prefault power exported from R to S)

$Z_{S0}/Z_{S1} = 1.0$

sen. end s.c.l = 1500 MVA
rec. end s.c.l = 5000 MVA

T_1 = 5.6 ms

T_2 = 52.2 ms (after fault)

T_3 = 68.4 ms (after fault)

T_4 = 233.6 ms (after arc transition)

$V_r \simeq$ 106 kV (peak to peak)

(a) secondary arc current
(b) current in fault arc path
(c) secondary arc voltage

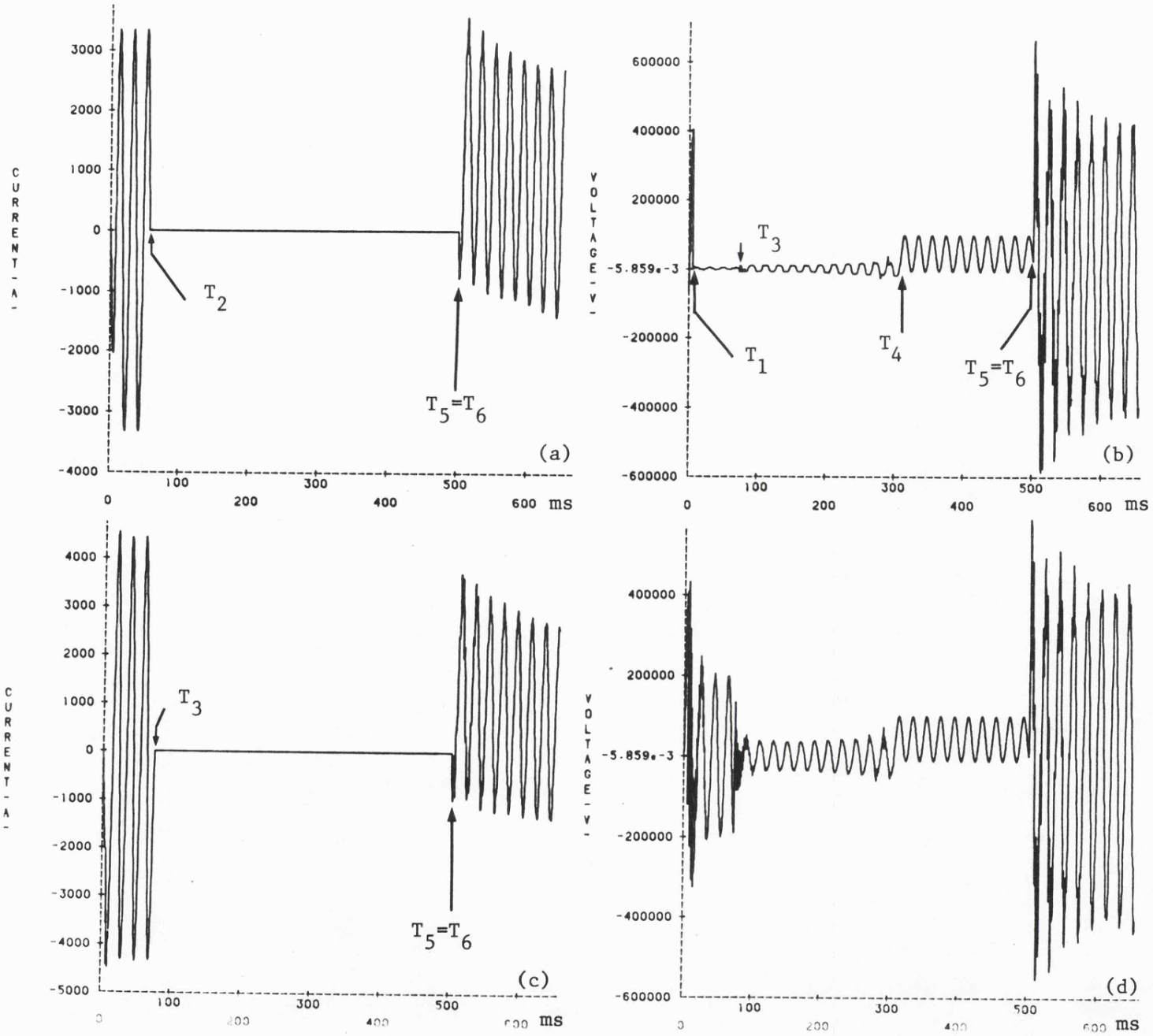

Fig. 8.14

Faulted phase-currents and voltages at ends S and R for fault at end S

T_5 = 497.4 ms (after fault)

T_6 = 497.4 ms (after fault)

Other fault conditions are stated in Fig. 8.13

(a) 'a'-phase current at end S
(b) 'a'-earth voltage at end S
(c) 'a'-phase current at end R
(d) 'a'-earth voltage at end R

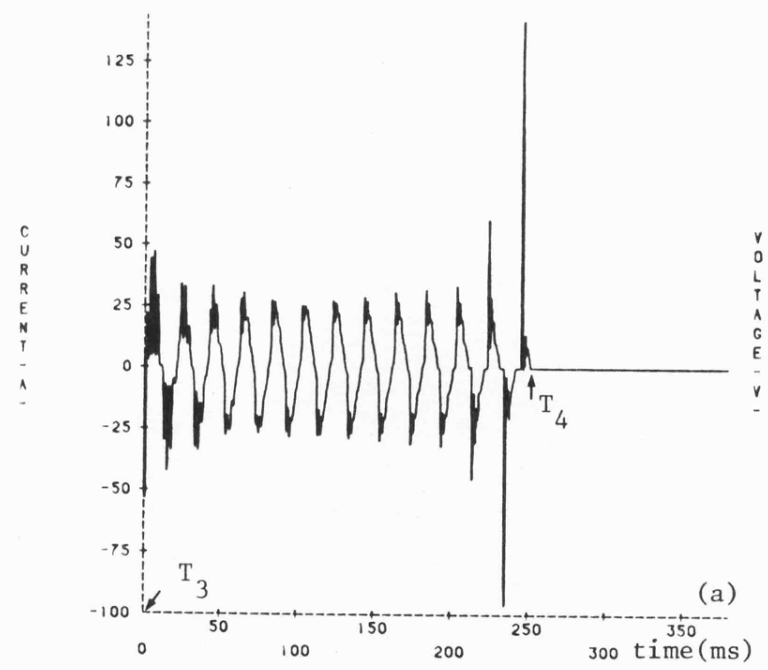

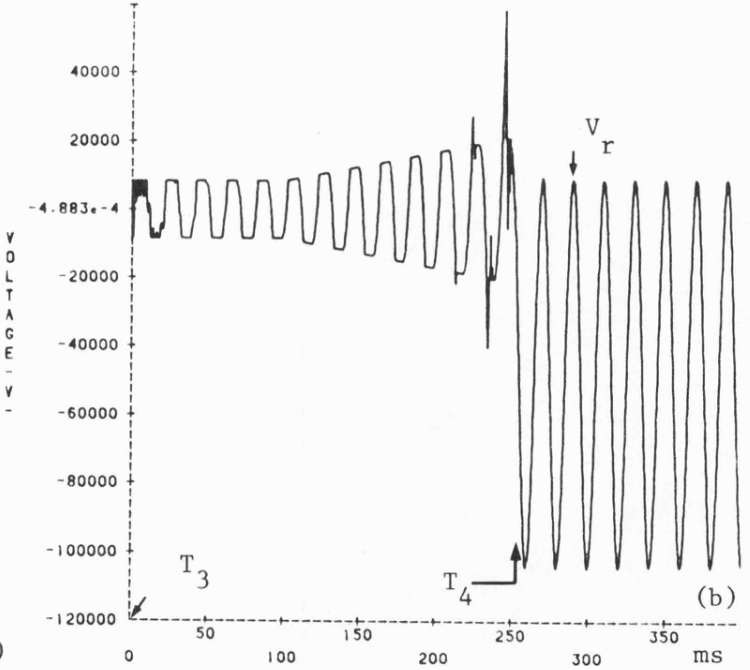

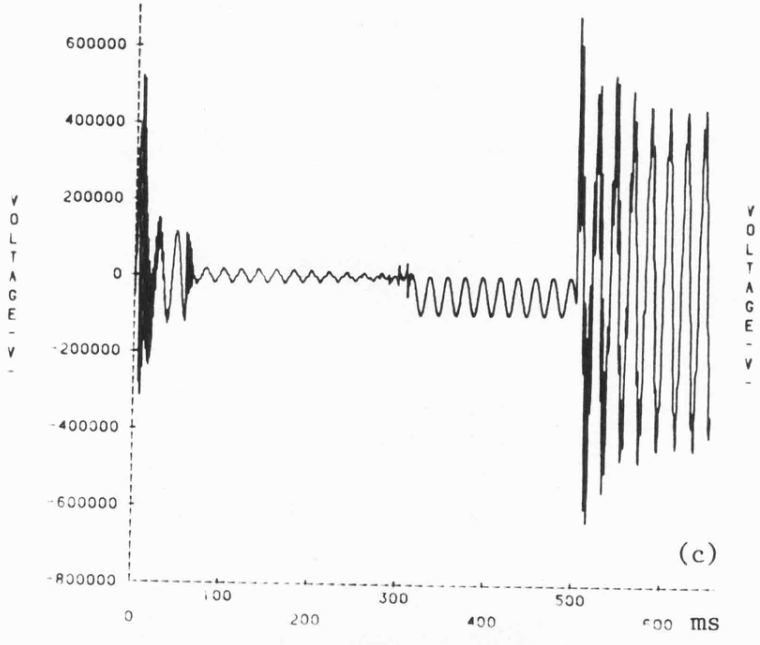

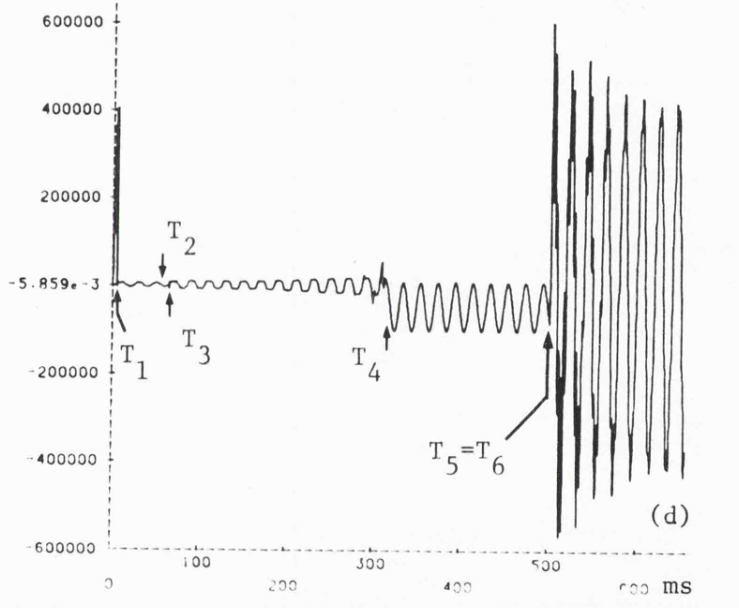

Fig. 8.15

Effect of fault position and power transfer direction on arc extinction

'a'-earth fault at peak of prefault 'a'-phase voltage

fault end R, x_f = 120 km

ℓ = 120 km, transposed

$V_S/V_R = \underline{1/10}^{o}$

Z_{SO}/Z_{S1} = 1.0

sen. end s.c.l = 1500 MVA

rec. end s.c.l = 5000 MVA

T_1 = 5 ms

T_2 = 52.8 ms (after fault)

T_3 = 59.4 ms (after fault)

T_4 = 252.8 ms (after arc transition)

T_5 = 497.6 ms (after fault)

T_6 = 497.6 ms (after fault)

$V_r \simeq$ 113.76 kV (peak to peak)

(a) secondary arc current
(b) secondary arc voltage
(c) 'a'-earth voltage at end S
(d) 'a'-earth voltage at end R

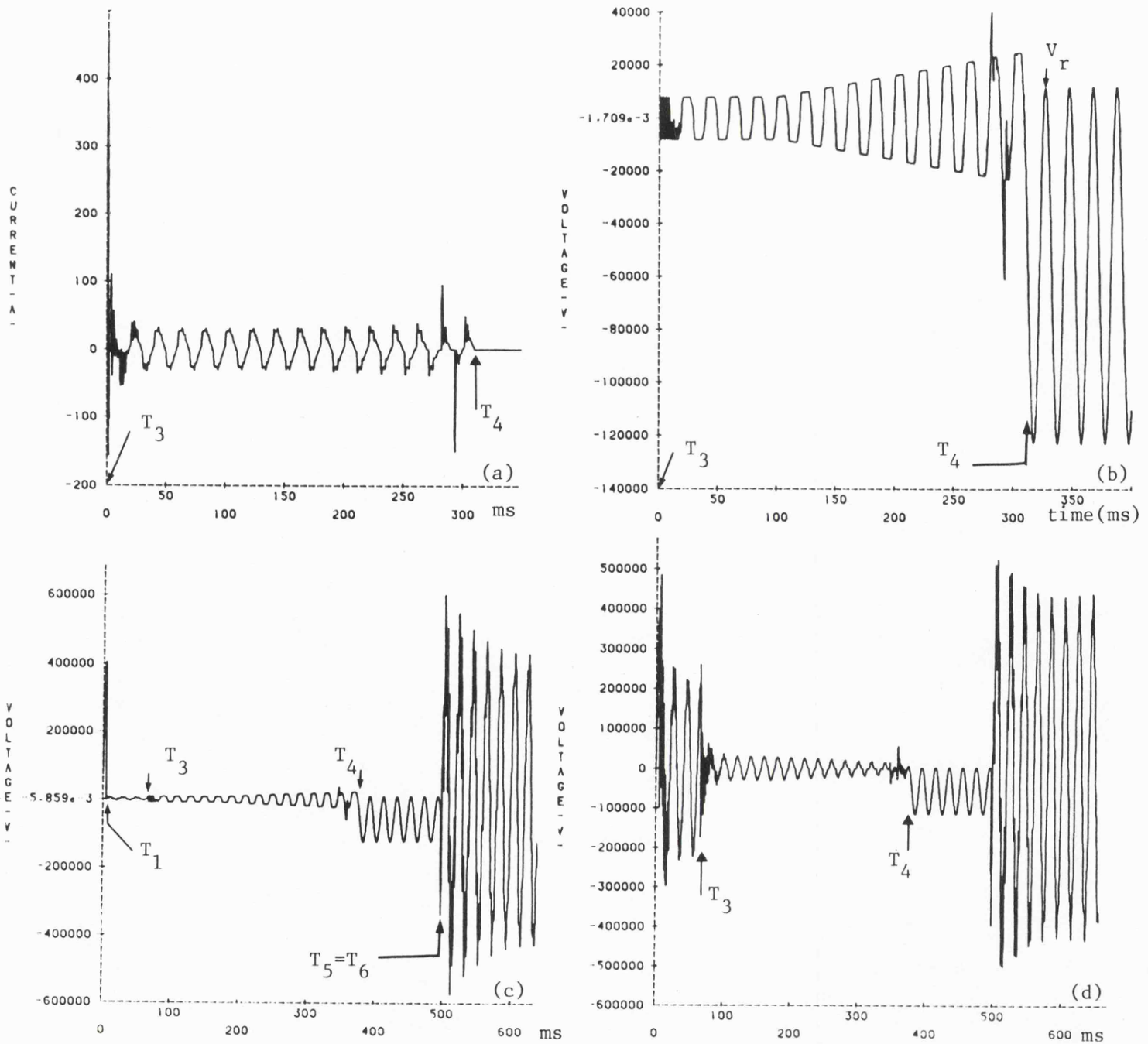

Fig. 8.16

Effect of source sequence impedance ratio (Z_{SO}/Z_{S1})

'a'-earth fault at peak of prefault 'a'-phase voltage

fault at end S, $x_f = 0$

ℓ = 120 km, transposed

$V_S/V_R = 1/10^o$

$Z_{SO}/Z_{S1} = 0.5$

sen. end s.c.l = 1500 MVA

rec. end s.c.l = 5000 MVA

T_1 = 4.5 ms

T_2 = 58.2 ms (after fault)

T_3 = 61.4 ms (after fault)

T_4 ≃ 310.4 ms (after arc transition)

T_5 = 493.2 (after fault)

T_6 = 493.2 (after fault)

V_r ≃ 134.6 kV (peak to peak)

(a) secondary arc current
(b) secondary arc voltage
(c) 'a'-earth voltage at end S
(d) 'a'-earth voltage at end R

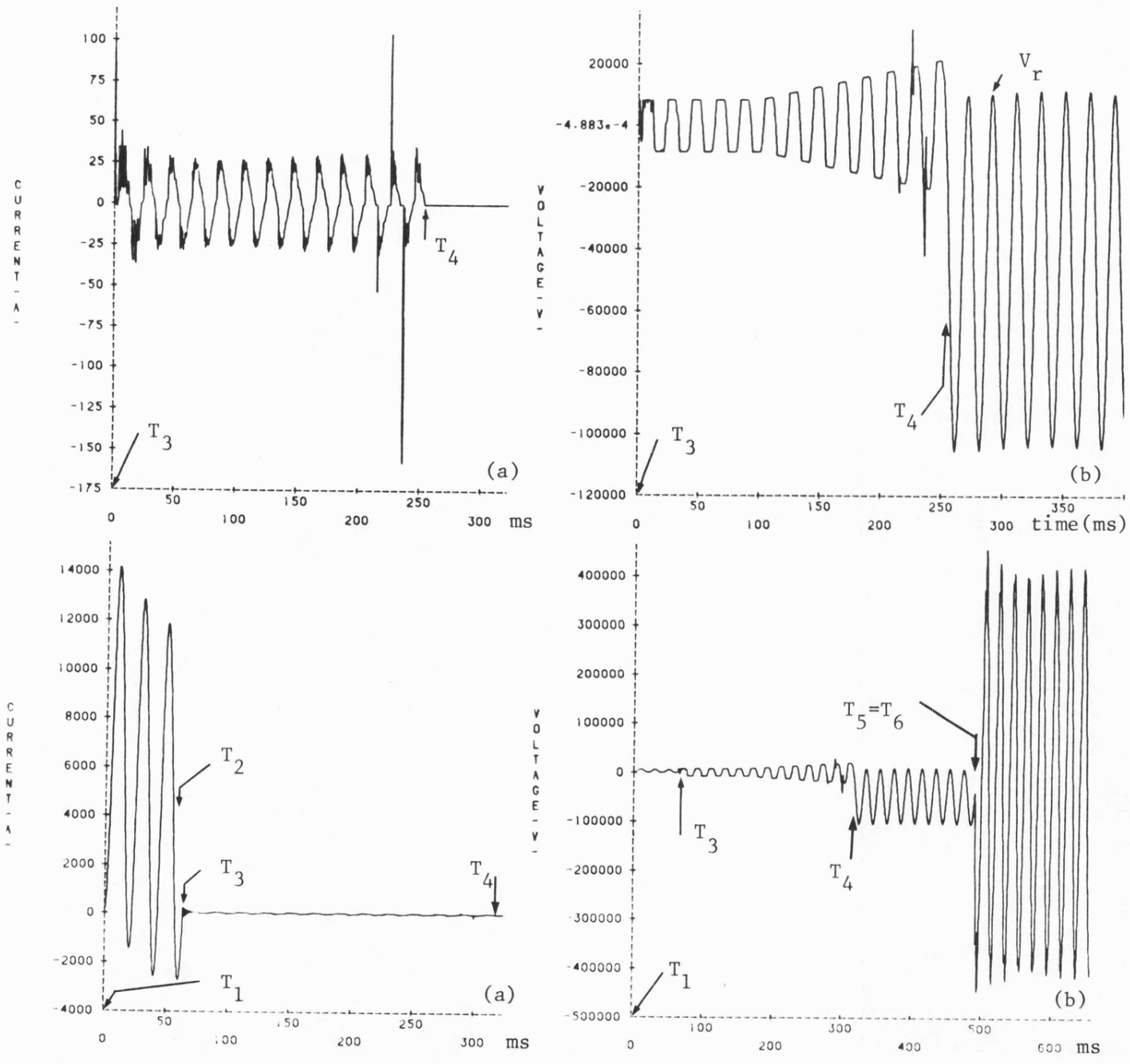

Fig. 8.17

Effect of fault inception time on secondary arc extinction

'a'-earth fault at zero of prefault 'a'-phase voltage

x_f = 60 km

ℓ = 120 km, transposed

$V_S/V_R = 1\underline{/0^o}$

Z_{SO}/Z_{S1} = 1

sen. end s.c.l = 1500 MVA

rec. end s.c.l = 5000 MVA

T_1 = 0

T_2 = 57.4 ms (after fault)

T_3 = 63.4 ms (after fault)

T_4 = 252.8 ms (after arc transition)

T_5 = 490.6 ms (after fault)

T_6 = 490.6 ms (after fault)

V_r = 115.2 kV (peak to peak)

(a) secondary arc current
(b) secondary arc voltage
(c) current in fault arc path
(d) fault point voltage

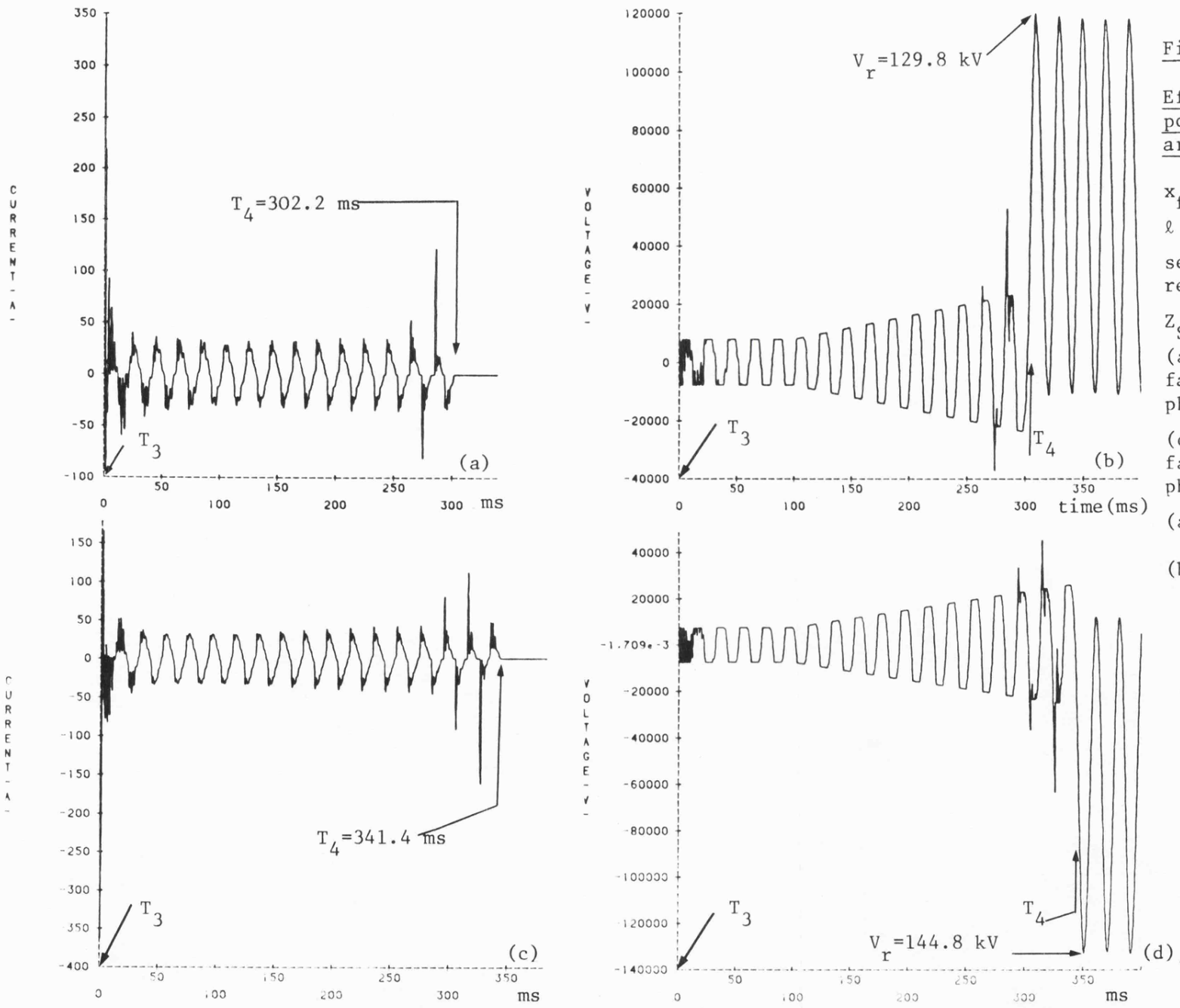

Fig. 8.18

Effect of line transposition on secondary arc extinction

x_f = 0

ℓ = 120 km, non-transposed

sen. end s.c.l = 1500 MVA
rec. end s.c.l = 5000 MVA

Z_{SO}/Z_{S1} = 1.0

(a),(b): $V_S/V_R = 1\underline{/10}^{o}$ fault on phase 'a' (outer phase)

(c),(d): $V_S/V_R = 1\underline{/0}^{o}$ fault on phase 'c' (middle phase)

(a),(c) secondary arc current

(b),(d) secondary arc voltage

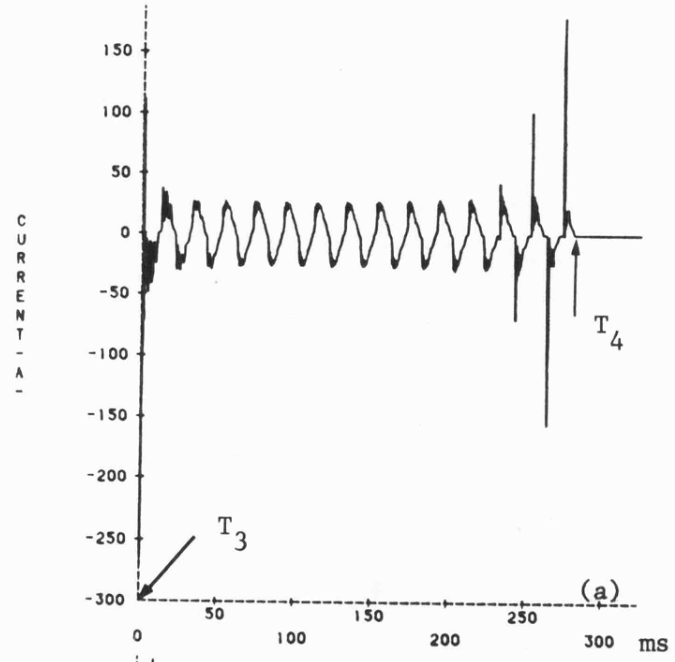

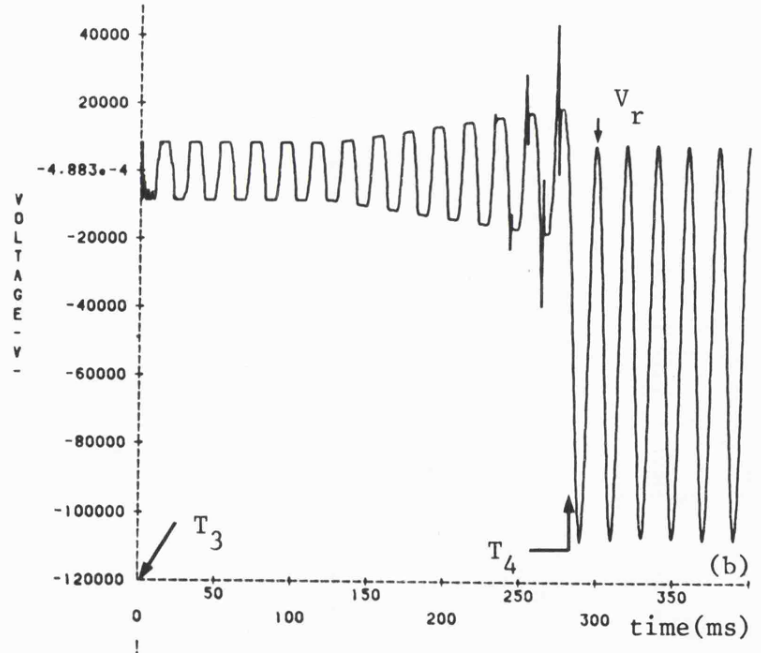

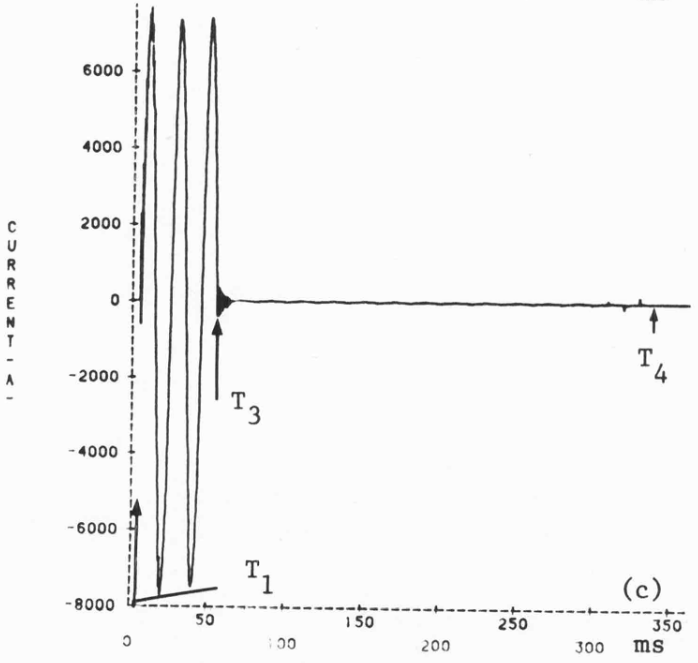

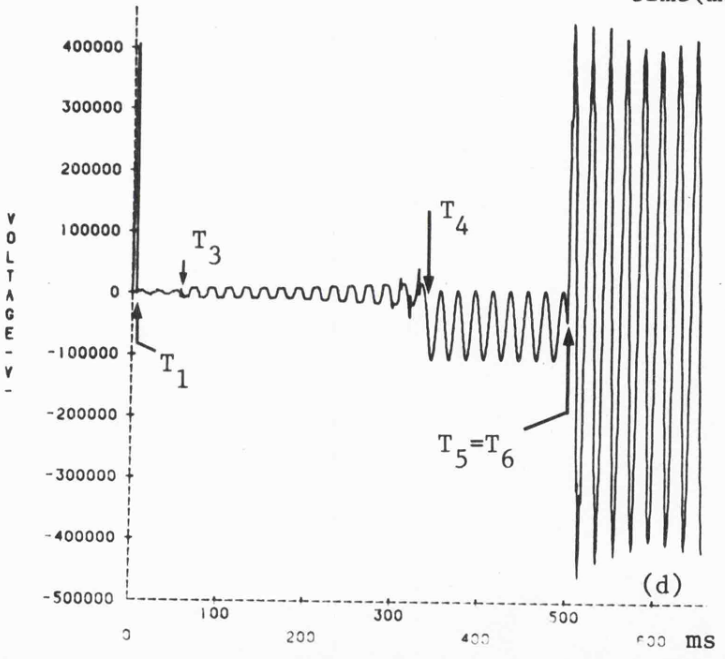

Fig. 8.19

Effect of the rate of increase of arc length on arc extinction

'a'-earth fault at peak of prefault 'a'-phase voltage

x_f = 60 km

ℓ = 120 km, transposed

sen. end s.c.l = 1500 MVA
rec. end s.c.l = 5000 MVA

Z_{S0}/Z_{S1} = 1.0

$V_S/V_R = 1\underline{/0^o}$

arc length/time variation is shown in eqn. 8.2

T_1 = 5 ms

T_2 = 50 ms (after fault)

T_3 = 50 ms (after fault)

T_4 ≃ 281.6 ms (after arc transition)

$T_5 = T_6$ = 495 ms (after fault)

V_r = 115.2 kV (peak to peak)

(a) secondary arc current
(b) secondary arc voltage
(c) current in fault arc path
(d) fault point voltage

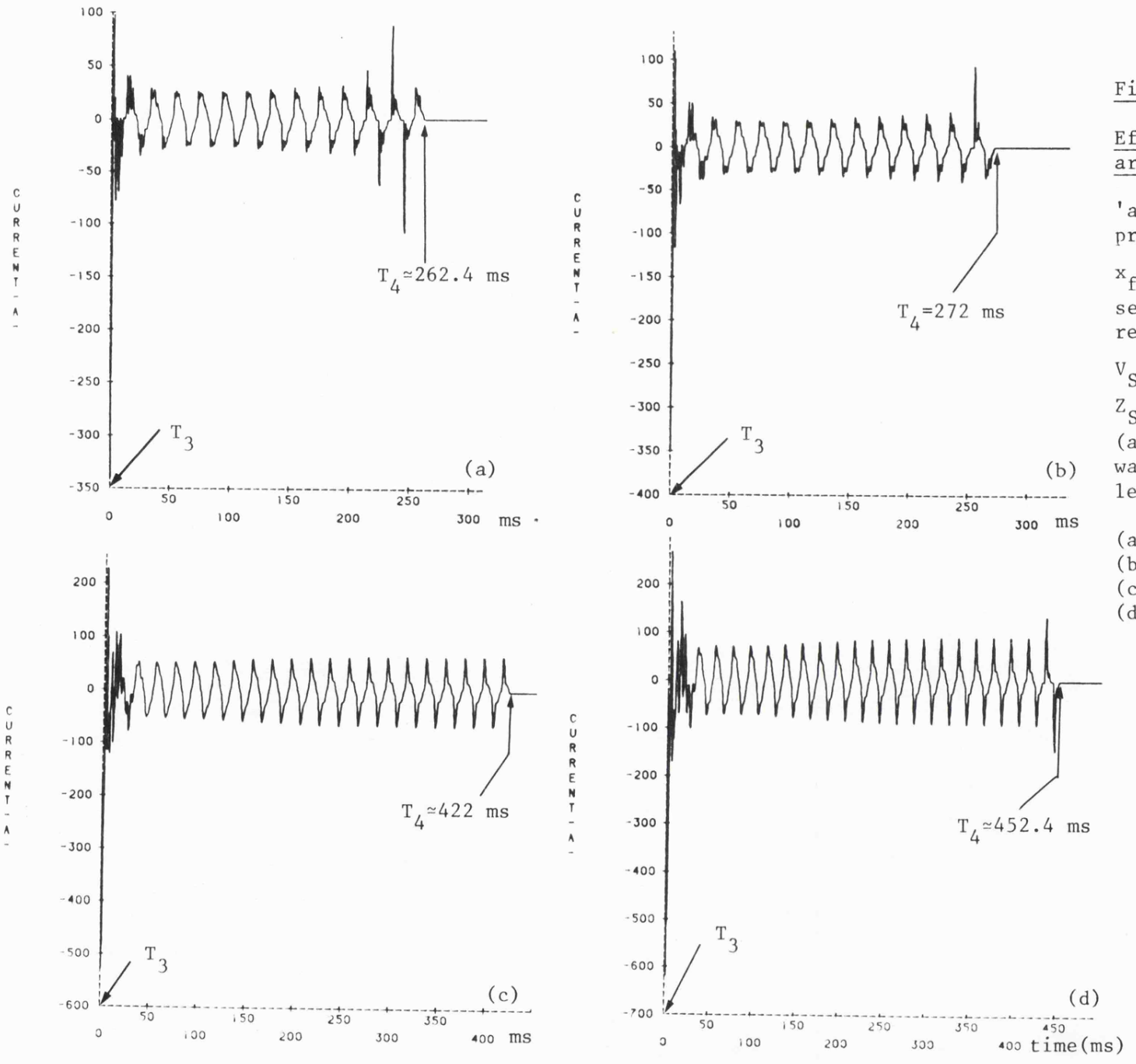

Fig. 8.20

Effect of the line length on arc extinction time

'a'-earth fault at peak of prefault 'a'-phase voltage

$x_f = 0$

sen. end s.c.l = 1500 MVA
rec. end s.c.l = 5000 MVA

$V_S/V_R = 1\underline{/0^o}$

$Z_{SO}/Z_{S1} = 1$

(a)-(d) secondary arc current waveforms for different line length

(a) ℓ = 120 km, transposed
(b) ℓ = 135 km, transposed
(c) ℓ = 240 km, transposed
(d) ℓ = 300 km, transposed

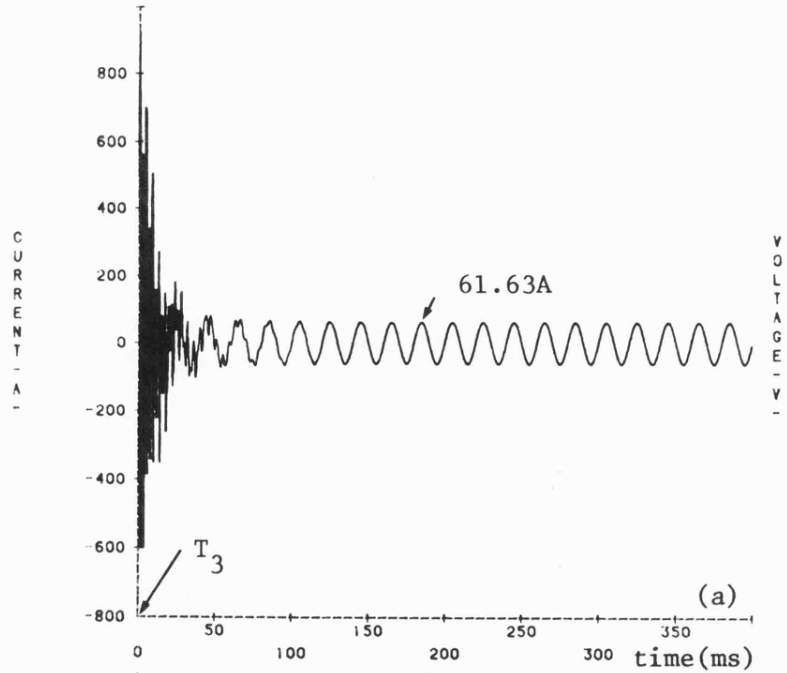

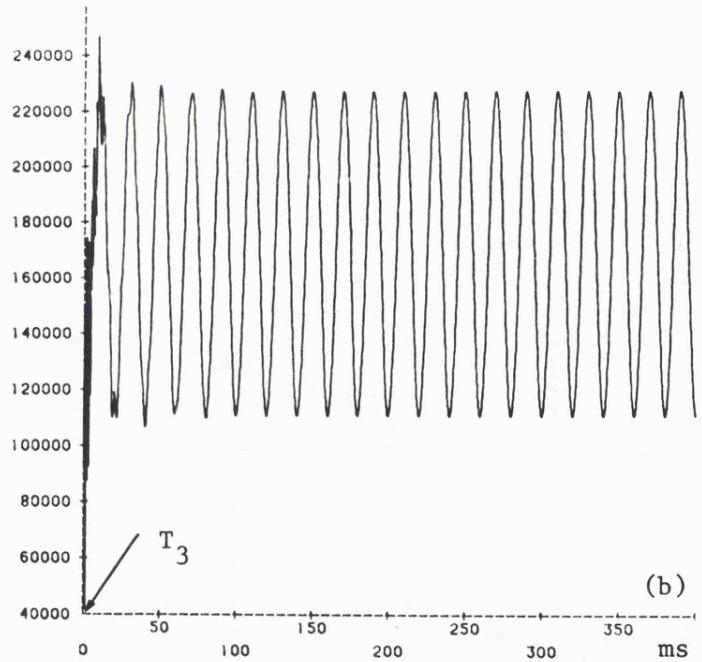

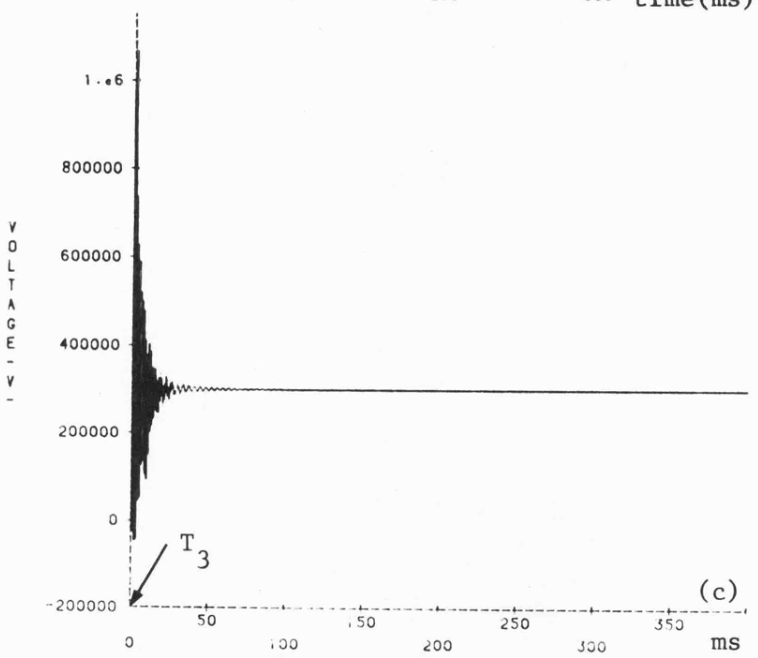

Fig. 8.21

Effect of the line length on arc extinction

'a'-earth fault at peak of prefault 'a'-phase voltage

$x_f = 0$

ℓ = 300 km, transposed

sen. end s.c.1 = 1500 MVA
rec. end s.c.1 = 5000 MVA

$R_f = 0.5\Omega$

$V_S/V_R = 1\underline{/0^o}$

$Z_{S0}/Z_{S1} = 1.0$

(a) secondary arc current (constant arc resistance of 0.5Ω)
(b) Thevenin voltage
(c) Thevenin impedance

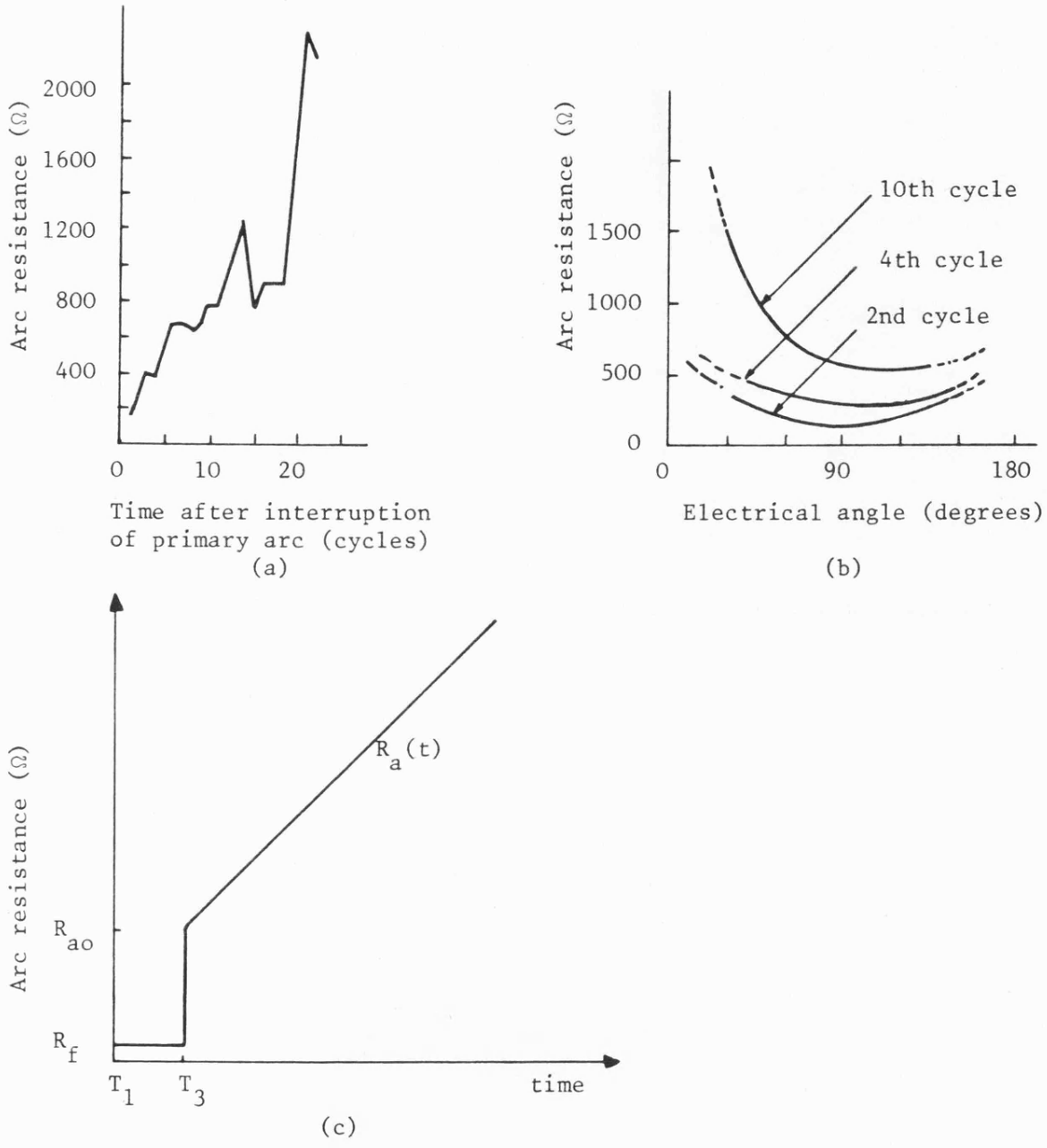

Fig. 8.22 Variation of the secondary arc resistance

(a) Typical arc resistance variation

primary arc = 8 kA, 5.74 cycles,
secondary arc = 31.5 A
self extinction time of 22.6 cycles

(b) Relation between secondary arc resistance and phase angle

(c) Linearised characteristics used in present study

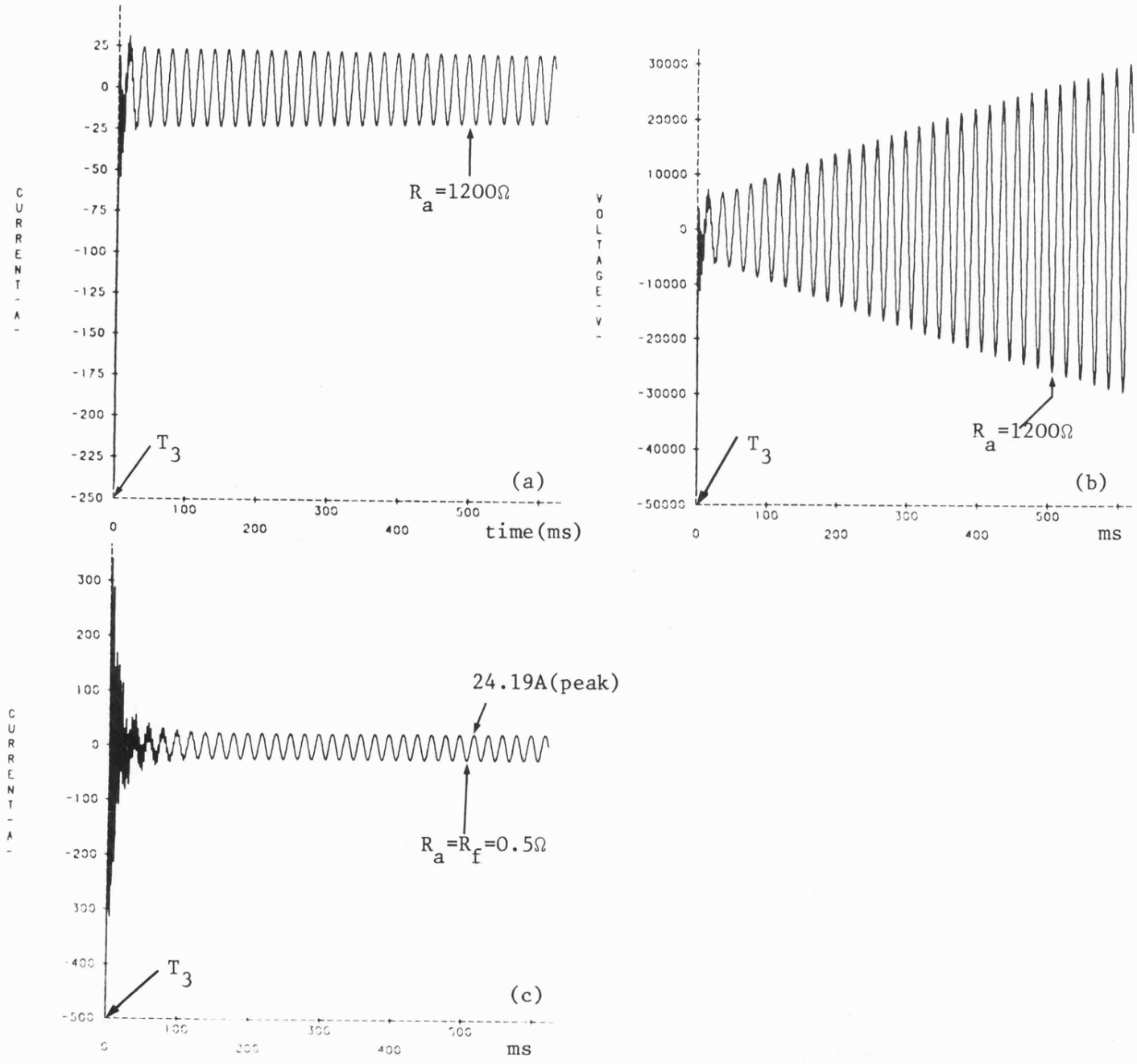

Fig. 8.23

Representation of the secondary arc path by a time dependent linear resistance

'a'-earth fault at peak of prefault 'a'-phase voltage

x_f = 0

ℓ = 120 km, transposed

sen. end s.c.l = 1500 MVA
rec. end s.c.l = 5000 MVA

R_f = 0.5Ω

$V_S/V_R = 1\underline{/0^o}$

Z_{S0}/Z_{S1} = 1.0

(a) secondary arc current with time dependent linear arc resistance
(b) secondary arc voltage with time dependent linear arc resistance
(c) secondary arc current with constant arc path resistance of 0.5Ω

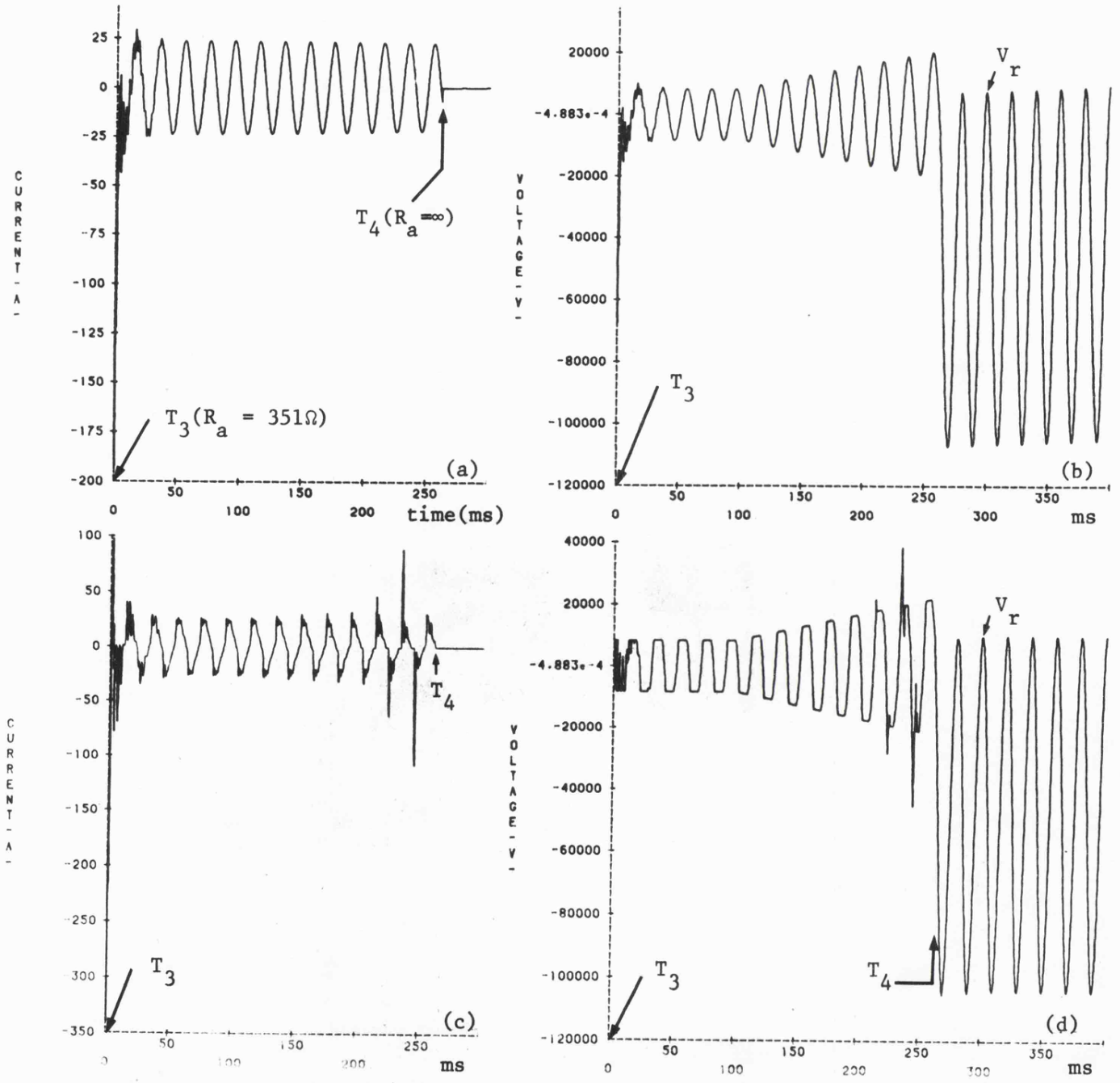

Fig. 8.24

Comparison between the secondary arc current and voltage waveforms under different arc path representation

(a),(b) arc path represented by a time dependent linear resistance, stated in eqn. 8.5.

fault conditions are stated in Fig. 8.23.

(c),(d) arc path represented by the non-linear arc characteristics

fault conditions are stated in Fig. 8.2

(a),(c) secondary arc current
(b),(d) secondary arc voltage

CHAPTER 9

SYSTEM STUDIES: COMPENSATED LONG LINE

9.1 Introduction

The mathematical model of the secondary arc path, as developed in chapters 4 and 5, is used here to obtain the system response. Two symmetrical shunt reactors are connected at the line(s) remote ends. The studies are carried out for a one feeder system, with two similar sources 5 GVA each, except in section 9.7 where a 4-feeder system is studied.

The effects of some factors on the extinction time are here investigated. These include fault location, transmission line loading, parameters of the shunt reactors and the parameters of the terminal stations. The effect of the shunt reactors, with directly grounded neutral, on the extinction time is also investigated. The possibility of using two symmetrical shunt reactors on an untransposed 200 km line is also studied.

The line length under study in this chapter is 300 km, except in section 9.11, and it is transposed at 100 km intervals. The pre-fault power transfer is considered either zero or approximately 1262 MW. The results presented here are for fault on phase 'a', except in section 9.10 (where the line is untransposed) two different phases are considered.

9.2 Effect of the Optimum Neutral Reactor

The four reactor scheme employing the optimum value for the neutral reactor, effectively compensates the capacitive coupling between the

energized and de-energized phases but has less effect on the inductive coupling. To effectively compensate both the capacitive and the inductive coupling would require that the phase reactors compensate the line to 100%. This is undesirable for many reasons not the least of which are the expense, low voltage under normal load flow, and the possibility of a potentially damaging resonance condition. For the purpose of this study the phase reactor is chosen to compensate the line to 75% (i.e. $h_1 = 0.75$), and this compares well with the values used in practice[82,71].

Two symmetrical four-legged reactors are connected at the remote ends of the line, with $h_1 = 0.75$ and $h_o = 0.6016$, to reduce the capacitive component of the secondary arc current and the recovery voltage to a theoretical value of zero. Fig. 9.1a shows the secondary arc current waveform for unloaded line, following a mid-point fault ($x_f = 150$ km), assuming a constant secondary arc resistance of 0.5 Ω. The corresponding Thevenin voltage and impedance waveforms are shown in fig. 9.1b,c. It can be seen from fig. 9.1 that the secondary arc current is reduced to a very small value but it does not reach zero within the time observed. This is mainly due to the time constant of the circuit, i.e. it requires approximately 2s to reach the steady-state, if the arc resistance is ignored. Figs. 9.2 and 9.3 show several features of the system throughout the whole process of single phase fault clearing and autoreclosure when the non-linear arc characteristic is included. It is evident from fig. 9.2 that the secondary arc extinguishes in a very short time after arc transition (approximately 25 ms). It is of interest to note that the magnitude of the recovery voltage subsequent to the arc extinction is only 4 kV (peak) and it has the beating characteristics which have been observed experimentally[10,5,71].

However such a degree of compensation is usually not required in practice for two reasons:

1. The voltage across the neutral reactor is high, which will increase the cost of the reactor[17].

2) If the secondary arc extinguishes immediately after fault isolation, then the insulator recovery characteristic will take the form of the three phase autoreclosure. According to the information reported in the literature [70,73,69], it requires about 0.3-0.38s to withstand the reclosing voltage.

Therefore, it is felt necessary to examine the system under the case when the shunt reactor is chosen to reduce the capacitive component of the secondary arc current to 20A (r.m.s.). It can be seen from eqn. 2.16 that there are infinite values for h_1 and h_o which could be used to reduce the secondary arc current to 20A (capacitive). However, the value of h_1 is normally chosen so that the shunt reactor limits the system overvoltage under light load conditions. Typically this value is between 0.7-0.85, and it is chosen in this study as 0.75[82].

9.3 Effect of Fault Position on Unloaded Line: Compensation to -20A (r.m.s.)

The parameters of the shunt reactors are chosen to reduce the capacitive component of the secondary arc current to 20A (r.m.s.). According to the simple calculations, shown in chapter 7, the value of h_o is equal to 0.8787121 when $h_1 = 0.75$. The secondary arc current waveform, assuming a constant secondary arc resistance (0.5 Ω), following a fault at the sending end of an unloaded line is shown in fig. 9.4a. It is evident from this figure that the steady-state value

of the secondary arc current is approximately 20.2A (r.m.s.). Fig. 9.4b,c,d illustrates the secondary arc behaviour, when the non-linear arc characteristic is included. The secondary arc current and voltage waveforms have some differences compared with the uncompensated case. The extinction time is approximately 30 ms shorter than the case when the line is uncompensated and its secondary arc current is 20A (r.m.s.), i.e. 135 km transposed line. The high current spike which is observed in the uncompensated case, before the final extinction, is much lower in this case. The recovery voltage waveform has no off-set, but it is oscillating with a beating frequency.

The steady-state calculations, described in chapter 2, show that for this degree of compensation the steady-state recovery voltage has a peak value of 123.3 kV. However, the recovery voltage waveform shows that the first peak immediately after extinction is 47 kV, succeeded by a second peak of 88.8 kV and 128.4 kV reaching a maximum value of 224 kV at the 7th halfcycle and then starts decreasing. This phenomenon has been explained by Kimbark. Kimbark in his discussion of reference 18 pointed out that this beating (in the recovery voltage) is described by T. Udo among others. It occurs due to the fact that the recovery voltage consists of a sinusoidal voltage of source frequency and a damped sinusoidal voltage of the natural frequency of the system, the latter generally being the lower of the two. Kimbark goes on to say that as a consequence of the beat and of the initial conditions, the first few voltage peaks are lower than the steady-state peak voltage and this circumstance may aid extinction of the secondary arc current. Even though reference 32 disagrees with Kimbark's explanations, however, the recovery voltage waveform conforms to Kimbark's[18] and other's explanations[12,13,17].

A close examination of the recovery voltage waveform shows that the rate of increase of the recovery voltage subsequent to arc extinction is approximately 9.4 kV/ms, and this compares with 11.5 kV/ms in the uncompensated line (fig. 8.5c). This decrease in the rate of increase of the recovery voltage aids the extinction time as seen from a comparison of figs. 9.5c and 8.20b.

The faulted phase response at the sending and receiving end is shown in fig. 9.5. It can be seen from this figure that the voltage observed at the end R remote from the fault exhibits the usual high frequency travelling wave induced distortion during the primary arc period[47]. Considerable high frequency distortion also occurs subsequent to clearance at end R at time T_3, the most likely cause of which is low level clearing induced travelling waves within the faulted phase being in transient between the secondary arc point and the now open-circuited R end. Similar effects are also observed during the dead time T_3 to T_4.

Fig. 9.6 shows the secondary arc behaviour following a mid point fault. It is of interest to note that the extinction time in this case is approximately 40 ms lower than the case of a sending end fault. The first peak of the recovery voltage does not show any significant difference from that of fig. 9.4. However, a close examination of the Thevenin voltage waveform indicates that the latter is higher in case of a fault at the sending end, in consequence the extinction time is also greater.

9.4 Effect of the Prefault Loading and Fault Position

9.4.1 Fault at the sending end: power transfer from sending to receiving end (V_S/V_R = 1/25.73)

Fig. 9.7 illustrates the secondary arc behaviour, following a-e fault at the sending end S, when the pre-fault power transfer from end S is approximately 1262 MW. A comparison with fig. 9.4 shows that the extinction time is approximately 107 ms longer for the loaded case. The same figure indicates that the first peak of the recovery voltage is 19 kV greater for the loaded case.

In this case, the sound-phase current induces significant longitudinal voltages in the faulted phase during the secondary arc period. These longitudinal electromagnetically induced voltages contribute to the total current that circulates through the secondary arc path and to the recovery voltage across it after each partial or final extinction. Even though the shunt reactor compensates part of the electromagnetically induced current, the steady-state value of the secondary arc current has increased approximately to 28A (r.m.s.) as shown in fig. 9.7c.

The faulted phase voltage and current waveforms, at the remote end R, throughout the whole process of single phase fault clearing and autoreclosure are shown in fig. 9.8. It is of interest to note that the voltage at the receiving end, during the dead time, is relatively high compared to the sending end voltage (fig. 9.7). It can be seen that this voltage is almost constant for the first 100 ms after arc transition then starts decreasing. This indicates that the electromagnetically induced voltage component is in antiphase with the arc path voltage component.

9.4.2 Mid point fault: power transfer from sending to receiving end (V_S/V_R = 1/25.73)

Fig. 9.9 illustrates the behaviour of the secondary arc following a mid point fault, when the power transfer from the sending end is approximately 1262 MW. It is of interest to note that the extinction time is significantly reduced, however, it is still 68 ms greater than the case of an unloaded line under the same fault condition (fig. 9.6). The fact that the electromagnetic coupling has a significant effect on the extinction time even if the fault is at the middle of the line, is mainly due to the effect of transposition. Transposition alters the point at which the electromagnetic coupling is zero and makes it a function of each phase[46,6,14].

A comparison of figs. 9.9b and 9.7b shows that the first peak of the recovery voltage is significantly lower in this case. This indicates that as the value of the first peak increases the extinction time also increases.

Considerable difference between the sending and receiving end voltage waveforms, during the dead time, can be seen from fig. 9.10. This phenomenon is mainly due to the phase difference between the electromagnetic and electrostatic voltage components along the line. The high transient overvoltage which is observed after breaker reclosure (fig. 9.10b,d) is partly due to the delay of the receiving end breaker reclosure. However, in a loaded line even if the two breakers reclose at the same instant significant overvoltage still can be observed.

9.4.3 Fault at the receiving end: power transfer from sending to receiving end ($V_S/V_R = 1\angle 25.73$)

Fig. 9.11 shows several features of the response of the system throughout the whole process of single phase fault clearing and auto-reclosure. It is evident from this figure that the extinction time is approximately 28 ms lower than the case of a sending end fault (fig. 9.7). The first peak of the recovery voltage is also lower. The sending end voltage waveform (fig. 9.11d) is of special interest. During the dead time the healthy phase induces significant electromagnetic voltage on the open phase, which is in phase with the voltage across the arc path, in this case. It is noticed that the total voltage on the sending end S, during the dead time is constant, during the first 100 ms after the arc transition, then starts increasing as the arc length increases.

From these results (section 9.4) it can be concluded that, under heavy load conditions the extinction time can vary significantly with fault position. It is concluded also that the first peak of the recovery voltage is much lower than the steady-state value of the recovery voltage. It is of interest to note that similar recovery voltage waveforms, and the characteristic of the first peak, has been observed experimentally[10,71]. Several studies indicate that the magnitude of the first peak in the recovery voltage always increases as the extinction time increases.

9.5 Effect of Power Transfer Direction

It has been indicated in the previous chapter that the extinction time, for a fault on phase 'a', in case of power transfer from sending end S to receiving end R is much higher than the case when the power transfer from end R to S. However, this phenomenon is only true when the line is discretely transposed and it depends on the faulted phase

and the number of cycles of transposition.

Fig. 9.12 illustrates the system behaviour, following a fault at the sending end S, when the pre-fault power transfer from end R is approximately 1262 MW. A comparison with fig. 9.7 shows that the extinction time is 214 ms lower in this case. The steady-state value of the secondary arc current waveform, calculated on the assumption of a constant arc path resistance (0.5 Ω), fig. 9.12c, has a peak value of 18.13A. This value is much lower than the case when the line is unloaded (28.8A). It can be noticed that the first peak of the recovery voltage is only 30 kV.

A fault at the receiving end R, under the same previous conditions, shows that the extinction time is only 27 ms greater (fig. 9.13). The first peak of the recovery voltage is also 3 kV higher than the previous case. These results conform to the conclusion drawn in the previous chapter that the extinction time is greater when the fault occurs at the power exporting end. The effect of the power transfer on the sending end voltage waveform, during the dead time, is also evident from a comparison of fig. 9.13 and 9.11. It can be noticed that when there is a fault at the receiving end R, the voltage which appears at the sending end S, during the dead time, is much higher when the power transfer is from S to R than the case when the power transfer is from R to S.

The significant effect of the power transfer direction on the extinction time, which is observed here, has not been reported in the literature. These findings may be very important from a practical point of view. A TNA study for a transposed and compensated long line indicates that the maximum value of the secondary arc current observed, when power flow from end S to R is significantly higher than that when power flow from end R towards S[6]. However, the authors explain the difference

as the direct result of the change in the equivalent source reactances behind the terminal buses as well as the pre-fault voltage profile. Apparently, this phenomenon is due to the effect of the discrete transposition and its interaction with the power flow direction, rather than the source capacity, because the sources used in this study are identical.

9.6 Effect of Fault Inception Time

The results presented so far assume the fault to occur at an instant of time corresponding to the peak voltage of the faulted phase. Such a type of fault produces maximum travelling wave distortion. Faults at an instant of time corresponding to zero faulted phase voltage to earth, however, produce maximum offset of the waveform particularly in the currents. This can be observed from fig. 9.14a,b, which shows the primary and secondary arc current waveforms following a mid point fault for an unloaded line when $V_a = 0$. This figure clearly indicates the offset in the secondary arc current for the first 70 ms. The extinction time in this case is greater than the case of a fault at the peak voltage (fig. 9.6) by approximately 20 ms. It is of interest to note that the secondary arc current extinguished partially 64 ms after the arc transition then restrikes again when the arc voltage becomes higher than the re-ignition voltage.

The faulted phase voltage waveform at the sending end is shown in fig. 9.14d. No significant high frequency distortion in the sending end voltage waveform during the fault period can be observed.

9.7 Response of 4-Section Feeder System

The results presented so far assume that there are no other lines connected to the sending or receiving end of the line under study (fig. 9.15a). However, this is not always the case in practice,

therefore, it is felt necessary to examine a practical system as shown in fig. 9.15b. The effect of the busbar termination of the line S-R (see fig. 9.15b) is examined under different fault positions. Each of the four lines is transposed through three equal points along its length. Two identical shunt reactors are connected at the remote ends of each line so that the capacitive component of the secondary arc current of each line is reduced to 20A (r.m.s.). The studies carried out when the pre-fault power flow from end S to R is approximately 1262 MW.

Fig. 9.16a,b illustrates the secondary arc behaviour following a fault at the receiving end R. A comparison with fig. 9.11 shows that the secondary arc extinction time is approximately 3 ms greater in the case of 4-section feeder system. It is of interest to note that the duration of the high noise period in the secondary arc current and voltage waveform is much longer in the case of 4-section feeder system. This is mainly due to wave reflection from other line ends.

Several faults at different positions along the line are studied. It is found that the busbar terminations have no significant effect on the extinction time, however, the high noise period, in the secondary arc current and voltage waveforms, is relatively longer. Fig. 9.16c,d shows the secondary arc current and voltage waveforms, following a fault at end S. A comparison with fig. 9.16a,b indicates that the extinction time is approximately 25 ms greater in this case, the first peak of the recovery voltage is also higher. Therefore, it is concluded that the line termination has no significant effect on the extinction time.

9.8 Voltage Across the Neutral Reactor

The digital computer program developed in this work can be used to predict the system overvoltages during the whole process of single line to ground fault followed by single pole opening and reclosure. However, of special interest is the voltage across the neutral reactor.

The ratio between the reactance of the neutral and that of the main reactor, which would eliminate the capacitively induced secondary arc, was calculated as 0.3287 (or, $x_o/x_1 = 1.986$). The neutral point voltage in this case (optimum neutral value) following a mid point fault, unloaded line, is shown in fig. 9.17a,b. It can be noticed that the voltage across the neutral reactor passes through different stages:

1. Transient high voltage following the fault inception at T_1, settled to a lower voltage during the fault period.

2. High transient voltage following the fault isolation at T_3, settled to a lower value during the dead time.

3. Zero voltage after breakers reclosure at T_5 and T_6. Different fault position indicated that the mid point fault at maximum voltage produces maximum fault overvoltage across the neutral reactor. It is evident from this figure that the overvoltages due to the fault and the breaker opening is much higher than the steady state voltage during the dead time. However, such a reactor would be too expensive and a smaller neutral reactor is normally used[17,13].

The ratio between the reactance of the neutral reactor and that of the main reactor, which would reduce the capacitively induced secondary arc current to 20A is found to be equal to 0.12 (or, $x_o/x_1 = 1.359$). This would result in a lower voltage across the neutral point reactor

and thus reduce the insulation level of the whole reactor. Fig. 9.17c,d illustrates the neutral reactor voltages following a mid point fault when the pre-fault power transfer is zero. It can be noticed from this figure that the voltage across the neutral reactor after the arc extinction is higher than that before the final extinction. The point on wave at which the fault is applied affects the overvoltages produced due to the fault inception only. This is shown in fig. 9.18a,b, where the fault is applied at zero point on wave for a mid point fault. It can be noticed that no overvoltage is observed during this type of fault, and the voltage across the neutral reactor after the arc transition is similar to the case of a maximum point on wave fault.

Several investigations have indicated that the pre-fault power transfer has no significant effect on the maximum voltage across the neutral reactors. This can be seen from fig. 9.18c,d which shows the neutral voltages following a mid point fault when the pre-fault power transfer from end S is approximately 1262 MW.

Several studies indicated that the maximum voltage across the neutral is approximately 70 kV. This corresponds to a mid point fault at maximum voltage. The voltage across the neutral reactor after the arc transition and before the final extinction is generally less then 40 kV, and it confirms the steady-state calculation shown by Carlson[17]. However, this voltage may increase up to 60 kV after arc extinction, this value is relatively higher than the steady-state calculation shown by Carlson. This is mainly due to the fact that the voltage waveform is not in a steady-state and it has the beating characteristics.

The busbar termination can affect the maximum overvoltage due to the fault inception, however, the neutral voltage after the arc transition is almost independent of the busbar termination. This is evident from

fig. 9.19 which shows the neutral reactor voltage following a fault at the sending end S, when the pre-fault power transfer from end S is approximately 1262 MW, for the two different systems studied in section 9.7.

The power transfer direction has some effects on the maximum voltage across the neutral reactor. It can be seen from figs. 9.18a,b and 9.20a,b that the voltage across the neutral reactor, following a fault at the sending end, is greater when the pre-fault power transfer is from end S to R. This is mainly due to the effect of the electromagnetic coupling and its interaction with the line transposition. Some voltage difference can be observed, for the same reason, in the neutral reactors of the same line. It can be noticed that the voltage across the neutral reactor at the power exporting end is relatively higher than that at the importing end.

9.9 Representation of the Secondary Arc Path by a Time Dependent Linear Resistance

The method which is described in section 8.10 is used here to obtain the secondary arc current and voltage waveforms. In this case the initial arc resistance and its rate of increase is chosen to produce an arc voltage approximately equal to the one previously observed. The time at which the secondary arc resistance increases to infinity is taken to be equal to the extinction time predicted by the non-linear arc representation.

Fig. 9.21a,b illustrates the secondary arc current and voltage waveforms following a fault at the sending end, for a transposed and an unloaded line. The first peak in the recovery voltage is smaller than that which is observed using the non-linear arc characteristics by approximately 2.8 kV (fig. 9.21c,d). No significant difference in

the recovery voltage waveform can be observed. However, the secondary arc current waveform is rather different from that which is observed using the non-linear arc characteristics.

To examine the effect of the extinction time on the magnitude of the first peak in the recovery voltage, the point at which the secondary arc resistance increases to infinity is increased to 0.4s. Under these conditions the secondary arc resistance has a constant value of 278.7 Ω during the first 100 ms then it increases to 1115 Ω at 0.4s. The secondary arc current and voltage waveforms under these conditions are shown in fig. 9.21e,f. It can be noticed from this figure that the first peak in the recovery voltage has increased to 54 kV compared to 44 kV in the previous case (fig. 9.21b). No other significant difference in the recovery voltage waveform can be observed.

9.10 Effect of Shunt Reactors with Directly Grounded Neutrals ($x_o/x_1 = 1$) on the Secondary Arc Extinction Time

One primary reason for using shunt reactors on e.h.v. transmission systems is to control steady-state voltages when energizing long lines or when operating long lines under light-load conditions[42,83,12]. If reactors are not used, the Mvar's generated by the line capacitance can cause high voltages at the receiving end of the lines due to Ferranti effect. Further, if the lines are energized from a weak system, high voltages can arise at the sending end of the lines due to the passage of the Mvar's generated by the lines through the reactance of the supply system.

Reactors with directly grounded neutrals ($x_o/x_1 = 1$) have no effect on the magnitude of the secondary arc current, if the resonance region is avoided ($h_1 < 1$). However, the steady-state value of the recovery voltage on the open phase, due to resonance of the reactor inductance

and line capacitance, is much greater than if no reactor were present. Simple steady-state calculations show that the magnitude of the recovery voltage, in 300 km transposed line, equipped with two directly grounded shunt reactors (h_1 = 0.75), is approximately 91% of the peak phase voltage (408.2 kV). However, the extinction time is mainly affected by the magnitude of the secondary arc current, and by the rate of rise of the first peak in the transient recovery voltage. The fact that the first peak in the recovery voltage is always lower than the steady-state value makes possible single pole autoreclosure, in lines equipped with directly grounded reactors.

Fig. 9.22 illustrates the secondary arc behaviour following a fault at the sending end S, when such reactors are used. It can be noticed from this figure that the steady-state value of the secondary arc current is approximately 61A (peak), and this compares with 60.6A based on steady-state calculations (chapter 7). This indicates clearly that the directly grounded reactors have no effect on the magnitude of the secondary arc current. A close examination of the recovery voltage waveform shows that the rate of rise of the first peak in the recovery voltage is approximately 16 kV/ms. This value is higher than the rate of rise for the uncompensated line (11.5 kV/ms). In consequence the extinction time is approximately 58 ms greater in this case (see fig. 8.20d).

These findings indicate that single pole autoreclosure can be used in long lines equipped with directly grounded shunt reactors but the dead time required is increased. However, it must be pointed out that under this condition high transient overvoltages might occur after reclosure because the recovery voltage in this case is much higher than the system voltage.

Maikopar has pointed out that the recovery voltage in this case can be dangerous for voltage transformers connected to the line. The latter has suggested the use of voltage transformer of capacitive type to eliminate such a problem[12].

9.11 The Possibility of Using 4-Legged Reactor Scheme in Untransposed Long Line

In some e.h.v. transmission lines, transposition is not required[71,21,22]. In such cases the magnitude of the negative sequence current component in machines connected to the system does not exceed the continuous negative sequence current carrying capability. The capacitance between two outer phases of a flat line is found to be only 31% of the capacitance between the middle phase and either outer phase. However, the simple symmetrical four-legged reactor bank can correctly compensate only lines with equal phase-to-phase capacitances.

Recently, a modified four-legged reactor scheme has been developed to be used in an untransposed line[71]. The modified reactor bank includes four switches whose operations are coordinated with the line breakers. However, such a scheme may increase the complexity of single pole autoreclosure.

It is therefore felt necessary to investigate the possibility of using simple four-legged reactors in an untransposed 200 km line. These studies include: (1) uncompensated line, (2) ideal compensation, (3) un-ideal compensation, and (4) voltages developed across the neutral reactors.

9.11.1 Uncompensated Line

As stated previously, ignoring the electromagnetic coupling effect, the centre phase of an untransposed line possesses the greatest mutual coupling and hence experiences more severe arcing conditions. Fig. 9.23a,b illustrates the secondary arc behaviour following a fault at the sending end, on the centre phase, for an unloaded line. It is of interest to note that the extinction time in this case is approximately 20 ms greater than that of the 300 km transposed line (fig. 8.20d). Although the steady-state value of the secondary arc current is lower in this case (about 53A (peak)), the recovery voltage is approximately 31 kV greater. A fault at the outer phase under the same conditions indicates that the extinction time is approximately 58 ms lower than the middle phase fault case (fig. 9.23a,b). It must be pointed out that even for a fault at the outer phase, the secondary arc current and the recovery voltage are much higher than that for the transposed line (fig. 9.23c,d), in consequence the extinction time is greater.

9.11.2 Effect of ideal compensation ($h_1 = 0.75$, $h_o = 0.6017$)

Fig. 9.24 illustrates the system behaviour following a fault at the sending end, outer phase, for an unloaded line equipped with two shunt reactors under optimum neutral conditions. A comparison with fig. 9.23a shows that the extinction time is approximately 165 ms greater for the uncompensated line. It is interesting to note that no significant overvoltages are developed at the receiving end when both breakers simultaneously reclose at T_5. A fault is applied on the middle phase under the previously mentioned conditions, and no significant difference in the extinction time can be observed.

The effect of the prefault power transfer on the extinction times is shown in fig. 9.25. It can be seen from this figure that the extinction time does not exceed 340 ms, when the pre-fault power transfer is approximately 1262 MW.

9.11.3 Effect of nonideal compensation (h_1 = 0.75, h_o = 1.0172)

In these studies, the shunt reactor parameters are chosen, so that the capacitive component of the secondary arc current can be reduced to 20A (r.m.s.), if the line is transposed. Fig. 9.26 illustrates the system behaviour following a fault at the sending end S, on the middle phase, when the pre-fault power transfer from end S is approximately 1262 MW. It can be noticed from this figure that the steady-state value of the secondary arc current (fig. 9.26a) is approximately 28A (r.m.s.). The extinction time is relatively higher than the maximum time observed under the optimum neutral reactor conditions. It is of interest to note that the maximum peak in the recovery voltage waveform is higher than the peak phase voltage (408.2 kV). However, this voltage can be tolerated if controlled reclosure is used as shown in fig. 9.26c. A fault at the receiving end R, under the same conditions, shows no difference in the extinction time (fig. 9.27a,b).

The power transfer direction has no significant effect on the extinction time if the line is not transposed. This can be seen from fig. 9.27c,d, which shows the secondary arc current and voltage waveform for a fault at the sending end, middle phase, when the pre-fault power transfer from end R is approximately 1262 MW. A comparison with fig. 9.27a,b shows no significant difference in the extinction time.

Several digital studies, for faults on the middle and the outer phases, at different fault positions indicates that the extinction time

does not exceed 380 ms. No significant difference in the extinction time can be observed whether the fault is on the middle or the outer phase. However, it is noticed that the maximum recovery voltage in the outer phase fault is higher than the middle phase fault. Fig. 9.28 shows the system behaviour following a fault at the end S, on the outer phase, when the pre-fault power transfer from end R is approximately 1262 MW. It can be noticed from this figure that the maximum peak in the recovery voltage is approximately 600 kV, while in case of a middle phase fault it does not exceed 500 kV. This increase in the recovery voltage may affect the maximum transient voltage that occurs after breaker reclosure, even if controlled reclosure is used as can be seen from fig. 9.28d.

9.11.4 Voltage across the neutral reactor

Significant differences in the voltage across the neutral reactor are observed for the two values of h_o used. This can be seen from fig. 9.29, which shows the neutral voltage waveform, during the whole process of single pole autoreclosure, following a fault at end S (on the outer phase) when the prefault power transfer from end R is approximately 1262 MW. It is evident from this figure that both the transient and the steady-state voltages are much higher in the case of optimum neutral reactor (h_o = 0.6017). However, the difference between the maximum extinction time observed in the two cases is only 41 ms.

9.12 Discussion

After arc extinction, the recovery voltage on the opened phase of a shunt reactor compensated line builds up in a transient beating process. Both the rate of rise of the first peak and the steady-state value of the recovery depends mainly on line and reactor parameters and, therefore,

on the transmission line compensation factor.

The extinction time of the secondary arc depends mainly on the steady-state value of the secondary arc current and on the rate of rise of the first peak of the recovery voltage. The results indicate clearly that as the extinction time is increased, the first peak in the recovery voltage is also increased. This is evident from fig. 9.30 which shows the magnitude of the first peak in the recovery voltage and the steady-state value of the secondary arc current vs extinction time.

It is noticed that, for the same line and shunt reactor parameters, power transfer direction significantly affects the magnitude of the secondary arc current and the first peak of the recovery voltage. In consequence the extinction time is significantly affected by the power transfer direction if the line is transposed. This indicates that the effect of the electromagnetic coupling is more significant if the line is transposed.

The results indicate that simple four reactor scheme can be applied to an untransposed line but a longer dead time is required. It is also found that shunt reactors with directly grounded neutrals can be used on a line equipped with single pole autoreclosure. However, the extinction time is relatively longer than the case without shunt reactor, even for 75% positive sequence compensation. The maximum recovery voltage observed under these conditions is approximately 72% higher than the peak value of the phase voltage.

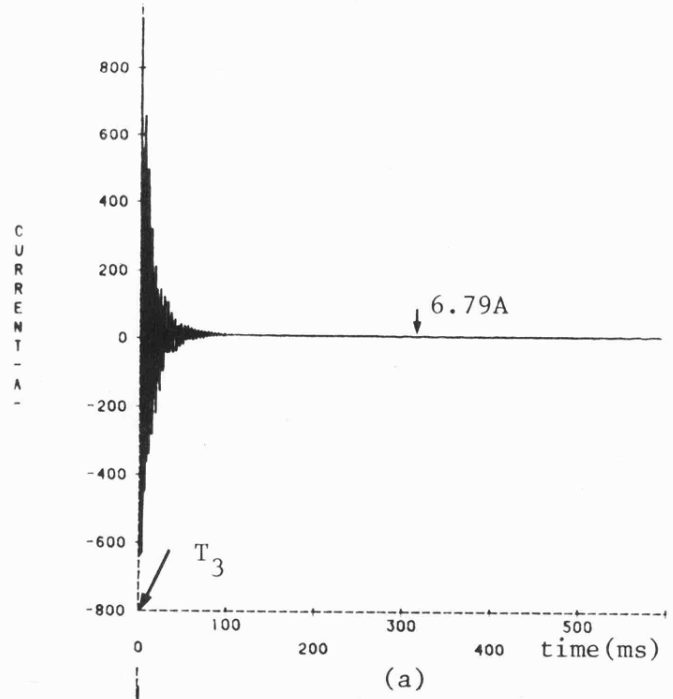

(a)

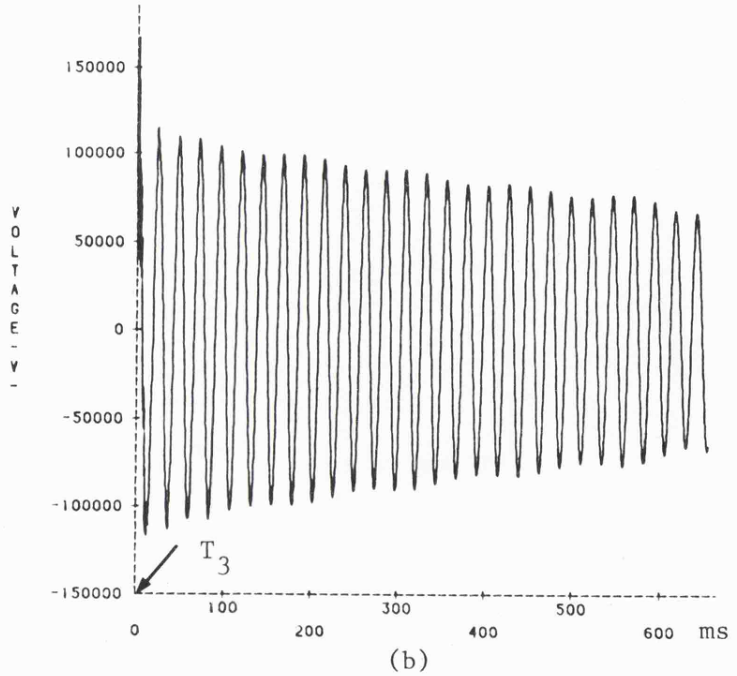

(b)

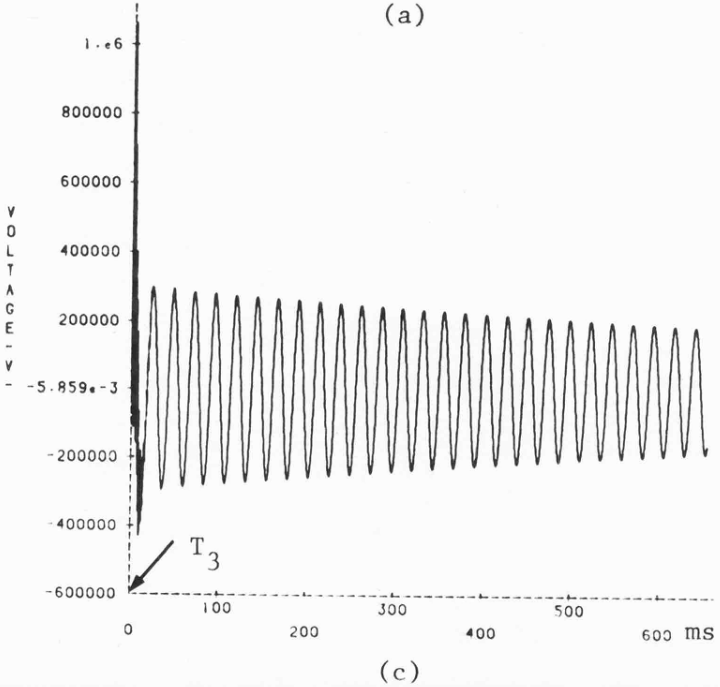

(c)

Fig 9.1

System response for midpoint fault under optimum neutral reactor condition

'a'-earth fault at peak of prefault 'a'-phase voltage

x_f = 150 km

ℓ = 300 km, transposed

sen. end s.c.l = 5000 MVA
rec. end s.c.l = 5000 MVA

R_f = 0.5Ω

$V_S/V_R = 1\underline{/0^o}$

Z_{S0}/Z_{S1} = 1.0

h_1 = 0.75, h_o = 0.60166

T_3 = clearance by breaker at end R (60 ms after fault) = time of arc transition

(a) secondary arc current (constant arc resistance of 0.5Ω)
(b) Thevenin voltage
(c) Thevenin impedance

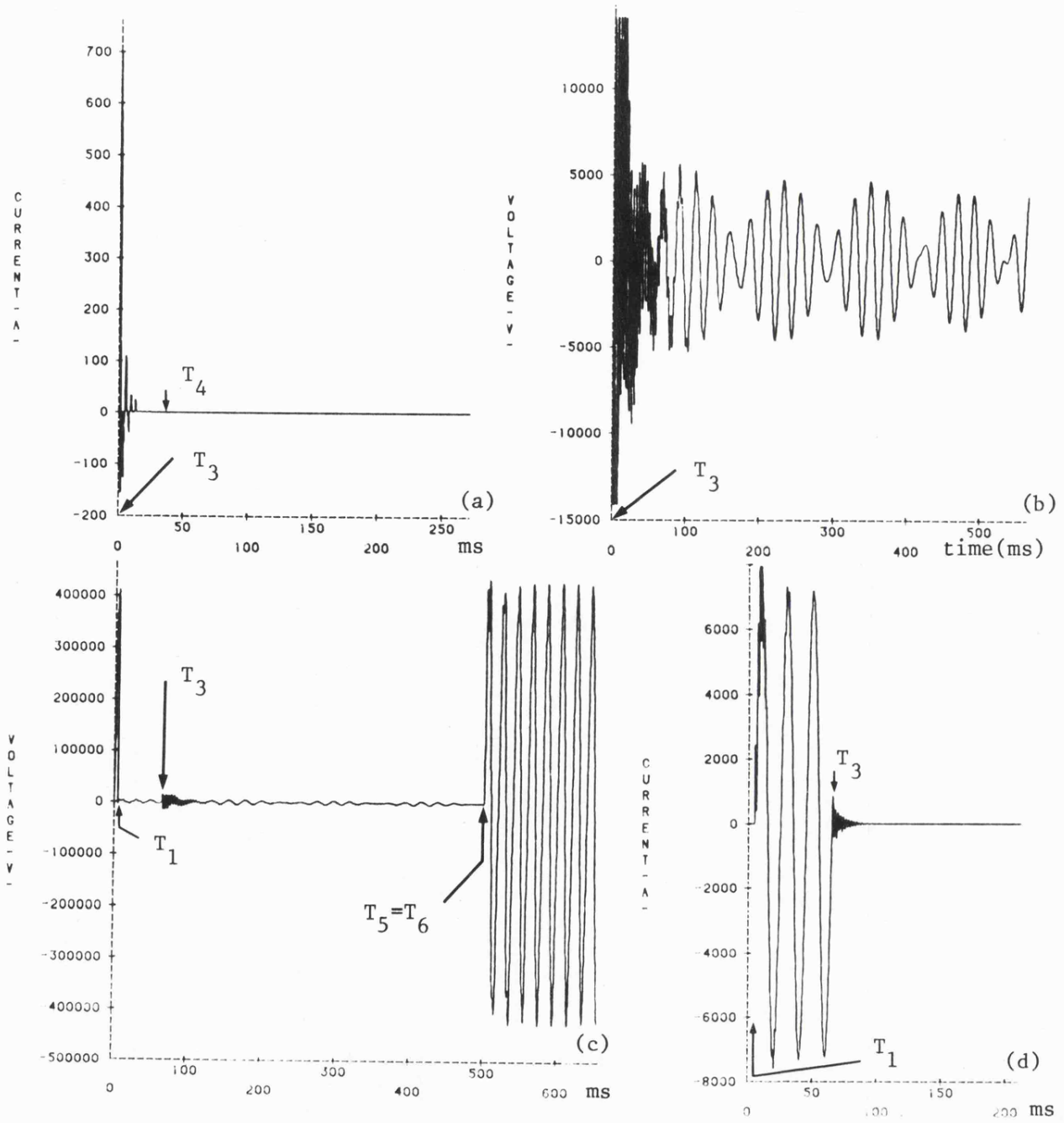

Fig. 9.2

Secondary arc behaviour

T_1 = 5 ms
T_2 = T_3 = 60 ms (after fault)
T_4 = 25 ms (after arc transition)
T_5 = T_6 = 495.2 ms (after fault)

(a) secondary arc current
(b) secondary arc voltage
(c) fault point voltage
(d) current in fault arc path

Fault conditions are stated in fig. 9.1.

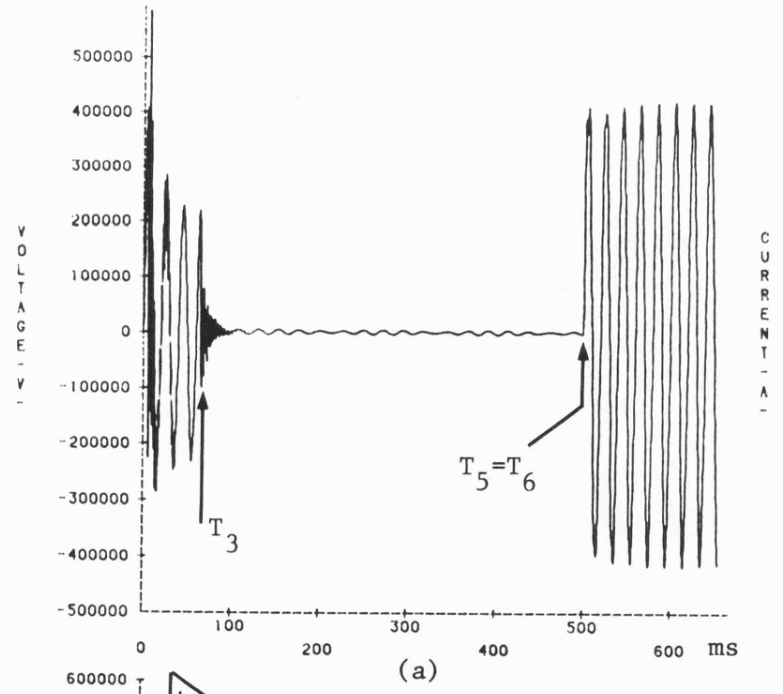

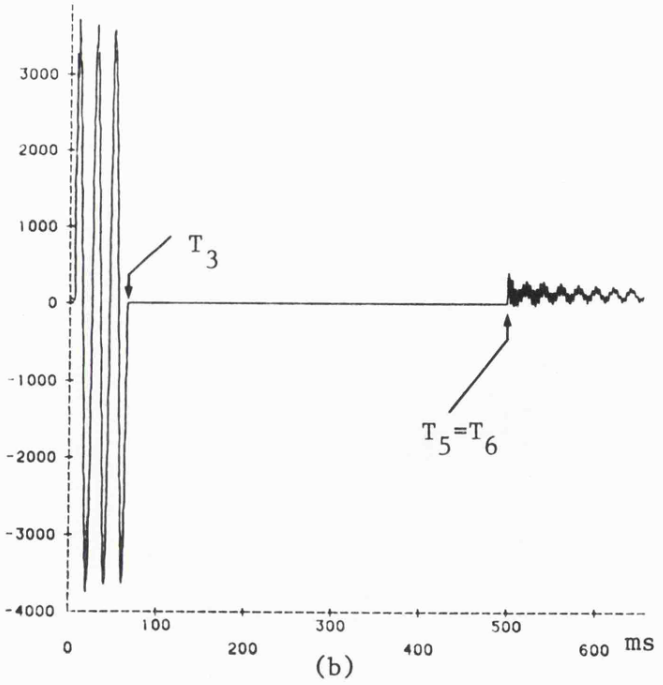

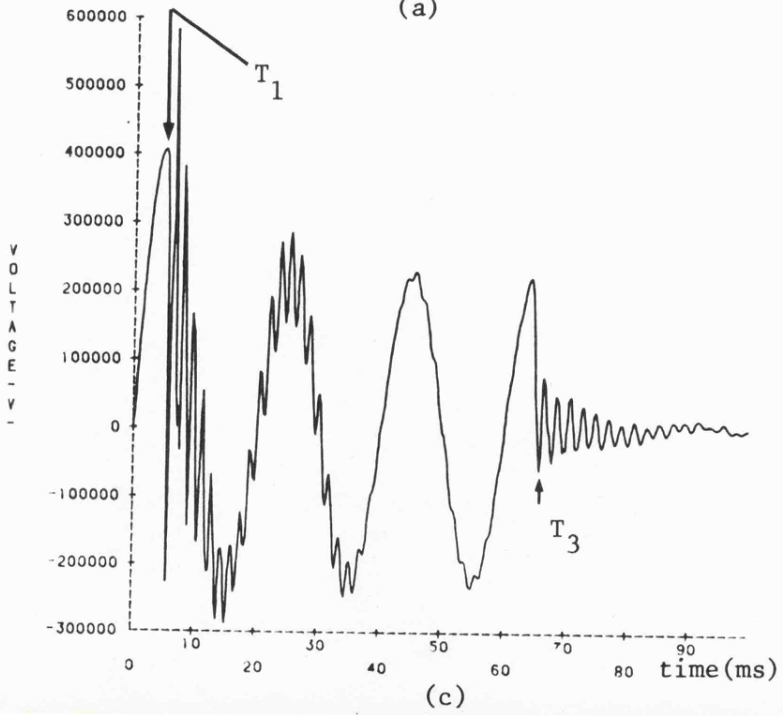

Fig. 9.3

Faulted phase voltage and current at end S

fault conditions are stated in Fig. 9.1

(a) 'a'-earth voltage at end S
(b) 'a'-phase current at end S
(c) enlargement of (a)

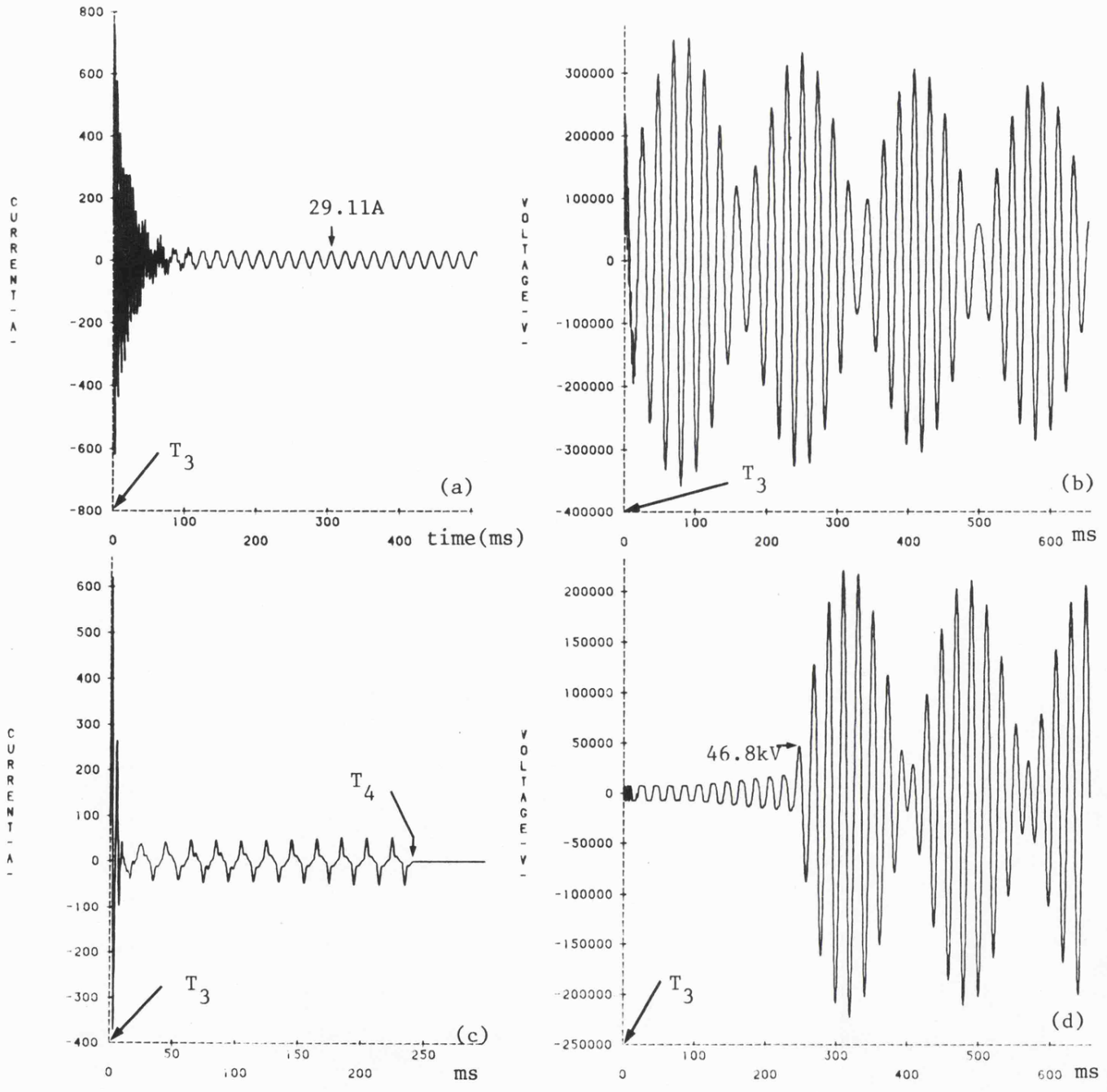

Fig. 9.4

Effect of fault position on arc extinction: compensation to 20A

'a'-earth fault at peak of prefault 'a'-phase voltage

$x_f = 0$

ℓ = 300 km, transposed

sen. end s.c.1 = 5000 MVA
rec. end s.c.1 = 5000 MVA

$V_S/V_R = 1\underline{/0^o}$, $Z_{S0}/Z_{S1} = 1$

$R_f = 0.5\Omega$

$h_1 = 0.75$, $h_o = 0.8787121$

T_3 = 60 ms (after fault)

T_4 = 241.6 ms (after arc transition)

(a) secondary arc current (constant arc path resistance of 0.5Ω)
(b) Thevenin voltage
(c) secondary arc current
(d) secondary arc voltage

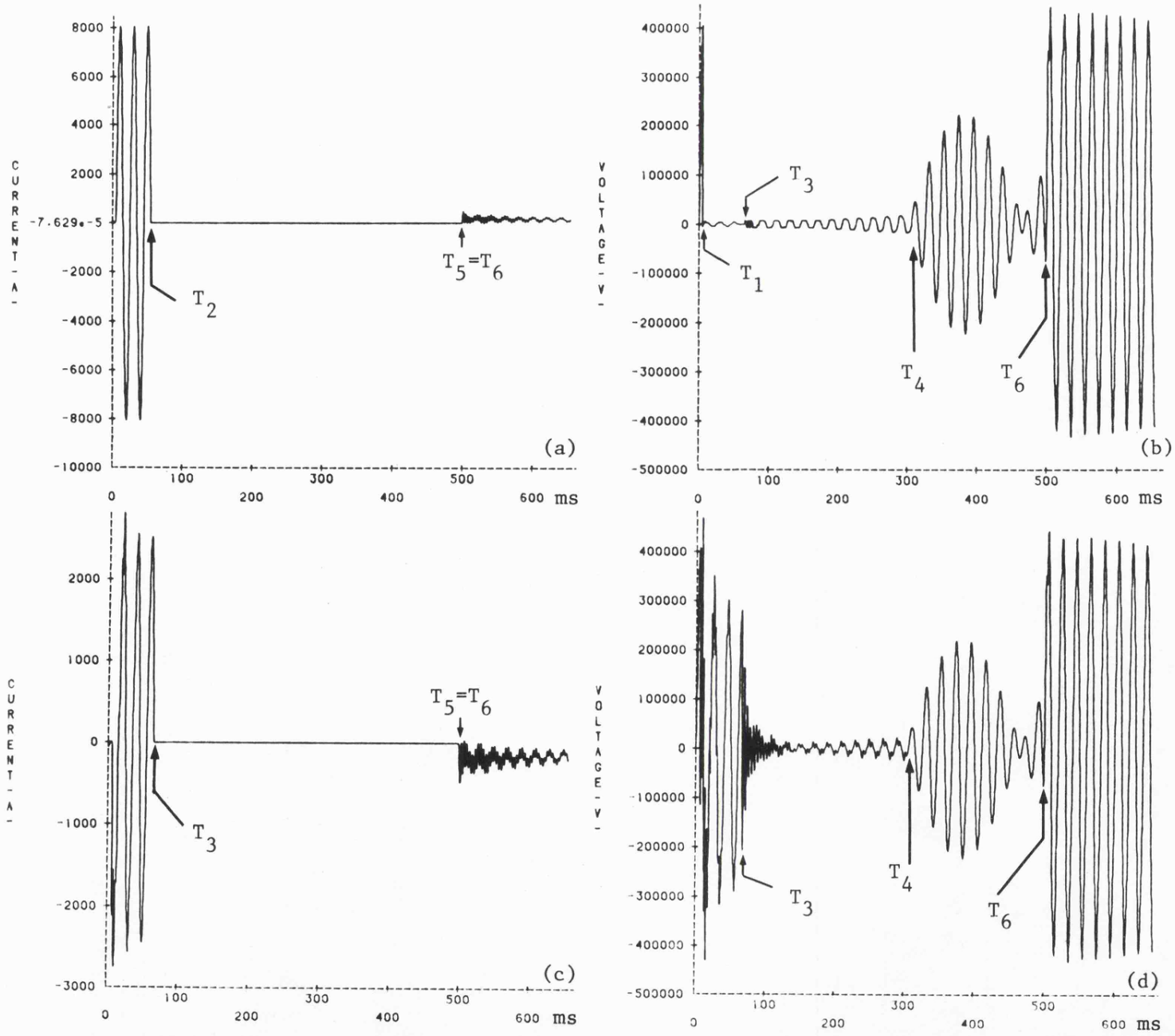

Fig. 9.5

Faulted-phase currents and voltages at ends S and R

Fault conditions are stated in Fig. 9.4

T_1 = 5 ms

T_2 = 50.2 ms (after fault)

$T_5 = T_6$ = 494.6 ms (after fault)

(a) 'a'-phase current at end S
(b) 'a'-earth voltage at end S
(c) 'a'-phase current at end R
(d) 'a'-earth voltage at end R

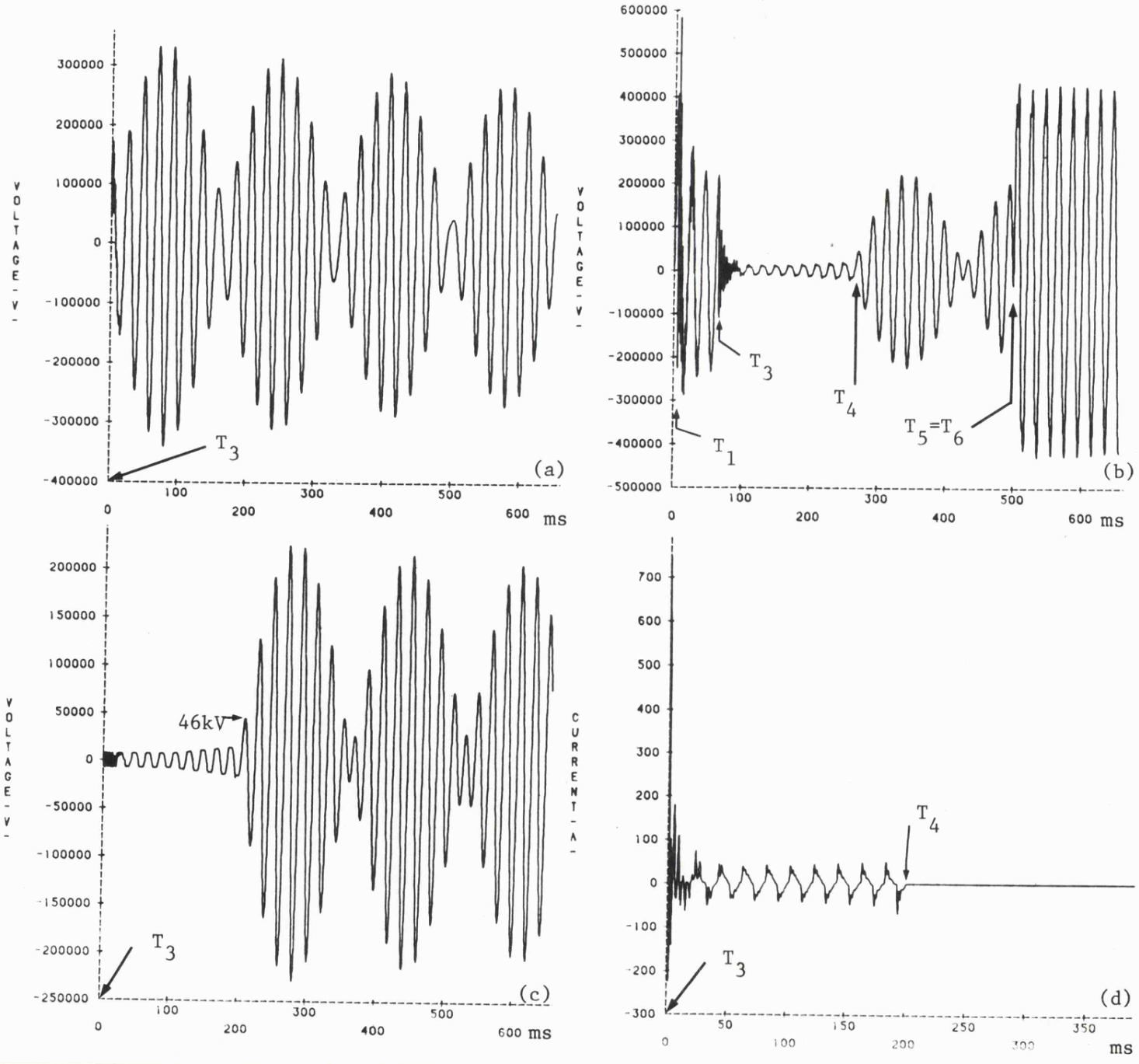

Fig. 9.6

Secondary arc behaviour for midpoint fault

'a'-earth fault at peak of prefault 'a'-phase voltage

x_f = 150 km, R_f = 0.5Ω

ℓ = 300 km, transposed

sen. end s.c.l = 5000 MVA
rec. end s.c.l = 5000 MVA

$V_S/V_R = 1\underline{/0^o}$, $Z_{SO}/Z_{S1} = 1$

$h_1 = 0.75$, $h_o = 0.8787121$

T_1 = 5 ms

T_2 = 60 ms (after fault)

T_3 = 60 ms (after fault)

T_4 = 200 ms (after arc transition)

$T_5 = T_6$ = 495 ms (after fault)

(a) Thevenin voltage
(b) 'a'-earth voltage at end S
(c) secondary arc voltage
(d) secondary arc current

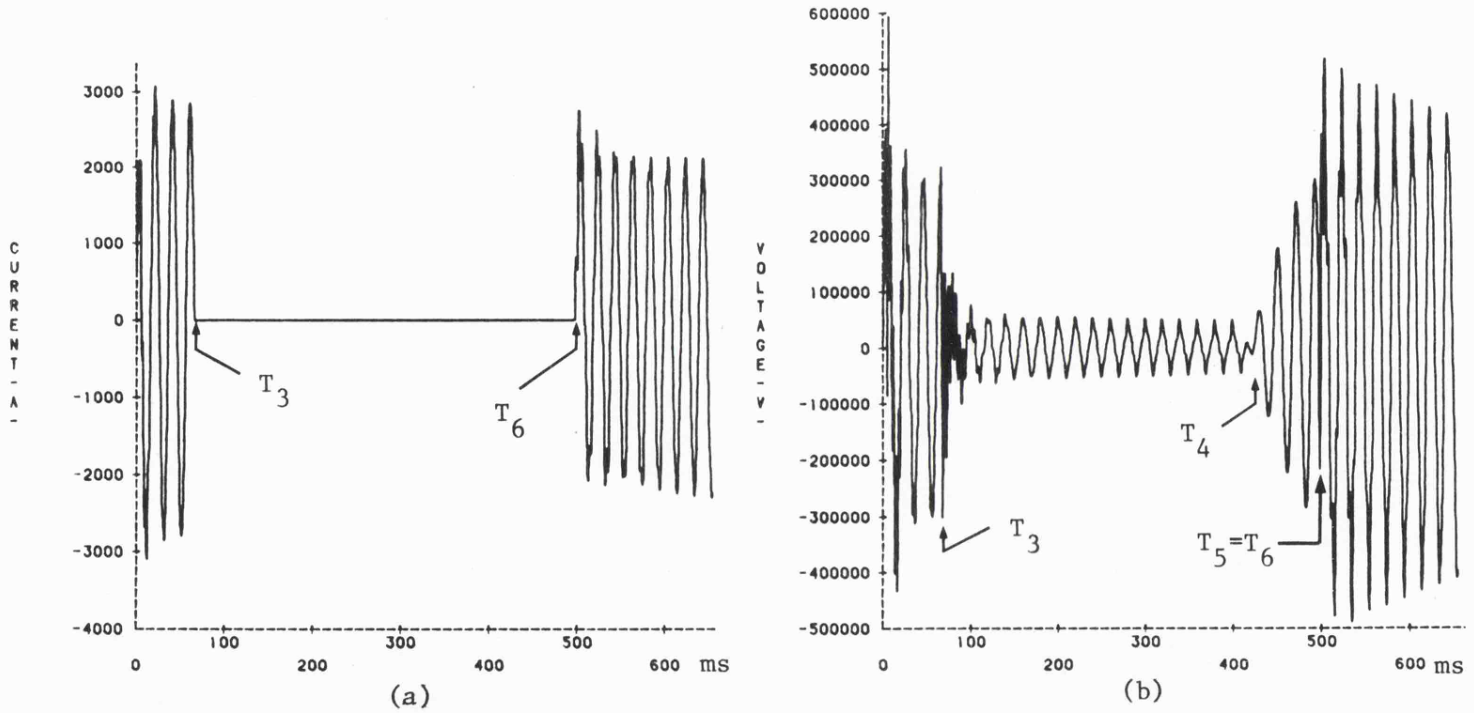

Fig. 9.8

Faulted phase current and voltage at end R

fault conditions are stated in Fig. 9.7

(a) 'a'-phase current
(b) 'a'-earth voltage

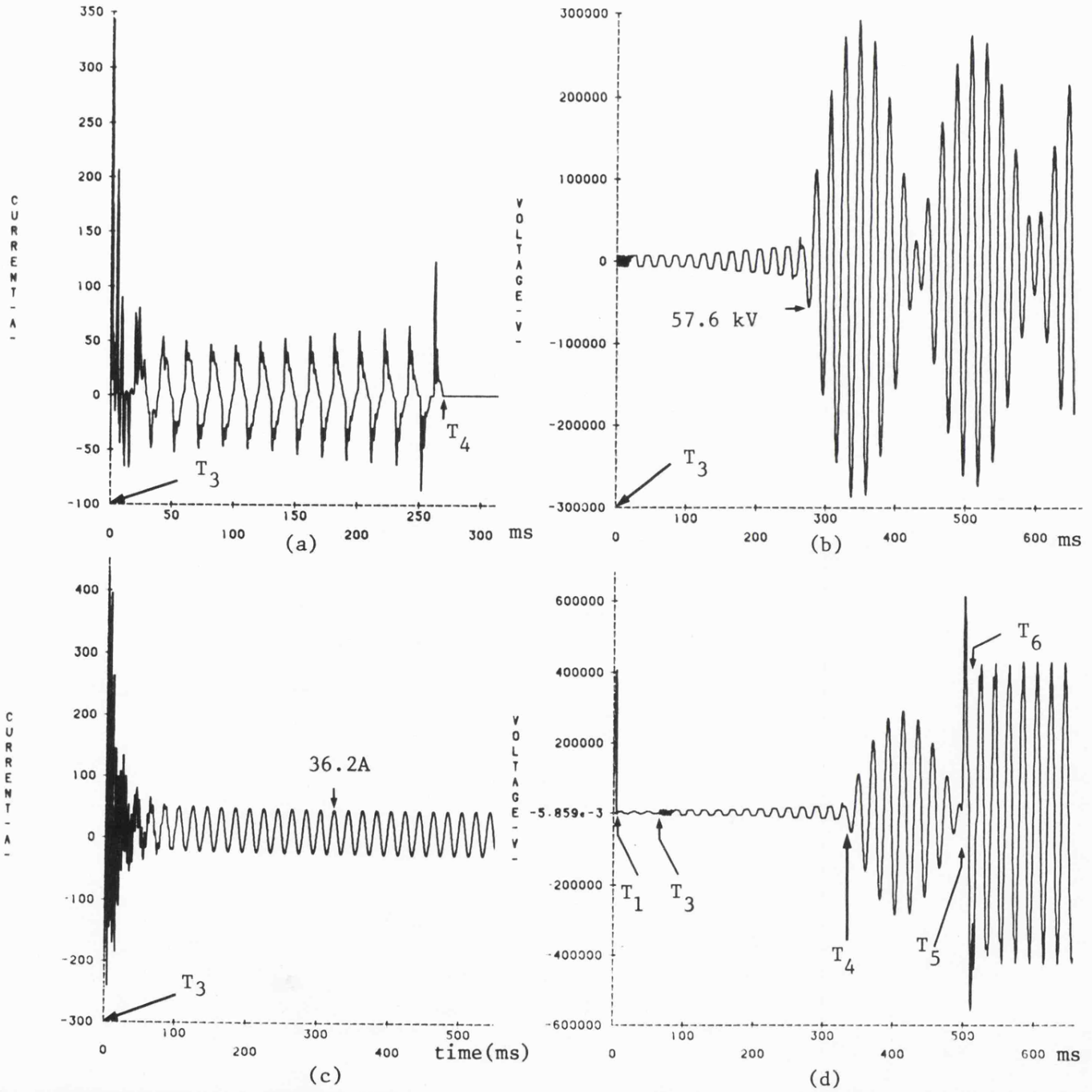

Fig. 9.9

Secondary arc behaviour for mid point fault

'a'-earth fault at peak of prefault 'a' phase voltage

x_f = 150 km, R_f = 0.5Ω

ℓ = 300 km, transposed

sen. end s.c.1 = 5000 MVA
rec. end s.c.1 = 5000 MVA

V_S/V_R = 1/25.73, Z_{SO}/Z_{S1} = 1

h_1 = 0.75, h_o = 0.8787121

T_1 = 4.28 ms

T_2 = 58.2 ms (after fault)

T_3 = 61.6 ms (after fault)

T_4 = 268.8 ms (after arc transition)

T_5 = 493.8 ms (after fault)

T_6 = 509.8 ms (after fault)

(a) secondary arc current
(b) secondary arc voltage
(c) secondary arc current (0.5Ω arc path resistance)
(d) fault point voltage

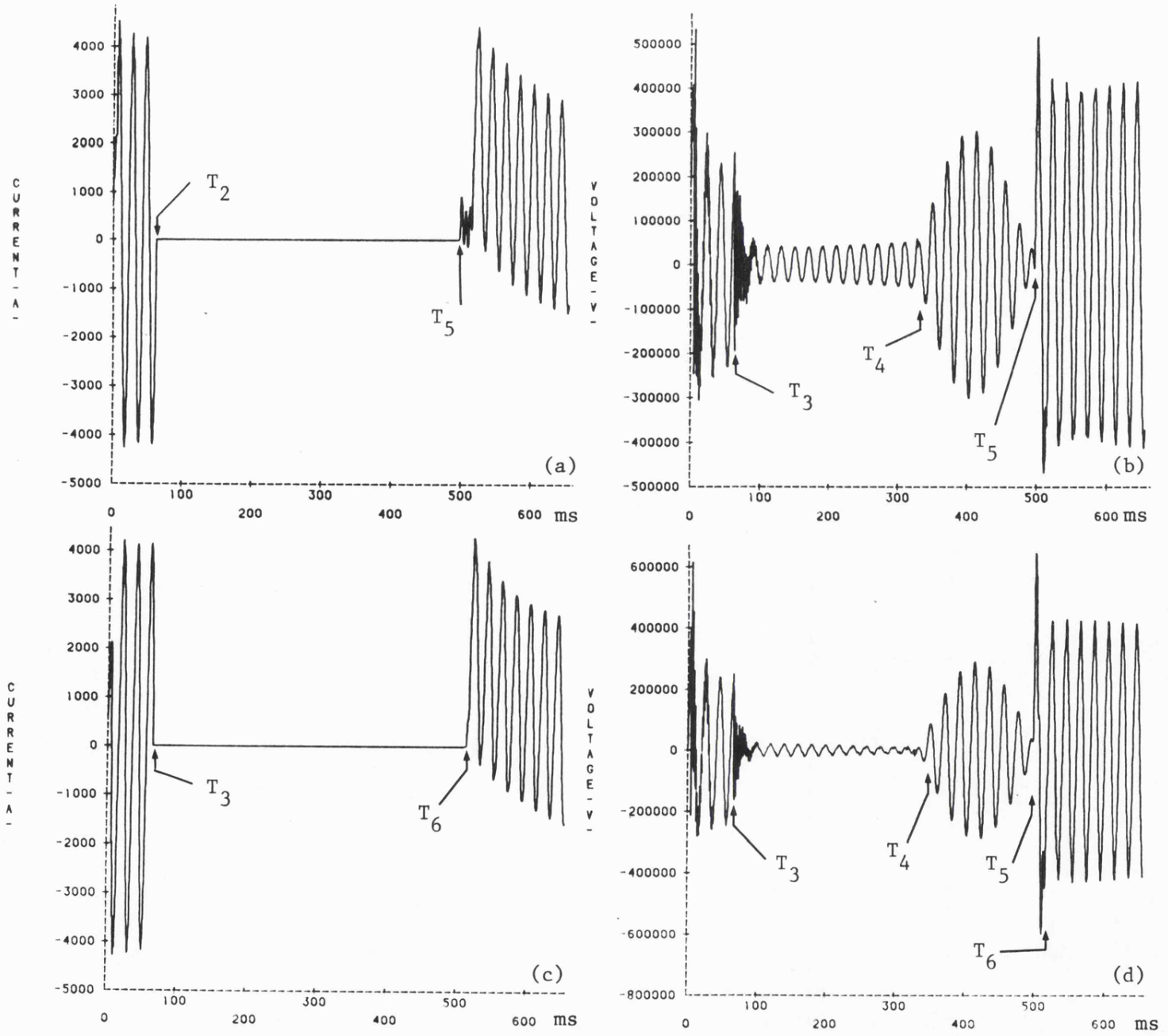

Fig. 9.10

Faulted phase currents and voltages at ends S and R

Fault conditions are stated in Fig. 9.9.

(a) 'a'-phase current at end S
(b) 'a'-earth voltage at end S
(c) 'a'-phase current at end R
(d) 'a'-earth voltage at end R

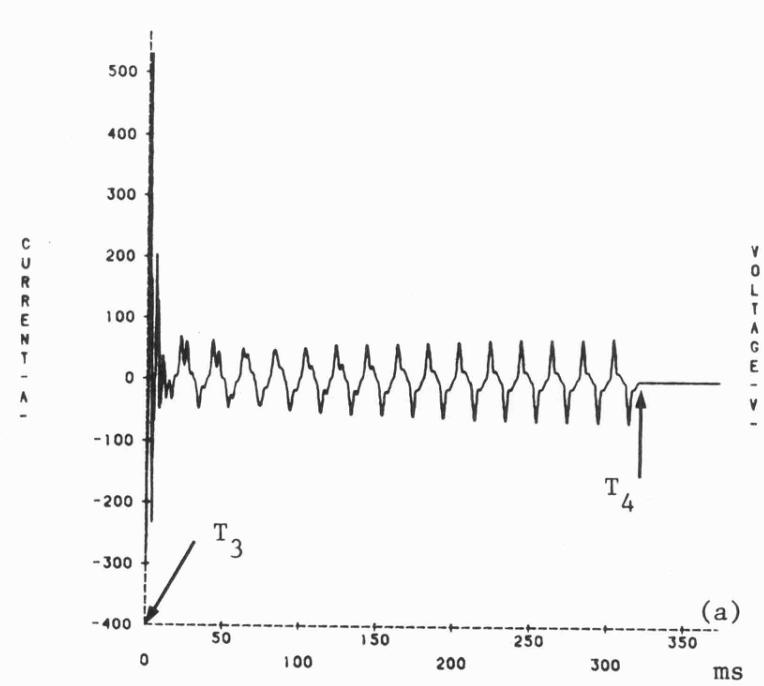

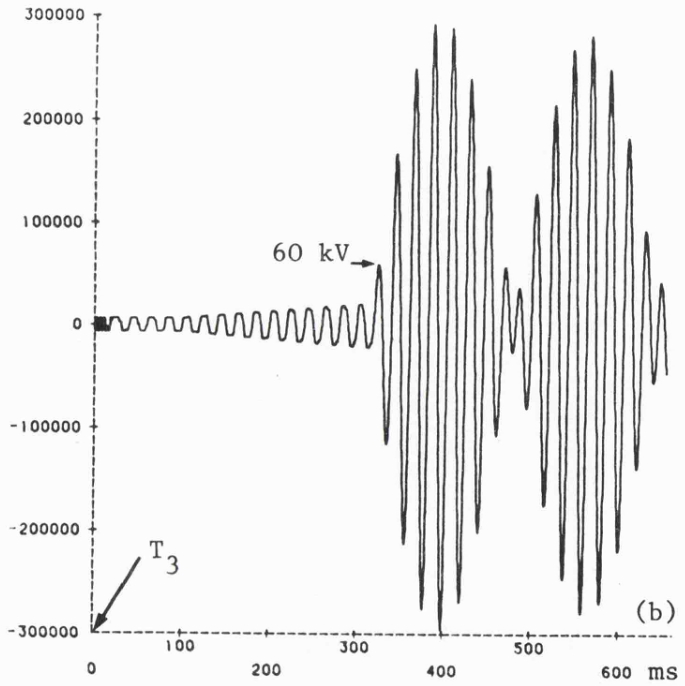

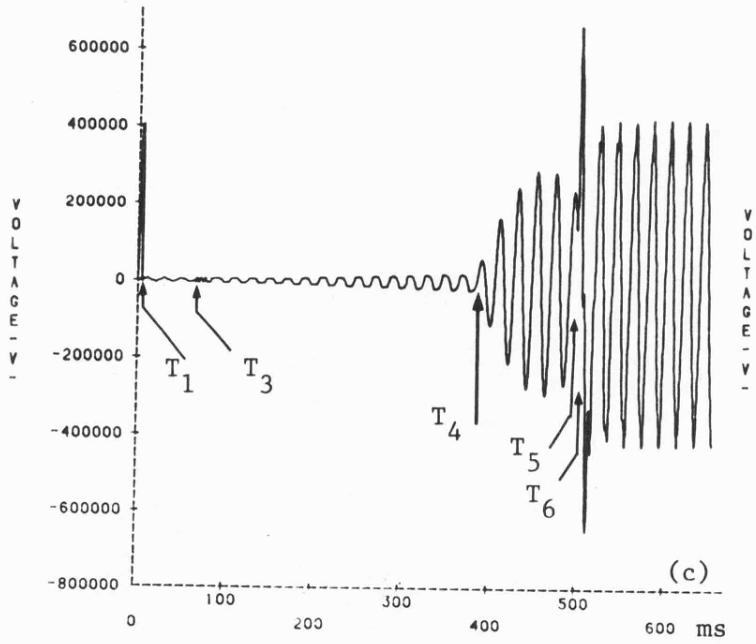

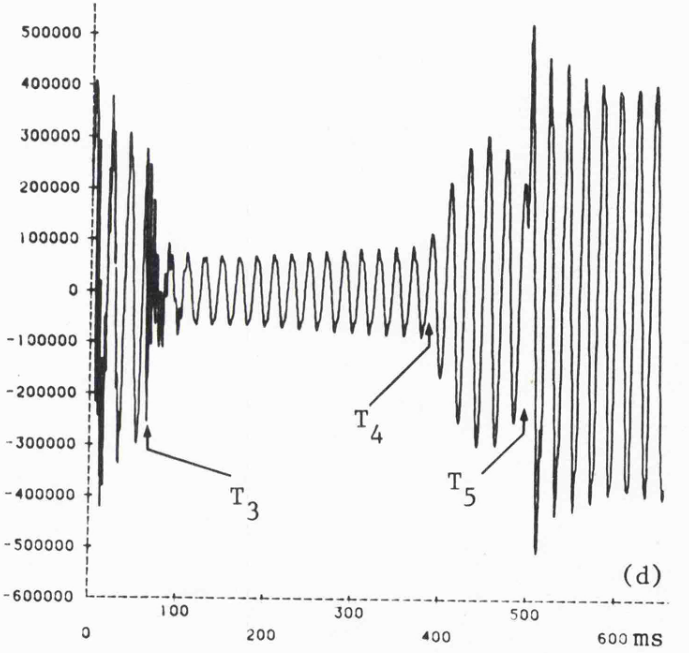

Fig. 9.11

Secondary arc behaviour for fault at end R

x_f = 300 km, R_f = 0.5Ω

ℓ = 300 km, transposed

sen. end s.c.l = 5000 MVA
rec. end s.c.l = 5000 MVA

$V_S/V_R = 1/25.73$, $Z_{SO}/Z_{S1} = 1$

$h_1 = 0.75$, $h_o = 0.8787121$

T_1 = 5 ms

T_2 = 57.4 ms (after fault)

T_3 = 60.8 ms (after fault)

T_4 = 320 ms (after arc transition)

T_5 = 494 ms (after fault)

T_6 = 509.4 ms (after fault)

(a) secondary arc current
(b) secondary arc voltage
(c) 'a'-earth voltage at end R
(d) 'a'-earth voltage at end S

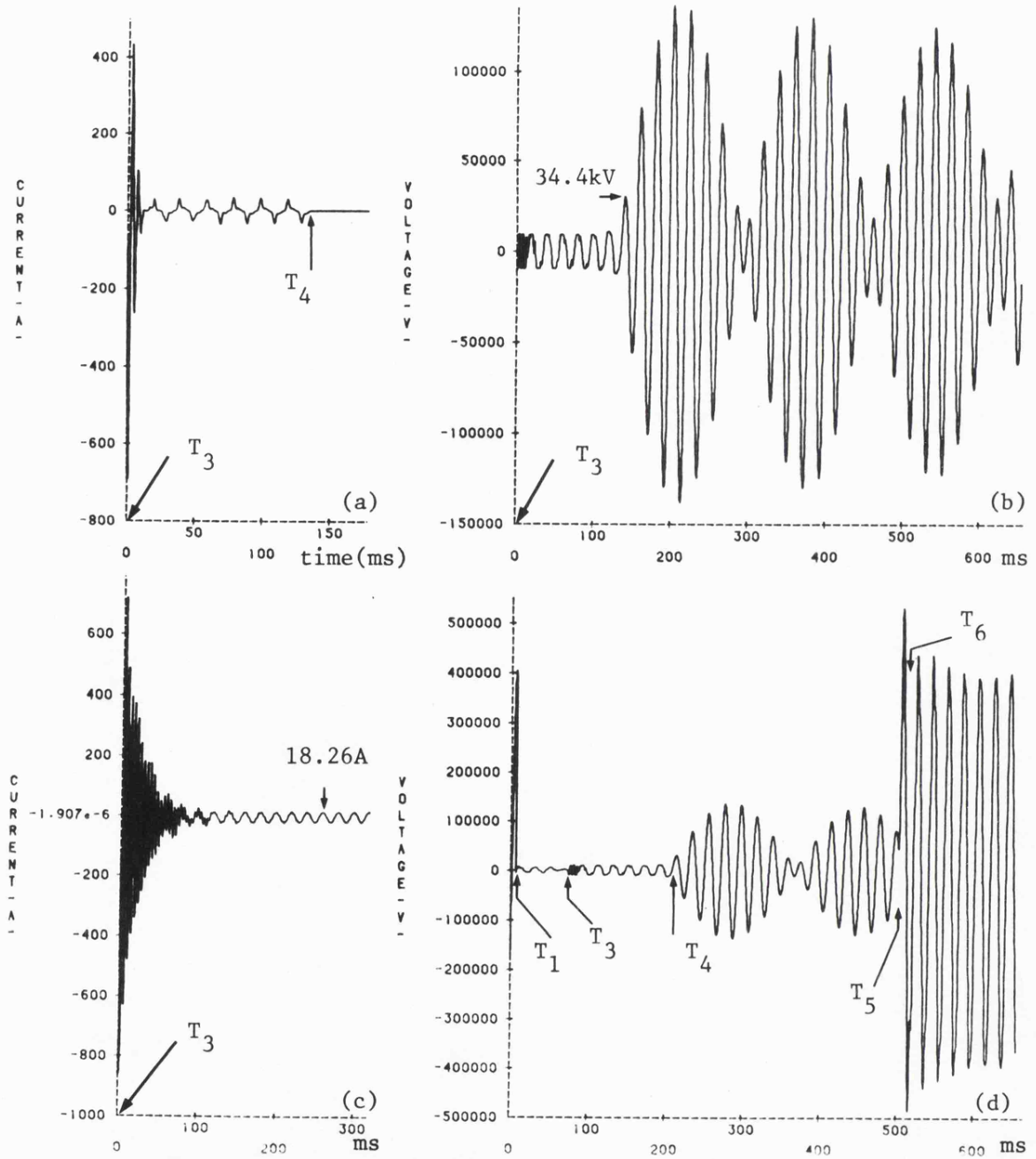

Fig. 9.12

Effect of power transfer direction on arc extinction

'a'-earth fault at peak of prefault 'a'-phase voltage

x_f = 0, R_f = 0.5Ω, ℓ = 300 km (transposed)

sen. end s.c.l = rec. end s.c.l = 5000 MVA

$V_S/V_R = 1\angle -25.73$, Z_{SO}/Z_{S1} = 1.0

h_1 = 0.75, h_o = 0.8787121

T_1 = 3.6 ms

T_2 = 51 ms (after fault)

T_3 = 67.4 ms (after fault)

T_4 = 134.4 ms (after arc transition)

T_5 = 496.4 ms (after fault

T_6 = 509 ms (after fault)

(a) secondary arc current
(b) secondary arc voltage
(c) secondary arc current (constant arc path resistance of 0.5Ω)
(d) fault point voltage

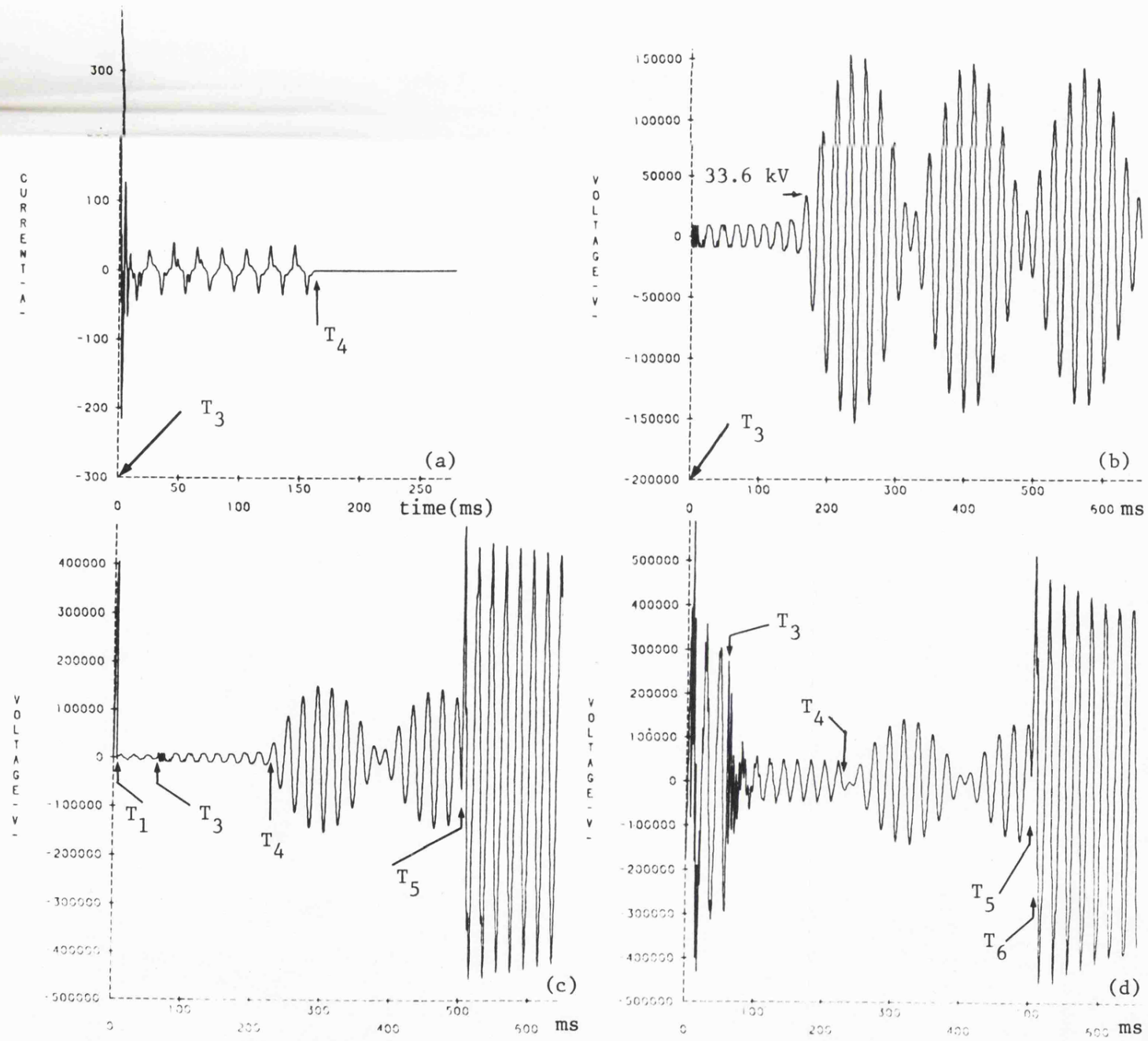

Fig. 9.13

Secondary arc behaviour for fault at end R

'a'-earth fault at peak of prefault 'a'-phase voltage

x_f = 300 km, R_f = 0.5Ω

ℓ = 300 km, transposed

sen. end s.c.1 = 5000 MVA
rec. end s.c.1 = 5000 MVA

$V_S/V_R = 1\angle -25.73$, $Z_{SO}/Z_{S1} = 1$

$h_1 = 0.75$, $h_o = 0.8787121$

T_1 = 5 ms

T_2 = 52.4 ms (after fault)

T_3 = 59.4 ms (after fault)

T_4 = 161.6 ms (after arc transition)

T_5 = 497.6 ms (after fault)

T_6 = 500.8 ms (after fault)

(a) secondary arc current
(b) secondary arc voltage
(c) 'a'-earth voltage at end R
(d) 'a'-earth voltage at end S

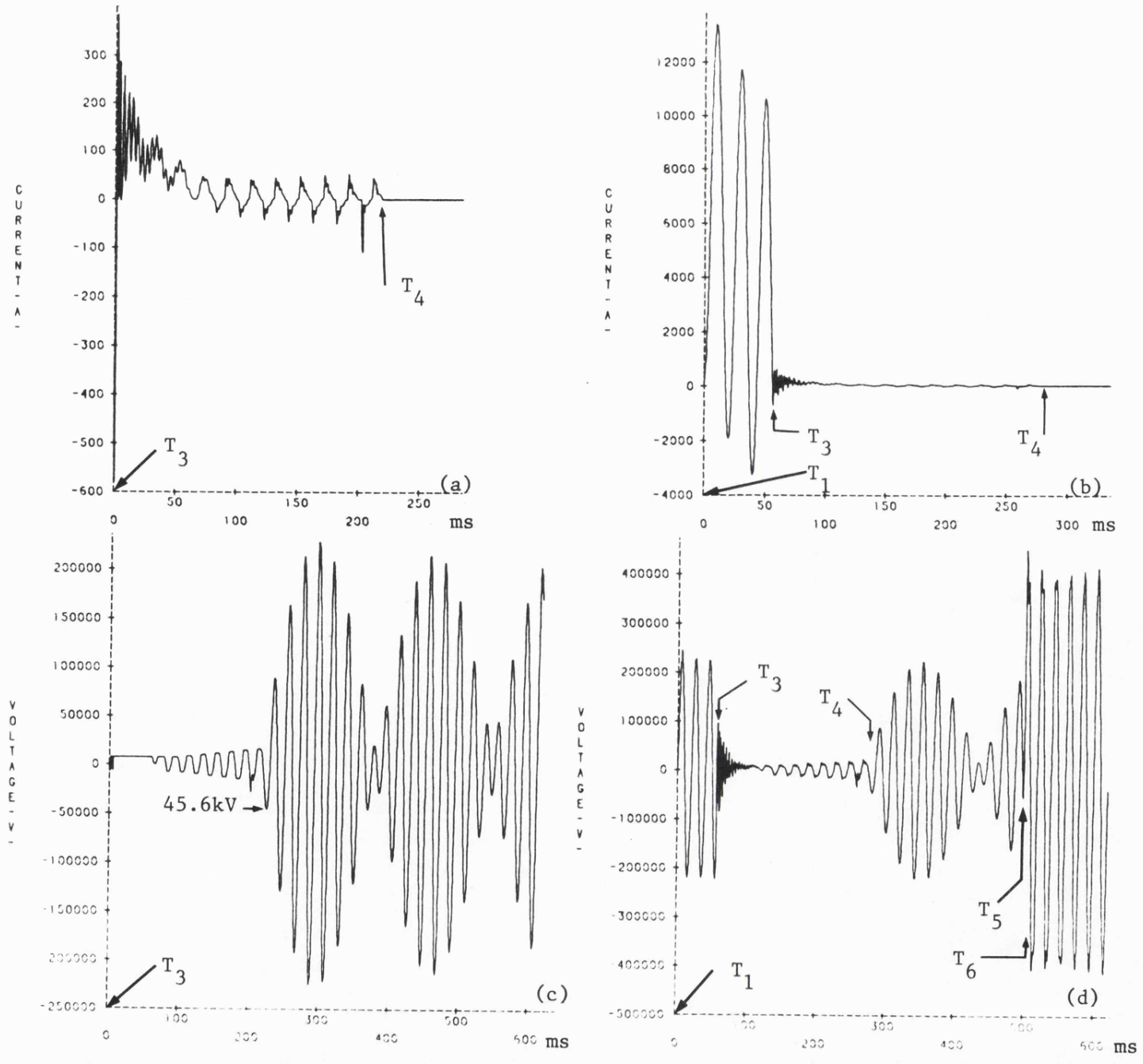

Fig. 9.14

Effect of fault inception time on arc extinction

'a'-earth fault at zero of prefault 'a'-phase voltage

x_f = 150 km, R_f = 0.5Ω

ℓ = 300 km, transposed

sen. end s.c.l = 5000 MVA
rec. end s.c.l = 5000 MVA

$V_S/V_R = 1\underline{/0^o}$, $Z_{SO}/Z_{S1} = 1$

$h_1 = 0.75$, $h_o = 0.8787121$

T_1 = 5 ms

$T_2 = T_3$ = 56.4 ms (after fault)

T_4 = 219.2 ms

T_5 = 499.8 ms (after fault)

T_6 = 503 ms (after fault)

(a) secondary arc current
(b) current in fault arc path
(c) secondary arc voltage
(d) 'a'-earth voltage at end S

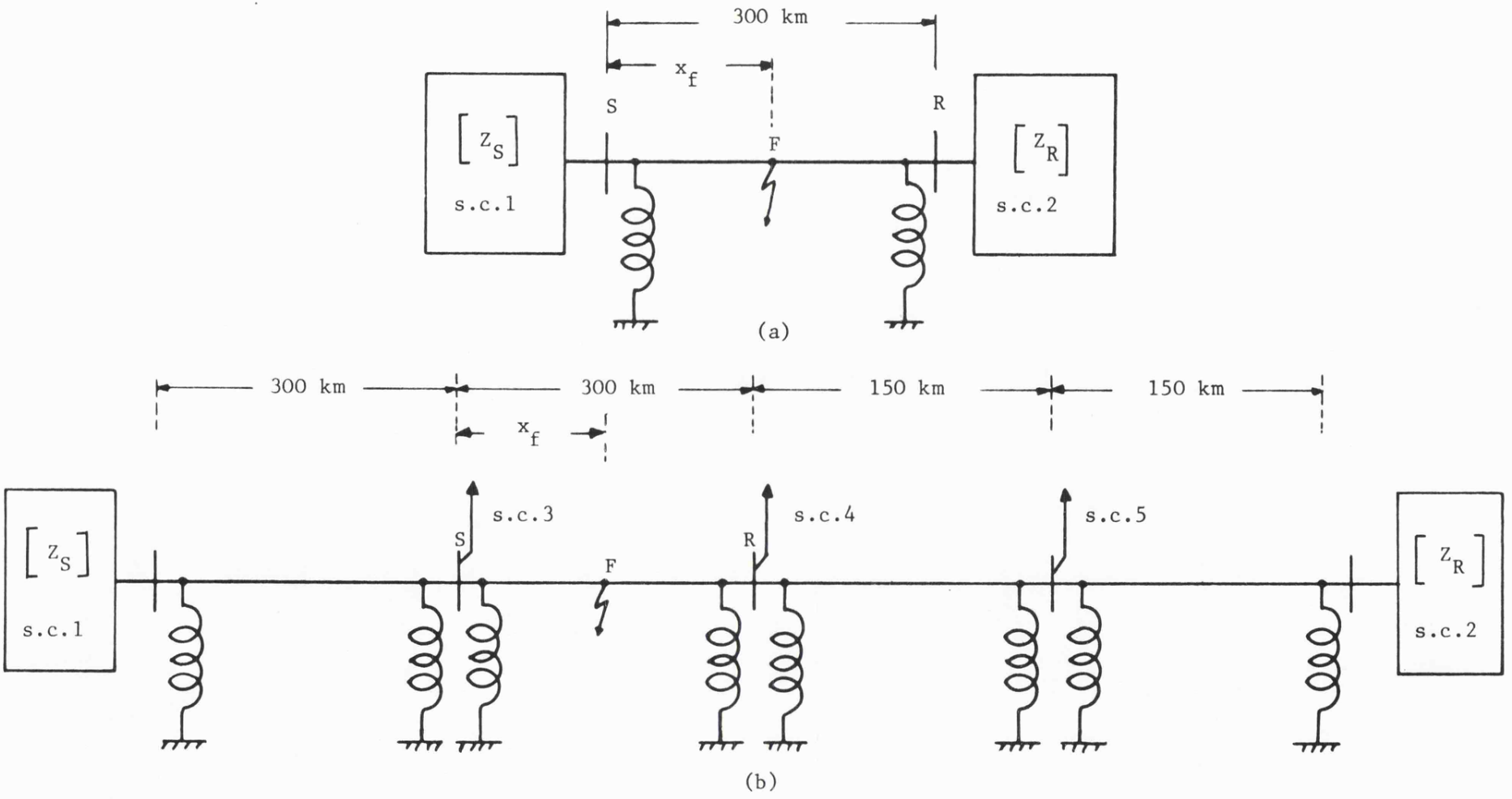

Fig. 9.15 Schematic diagram of the shunt-compensated systems studied

(a) single-section feeder system
(b) four-section feeder system

s.c.1-s.c.5 are staed in chapter 7

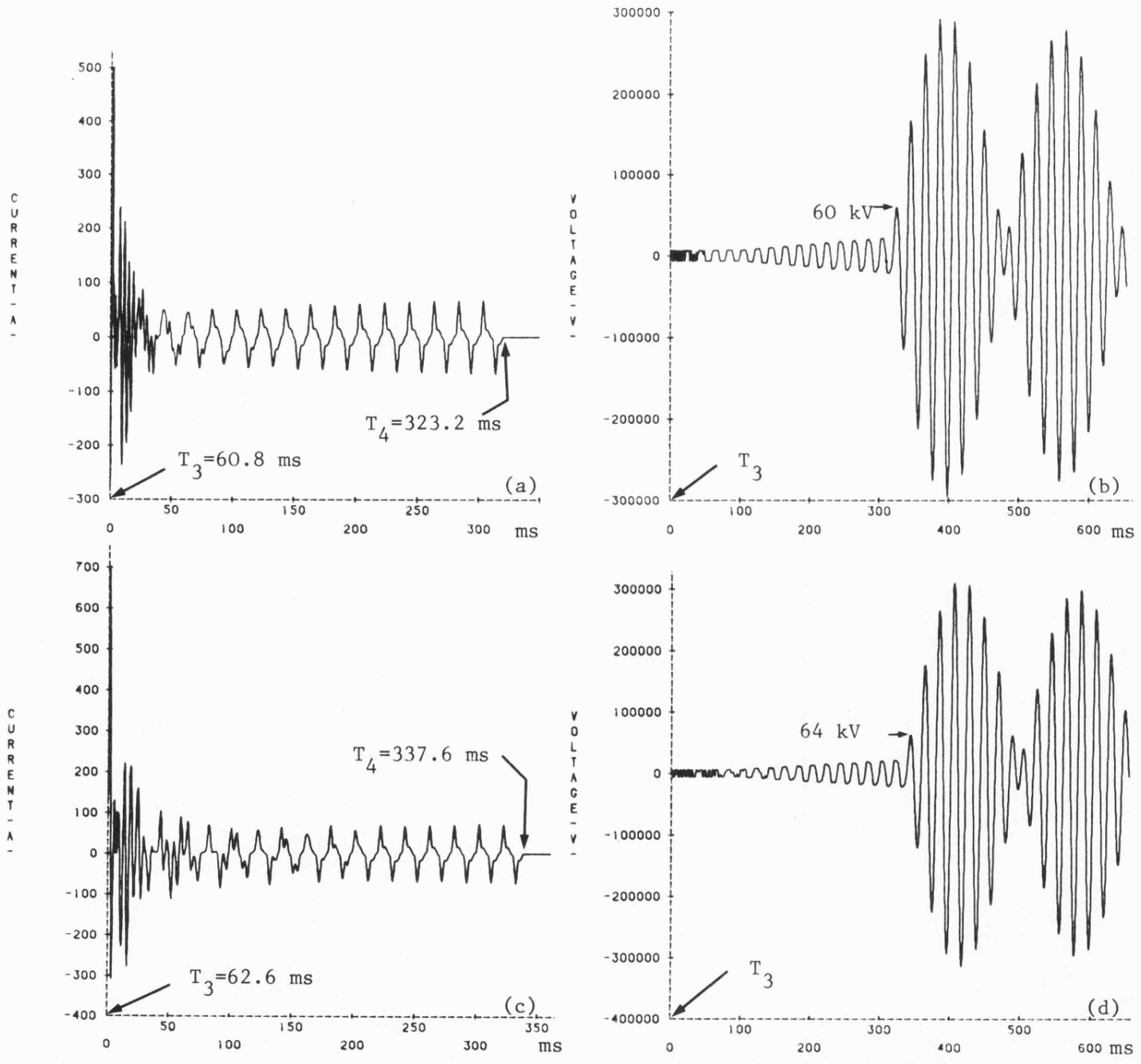

Fig. 9.16

Response of 4-section feeder system

$V_S/V_R = 1\angle 25.73^{\circ}$, $Z_{SO}/Z_{S1} = 1$

$h_1 = 0.75$, $h_o = 0.8787121$

$\ell = 300$ km, transposed

System configuration is shown in Fig. 9.15(b)

(a),(b): secondary arc current and voltage for fault at end R

(c),(d): secondary arc current and voltage for fault at end S

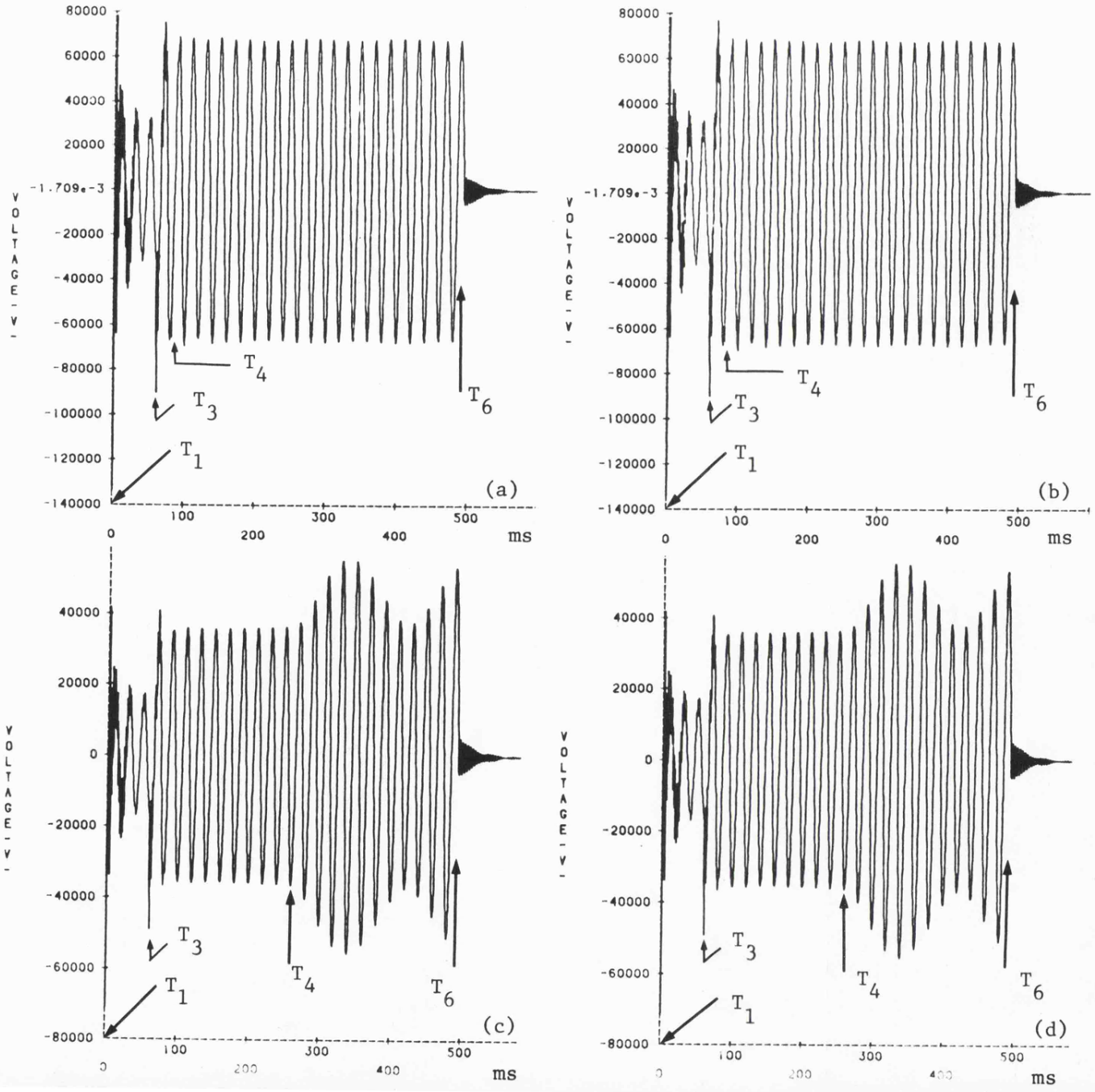

Fig. 9.17

Effect of the shunt reactor parameters on the voltage across the neutral reactors

(a),(b) voltage across the neutral reactors at the sending and receiving ends respectively

Fault conditions are stated in Figs. 9.1-9.2

(c),(d) voltage across the neutral reactors at the sending and receiving ends respectively

Fault conditions are stated in Fig. 9.6

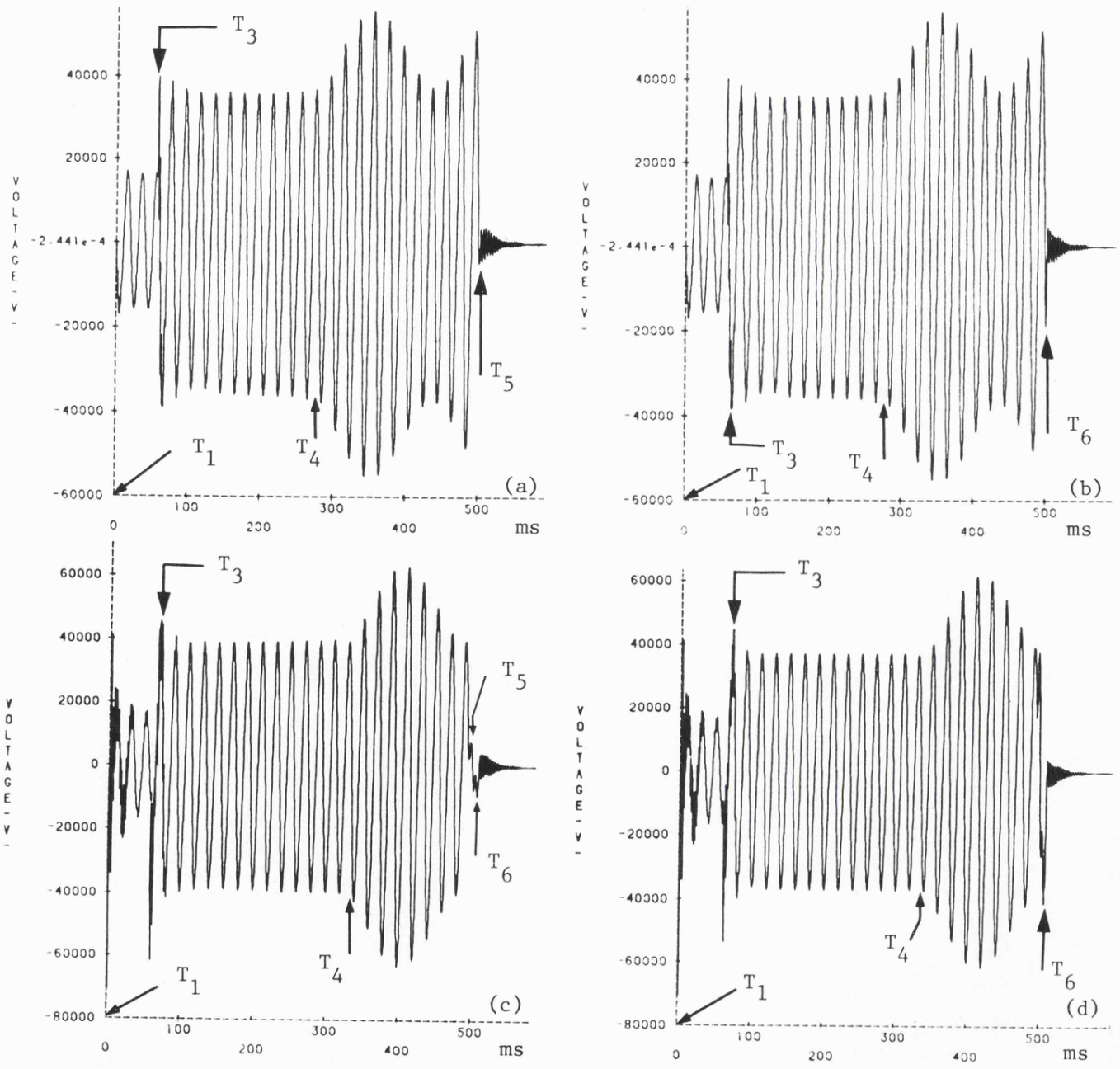

Fig. 9.18

Effect of fault inception time and pre-fault power transfer on the voltage across the neutral reactor

(a),(b) voltage across the neutral reactors at the sending and receiving ends respectively

Fault conditions are stated in Fig. 9.14

(c),(d) voltage across the neutral reactors at the sending and receiving ends respectively

Fault conditions are stated in Fig. 9.9

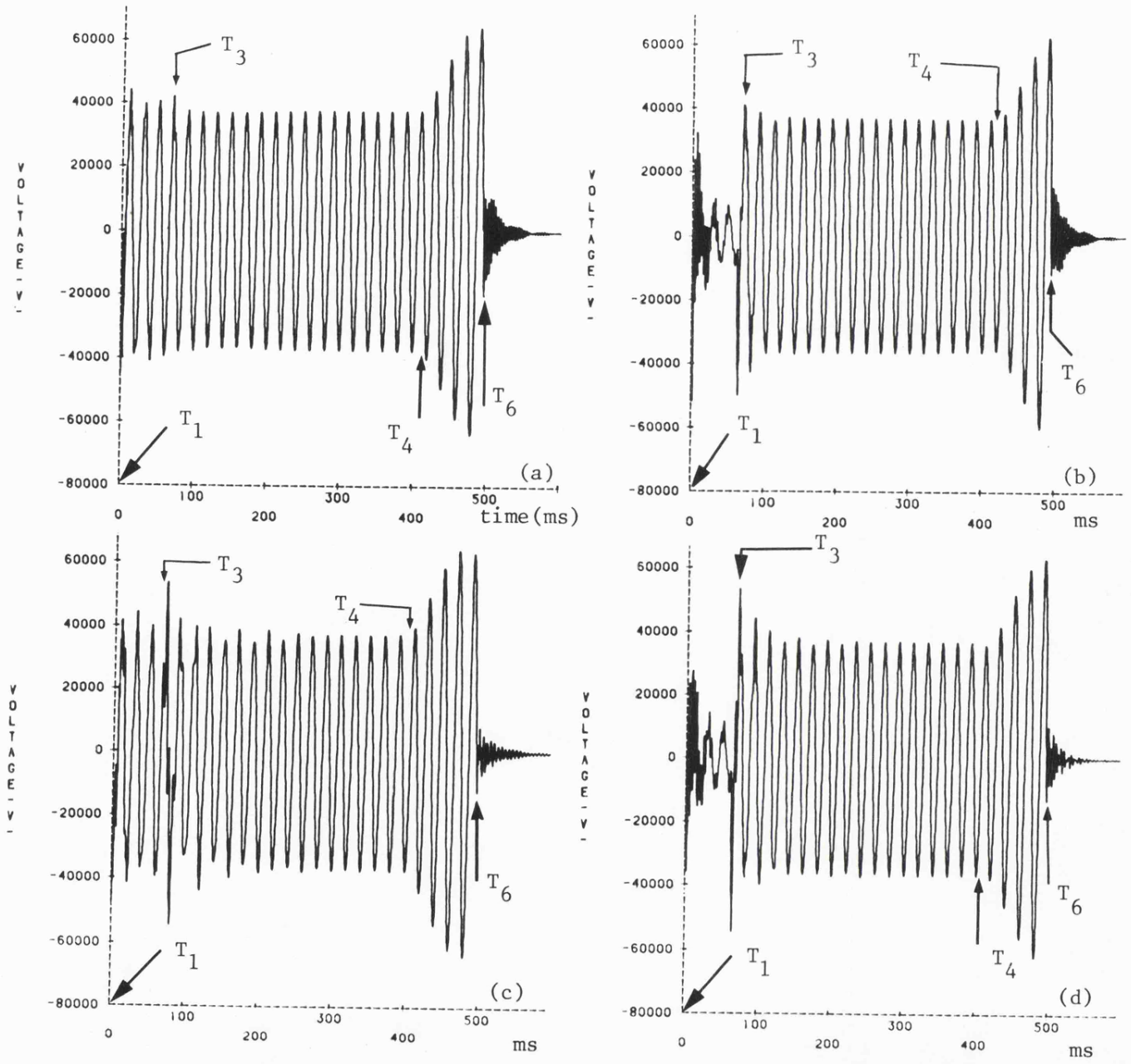

Fig. 9.19

Effect of the busbar termination on the voltage across the neutral reactors

(a),(b) voltage across the neutral reactors at the sending and receiving ends respectively

x_f = 0, two feeder system

Fault conditions are stated in Fig. 9.7.

(c),(d) voltage across the neutral reactors at the sending and receiving ends respectively

x_f = 0, four feeder system

Fault conditions are stated in Fig. 9.16

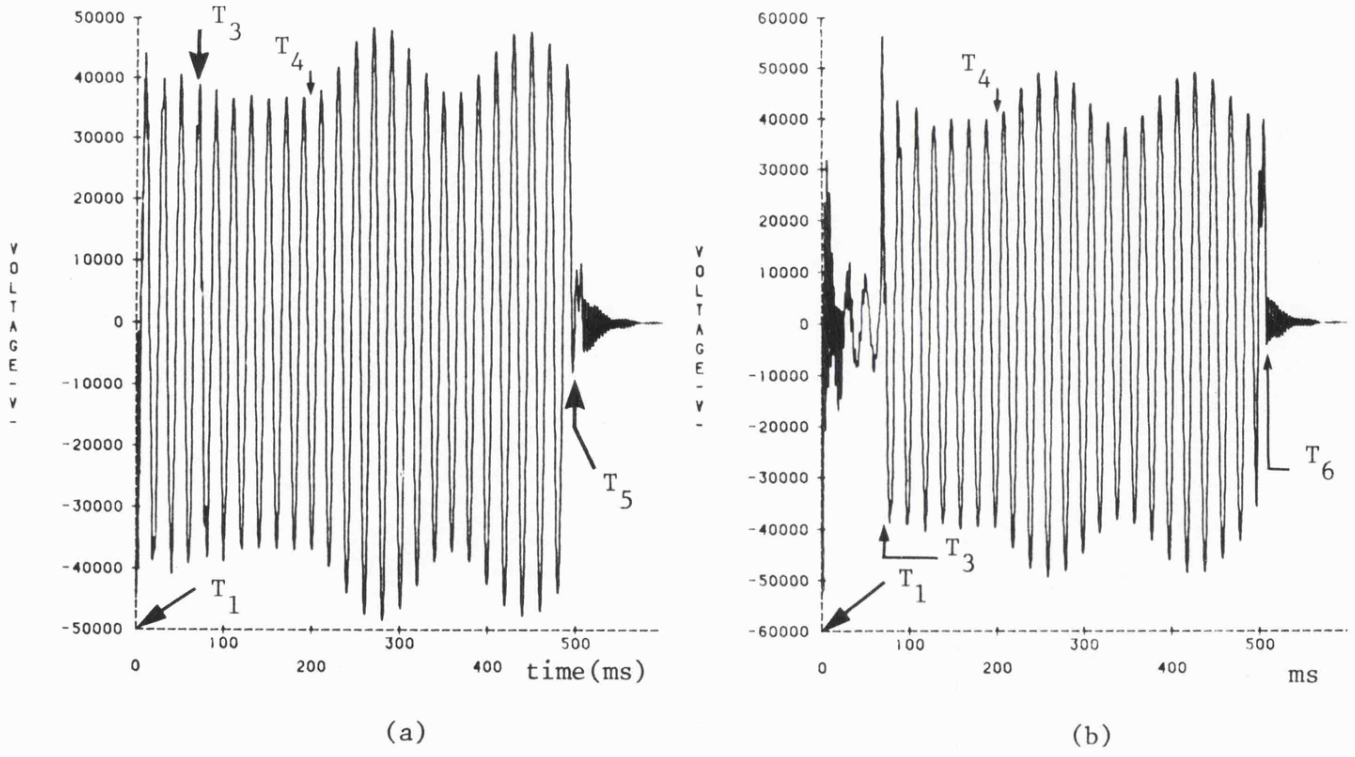

Fig. 9.20

Effect of power transfer direction on voltage across the neutral reactors

$x_f = 0$

ℓ = 300 km, transposed

Fault conditions are stated in Fig. 9.12

(a) neutral reactor voltage at end S
(b) neutral reactor voltage at end R

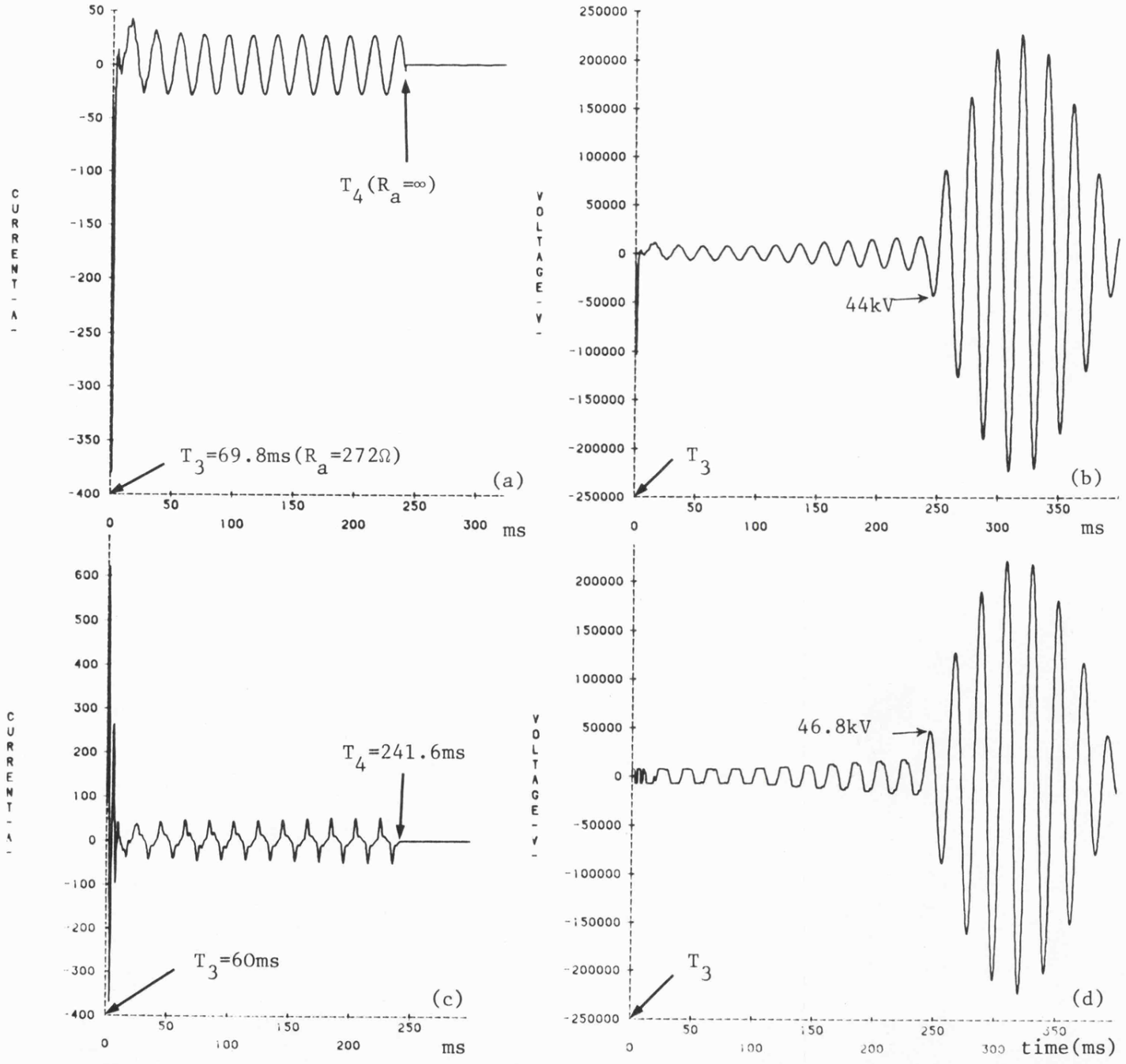

Fig. 9.21

Representation of the secondary arc path by a time dependent linear resistance

(a),(b):

$x = 0$, $R_f = 0.5\Omega$

ℓ = 300 km, transposed

$R_a(t) = V_p \ell_a(t)/I_p$, $t < 0.241$s

$R_a(t) = \infty$, $t > 0.241$ s

$\ell_a(t)/\ell_o = 1$, $t < 0.1$s

$= 10t$, $t > 0.1$s

(a) secondary arc current
(b) secondary arc voltage

(c),(d):

$x = 0$, $R_f = 0.5\Omega$

ℓ = 300 km, transposed secondary arc current and voltage waveform using the non-linear arc characteristic

Fault conditions are stated in Fig. 9.4

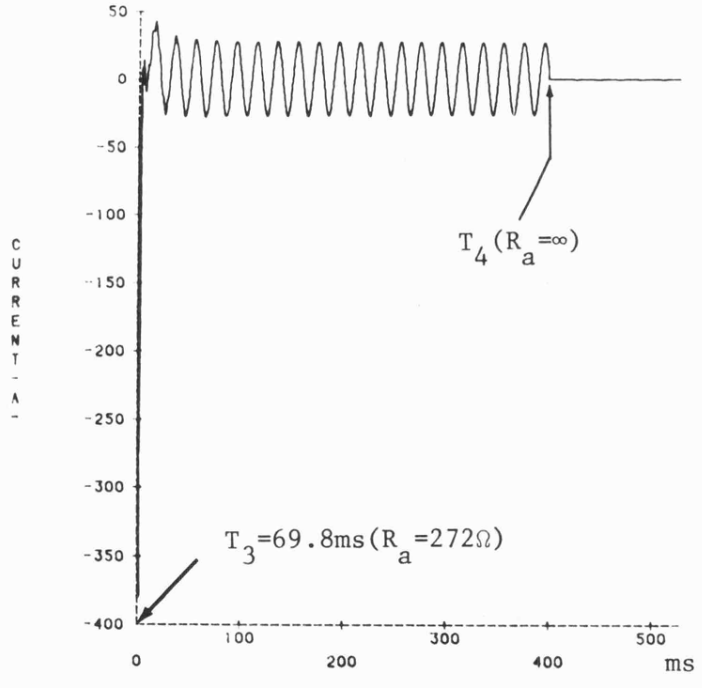

(e)

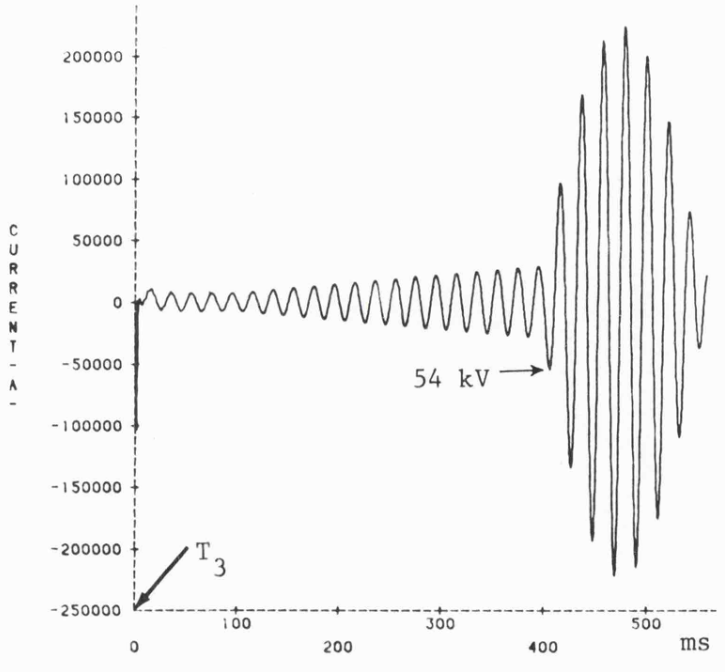

(f)

Fig. 9.21 (continued)

(e),(f):

$x = 0$, $R_f = 0.5\Omega$

$\ell = 300$ km, transposed

$R_a(t) = V_p \ell_a(t)/I_p$, $t < 0.4s$

$R_a(t) = \infty$, $t > 0.4s$

$\ell_a(t)/\ell_o = 1$, $t < 0.1s$

$= 10t$, $t > 0.1s$

(e) secondary arc current
(f) secondary arc voltage

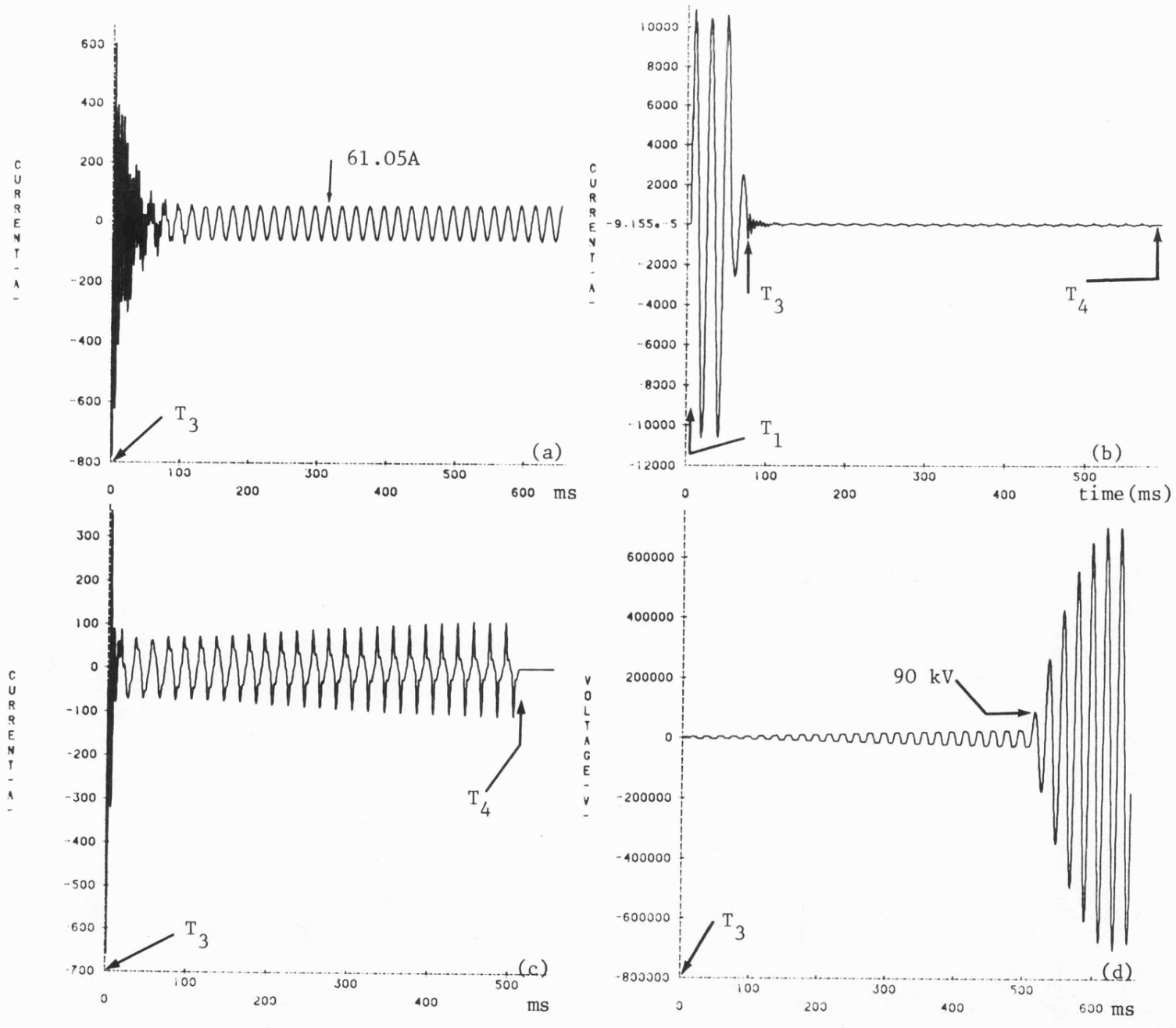

Fig. 9.22

Effect of shunt reactors with directly grounded neutrals on arc extinction

'a'-earth fault at peak of prefault 'a'-phase voltage

$x_f = 0$, $R_f = 0.5\Omega$

$\ell = 300$ km, transposed

$V_S/V_R = 1/0^o$, $Z_{SO}/Z_{S1} = 1$

sen. end s.c.1 = 5000 MVA

rec. end s.c.1 = 5000 MVA

$h_1 = 0.75$, $h_o = 1.195$

$T_1 = 5$ ms

$T_2 = 50.2$ ms

$T_3 = 69.8$ ms

$T_4 = 511.6$ ms

$T_5 = T_6 = 495$ ms

(a) secondary arc current (secondary arc path = 0.5Ω)

(b) current in fault arc path

(c) secondary arc current

(d) secondary arc voltage

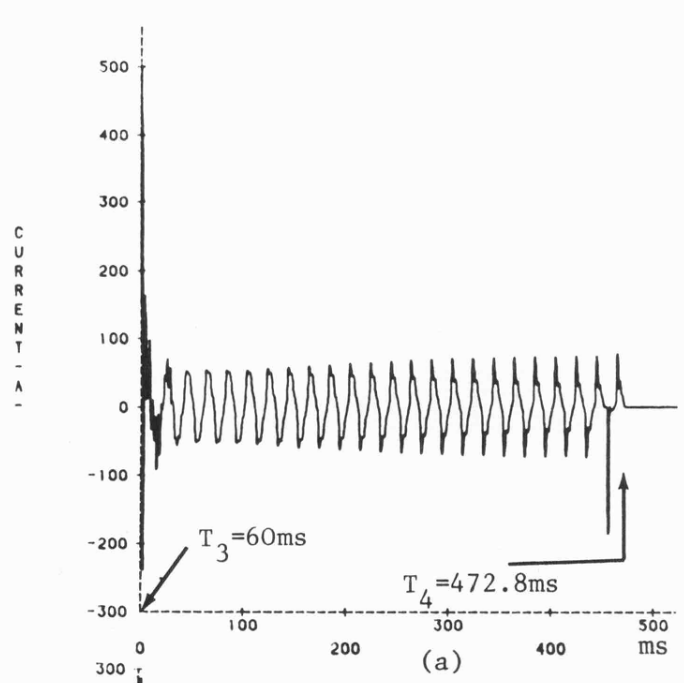

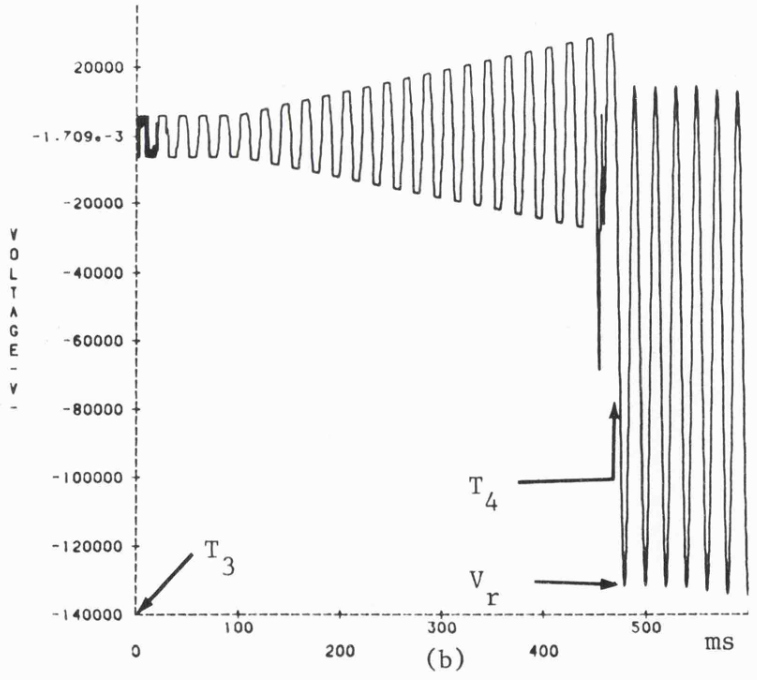

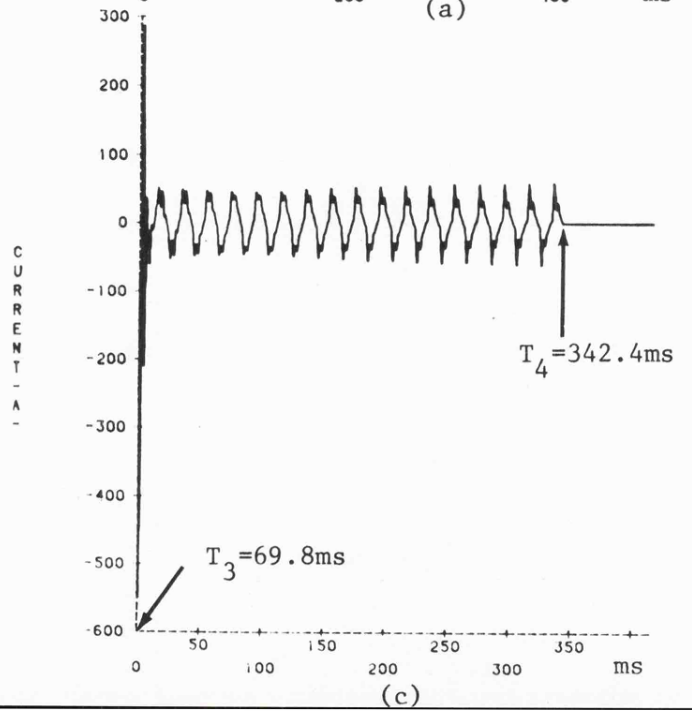

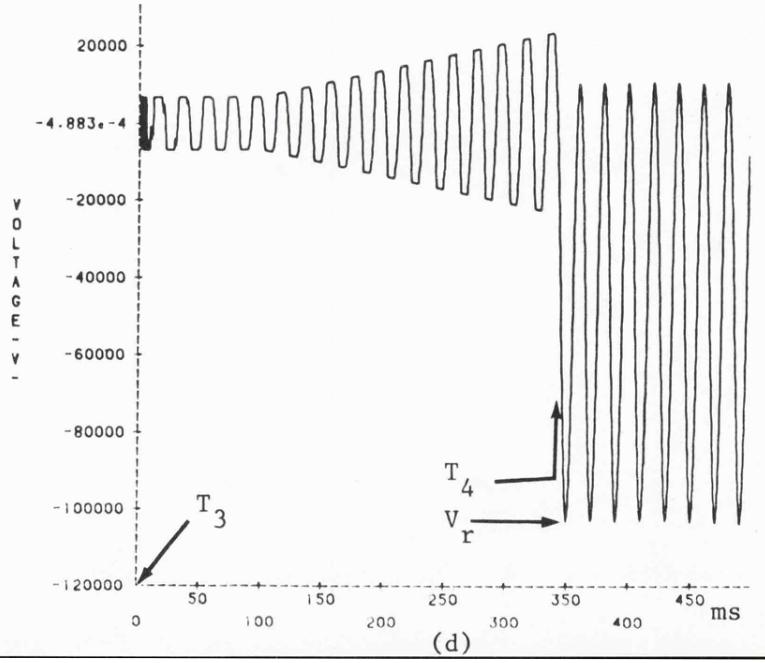

Fig. 9.23

Extinction of the secondary arc in 200 km non-transposed and uncompensated line

$x_f = 0$, $R_f = 0.5\Omega$

sen. end s.c.l = 5000 MVA

rec. end s.c.l = 5000 MVA

$V_S/V_R = 1\underline{/0^o}$, $Z_{SO}/Z_{S1} = 1$

(a),(b):

secondary arc current and voltage waveforms for a fault on phase 'c' (middle phase).

ℓ = 200 km, non-transposed

V_r = 146.3 kV (peak to peak)

(c),(d):

secondary arc current and voltage waveforms for a fault on phase 'c'

ℓ = 200 km, transposed

V_r = 115.2 kV (peak to peak)

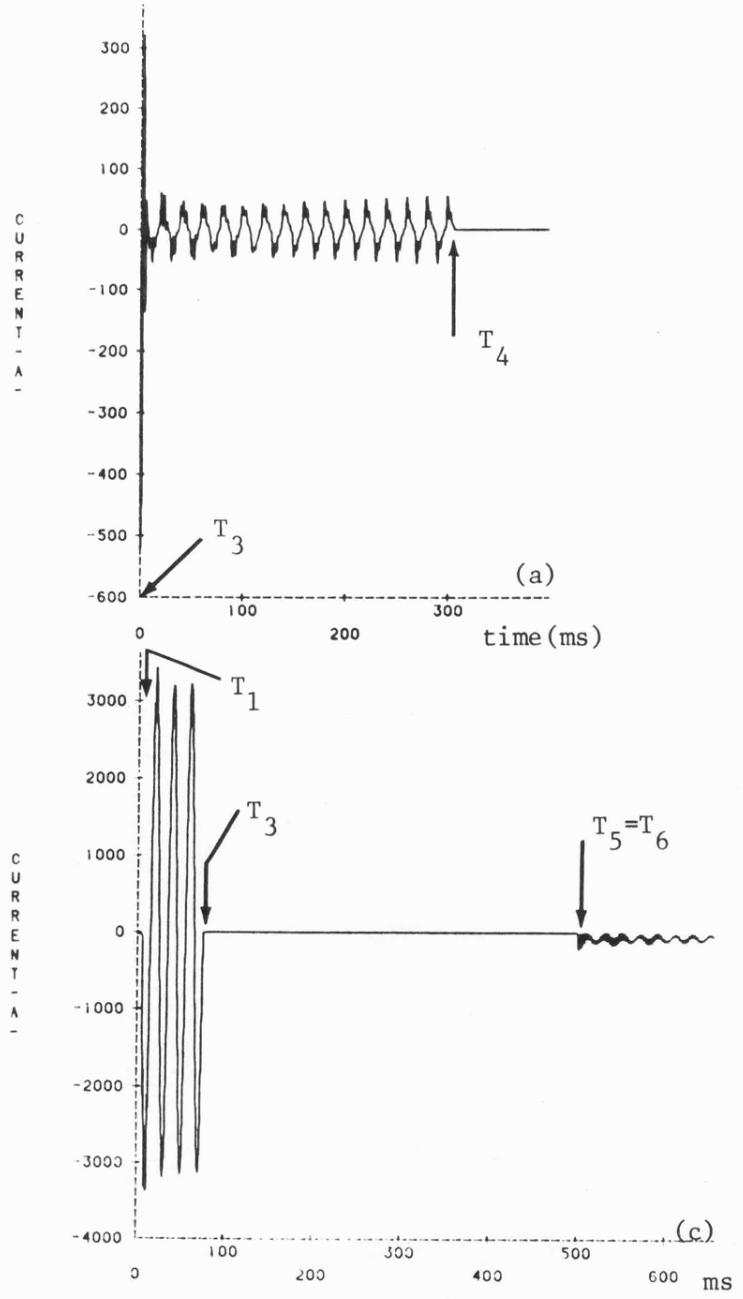

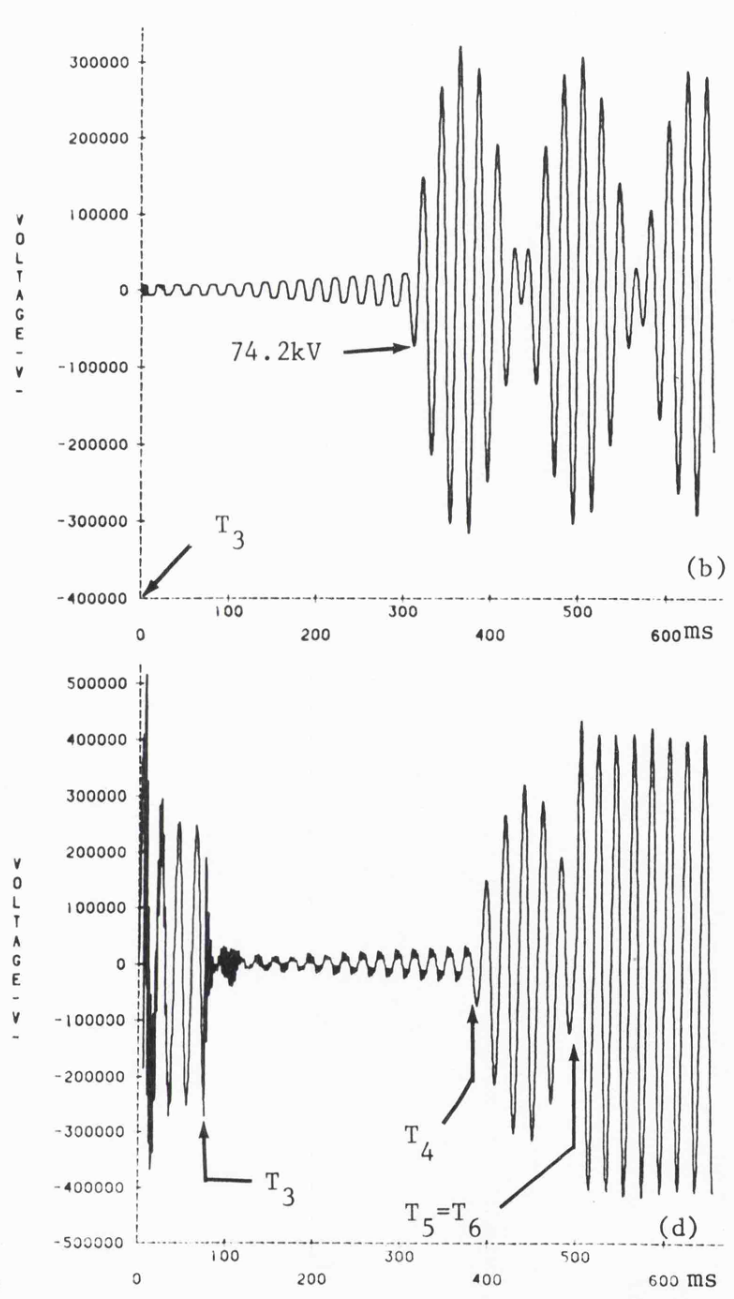

Fig. 9.24

Effect of 4-legged shunt reactors on the arc extinction in non-transposed line

$x_f = 0$, $R_f = 0.5\Omega$

ℓ = 200 km, non-transposed

sen. end s.c.l = 5000 MVA
rec. end s.c.l = 5000 MVA

$V_S/V_R = 1\underline{/0^o}$, $Z_{SO}/Z_{S1} = 1$

$h_1 = 0.75$, $h_o = 0.60166$

T_1 = 5 ms

T_2 = 50.2 ms

T_3 = 69.8 ms

T_4 = 307.2 ms

$T_5 = T_6$ = 495.6 ms

(a) secondary arc current
(b) secondary arc voltage
(c) 'a'-phase current at end R
(d) 'a'-earth voltage at end R

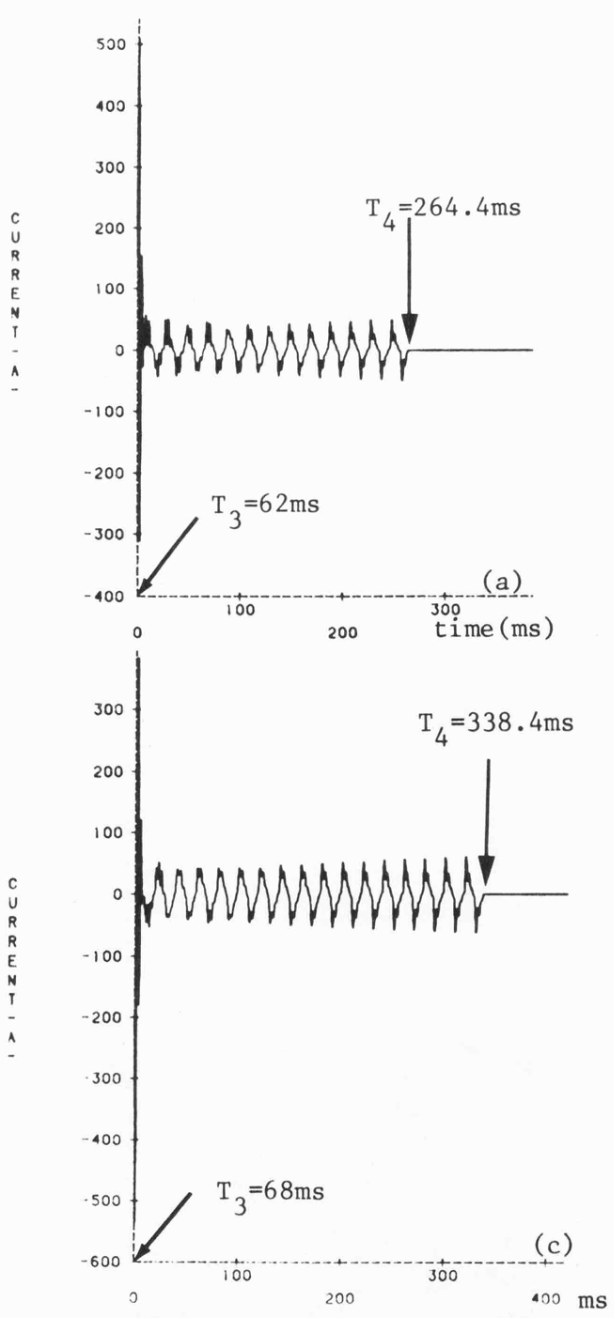

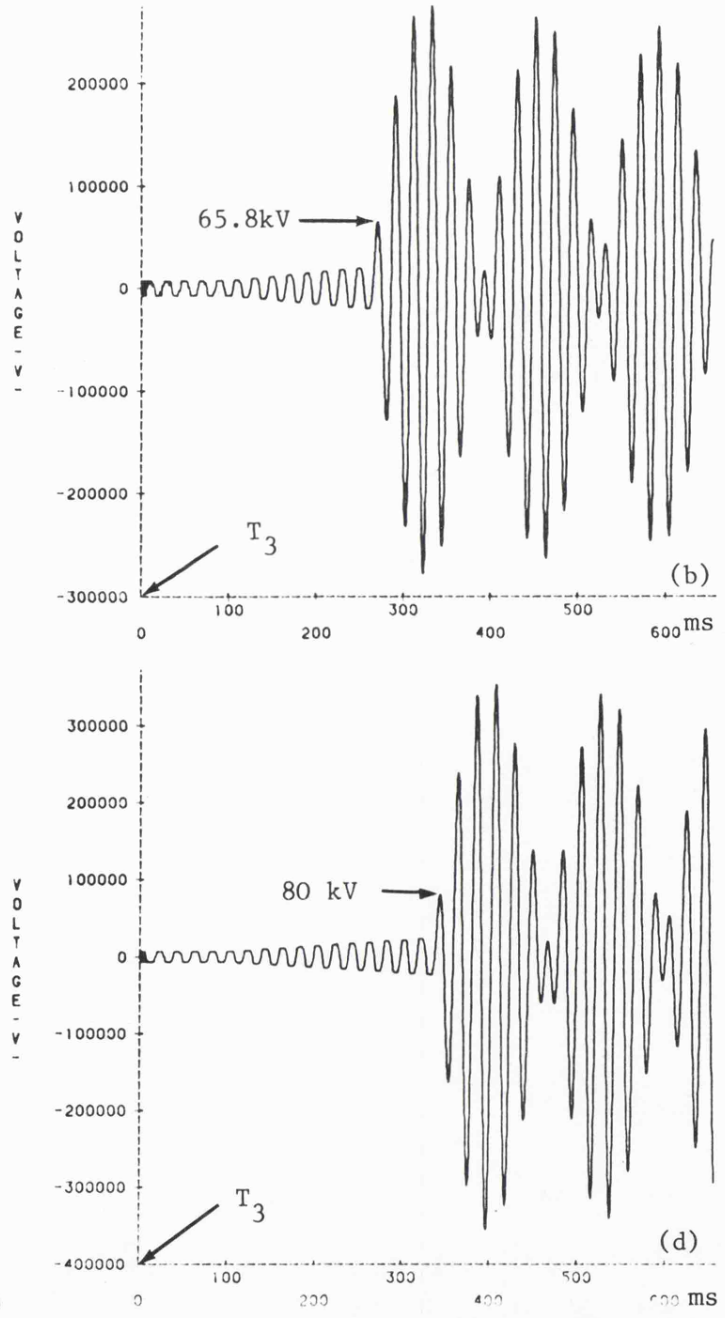

Fig. 9.25

Effect of pre-fault power transfer on the arc extinction

'a'-earth fault at peak of prefault 'a'-phase voltage

x_f = 0, ℓ = 200 km (non-transposed)

h_1 = 0.75, h_o = 0.60166

Z_{SO}/Z_{S1} = 1, R_f = 0.5Ω

sen. end s.c.l = rec. end s.c.l = 5000 MVA

(a),(b): secondary arc current and voltage waveforms respectively

$V_S/V_R = 1\underline{/}16.82^o$ (power exported from S to R is approximately 1262 MW)

(c),(d): secondary arc current and voltage waveforms respectively

$V_S/V_R = 1\underline{/}-16.82^o$

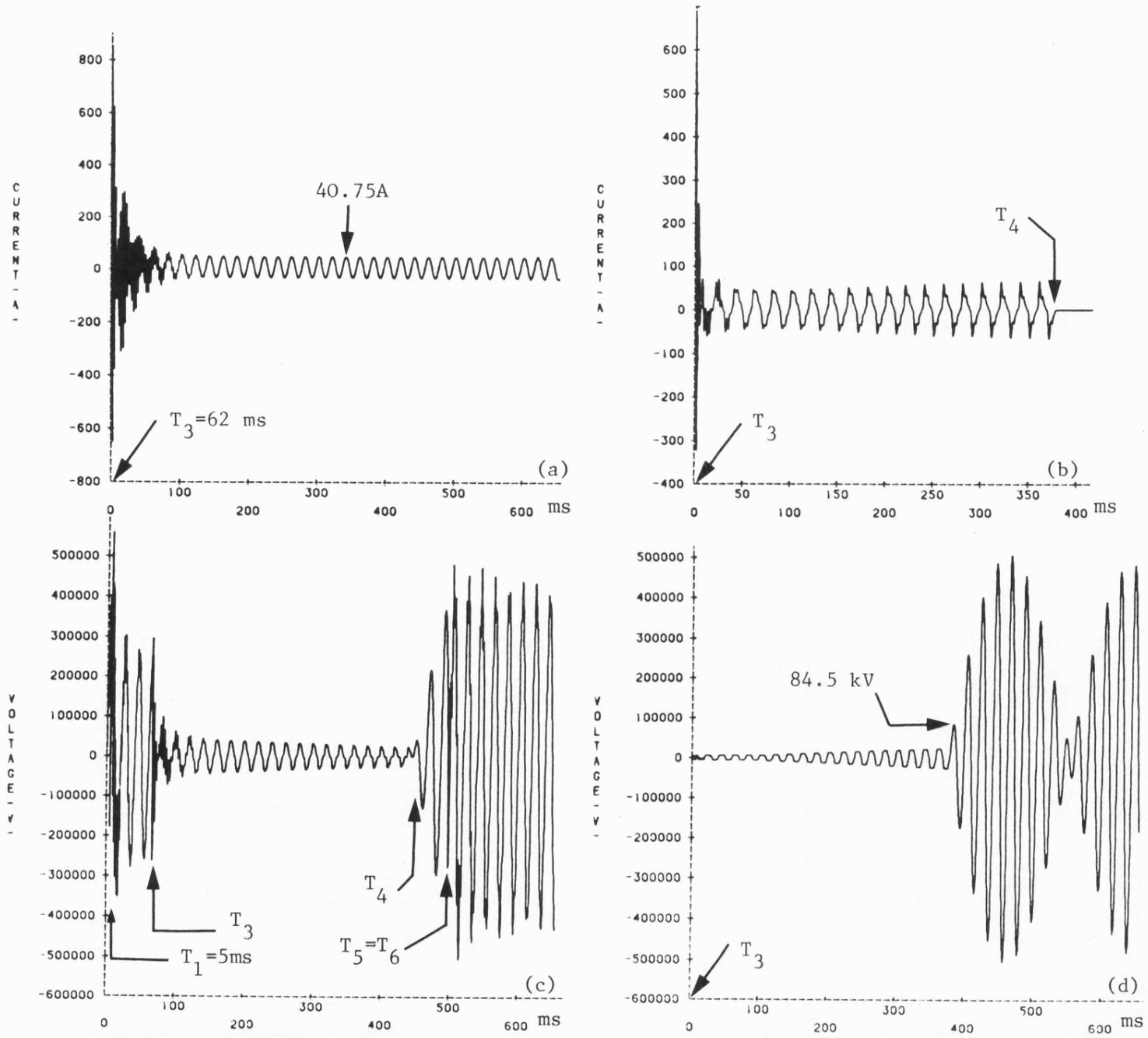

Fig. 9.26

Effect of the shunt reactor parameter on the arc extinction

Fault on the middle phase

x_f = 0, ℓ = 200 km, non-transposed

V_S/V_R = $1\underline{/}16.82^o$

Z_{SO}/Z_{S1} = 1

sen. end s.c.1 = 5000 MVA

rec. end s.c.1 = 5000 MVA

h_1= 0.75, h_o = 1.0172

T_2 = 59.2 ms (after fault)

T_3 = 62 ms (after fault)

T_4 = 380 ms (after arc transition)

T_5=T_6=494.2 ms (after fault)

(a) secondary arc current (0.5Ω arc path resistance)
(b) secondary arc current
(c) 'c'-earth voltage at end R
(d) secondary arc voltage

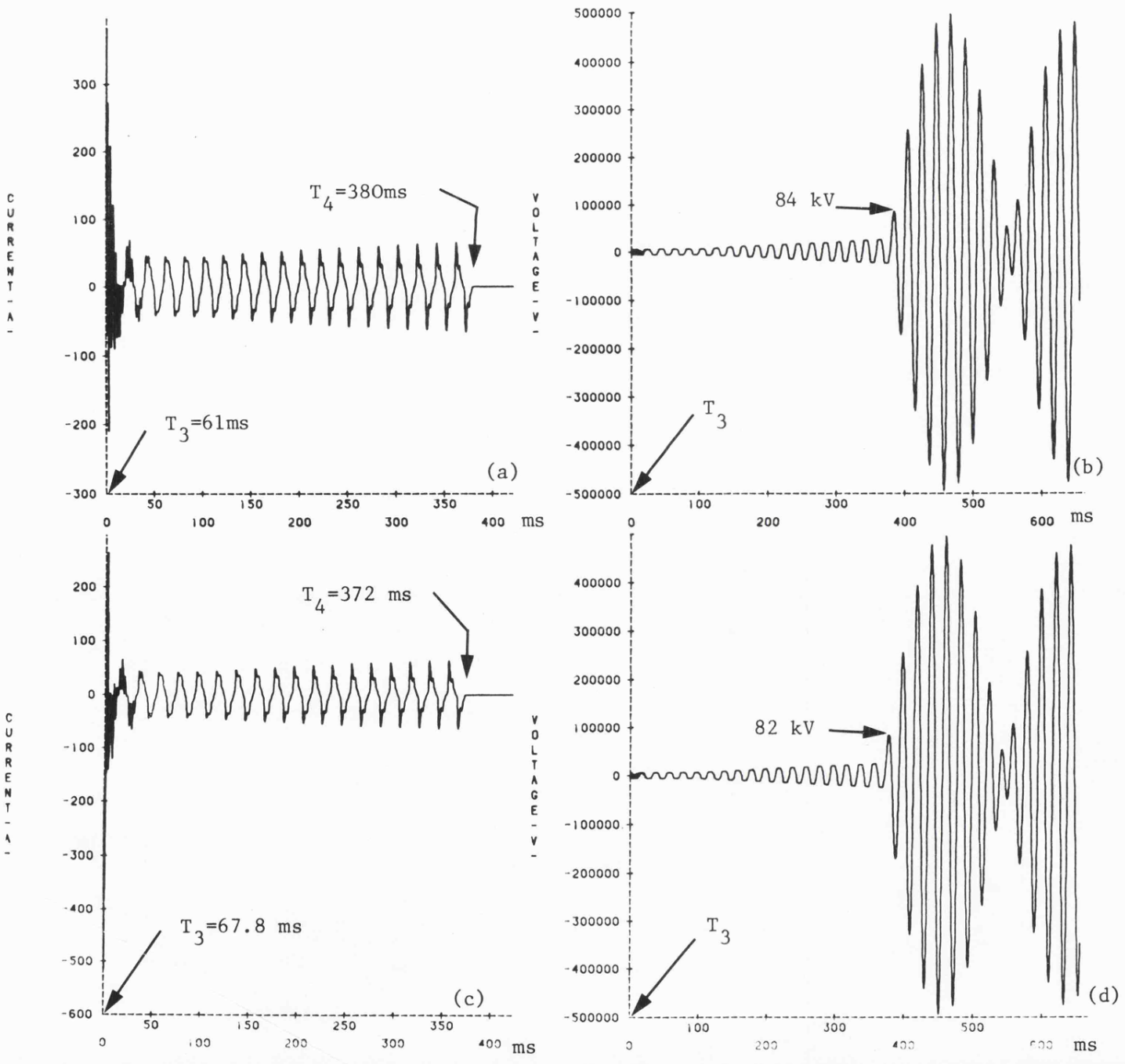

Fig. 9.27

Effect of fault position and power transfer direction on the arc extinction

h_1 = 0.75, h_o = 1.0172
fault on the middle phase

ℓ = 200 km, non-transposed

sen. end s.c.1 = 5000 MVA
rec. end s.c.1 = 5000 MVA

(a),(b): secondary arc current and voltage waveforms respectively

x_f = 200 km,
$V_S/V_R = 1\underline{/16.82}^o$

(c),(d): secondary arc current and voltage waveforms respectively

x_f = 0, $V_S/V_R = 1\underline{/-16.82}^o$

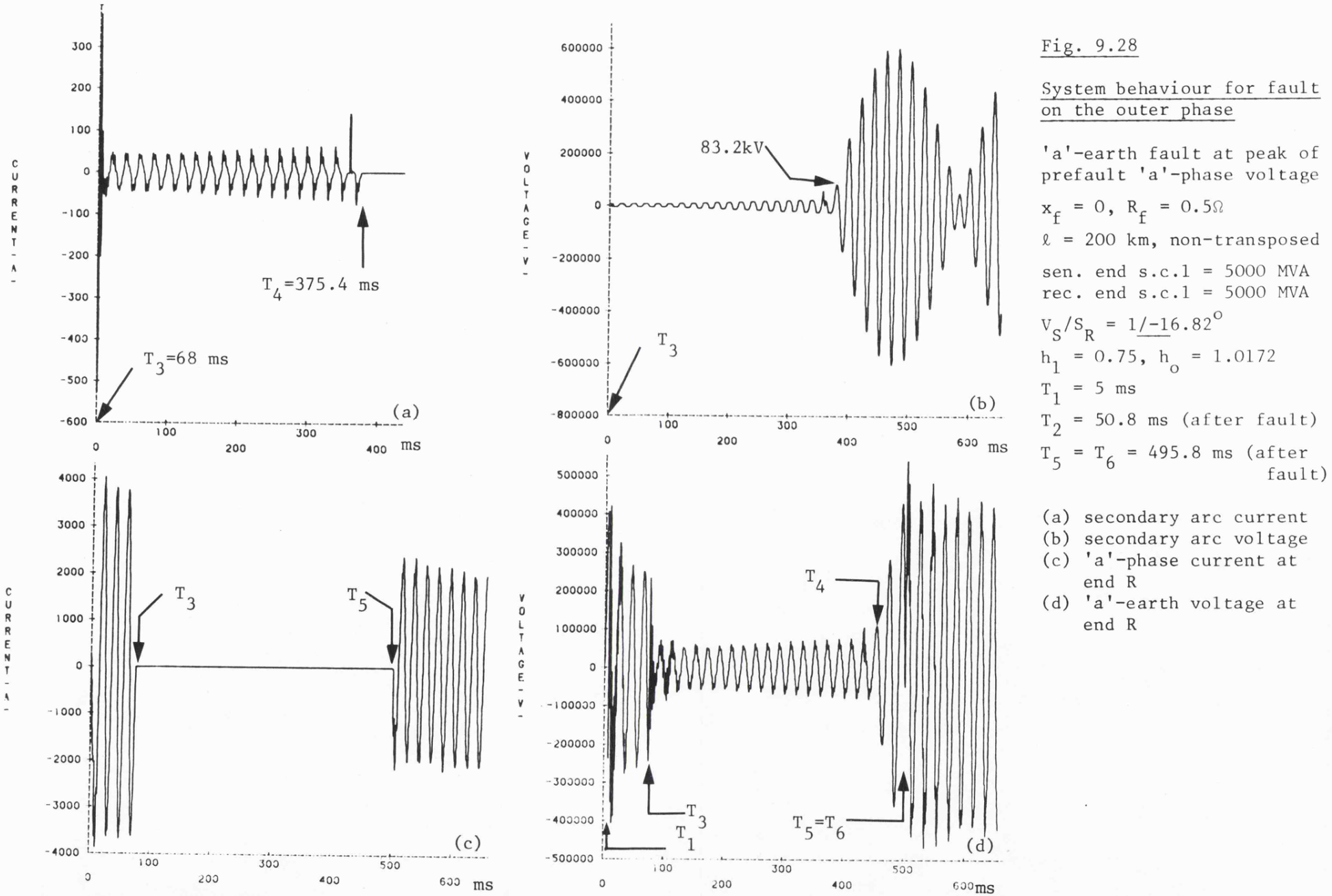

Fig. 9.28

System behaviour for fault on the outer phase

'a'-earth fault at peak of prefault 'a'-phase voltage

$x_f = 0$, $R_f = 0.5\Omega$

ℓ = 200 km, non-transposed

sen. end s.c.l = 5000 MVA
rec. end s.c.l = 5000 MVA

$V_S/S_R = 1/\underline{-16.82}^{o}$

$h_1 = 0.75$, $h_o = 1.0172$

T_1 = 5 ms

T_2 = 50.8 ms (after fault)

$T_5 = T_6$ = 495.8 ms (after fault)

(a) secondary arc current
(b) secondary arc voltage
(c) 'a'-phase current at end R
(d) 'a'-earth voltage at end R

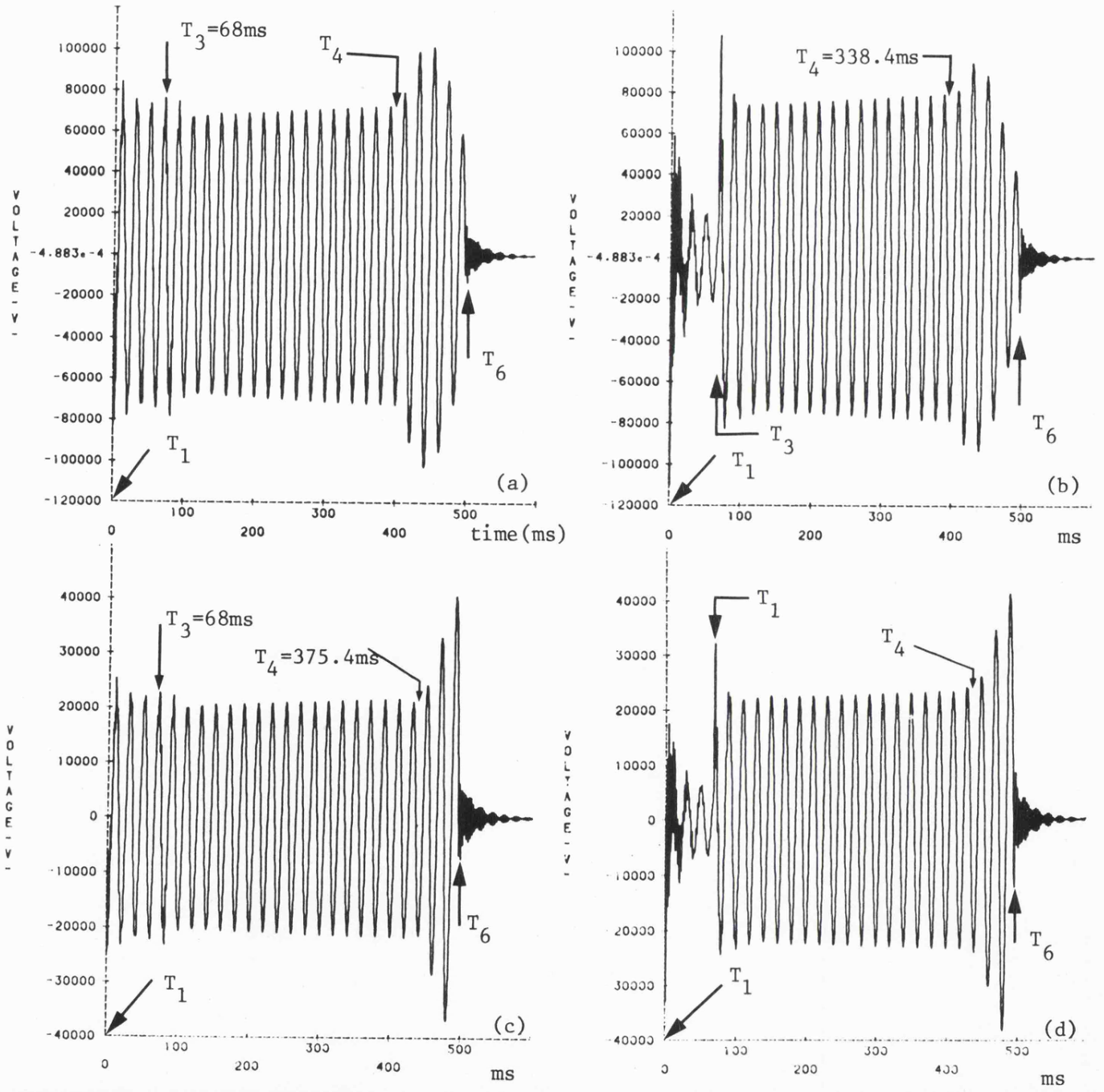

Fig. 9.29

Voltages across the neutral reactors for different values of h_o

a'-earth fault at peak of prefault 'a'-phase voltage

$x_f = 0.0$, $R_f = 0.5\Omega$

$\ell = 200$ km, non-transposed

$V_S/V_R = 1/-16.82^o$, $Z_{SO}/Z_{S1} = 1$

sen. end s.c.l = 5000 MVA

rec. end s.c.l = 5000 MVA

(a),(b): Voltage across the neutral reactors at the sending and receiving ends respectively

$h_1 = 0.75$, $h_o = 0.60166$

(c),(d): Voltage across the neutral reactors at the sending and receiving ends respectively

$h_1 = 0.75$, $h_o = 1.0172$

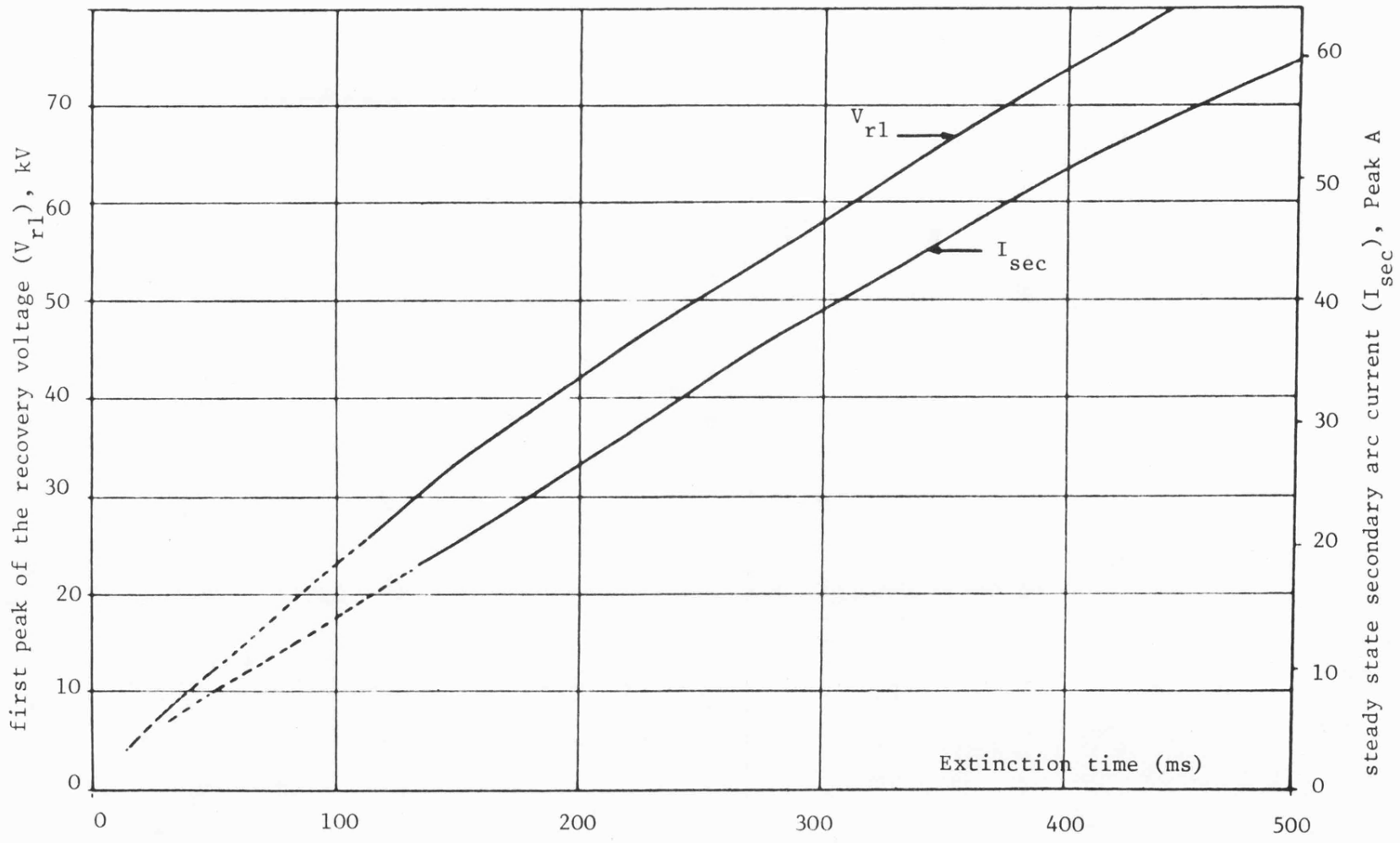

Fig. 9.30 Variation of the extinction time

CHAPTER 10

CONCLUSIONS AND FUTURE WORK

10.1 Conclusions

The effectiveness of single-pole autoreclosure in maintaining power system stability is largely determined by the speed with which secondary arc extinction and hence autoreclosure can be achieved. Realistic simulation techniques are of obvious importance in relation to the design of systems employing s.p.s. and, in this work, methods have been developed to enable the faulted response of e.h.v. feeders subjected to secondary arcing phenomena to be more realistically simulated than has hitherto been possible.

The simulation of the secondary arc path, in particular, has hitherto represented a particularly difficult problem in both analog or digital based system studies, but the present work indicates clearly that it is now feasible to incorporate realistic arc models into practical system studies. The new techniques are particularly applicable to power transmission system planning activity, and in view of the complexity of the secondary arcing process and its interaction with the system, emphasis has been placed upon developing methods that enable experimental data relating to arc behaviour to be incorporated into a particular study.

To some extent, the work underlines the desirability of further experimentation to define more fully some of the behavioural characteristics of long low current unconstrained arcs. Nevertheless, the results here obtained using current available information are encouraging in that

many of the features of the response of systems, as observed during actual field tests, have been observed .

The simulation methods developed in this work are general, and they can be used for different system configurations. The fault can be applied anywhere along the line at any instant, i.e. the angle of the voltage at the fault point can be varied freely. Breaker opening and reclosure can occur at any point on wave. Secondary arc path can be represented by a zero or small constant linear resistance, by a time dependent linear resistance or more realistically by the non-linear representation developed. Furthermore , the fault can be applied on any phase with the line transposed or non-transposed and sources can be arbitrarily chosen.

However, the digital computer program has been specifically used in the following studies on 500 kv system .

1. To obtain more realistic assessment of the likely extinction times associated with 120 km uncompensated line.

2. The effect of the 4-legged reactors on reducing the dead time, in 300 km transposed line.

3. The possibility of using 4-legged shunt reactors on 200 km untransposed line.

4. The effect of shunt reactor with directly grounded neutral on the extinction time and reclosing overvoltages.

5. To determine the system and neutral reactor overvoltages during the whole process of single pole autoreclosure.

6. To obtain more realistic current and voltage waveforms which are used as data for the power line protection equipment.

The computational results presented in chapters (8) and (9) cover in detail the above mentioned effects and the conclusions to be drawn are given below.

a) Without shunt compensation:

1. The recovery voltage waveform is almost fully offset. Its peak to peak value is approximately $2\sqrt{2}$ times the steady-state r.m.s. value.

2. The secondary arc current waveform is very non-linear and it has very high transient peaks before final arc extinction.
Findings 1 and 2 have been observed experimentally, and the waveforms obtained here compare very favourably with experimental results[3,5,8,10,31]. This provides very valuable indirect validation which is evidence of the validity of the new computational method developed.

3. For the 120 km transposed line under study, extinction times of the order of 0.31s have been predicted. In this respect, it is worth recording that such results confirm the validity of the practice of setting dead times to approximately 0.5s in applications where the secondary arc current is limited to about 20A on a simple steady-state basis. Hence, the steady-state values of the secondary arc current and induced recovery voltage may be taken as effective parameters to indicate the condition of the arc extinction.

4. The conditions for secondary arc extinction are greatly improved by transpositions, because they considerably reduce secondary arc current and induced recovery voltage.

5. Extinction time is increased as the line length increases, even for the same recovery voltages. The result shows that the extinction time for a 20A (r.m.s.) current with 115 kV peak to peak recovery voltage is approximately 275 ms, while the extinction time for 43.5A with the same recovery voltage is approximately 450 ms. These findings compare very favourably with experimental results[8,5,10,31].

6. Representation of the secondary arc path by a time dependent resistance cannot be used to predict the extinction time, or predict accurately the secondary arc current and voltage waveforms.

b) With shunt compensation:

1. The recovery voltage waveform in the shunt compensated system is symmetrical but it has the beating characteristics. Steady-state value is not reached before one second. The first peak in the recovery voltage is much lower than the steady-state value, however, its rate of rise depends on the shunt reactor parameters. These findings compare very favourably with experimental results observed by several authors[71,18,21,13,17].

2. Secondary arc extinction time is found to depend on the steady-state value of the secondary arc current and on the first peak of the recovery voltage.

3. The extinction time of the secondary arc for a 300 km transposed line is found to vary between 0.15s and 0.35s, when the line is equipped with two 4-legged reactors designed to reduce the capacitive component of the secondary arc current to 20A (r.m.s.)

4. The capacitive component of the secondary arc current and voltage can be reduced to a very small value if an optimum neutral

reactor is used and the line is transposed.

5. Power transfer direction is found to have a very significant effect on the extinction time if the line is transposed. It is found that the extinction time is always higher at the power exporting end.

6. The first peak in the recovery voltage waveform is found to increase as the extinction time increases.

7. The very high transient peaks in the secondary arc current and voltage waveforms are found to be less than that in the uncompensated line. However, it is found that the magnitude of the peaks just before the final extinction could be twice the peak which is observed in linear arc path simulation.

8. The steady-state value of the recovery voltage cannot be used to predict the extinction time in shunt compensated system.

9. Shunt reactors with directly grounded neutrals do not aid the extinction of the secondary arc, even if the resonance region is avoided. For the system considered it is found that the recovery voltage could reach 175% of the peak phase voltage. However, simple steady-state calculations show that the recovery voltage is only 92% of the peak phase voltage.

10. The transient overvoltage across the neutral reactor can be reduced if the neutral reactor is chosen to reduce the capacitive component of the secondary arc current to 20A (r.m.s.). However, no significant voltage reduction during the dead time can be achieved because the voltage after arc extinction is not in a steady-state.

11. Four reactor schemes can be applied to 200 km untransposed line. In this case the extinction time is found to be approximately 380 ms.

12. The effect of the electromagnetic coupling is found to be more significant in the transposed line, and the power transfer direction has no significant effect on the extinction time if the line is not transposed.

13. Busbar termination is found to have no significant effect on the extinction time. However, it may affect the duration of the high noise period in the current and voltage waveforms.

14. Maximum overvoltage across the neutral reactor is found to occur for a fault at the middle of the line at maximum point on wave.

10.2 Future Work

The work presented in this thesis may form the basis for future investigations of short and long lines employing single pole auto-reclosure with particular reference to the attaining of both feasible and more economic system designs.

Future work may therefore be carried out along the following lines:

1. The simulation techniques developed in this thesis may be used as a reference to other work in the same field.

2. The simulation techniques developed can be used in the process of programmable based real-time testing of power line protection equipment. In this respect, the implication of protection malfunction caused by severe waveform distortion can be serious and it is clear from the present work that even disregarding the relatively severe arc re-ignition

transients that are observed near final extinction, a linear resistance approximation to the arc path would not reproduce the significant non-linear voltage waveforms that are fed to protective gear utilising voltage transformers connected to the line side of the circuit breakers.

3. In the present work, only a single-circuit 3-phase system has been considered. However, the secondary arc simulation technique presented is very general and its application to double-circuit systems is a future possibility.

4. A single line to ground fault may lead to faults involving more than one phase and hence the simulation of the simultaneous faults could be considered. In this case, the prefault conditions are effectively no longer steady-state but a single line to ground fault has to be simulated.

5. The simulation techniques developed for the secondary arc can be used to simulate the surge diverters across both the main and neutral reactors.

6. The simulation techniques developed here for the secondary arc can be used to predict the extinction time and the system behaviour in system employing high-speed grounding switches for s.p.s.[84].

7. The simulation techniques developed here can be used as a basis to predict the secondary arc extinction time in system employing modified four reactor switches[71].

8. The simulation techniques developed here could be extended to include the use of series capacitors in e.h.v. and u.h.v. systems employing shunt reactors[85].

9. In predicting system and reactor overvoltages, high frequency voltage components up to only 2.5 kHz were covered in the present work. To cover higher frequency voltage components and hence more accurate prediction of overvoltages, a larger computer capacity is necessary. As the present work carried out in ICL 2980. However, high frequency overvoltages due to the fault inception and breaker opening can be predicted within the present available capacity.

10. The future work should include the surge diverter of the neutral reactor.

11. The present breaker simulation technique can be used to incorporate closing resistor(s), if necessary.

12. Further practical work in the following area would be useful.

a) Effect of the magnitude of the secondary arc current on the rate of increase of the arc length.

b) Effect of the primary arc on the voltage gradient of the secondary arc.

c) Effect of the magnitude of the secondary arc current on the rate of rise of the re-ignition voltage.

REFERENCES

1. Hobson, J.E. and Muller, H.N., Jr.: "Single-pole fault clearing for greater stability", Westinghouse Engineer, 1942, (1), pp.23-25.

2. Cabanes, L., Dietsch, C. and Divan, M.: "Does the length of line limit the application of single-phase automatic reclosure in very high voltage transmission systems?": CIGRE, Paris, Paper No.142, 1954.

3. Maury, M.E.: "Extinction of arcs in single-phase high-speed reclosure of 220 kV transmission lines", Revue General de l'Electricite, 1944, 53, (5), pp.79-90.

4. Annino, E., Clerici, A. and Colombo, A.: "Analog determination of secondary currents and induced voltages in a 400 kV double-circuit line", IEEE, Paper No.31, PP 66-385, 1966.

5. Haubrich, H.J., Hosemann, G., and Thomas, R.: "Single-phase auto-reclosing in e.h.v. systems", CIGRE, Paris, Paper No. 31-09, 1974.

6. Lambert, S.R., Koschik, V., Wood, C.E., Worner, G. and Pocamora, R.G.: "Long line single-phase switching transients and their effect on station equipment", IEEE Trans., 1978, PAS-97, No.3, pp.857-865.

7. Jahn, D., Koettnitz, H. and Schulze, H.: "Earth wires as a means of improving single-pole rapid reclosing of long high-voltage lines", CIGRE, Paris, Paper No.401, 1964.

8. Ozaki, Y.: "Arc characteristics of insulator strings for e.h.v. transmission lines", IEEE Paper No.31, CP 65-18, 1965.

9. Maikopar, A.S.: "Minimum time of automatic reclosing", Electric Technology (USSR), 1960, pp.302-315.

10. Balossi, A., Malaguti, M. and Ostano, P.: "Laboratory full-scale tests for the determination of the secondary arc extinction time in high-speed reclosing", IEEE, Paper No.31, PP 66-382, 1966.

11. Spron, P. and Prince, D.C.: "Ultra high-speed reclosing of high-voltage transmission lines", Trans.AIEE, 1937, 56, (1), pp.81-90.

12. Maikopar, A.S.: "Prospects of single-phase automatic reclosure on 500-kV long distance lines 500 km in length when using shunting reactors", Electric Technology (USSR), 1964, 3, pp.348-355.

13. Carlsson, L., Groza, L., Cristovici, A., Necsulescu, D.S. and Ionescu, A.: "Single-pole reclosing on e.h.v. lines", CIGRE, Paris, Paper No. 31-03, 1974.

14. Knudsen, N.: "Single-phase switching of transmission lines using reactors for extinction of the secondary arc", CIGRE, Paris, Paper No. 310, 1962.

15. Kimbark, E.W.: "Suppression of ground-fault arcs on single-pole-switched e.h.v. lines by shunt reactors", IEEE Trans., 1964, PAS-83, pp.285-290.

16. Edwards, L., Chadwick, J.W., Jr., Riesch, H.A. and Smith, L.E.: "Single-pole switching on TVA's Paradise-Davidson 500-kV line: design concepts and staged fault test results", IEEE Trans., 1971, PAS-90, No.6, pp.2436-2450.

17. Carlsson, L.: "The use of a neutral-point reactor for single-pole reclosing on e.h.v. lines", ASEA Journal, 1976, 49, (4), pp.91-94.

18. Peterson, A.H. and Dravid, N.V.: "A method for reducing dead time for single-pole reclosing in e.h.v. transmission", IEEE Trans., 1969, PAS-88, No.4, pp.286-291.

19. Muller, M., Gygax, F., Hahn, C. and Baltensperger, P.: "Protection of e.h.v. systems, taking into account single-phase automatic reclosure on very long line", Brown Boveri Rev., 1958, 45, (6), pp.243-253.

20. Heinemann, T.: "Single-pole rapid reclosing", Elec. Rev., 1965, 176, (18), pp.668-671.

21. Shperling, B.R., Fakheri, A. and Ware, B.J.: "Compensation scheme for single-pole switching on untransposed transmission lines", IEEE Trans., 1978, PAS-97, No.4, pp.1421-1429.

22. Shperling, B.R. and Fakheri, A.: "Single-phase switching parameters for untransposed e.h.v. transmission lines", ibid., 1979, PAS-98, No.2, pp.643-654.

23. Shipley, R.B., Holly, H.J. and Coleman, D.W.: "Digital analysis of single-pole switching on e.h.v. lines", ibid., 1968, PAS-87, No.8, pp.1679-1687.

24. Eaton, J.R. and Kozak, E.: "Single-pole switching on reactor compensated lines: optimum operating conditions", IEEE, Paper No. C74 075-8, 1974.

25. Schaer, F. and Baltensperger, P.: "Short-circuit tests with rapid reclosure on the 220-kV Mettlen-Lavorgo line", Trans.AIEE, 1956, 75, part III, pp.1137-1146.

26. Milne, K.H.: "Single-pole reclosing tests on long 275-kV transmission lines", IEEE Trans., 1963, PAS-82, pp.658-661.

27. Ozaki, Y.: "Extinction of secondary arc current in a single-pole reclosing system", Elec. Engg. in Japan, 1964, 84, (6), pp.53-63.

28. Dobson, W.P. and Mason, V.V.: "Single-pole reclosing: relaying problems and arc extinction times", CIGRE, Paris, Paper No.316, 1952.

29. Belyakov, N.N., Rashkes, V.S. and Rozhavskaya, S.N.: "The use of compensation reactors to improve single-phase automatic reclosing conditions on high voltage lines", Electr. Stantsii (USSR), 1975, No.12, pp.68-72.

30. Anjo, K., Terase, H. and Kawaguchi, Y.: "Self-extinction of arcs created in long air gaps", Elec. Engg. in Japan, 1968, 88, (4), pp.83-93.

31. Gary, C., Hesketh, S. and Moreau, M.: "Tests of self-extinction of secondary arcs in case of single-pole switching. Application to 750-kV lines", Revue General de l'Electricite, 1971, 80, (5), pp.406-412.

32. Balser, S.J., Eaton, J.R. and Krause, P.C.: "Single-pole switching. A comparison of computer studies with field test results", IEEE Trans., 1974, PAS-93, No.1, pp.100-108.

33. Goodridge, H.L., Sasdi, G.P. and Stadtfeld, N., Jr.: "Single-pole reclosing and underlying system protection during the single-phasing period", IEEE Paper No. 31, CP 67-537, 1967.

34. Johns, A.T. and Aggarwal, R.K.: "Digital simulation of fault auto-reclosure sequences with particular reference to the performance evaluation of protection for e.h.v. transmission lines", Proc. IEE, 1981, 128, Pt.C., No.4, pp.183-195.

35. Barthold, L.O. and Carter, G.K.: "Digital travelling wave solutions", Trans.AIEE, Dec. 1961, pp.812-820.

36. Domel, H.W.: "Digital computer solution of electromagnetic transients in single and multi-phase networks", IEEE Trans., 1969, PAS-88, No.4, pp.388-399.

37. Boonyubol, C., Calabrese, C. and Tudor, J.R.: "A mathematical analysis of transmission-line parameters related to fault surges", ibid., 1970, PAS-89, No.6, pp.1207-1215.

38. Battison, M.J., Day, S.J., Mullineux, N., Parton, K.C. and Reed, J.R.: "Calculation of switching phenomena in power systems", Proc.IEE, 1967, 114, (4), pp.478-486.

39. Wedepohl, L.M. and Mohamed, S.E.T.: "Multiconductor transmission lines. Theory of natural modes and fourier integral applied to transient analysis", ibid., 1969, 116, (9), pp.1553-1563.

40. Cornick, K.J., Ko, Y.M. and Pek, B.: "Power system transients caused by arcing faults", ibid., 1981, 128, Pt.C., No.1, pp.18-27.

41. Bickford, J.P., Sanderson, J.V.H., Abelsalem, M.M., Mohamed, S.E.T., Morais, S.A. and Olipade, O.: "Developments in the calculation of waveforms and frequency spectra for transients fault currents and voltages", ibid., 1980, 127, Pt.C., No.3, pp.145-152.

42. Edlinger, A., Glavitsch, H. and Ritter, A.: "The use of high-voltage reactors for the compensation of e.h.v. transmission lines", CIGRE, Paris, Paper No.402, 1964.

43. Kimbark, E.W.: "Charts of three quantities associated with single-pole switching", IEEE Trans., 1975, PAS-94, No.2, pp.388-395.

44. Kimbark, E.W.: "Selective pole switching of long double-circuit e.h.v. lines", ibid, 1976, PAS-95, No.1, pp.219-230.

45. Johns, A.T., El-Nour, M. and Aggarwal, R.K.: "Performance of distance protection of e.h.v. feeders utilising shunt-reactor arrangements for arc suppression and voltage control", Proc.IEE, 1980, 127, Pt.C., No.5, pp.304-316.

46. Martins, N.: "Computation of residual fault currents in single-phase switched transmission lines", M.Sc. Dissertation, UMIST, 1974.

47. Johns, A.T. and Aggarwal, R.K.: "Digital simulation of faulted e.h.v. transmission lines with particular reference to very-high speed protection", Proc.IEE, 1976, 123, (4), pp.353-359.

48. Berglund, R.O., Mittelstadt, W.A., Shelton, M.L., Barkan, P., Dewey, C.G. and Skreiner, K.M.: "One-cycle fault interruption at 500 kV: system benefits and breaker design", IEEE Trans., 1974, PAS-93, pp.1240-1251.

49. Hicks, K.L. and Butt, W.H.: "Feasibility and economics of ultra-high speed fault clearing", ibid, 1980, PAS-99, No.6, pp.2138-2145.

50. Maury, E.: "Synchronous closing of 525 and 765 kV circuit breakers: a means of reducing switching surges on unloaded lines", CIGRE, Paris, Paper No. 143, 1966.

51. Konkel, H.E., Legate, A.C. and Ramberg, H.C.: "Limiting switching surge overvoltages with conventional power circuit breakers", IEEE Trans., 1977, PAS-96, No.2, pp.535-542.

52. Wedepohl, L.M. and Mohamed, S.E.T.: "Transient analysis of multiconductor transmission lines with special reference to nonlinear problems", Proc.IEE, 1970, 117, (5), pp.979-988.

53. Bickford, J.P. and Doeple, P.S.: "Calculation of switching transients with particular reference to line energization", ibid, 1967, 114, (4), pp.465-477.

54. Wedepohl, L.M.: "Application of matrix methods to the solution of travelling-wave phenomena in polyphase systems", ibid., 1963, 110, (12), pp.2200-2212.

55. Edels, H.: "Properties and theory of the electric arc", ibid., 1961, 108A, pp.55-69.

56. Kompton, K.T.: "The electric arc", Trans.AIEE, June 1927, 46, pp.868-878.

57. King, L.A.: "The voltage gradient of the free burning arc in air or nitrogen", ERA Report, Ref. G/XT 172, 1961.

58. Storm, A.P.: "Lone 60-cycle arcs in air", Trans.AIEE, March 1946, 65, pp.113-117.

59. Maikopar, A.S.: "The quenching of an open arc", Electrichestvo (USSR), 1960, No.4, pp.64-69.

60. Eaton, J.R., Peck, J.K. and Dunham, J.M.: "Experimental study of arcing faults on a 75-kV transmission system", Trans.AIEE, 1931, 50, pp.1469-1479.

61. Browne, T.E., Jr.: "The electric arc as a circuit element", Journal of the Electrochemical Society, 1955, 102, (1), pp.27-37.

62. Eaton, J.R.: "Factor affecting arc extinction on a Peterson-coil system", Trans.AIEE, Nov. 1939, 58, pp.576-581.

63. Slepian, J.: "Extinction of a long a-c arc", ibid., 1930, 49, (2), pp.421-430.

64. Terase, H., Sadamoto, K., Abe, K. and Kawaguchi, Y.: "Dielectric strength recovery characteristics after fault arc extinction in 500-kV transmission lines", Elec. Engg. in Japan, 1969, 89, (2), pp.29-38.

65. Fukunishi, M. and Terase, H.: "Study of insulator strings for reducing dead time of high-speed reclosing", ibid., 1971, 91, (3), pp.125-131.

66. Boisseau, A.C., Wyman, B.W. and Sheats, W.F.: "Insulator flashover deionization times as a factor in applying high-speed reclosing circuit breakers", Trans.AIEE, 1949, 68, Part II, pp.1058-1067.

67. Maikopar, A.S. and Snitovskaya, G.Z.: "Tests of automatic reclosing on a test-industrial 750 kV overhead line", Electr. Stantsii (USSR), 1973, No.7, pp.506-508.

68. Johnson, I.B., Barthold, L.O., Dorsa, C., Hagenguth, J.H., Hauspurg, A., Kinghorn, J.H., Naef, O., Phelps, J.D.M., Phillips, V.E., Skeats, W.F., Titus, C.H. and Vose, F.C.: "Fault arc deionization and circuit breaker reclosing on e.h.v. lines - field, laboratory and analytical results", CIGRE, Paris, Paper No. 307, 1962.

69. Terase, H., Sadamoto, K., Hashimoto, Y. and Kawaguchi, Y.: "Dielectric recovery of heavy-circuit arc in a long air gap", Elec. Engg. in Japan, 1968, 88, (7), pp.80-87.

70. Fukunishi, M., Anjo, K., Terase, H., Ozaki, Y., Yano, K. and Kawaguchi, Y.: "Laboratory study on dead time of high speed reclosing of 500-kV systems", CIGRE, Paris, Paper No. 31-03, 1970.

71. Shperling, B.R., Fakheri, A.J., Shih, C.H. and Ware, B.J.: "Analysis of single-phase switching field tests on the AEP 765 kV system", IEEE Trans., 1981, PAS-100, No.4, pp.1729-1735.

72. Maikopar, A.S. and Snitovskaya, G.Z.: "Tests of automatic reclosing on an industrial 750 kV line", Electr·Stantsii (USSR), 1977, No.2, pp.59-62.

73. Terase, H., Hashimoto, Y., Arakane, M. and Kawaguchi, Y.: "Self-extinction of secondary arcs of 500-kV insulator strings", Elec. Engg. in Japan, 1969, 89, (6), pp.11-19.

74. Higham, J.B. and Meek, J.M.: "Voltage gradients in long gaseous spark channels", The Proc. of Physical Society, 1950, Section B, 63, Pt.9, pp.633-648.

75. Wanger, C.F., Lane, C.M. and Lear, C.M.: "Arc drop during transition from spark discharge to arc", Trans.AIEE, 1958, 77, (3), pp.242-247.

76. Bdrgonovo, G., Santagostino, G., Gamelli, G., Lagostena, L. and Porrino, A.: "Evaluation of the risk of failure due to switching surges in u.h.v. networks", CIGRE, Paris, Paper No. 33-14, 1978.

77. Fukuda, S., Ozaki, Y. and Furuno, K.: "Switching surges reduction with circuit-breaker resistor in e.h.v. system", ibid, Paper No. 13-09, 1978.

78. McClymont, K.R.: "Single-pole reclosing: results of staged-fault tests", Ontario Hydro Research News, 1954, 6, (2), pp.9-13.

79. Ametani, A.: "The application of fast fourier transform to electrical transient phenomena",Int.J. Elect. Eng. Educ., 1973, 10, pp.277-287.

80. Wilox, D.J.: "Numerical Laplace transformation and inversion", ibid., 1978, 15, pp.247-265.

81. Day, S.J., Mullineux, N. and Reed, J.R.: "Developments in obtaining transient response using fourier transforms", ibid., 1965, 3, pp.501-506.

82. Kennedy and Donkin Consulting Engineers: "500 kV interconnection between the central system and the Atlantic Coast of Colombia", Report No.10, June 1976.

83. Janke, G., Jenkins, R., Nordstorm, B. and Norlin, L.: "The choice of shunt reactors for the Swedish 400-kV system", CIGRE, Paris, Paper No.412, 1962.

84. Hasibar, R.M., Legate, A.C., Brunke, J. and Peterson, W.G.: "The application of high-speed grounding switches for single-pole reclosing on 500-kV power systems", IEEE Trans., 1981, PAS-100, No.4, pp.1512-1515.

85. Thanassoulis, P., De Franco, N., Clerici, A. and Cazzani, M.: "Overvoltages on a series-compensated 750 kV system for the 10,000 MW Itaipu project", ibid., 1975, PAS-94, No.4, pp.622-631.

86. Galloway, R.H., Shorrocks, W.B. and Wedepohl, L.M.: "Calculation of electrical parameters for short and long polyphase transmission lines", Proc.IEE, 1964, 111, (12), pp.2051-2059.

87. Johns, A.T.: "Computer simulation studies of new methods of distance protection for e.h.v. lines", Report on Science Research Council Research, Grant B/RG/4534/1, Nov. 1975, University of Bath.

88. Banerjee, A.R.: "Fault transient analysis of power transmission line", Ph.D. Thesis, University of Bath, 1976.

89. Carson, Jr.: "Wave propagation in overhead wires with ground return", Bell System Technology Journal, 1926, 5, pp.539-554.

APPENDIX 2.1

STEADY-STATE CALCULATIONS ASSOCIATED WITH SINGLE-POLE SWITCHING

If s.p.s. is adopted, care must be taken that the secondary arc current is promptly extinguished, say in time to permit successful reclosure in one-half second. The secondary arc is maintained by (1) shunt capacitive coupling and (2) longitudinal coupling from mutual inductance and resistance, between the disconnected, faulted phase and the energized, unfaulted phases. Both components increase with length of the line. The capacitive component is more important, being independent of line loading, and is the only one considered here[43].

4-legged shunt reactor can neutralize the capacitive component of the secondary arc current and voltage, but it has less effect on the electromagnetic coupling. The value of the neutral reactor which would neutralize the capacitive components of the secondary arc current and voltage, depends on the inductance of the phase reactor and on the line capacitance ratio (C_o/C_1). The effect of the 4-legged shunt reactor on the magnitudes of the secondary arc current, steady-state recovery voltage, and natural frequency of transient recovery voltage is derived here[43].

Consider a three-phase transposed line as shown in fig. 2.6a. The fault is assumed to occur on phase 'a' by closure of switch F and is isolated by opening of circuit breaker CB, whereupon it becomes a secondary arc current I_{sec}. Extinction of the fault arc is represented by opening switch F. The voltage V_r across the open switch is then the

recovery voltage. I_{sec} and V_r can be calculated more simply from the reduced circuit of fig. 2.6b, where the sound phases 'b' and 'c' are replaced by phase 'bc' having an applied voltage equal to the average of E_b and E_c. In any reactor scheme designed for quenching the secondary arc, the inductance of the upper arm resonates with the corresponding capacitance at the supply frequency, giving a high (theoretically infinite) impedance, the lower arm generally does not resonate. Hence, the recovery voltage $V_r = 0$.

While the secondary arc is present, it bypasses the lower arm, and the current I_{sec} is proportional to the susceptance of the upper arm. With this arm adjusted for resonance, I_{sec}, as well as V_r, is zero.

On any line with shunt reactors, the recovery voltage has, in addition to the steady-state components a transient component of a natural frequency f_r, generally different from the supply frequency f_o. The result is a beat frequency $f_o - f_r$. The circuit for determining the natural frequency is that of fig. 2.6c, formed from that of fig. 2.6b by setting the applied voltage equal to zero, thus making nodes 'bc' and 'g' become one.

A 2.1.1 Calculation of the Secondary Arc Current

The upper arm of fig. 2.6a has the susceptance

$$B_u = \frac{2}{3}\left[\omega_o(C_1 - C_o) - (\Gamma_1 - \Gamma_o)/\omega_o\right] \qquad (A2.1.1)$$

and the lower arm has

$$B_\ell = \omega_o C_o - \Gamma_o/\omega_o \qquad (A2.1.2)$$

The degrees of shunt compensation are:

$$\text{Positive sequence } (h_1) = \frac{B_{L1}}{B_{C1}} = \frac{\Gamma_1/\omega_o}{C_1\omega_o} = \frac{1}{\omega_o^2 L_1 C_1} \qquad \text{(A2.1.3)}$$

$$\text{Zero sequence } (h_o) = \frac{B_{LO}}{B_{CO}} = \frac{\Gamma_o/\omega_o}{C_o\omega_o} = \frac{1}{\omega_o^2 L_o C_o} \qquad \text{(A2.1.4)}$$

From eqns. A2.1.1-A2.1.4 it can be shown that[43]:

$$B_u = \frac{2}{3}\omega_o\left[C_1(1 - h_1) - C_o(1 - h_o)\right] \qquad \text{(A2.1.5)}$$

$$B_\ell = \omega_o C_o(1 - h_o) \qquad \text{(A2.1.6)}$$

or

$$B_u + B_\ell = \frac{1}{3}\omega_o\left[2C_1(1 - h_1) + C_o(1 - h_o)\right] \qquad \text{(A2.1.7)}$$

When switch F in fig.2.6 is closed, the secondary arc current is:

$$I_{sec} = j(-E/2)B_u = j(E/2)(2\omega_o/3)\left[C_1(1 - h_1) - C_o(1 - h_o)\right]$$

$$= -j(E\omega_o/3)\left[C_1(1 - h_1) - C_o(1 - h_o)\right] \qquad \text{(A2.1.8)}$$

The base current is the normal charging current:

$$I_b = j\omega_o E C_1 \qquad \text{(A2.1.9)}$$

The normalized secondary arc current is:

$$I_{sec(p.u.)} = I_{sec}/I_b = -(H_1 - kH_o)/3 \qquad \text{(A2.1.10)}$$

where

$$H_1 = (1 - h_1), \quad H_o = (1 - h_o), \quad \text{and } k = \frac{C_o}{C_1}$$

Here, it must be pointed out that if two shunt reactors are required to reduce the secondary arc current to 20A (r.m.s.), I_{sec} in eqn. A2.1.10 should be set equal to -j20, and I_b should be taken for the whole line.

A2.1.2 Calculation of the Steady-State Recovery Voltage

When switch F in fig. 2.6b is open, the recovery voltage is that across the lower arm when voltage -0.5E is applied to the upper and lower arms in series.

$$V_r = -0.5E \frac{B_u}{B_u + B_\ell} = -E \frac{H_1 - kH_o}{2H_1 + kH_o} \qquad \text{(A2.1.11)}$$

The base voltage is normal line-to-ground voltage E.

$$V_{r(p.u.)} = \frac{V_r}{E} = - \frac{H_1 - kH_o}{2H_1 + kH_o} \qquad \text{(A2.1.12)}$$

A 2.1.3 Calculation of the Natural Frequency of Transient Component of Recovery Voltage

This is the natural frequency of fig. 2.6c, having a susceptance

$$B_u + B_\ell = \left[\omega(2C_1 + C_o) - (2\Gamma_1 + \Gamma_o)/\omega\right]/3 \qquad \text{(A2.1.13)}$$

The natural angular frequency is that which makes the susceptance vanish; it is

$$\omega_r = \left(\frac{2\Gamma_1 + \Gamma_o}{2C_1 + C_o}\right)^{\frac{1}{2}} \qquad \text{(A2.1.14)}$$

The base frequency is the supply frequency ω_o, which from the definitions of h_1 and h_o

$$\omega_o = \left(\frac{\Gamma_1}{h_1 C_1}\right)^{\frac{1}{2}} = \left(\frac{\Gamma_o}{h_o C_o}\right)^{\frac{1}{2}} \qquad \text{(A2.1.15)}$$

The natural frequency, normalized on this base is:

$$f_{r(p.u.)} = \frac{\omega_r}{\omega_o} = \left(\frac{2h_o + kh_o}{2 + k}\right)^{\frac{1}{2}} \qquad \text{(A.2.1.16)}$$

Eqns. A2.1.10 and A2.1.12 are the basic equations used in this thesis to determine the shunt reactor parameters.

It must be pointed out that the optimum neutral reactor for high voltage lines of over 300 km should be selected from the full theoretical equivalent circuit[29]. This provides an additional decrease in the secondary arc current in comparison with the case where the neutral is selected for compensation of the capacitive component only. For lines of less than 300 km in length eqn. A2.1.10 can be used for determination of the neutral reactor.

APPENDIX 2.2

CALCULATION OF TRANSMISSION LINE PARAMETERS AND SOLUTION OF THE TRAVELLING WAVE EQUATION

The basic line parameter matrices are the series impedance (Z) and the shunt admittance (Y) matrices which are uniformly distributed along its length. For a multi-conductor line, the basic line parameter matrices have been formulated[86] for realistic transient studies, and are presented in this Appendix. Other line parameter matrices such as surge impedance (Z_o), surge admittance (Y_o), and propagation constant are derived from these basic parameters.

A 2.2.1 Series Impedance Matrix

The series impedance matrix, $[Z]$, consists of three main components namely:

1. The impedance due to the physical geometry of the conductors, $[Z_g]$, which is due to the electromagnetic couplings between them.
2. The internal or self impedance, $[Z_c]$.
3. The impedance which accounts for the earth return path, $[Z_e]$.

Thus the series impedance matrix of a multi-conductor line is of the form:

$$[Z] = [Z_g + Z_c + Z_e] \qquad \text{(A2.2.1)}$$

The series impedance matrix $[Z]$ and each of its component matrices are of the order 3p + q where:

p = number of circuits

q = number of earth wires

A 2.2.1a Impedance Due to Physical Geometry

The impedance matrix due to the physical geometry of the line conductors shown in fig. A2.2.1 is of the form:

$$[Z_g] = jX_g = j\frac{\omega u}{2\pi}[B] \qquad \text{(A2.2.2)}$$

B is known as the charge-coefficient matrix and its elements are defined as:

$$B_{ij} = \log_e (D_{ij}/d_{ij}) \qquad \text{(A2.2.3)}$$

where:

$[D_{ij}]$ = distance between the ith conductor and the image of the jth conductor

d_{ij} = distance between the ith conductor and the jth conductor (for $i \neq j$)

= radius of the ith conductor for ($i = j$)

A 2.2.1b The Self Impedance of the Conductors

Considering a single-circuit e.h.v. line with two earth wires, the self impedance matrix of the conductors is one where diagonal elements represent the self impedances of the phase conductors and earth wires and whose off-diagonal terms are zero as given by eqn. A2.2.4.

$$[Z_c] = [Z_{sc} \quad Z_{sc} \quad Z_{sc} \quad Z_{se} \quad Z_{se}]_{diag} \qquad \text{(A2.2.4)}$$

Since it is a common practice to bundle the conductors of e.h.v. lines, the self impedance of the bundled conductors is:

$$Z_{sc} = Z_{ssc}/N_b$$

where

Z_{ssc} = self impedance of a sub-conductor of the bundle.

N_b = number of sub-conductors consisting the bundle.

The calculation of the self impedance of the conductors is complicated mainly due to the fact that it depends on too many factors such as stranding of the conductors, presence of steel core (in ACSR conductors), non-uniform current density (due to skin effect), frequency and other design features.

In practice two equations are commonly used. One is used for the low frequency range, less than or equal to 500 Hz, and the other for high frequency range, greater than 500 Hz.

For low frequencies, $\left[Z_c\right]$ can be calculated by assuming a uniform current distribution in the conductors, (and also the influence of stranding and the steel core of the conductor can be neglected). In this case the elements of the matrix given by eqn. A2.2.4 are:

$$\left[Z_c\right] = R_{dc} + j \frac{\omega\mu}{2\pi} \log_e (r/r_{gm}) \qquad \text{(A2.2.6)}$$

where:

R_{dc} = dc resistance

r = phase conductor or earth wire radius

r_{gm} = phase conductors or earth wire geometric mean radius, which is given by the cable manufacturer

$$R_{dc} = \frac{\rho}{n\pi r_s^2} \qquad \text{(A2.2.7)}$$

where:

ρ = conductor resistivity

n = number of conducting strands

r_s = radius of each strand

As the frequency increases, the skin effects become more and more important. Due to the skin effect, the current density is not uniform throughout the overall radius of the conductors. The self impedance of the conductors is very much affected by the non-uniformity of current distribution. The conductor resistance increases with frequency where its inductance decreases as the frequency increases. Fig. A2.2.2 shows a typical variation of self inductance and resistance with frequency, which for computational efficiency, is stored in piecewise linearised form[87].

The self impedance of the conductors at higher frequencies (above 2.5 kHz) may be calculated by the method suggested by Galloway et al[86] as follows:

For phase conductors (the same thing applies to earth wires):

$$Z_c = R_c + jX_c$$

where:

$$R_c = X_c = \frac{K_1 \rho m}{\sqrt{2r_o(n_o + 2)\pi}} \qquad \text{(A2.2.8)}$$

and

$m = \sqrt{\omega\mu/\rho}$

r_o = radius of each outer strand

n_o = number of strands in the outer layer

k_1 = factor accounts for conductor stranding $\simeq$ 2.25

In the present work, the standard conductor is substituted by a solid aluminium conductor of the same overall radius, and the self impedance is evaluated on the basis of non-uniform current density due to skin effect. This method is commonly used for design purposes for evaluating the self impedance of ACSR conductors[88].

A 2.2.1c Impedance due to Earth-Return Path

The contribution to the line series impedance due to the earth-return path, is calculated by using the infinite series developed by Carson[89]. Carson's equations have been expressed in a form suitable for digital simulation by Galloway et al[86] and they are:

$$\left[Z_e\right] = \frac{2\omega\mu}{2\pi} \left[P + j\,Q\right] \qquad \text{(A2.2.9)}$$

$\left[P\right]$ and $\left[Q\right]$ are calculated in terms of r_{ij} and θ_{ij}, fig. A2.2.1 with

$$r_{ij} = \sqrt{(\omega\mu/\rho)\ D_{ij}} \qquad \text{(A2.2.10)}$$

and have two different formulae[86] according to the value of r_{ij} greater than 5 ($r_{ij} > 5$), or smaller or equal to 5 ($r_{ij} \leq 5$).

A 2.2.2 Shunt Admittance Matrix

On the assumption that the air conductance of free space is negligible, the shunt admittance matrix of the transmission line contains only imaginary terms which corresponds to the capacitive couplings between the conductors, and the conductors and earth. It is a matrix of the order 3p + q, where p is the number of circuit and q is the number of earth wires. It is defined as:

$$\left[Y\right] = j2\pi\omega\epsilon\left[B\right]^{-1} \qquad \text{(A2.2.11)}$$

where

$\left[B\right]^{-1}$ is the inverse of the matrix $\left[B\right]$ given by eqn. A2.2.2

A 2.2.3 Elimination of Earth Wires

Since the voltages and currents in the earth wires are not of importance, it is therefore necessary to eliminate elements in rows and columns corresponding to them in both series impedance and shunt admittance matrices. Thus the performance of the phase conductors, which is of interest, remains unchanged and the system analysis is very much simplified[87,88].

Earth wires are normally earthed at regular intervals, hence they can be assumed to have zero (or near zero) potentials if standing voltages between towers are neglected. In this case elements in rows and columns corresponding to the earth wires of the shunt admittance matrix can be discarded. For the series impedance matrix, the earth wire elimination is done by inverting the matrix and then eliminating elements in rows and columns corresponding to the earth wires, and then reinvert it back.

A 2.2.4 Solution of the Travelling Wave Equation

Expressing in Laplace form, the voltage and currents at a distance, x, from one end of the line of any homogeneous multi-conductor transmission line can be shown to be[52,39]:

$$\left[\frac{d\bar{V}}{dX}\right] = -\left[\bar{Z}\right]\left[\bar{I}\right] \qquad \text{(A2.2.12)}$$

$$\left[\frac{d\bar{I}}{dX}\right] = -\left[\bar{Y}\right]\left[\bar{V}\right] \qquad \text{(A2.2.13)}$$

$\bar{V}$ and $\bar{I}$ are column vectors having elements representing respectively the Laplace transforms of the voltage and currents in all phase conductors. $\bar{Z}$ and $\bar{Y}$ are respectively the Laplace transforms of the series impedance and shunt admittance matrices where the rows and columns corresponding to earth wires are eliminated.

From eqns. A2.2.12 and A2.2.13:

$$\left[\frac{d^2\bar{V}}{dX^2}\right] = [\bar{Z}][\bar{Y}][\bar{V}] = [\bar{P}][\bar{V}] \qquad \text{(A2.2.14)}$$

$$\left[\frac{d^2\bar{I}}{dX^2}\right] = [\bar{Y}][\bar{Z}][\bar{I}] = [\bar{P}]^T[\bar{I}] \qquad \text{(A2.2.15)}$$

where

$$[\bar{P}] = [\bar{Z}][\bar{Y}] \qquad \text{(A2.2.16)}$$

T = matrix transposition

The matrix $[\bar{P}]$ is a full matrix. Therefore the solution for $[\bar{V}]$ and $[\bar{I}]$ can be obtained by solving a set of simultaneous differential equations, eqns. A2.2.14 and A2.2.15. If, by some means of transformation, the eqn. A2.2.14 or A2.2.15 can be written in a form of a set of differential equations which can be solved independently, the solution is much simpler.

Let a matrix, $[S]$, a non-singular square matrix such that:

$$[\bar{V}] = [S][\bar{v}] \qquad \text{(A2.2.17)}$$

From eqn. A2.2.14 and A2.2.17:

$$\left[\frac{d^2\bar{V}}{dX^2}\right] = [D][\bar{v}] \qquad \text{(A2.2.18)}$$

where

$$[D] = [S]^{-1}[\bar{P}][S] \qquad \text{(A2.2.19)}$$

With a suitable choice of $[S]$, the matrix $[D]$ becomes a diagonal matrix. Hence eqn. A2.2.18 contains a set of differential equations which can be solved independently. From the matrix theory it can be shown that $[D]$ and $[S]$ are respectively the eigenvalue and eigenvector matrices of the matrix $[\bar{P}]$.

The solution of eqn. A2.2.18 is:

$$\bar{v} = \exp(-\gamma x)\,\bar{v}_s + \exp(\gamma x)\,\bar{v}_r \qquad \text{(A2.2.20)}$$

where

$$\gamma = \sqrt{D} \qquad \text{(A2.2.21)}$$

$\bar{v}_s$ and $\bar{v}_r$ are constants of integration

By analogy to the system of a single phase transmission line, it can be said that in multi-conductor transmission lines there are a number of waves, equal to the number of phase conductors, which propagate independently, each is characterised by its own propagation constant γ_i, where γ_i is an element in the matrix γ .

Expressing in terms of original phase voltages, eqn. A2.2.20 can be written as:

$$\bar{V} = S\,\exp(-\gamma x)\,S^{-1}\,\bar{V}_s + S\,\exp(\gamma x)\,S^{-1}\,\bar{V}_r \qquad \text{(A2.2.22)}$$

where

$$\bar{V}_s = S\,\bar{v}_s\,, \quad \bar{V}_r = S\,\bar{v}_r$$

From eqn. A2.2.15, the current in a multi-conductor transmission line can be shown to be:

$$\bar{I} = \bar{Y}_o\,S\,\exp(-\gamma x)\,S^{-1}\,\bar{V}_s - \bar{Y}_o\,S\exp(\gamma x)\,S^{-1}\,\bar{V}_r \qquad \text{(A2.2.23)}$$

where

$$\bar{Y}_o = \bar{Z}^{-1}\,S\,\gamma\,S^{-1} \qquad \text{(A2.2.24)}$$

Eqns. A2.2.22 and A2.2.23 show the voltages and currents at any point, distance x from one end of the line. But if only terminal quantities of multiconductor transmission line are of interest it is possible to formulate two-port matrix equations from eqns. A2.2.22 and A2.2.23 by

replacing x by zero and length of the line, ℓ, and can be shown to be:

$$\begin{bmatrix} \bar{V}_S \\ \bar{I}_S \end{bmatrix} = \begin{bmatrix} S \cosh \gamma\ell \, S^{-1} & S \sinh \gamma\ell \, S^{-1} \, Z_o \\ Y_o S \sinh \gamma\ell \, S^{-1} & Y_o S \cosh \gamma\ell \, S^{-1} \, Z_o \end{bmatrix} \begin{bmatrix} \bar{V}_R \\ \bar{I}_R \end{bmatrix} \qquad \text{(A2.2.25)}$$

where $\bar{Z}_o = S \, \gamma^{-1} \, S^{-1} \, \bar{Z}$

It can be seen that eqn. A2.2.25 gives the transmission network equations in terms of the well known 'ABCD' constant matrices, where

$$A = \cosh(\psi\ell) \quad , \quad B = \sinh(\gamma\ell) \, Z_o$$
$$C = Y_o \sinh(\psi\ell) \, , \quad D = Y_o \cosh(\gamma\ell) \, Z_o \qquad \text{(A2.2.26)}$$

and

$$\psi = S\gamma S^{-1}$$
$$\cosh(\psi\ell) = S \cosh(\gamma\ell) \, S^{-1}$$
$$\sinh(\psi\ell) = S \sinh(\gamma\ell) \, S^{-1}$$

For a single-circuit, the dimension of any of the matrices given in eqn. A2.2.26 is (3 x 3). Eqn. A2.2.25 is the basic equation used in the analytical and digital analysis presented in this thesis.

A2.2.5 Determination of Eigenvalues and Eigenvectors

In the case where lines cannot be assumed fully symmetrical, eigenvalues and eigenvectors of matrix $\bar{P}$ can be calculated by using the root squaring method[86] whose efficiency depends very much on the values of the eigenvalues. It might fail to converge if they are very close to each other but present a very quick convergence if they are widely different.

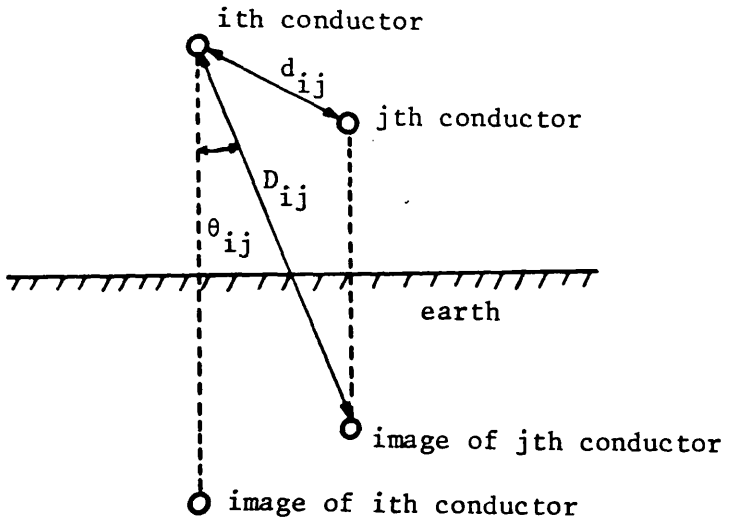

Fig. A2.2.1 Schematic diagram of conductor positions

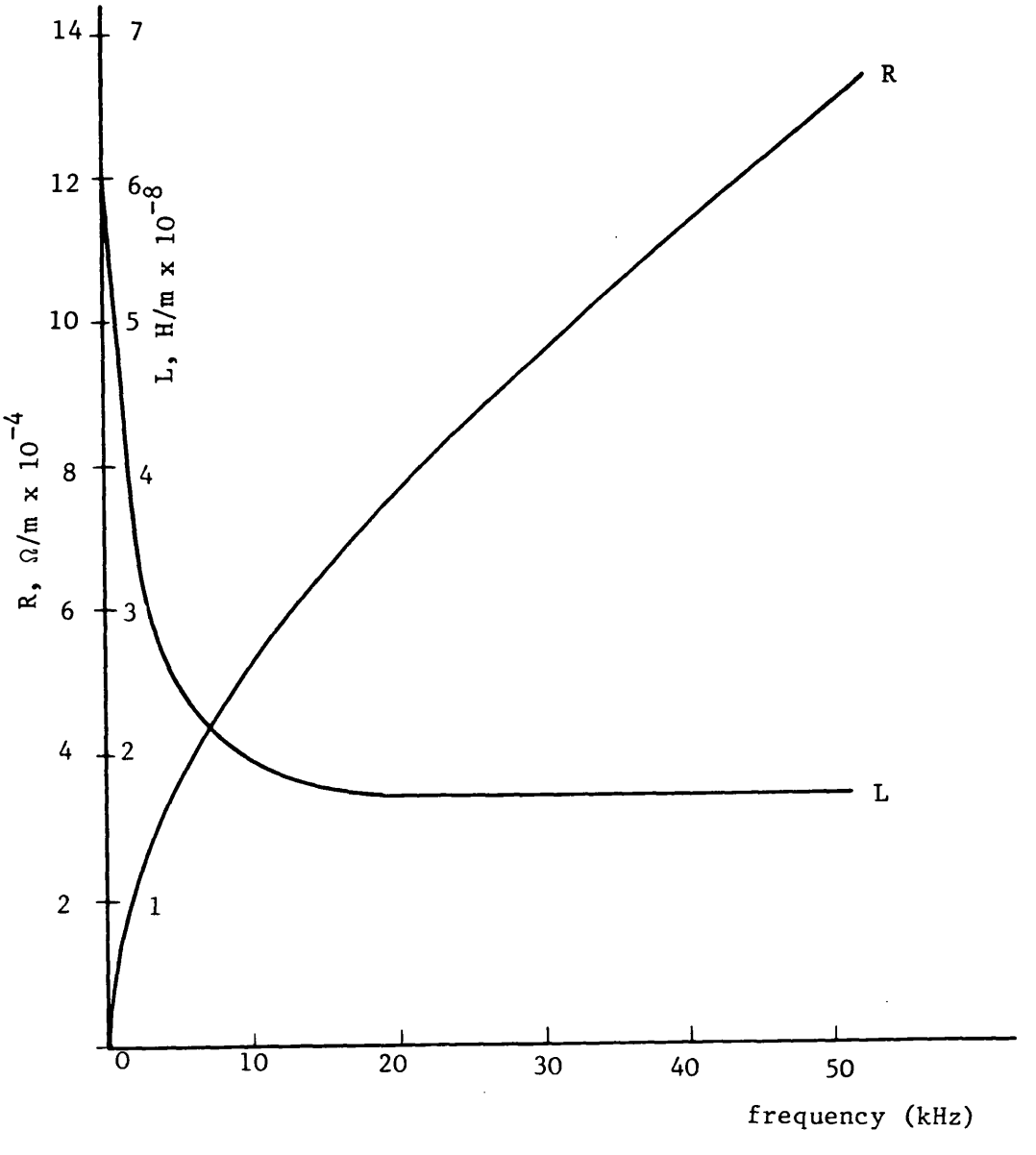

Fig. A2.2.2 Variation of line inductance (L) and resistance (R) with frequency

APPENDIX 2.3

SOURCE SIMULATION

For the purpose of confirming the digital simulation presented in this thesis, a general source model based upon defined short circuit levels (s.c.l.) at the terminating busbar has been used[47,87]. The model can further be modified to incorporate a lumped capacitance to represent any stray capacitance of the busbar to earth plus the capacitance of voltage transformers for metering or relaying purposes. However, this capacitance has been neglected in the course of the work presented, because it complicates the process of varifying the simulation as a whole[47]. The basic source model is shown in fig. 2.9 and the source impedance matrix can be calculated as follows:

$$\begin{bmatrix} \bar{E}_{Sa} \\ \bar{E}_{Sb} \\ \bar{E}_{Sc} \end{bmatrix} = \begin{bmatrix} Z_{S1} + Z_{n1} & Z_{n1} & Z_{n1} \\ Z_{n1} & Z_{S1} + Z_{n1} & Z_{n1} \\ Z_{n1} & Z_{n1} & Z_{S1} + Z_{n1} \end{bmatrix} \begin{bmatrix} \bar{I}_{Sa} \\ \bar{I}_{Sb} \\ \bar{I}_{Sc} \end{bmatrix} + \begin{bmatrix} \bar{V}_{Sa} \\ \bar{V}_{Sb} \\ \bar{V}_{Sc} \end{bmatrix} \qquad \text{(A2.3.1)}$$

In a more general form to suit a (6 x 6) matrix simulation, eqn. A2.3.2 can be used.

$$\begin{bmatrix} \bar{E}_S \\ \bar{I}_S \end{bmatrix} = \begin{bmatrix} U & Z_S \\ 0 & U \end{bmatrix} \begin{bmatrix} \bar{V}_S \\ \bar{I}_S \end{bmatrix} \qquad \text{(A2.3.2)}$$

where

$$[Z_S] = \begin{bmatrix} Z_{S1} + Z_{n1} & Z_{n1} & Z_{n1} \\ Z_{n1} & Z_{S1} + Z_{n1} & Z_{n1} \\ Z_{n1} & Z_{n1} & Z_{S1} + Z_{n1} \end{bmatrix}$$

$$U = \begin{bmatrix} 1 & 0 & 0 \\ 0 & 1 & 0 \\ 0 & 0 & 1 \end{bmatrix}, \quad 0 = \begin{bmatrix} 0 & 0 & 0 \\ 0 & 0 & 0 \\ 0 & 0 & 0 \end{bmatrix}$$

or

$$\begin{bmatrix} \bar{E}_S \\ \bar{I}_S \end{bmatrix} = \begin{bmatrix} Z_{S6} \end{bmatrix} \begin{bmatrix} \bar{V}_S \\ \bar{I}_S \end{bmatrix} \qquad \text{(A2.3.3)}$$

In eqn. A2.3.1 the elements Z_{S1} and Z_{n1} are calculated as follows:

$$Z_{S1} = |V_L|^2/\text{s.c.l.} \qquad \text{(A2.3.4)}$$

$$\text{but} \quad Z_{S1} = R_{S1} + j\omega L_{S1} = R_{S1} + jX_{S1} \qquad \text{(A2.3.5)}$$

Defining the X/R ratio (at power frequency) of the sending and receiving end sources, the two elements of eqn. A2.3.5 can be defined. This ratio may take any value between 30-100[47].

The neutral source impedance Z_{n1} is calculated by producing both the p.p.s. and z.p.s. impedances Z_1 and Z_{S0} for the circuit of fig. 2.9, where:

$$Z_1 = Z_{S1}$$

$$Z_{S0} = Z_{S1} + 3Z_{n1}$$

$$\therefore \quad Z_{S0} = Z_1 + 3Z_{n1}$$

$$\text{and} \quad Z_{n1} = (Z_{S0} - Z_{S1})/3 = Z_{S1}((Z_{S0}/Z_{S1}) - 1)/3 \qquad \text{(A2.3.6)}$$

The zero/positive phase sequence impedance ratio (Z_{S0}/Z_{S1}) is among other source parameters which have to be defined. The parameters are:

1. Short circuit levels, i.e. s.c.1,...,s.c.n
2. X/R ratios at power frequency
3. Z_{S0}/Z_{S1} ratios
4. System line voltage (V_L).

APPENDIX 2.4

FAULT SIMULATION

Fig. 2.14 shows the faulted system in which the fault is simulated by a suddenly applied voltage source at the point of fault. It has been shown in reference (47) that this voltage source is equal in magnitude and opposite in polarity to the prefault voltage of the faulted phase, at the point of fault.

Consider fig. 2.14, at the fault point two main equations can be written:

$$\begin{bmatrix} \bar{E}_{ff} \\ \bar{I}_{fRf} \end{bmatrix} = \begin{bmatrix} A_R & B_R \\ C_R & D_R \end{bmatrix} \begin{bmatrix} \bar{V}_{Rf} \\ \bar{I}_{Rf} \end{bmatrix} \qquad \text{(A2.4.1)}$$

$$\begin{bmatrix} \bar{E}_{ff} \\ -\bar{I}_{fSf} \end{bmatrix} = \begin{bmatrix} A_L & B_L \\ C_L & D_L \end{bmatrix} \begin{bmatrix} \bar{V}_{Sf} \\ -\bar{I}_{Sf} \end{bmatrix} \qquad \text{(A2.4.2)}$$

where $\bar{E}_{ff}$, $\bar{I}_{fRf}$, $\bar{V}_{Rf}$, $\bar{I}_{Rf}$, $\bar{I}_{fSf}$, $\bar{V}_{Sf}$ and $\bar{I}_{Sf}$ are the transforms of the respective voltages and currents shown in fig. 2.14.

$$\begin{bmatrix} A_R & B_R \\ C_R & D_R \end{bmatrix} = \begin{bmatrix} A_2 & B_2 \\ C_2 & D_2 \end{bmatrix} \begin{bmatrix} Y_{SR} \end{bmatrix}$$

$$\begin{bmatrix} A_L & B_L \\ C_L & D_L \end{bmatrix} = \begin{bmatrix} A_1 & B_1 \\ C_1 & D_1 \end{bmatrix} \begin{bmatrix} Y_{SR} \end{bmatrix}$$

where

A_1, B_1, C_1, and D_1 represent the line constant matrices between the fault point and the sending end S.

A_2, B_2, C_2, and D_2 represent the line constant matrices between the fault point and the receiving end R.

Y_{SR} is a 6 x 6 shunt reactor matrix.

If the shunt reactor is removed then Y_{SR} can be replaced by unity matrix.

Applying the superposition principle, $\bar{V}_{ff}$ is the only voltage source in the circuit of fig. 2.14.

$$\left[\bar{V}_{Sf}\right] = -\left[Z_{SS}\right]\left[\bar{I}_{Sf}\right] \qquad \text{(A2.4.3)}$$

$$\left[\bar{V}_{Rf}\right] = \left[Z_{SR}\right]\left[\bar{I}_{Rf}\right] \qquad \text{(A2.4.4)}$$

where Z_{SS} and Z_{SR} are the sending and receiving ends simple/composite source impedance matrices respectively.

Substituting eqn. A2.4.4 into eqn. A2.4.1 gives

$$\begin{aligned}\left[\bar{E}_{ff}\right] &= \left[A_R + B_R Z_{SR}^{-1}\right]\left[\bar{V}_{Rf}\right] \\ \left[\bar{I}_{fRf}\right] &= \left[C_R + D_R Z_{SR}^{-1}\right]\left[\bar{V}_{Rf}\right]\end{aligned} \qquad \text{(A2.4.5)}$$

from which

$$\left[\bar{E}_{ff}\right] = \left[A_R + B_R Z_{SR}^{-1}\right]\left[C_R + D_R Z_{SR}^{-1}\right]\left[I_{fRf}\right] \qquad \text{(A2.4.6)}$$

Likewise, using eqns. A2.4.2 and A2.4.3

$$\left[\bar{E}_{ff}\right] = -\left[A_L + B_L Z_{SS}^{-1}\right]\left[C_L + D_L Z_{SS}^{-1}\right]\left[I_{fSf}\right] \qquad \text{(A2.4.7)}$$

Now, considering any general earth fault

$$\left[\bar{E}_{ff}\right] = \left[\bar{V}_{ff}\right] + \left[Z_F\right]\left[\bar{I}_{fSf} - \bar{I}_{fRf}\right] \qquad \text{(A2.4.8)}$$

where Z_F is a diagonal matrix of the required values of fault resistance (R_f) in each phase. Using eqns. A2.4.6, A2.4.7

$$\left[\bar{I}_{fSf} - \bar{I}_{fRf}\right] = -\left\{\left[C_L + D_L Z_{SS}^{-1}\right]\left[A_L + B_L Z_{SS}^{-1}\right]^{-1} + \left[C_R + D_R Z_{SR}^{-1}\right]\left[A_R + B_R Z_{SR}^{-1}\right]^{-1}\right\}\left[\bar{E}_{ff}\right] \quad \text{(A2.4.9)}$$

Finally substituting eqn. A2.4.9 into eqn. A2.4.8

$$\bar{V}_{ff} = -\left[\left[\left[C_L + D_L Z_{SS}^{-1}\right]\left[A_L + B_L Z_{SS}^{-1}\right]^{-1}\right] + \left[C_R + D_R Z_{SR}^{-1}\right] A_R + B_R Z_{SR}^{-1}\right]\right]^{-1} + Z_F\left[\bar{I}_{fSf} - \bar{I}_{fRf}\right] \quad \text{(A2.4.10)}$$

Eqn. A2.4.10 relates the superimposed voltages $\bar{V}_{ff}$ to the fault current $\left[\bar{I}_{fSf} - \bar{I}_{fRf}\right]$ and can be written in the following form:

$$\begin{bmatrix} \bar{V}_{ffa} \\ \bar{V}_{ffb} \\ \bar{V}_{ffc} \end{bmatrix} = \begin{bmatrix} Z_{aa} & Z_{ab} & Z_{ac} \\ Z_{ba} & Z_{bb} & Z_{bc} \\ Z_{ca} & Z_{cb} & Z_{cc} \end{bmatrix} \begin{bmatrix} \bar{I}_{fa} \\ \bar{I}_{fb} \\ \bar{I}_{fc} \end{bmatrix} \quad \text{(A2.4.11)}$$

Consider now a single phase to earth fault involving the 'a' phase, $\bar{V}_{ffa}$ is the Fourier transform of a suddenly applied voltage of the form:

$$V_{ffa} = -V_{fSa} \sin(\omega_o t + \beta)h(t) \quad \text{(A2.4.12)}$$

V_{fSa} = peak of the fault point prefault voltage

β = phase displacement between the prefault voltage of phase 'a' and the reference voltage

$h(t)$ = a unit step function

The currents $\bar{I}_{fb}$ and $\bar{I}_{fc}$ are zero because their phases are healthy, and eqn. A2.4.11 takes the simplified form:

$$\begin{bmatrix} \bar{V}_{ffa} \\ \bar{V}_{ffb} \\ \bar{V}_{ffc} \end{bmatrix} = \begin{bmatrix} Z_{aa} \\ Z_{ba} \\ Z_{ca} \end{bmatrix} \begin{bmatrix} \bar{I}_{fa} \end{bmatrix} \qquad \text{(A2.4.13)}$$

With reference to eqn. A2.4.13, the voltage transform $\bar{V}_{ffa}$ is known, so that the superimposed voltages in the sound phases are easily evaluated. The vector of transformed superimposed voltages from each phase to earth, $\bar{E}_{ff}$, is obtained from eqn. A2.4.14.

$$\begin{bmatrix} \bar{E}_{ffa} \\ \bar{E}_{ffb} \\ \bar{E}_{ffc} \end{bmatrix} = \begin{bmatrix} \bar{V}_{ffa} \\ \bar{V}_{ffb} \\ \bar{V}_{ffc} \end{bmatrix} + \begin{bmatrix} R_f & 0 & 0 \\ 0 & R_f & 0 \\ 0 & 0 & R_f \end{bmatrix} \begin{bmatrix} \bar{I}_{fa} \\ \bar{I}_{fb} = 0 \\ \bar{I}_{fc} = 0 \end{bmatrix} \qquad \text{(A2.4.14)}$$

The final step in the process involves computing the spectrum of the voltages and currents at the sending and receiving ends.

At the sending end S, the currents and voltages are related to the fault-point variables by eqn. A2.4.2, so that

$$\begin{bmatrix} \bar{E}_{ff} \\ -\bar{I}_{fSf} \end{bmatrix} = \begin{bmatrix} A_L & B_L \\ C_L & D_L \end{bmatrix} \begin{bmatrix} \bar{V}_{Sf} \\ -\bar{I}_{Sf} \end{bmatrix}$$

but $\begin{bmatrix} \bar{V}_{Sf} \end{bmatrix} = - \begin{bmatrix} Z_{SS} \end{bmatrix} \begin{bmatrix} \bar{I}_{Sf} \end{bmatrix}$

Now $\begin{bmatrix} \bar{E}_{ff} \end{bmatrix} = \begin{bmatrix} A_L \end{bmatrix} \begin{bmatrix} \bar{V}_{Sf} \end{bmatrix} - \begin{bmatrix} B_L \end{bmatrix} \begin{bmatrix} \bar{I}_{Sf} \end{bmatrix}$

Therefore $\begin{bmatrix} \bar{V}_{Sf} \end{bmatrix} = \begin{bmatrix} A_L + B_L Z_{SS}^{-1} \end{bmatrix}^{-1} \begin{bmatrix} \bar{E}_{ff} \end{bmatrix}$ (A2.4.15)

and $\begin{bmatrix} \bar{I}_{Sf} \end{bmatrix} = - \begin{bmatrix} Z_{SS} \end{bmatrix}^{-1} \begin{bmatrix} \bar{V}_{Sf} \end{bmatrix}$ (A2.4.16)

Likewise, using eqns. A2.4.1, A2.4.4

$$\begin{bmatrix} \bar{V}_{Rf} \end{bmatrix} = \begin{bmatrix} A_R + B_R Z_{SR}^{-1} \end{bmatrix}^{-1} \begin{bmatrix} \bar{E}_{ff} \end{bmatrix} \qquad \text{(A2.4.17)}$$

and

$$\left[\bar{I}_{Rf}\right] = \left[Z_{SR}\right]^{-1}\left[\bar{V}_{Rf}\right] \qquad \text{(A2.4.18)}$$

Finally the voltage transforms of the voltage across the neutral reactor can be calculated as follows:

$$\bar{V}_{Sn} = (\bar{V}_{Sf}(1) + \bar{V}_{Sf}(2) + \bar{V}_{Sf}(3)) \frac{Z_n}{Z_p + 3Z_n}$$

$$\bar{V}_{Rn} = (\bar{V}_{Rf}(1) + \bar{V}_{Rf}(2) + \bar{V}_{Rf}(3)) \frac{Z_n}{Z_p + 3Z_n} \qquad \text{(A2.4.19)}$$

The faulted point, sending end, and receiving end voltages and currents transforms are converted to time domain via the inverse transform[47], and are added to the corresponding prefault steady-state variations to obtain the complete fault-transient waveforms.

It must be pointed out, that eqn. A2.4.15 is rather different from that which is shown in reference 47. This is due to the fact that the latter formulation applied to an untransposed line, and eqns. 19 and 29 (in reference 47) cannot be used at the same time in a transposed line. However, eqn. 19 is true only if the line constant matrices, in the transposed line, are multiplied from the fault point to the sending end. While eqn. 29 is true only if the line constant matrices, in the transposed line, are multiplied from the sending end to the fault point.

In this thesis, the matrices multiplication, due to the line transposition and the shunt reactors, are carried out from the sending to the receiving end in the steady-state formulation. While in the transient formulation, the multiplications are carried out from the fault point to the sending and receiving ends.

APPENDIX 3.1

EVALUATION OF THE GENERAL ADMITTANCE MATRIX

With reference to fig. 3.2 the transforms of the voltage components V_{S3} and V_{R3} on the line side of the breakers are obtained by noting that[34,47]:

$$\bar{V}_{S3} = \bar{E}_{SS3} - \bar{E}_{S3} = Z_{SS}\,\bar{I}_{S3} - \bar{E}_{S3} \qquad \text{(A3.1.1)}$$

$$\bar{V}_{R3} = \bar{E}_{RR3} + \bar{E}_{R3} = -Z_{SR}\,\bar{I}_{R3} + \bar{E}_{R3} \qquad \text{(A3.1.2)}$$

Also, the variation of the relaying point voltages and currents are related to the fault quantities by:

$$\begin{bmatrix} \bar{V}_{FF3} \\ \bar{I}_{FS3} \end{bmatrix} = \begin{bmatrix} A_1 & B_1 \\ C_1 & D_1 \end{bmatrix} \begin{bmatrix} \bar{V}_{S3} \\ \bar{I}_{S3} \end{bmatrix} \qquad \text{(A3.1.3)}$$

$$\begin{bmatrix} \bar{V}_{FF3} \\ -\bar{I}_{FR3} \end{bmatrix} = \begin{bmatrix} A_2 & B_2 \\ C_2 & D_2 \end{bmatrix} \begin{bmatrix} \bar{V}_{R3} \\ -\bar{I}_{R3} \end{bmatrix} \qquad \text{(A3.1.4)}$$

or

$$\bar{V}_{FF3} = A_1\bar{V}_{S3} + B_1\bar{I}_{S3} \qquad \text{(A3.1.5)}$$

$$\bar{I}_{FS3} = C_1\bar{V}_{S3} + D_1\bar{I}_{S3} \qquad \text{(A3.1.6)}$$

$$\bar{V}_{FF3} = A_2\bar{V}_{R3} - B_2\bar{I}_{R3} \qquad \text{(A3.1.7)}$$

$$\bar{I}_{FR3} = -C_2\bar{V}_{R3} + D_2\bar{I}_{R3} \qquad \text{(A3.1.8)}$$

At the fault point:

$$\bar{V}_{FF3} = \bar{E}_{FF3} + Z_F\left[\bar{I}_{FR3} - \bar{I}_{FS3}\right] \qquad \text{(A3.1.9)}$$

from eqns. A5.1.2 and A5.1.8

$$\bar{I}_{FR3} = \left[D_2 + C_2 Z_{SR} \right] \bar{I}_{R3} - C_2 \bar{E}_{R3}$$

from eqns. A5.1.1 and A5.1.6

$$\bar{I}_{FS3} = \left[D_1 + C_1 Z_{SS} \right] \bar{I}_{S3} - C_1 \bar{E}_{S3}$$

$$\therefore \left[\bar{I}_{FR3} - \bar{I}_{FS3} \right] = C_1 \bar{E}_{S3} - C_2 \bar{E}_{R3} + H_{11} \bar{I}_{R3} - H_{12} \bar{I}_{S3} \qquad \text{(A3.1.10)}$$

where

$$H_{11} = D_2 + C_2 Z_{SR}$$

$$H_{12} = D_1 + C_1 Z_{SS}$$

from eqns. A3.1.7, A3.1.9, A3.1.2

$$\bar{I}_{R3} = - \left[B_2 + A_2 Z_{SR} \right]^{-1} \bar{E}_{FF3} - \left[B_2 + A_2 Z_{SR} \right]^{-1} \left[Z_F \right] \left[\bar{I}_{FR3} - \bar{I}_{FS3} \right] + \left[B_2 + A_2 Z_{SR} \right]^{-1} \left[A_2 \right] \bar{E}_{R3}$$

or

$$\bar{I}_{R3} = AA_1 \bar{E}_{FF3} + AA_2 \left[\bar{I}_{FR3} - \bar{I}_{FS3} \right] + AA_3 \bar{E}_{R3} \qquad \text{(A3.1.11)}$$

where

$$AA_1 = - \left[B_2 + A_2 Z_{SR} \right]^{-1}$$

$$AA_2 = AA_1 Z_F$$

$$AA_3 = -AA_1 A_2$$

from eqns. A3.1.5, A3.1.1, A3.1.9

$$\bar{I}_{S3} = A_{11} \bar{E}_{FF3} + A_{22} \left[\bar{I}_{FR3} - \bar{I}_{FS3} \right] + A_{33} \bar{E}_{S3} \qquad \text{(A.1.12)}$$

where

$$A_{11} = \left[B_1 + A_1 Z_{SS} \right]^{-1}$$

$$A_{22} = A_{11} Z_F$$

$$A_{33} = A_{11} A_1$$

Substituting eqns. A3.1.11 and A3.1.12 into eqn. A3.1.10

$$\left[\bar{I}_{FR3} - \bar{I}_{FS3} \right] = Hk_{12}\bar{E}_{FF3} + Hk_{13}\bar{E}_{R3} - Hk_{14}\bar{E}_{S3} \qquad \text{(A3.1.13)}$$

where

$$Hk_{12} = Hk_1^{-1} Hk_2$$
$$Hk_{13} = Hk_1^{-1} Hk_3$$
$$Hk_{14} = Hk_1^{-1} Hk_4$$

and

$$Hk_1 = U + H_{12}A_{22} - H_{11}A_{22}$$
$$Hk_2 = H_{11}AA_1 - H_{12}A_{11}$$
$$Hk_3 = H_{11}AA_3 - C_2$$
$$Hk_4 = H_{12}A_{33} - C_1$$

Substituting eqn. A3.1.13 into eqn. A3.1.11

$$\bar{I}_{R3} = AA_{12}\bar{E}_{FF3} + AA_{13}\bar{E}_{R3} - AA_{14}\bar{E}_{S3} \qquad \text{(A3.1.14)}$$

where

$$AA_{12} = AA_1 + AA_2Hk_{12}$$
$$AA_{13} = AA_3 + AA_2Hk_{13}$$
$$AA_{14} = AA_2Hk_{14}$$

Substituting eqn. A3.1.13 into eqn. A3.1.12

$$\bar{I}_{S3} = HH_{12}\bar{E}_{FF3} + HH_{14}\bar{E}_{S3} + HH_{13}\bar{E}_{R3} \qquad \text{(A3.1.15)}$$

where

$$HH_{12} = A_{11} + A_{22}Hk_{12}$$
$$HH_{13} = A_{22}Hk_{13}$$
$$HH_{14} = A_{33} - A_{22}Hk_{14}$$

from eqns. A3.1.13, A3.1.14, and A3.1.15

$$\begin{bmatrix} \bar{I}_{FR3} - \bar{I}_{FS3} \\ \bar{I}_{S3} \\ \bar{I}_{R3} \end{bmatrix} = \begin{bmatrix} Hk_{12} & -Hk_{14} & Hk_{13} \\ HH_{12} & HH_{14} & HH_{13} \\ AA_{12} & -AA_{14} & AA_{13} \end{bmatrix} \begin{bmatrix} \bar{E}_{FF3} \\ \bar{E}_{S3} \\ \bar{E}_{R3} \end{bmatrix} \qquad \text{(A3.1.16)}$$

or

$$\begin{bmatrix} \bar{I}_{F3} \\ \bar{I}_{S3} \\ \bar{I}_{R3} \end{bmatrix} = \begin{bmatrix} Y_1 & Y_2 & Y_3 \\ Y_4 & Y_5 & Y_6 \\ Y_7 & Y_8 & Y_9 \end{bmatrix} \begin{bmatrix} \bar{E}_{FF3} \\ \bar{E}_{S3} \\ \bar{E}_{R3} \end{bmatrix} \qquad \text{(A3.1.17)}$$

It is important to note that the (9 x 9) admittance matrix in eqn. A3.1.17 is essentially a universal relationship which can be computed and stored at all spectral frequencies of interest. This eqn. can be used for fault simulation as well as breaker opening and closing. In this thesis the admittance matrix which is used is (9 x 5 x 4096). However, the choice of the five column depends on the faulted phase.

APPENDIX 5.1

NUMERICAL SOLUTION METHOD FOR SECONDARY ARC PATH

With reference to eqn. 5.5, the eqn. for solution is:

$$v_{arc}(t) = e_T(t) - \int_0^t Z_T(t-\tau) i_{arc}(\tau) d\tau \qquad \text{(A5.1.1)}$$

The integral part of eqn. A5.1.1 can be solved using the Trapezoidal rule in which time t is split into discrete intervals ΔT:

$$\int_0^{n\Delta T} Z_T(t-\tau) i_{arc}(\tau) d\tau \simeq \Big[Z_T(0) i_{arc}(n)/2 + Z_T(1) i_{arc}(n-1) + \ldots Z_T(n-1) i_{arc}(1) + Z_T(n) i_{arc}(0)/2 \Big] \Delta T \qquad \text{(A5.1.2)}$$

where $Z_T(m) = \frac{1}{2\pi} \int_{-\infty}^{\infty} Z_T \exp(j\omega m \Delta T) d\omega$, $m = 0,n$

Now at $t = 0$, $i_{arc}(t) = 0$. Thus $i_{arc}(0) = 0$ and eqn. A5.1.2 can be written in the more succinct form:

$$\int_0^{n\Delta T} Z_T(t-\tau) i_{arc}(\tau) d\tau \simeq \frac{Z_T(0) i_{arc}(n) \Delta T}{2} + \sum_{k=1}^{n-1} Z_T(n-k) i_{arc}(k) \Delta T \qquad \text{(A5.1.3)}$$

Eqn. A5.1.2 is strictly valid only for $n = 2,3,\ldots$, the Trapezoidal approximation for the first step $n = 1$ being:

$$\int_0^{\Delta T} Z_T(t-\tau) i_{arc}(\tau) d\tau = Z_T(0) i_{arc}(1) \Delta T/2 \qquad \text{(A5.1.4)}$$

Substituting eqn. A5.1.3 or A5.1.4 as appropriate into eqn. A5.1.1 and noting the discrete relationship between the arc voltage and current, given in eqn. 4.13, we obtain:

$$e_T(1) = f(i_{arc}(1),1) + Z_T(0)i_{arc}(1)\Delta T/2$$

$$e_T(n) = f(i_{arc}(n),n) + Z_T(0)i_{arc}(n)\Delta T/2 + \sum_{k=1}^{n-1} Z_T(n-k)i_{arc}(k)\Delta T,\ n = 2,3 \qquad \text{(A5.1.5)}$$

APPENDIX 8.1

STEADY-STATE CALCULATIONS OF THE SECONDARY ARC CURRENT

In order to determine the capacitive components of the secondary arc current and the recovery voltage, consider the equivalent circuit for a three phase line. This can be represented by a network of six capacitances, i.e. the three mutual capacitances C_{12}, C_{23}, C_{31} and the three zero sequence capacitances C_{10}, C_{20}, and C_{30} as shown in fig. A8.1a.

Assuming that the phases are non-symmetric, these capacitances are different but, for a transposed line, the transposition of the phases equalises the mutual capacitances on the one hand and self capacitances on the other. Therefore consider the average C_m of the capacitances C_{12}, C_{23}, C_{31} and the average C_o of the capacitances C_{10}, C_{20}, C_{30}. This simplifies the equivalent diagram of a three-phase line of fig. A8.1a to fig. A8.1b.

Consider a single line to earth fault on phase '2', and is then isolated from the source by opening the circuit breaker CB (fig. A8.1c). The secondary arc current (I_{sec}) which passes through the capacitance C_m when the arc resistance (assumed to be zero) is shunted to earth is[3]:

$$I_{sec} = j\omega_o C_m E_1 + j\omega_o C_m E_3 = -j\omega_o C_m E_2 \qquad \text{(A8.1.1)}$$

If the arc is extinguished (fig. A8.1d), phase 2 becomes charged capacitively. A simple calculation gives the recovery voltage charged in the isolated phase:

$$V_r = \frac{-E_2}{2 + \frac{C_o}{C_m}} \qquad \text{(A8.1.2)}$$

Maury[3] shows that if the secondary arc path resistance R_a (fig. A8.1e) is included in the calculation of the secondary arc current, eqn. A8.1.1 becomes:

$$I'_{sec} = \frac{-j\omega_o C_m E_2}{1 + jR_a(C_o + 2C_m)\omega_o} \qquad \text{(A8.1.3)}$$

$$\text{or} \quad I'_{sec} = \frac{I_{sec}}{1 + jR_a(C_o + 2C_m)\omega_o} \qquad \text{(A8.1.4)}$$

The resistance R_a introduces, therefore, a phase difference ϕ in the current whose tangent is:

$$\tan \phi = R_a(C_o + 2C_m)\omega_o \qquad \text{(A8.1.5)}$$

and reduces the secondary arc current by a factor of cos ϕ so that:

$$I'_{sec} = I_{sec} \cos \phi$$

The author states that, the secondary arc resistance does not exceed 1000 Ω, in a 220 km test. The author pointed out that, for a 400 km line, the drop in the secondary arc current due to 1000 Ω resistance is only 13%.

For the 120 km line, under study in chapter 8:

$$(C_o + 2C_m)\omega_o = 4.18934 \times 10^{-4}$$

$$\text{and} \quad I'_{sec(R_a=1200\Omega)} = 0.893452\ I_{sec(R_a=0.5\Omega)}$$

$$\text{or} \quad I'_{sec(R_a=1200\Omega)} = 21.83 \text{ A (peak)}$$

A closer examination of fig. 8.23a shows that the secondary arc current at $R_a = 1200\Omega$ (t = 0.5s) has a value of approximately 21.6A.

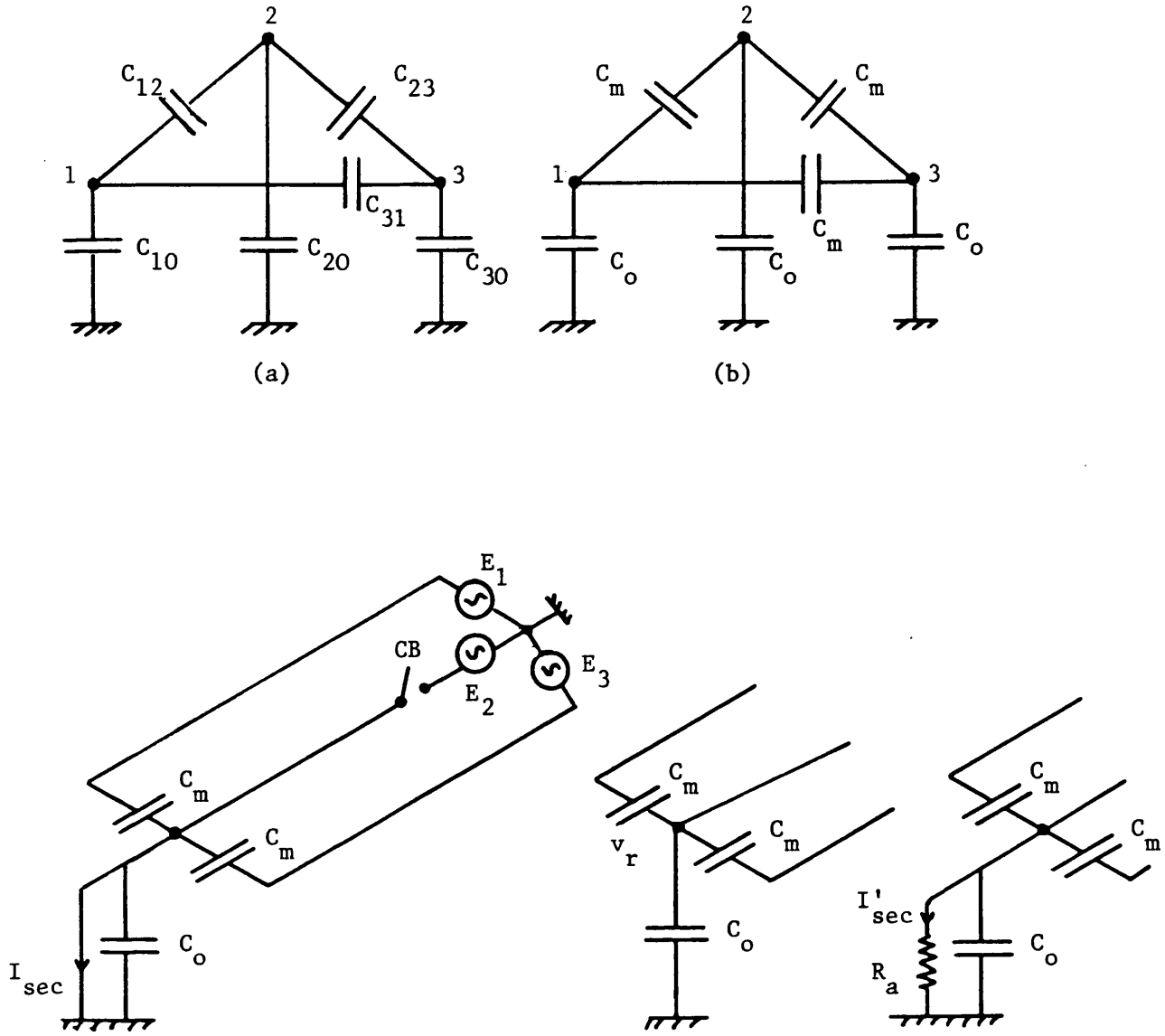

Fig. A8.1.1 Diagrams illustrating the calculation of the secondary arc current and the recovery voltage

(a) Equivalent circuit for a three-phase line

(b) Simplified diagram of a three-phase transposed line

(c) Circuit used to calculate the secondary arc current

(d) Circuit used to calculate the recovery voltage

(e) Circuit used to include the secondary arc resistance effect